

NATIONAL LIBRARY
OTTAWA



BIBLIOTHÈQUE NATIONALE
OTTAWA

8125

NAME OF AUTHOR..... *Beung C. So*

TITLE OF THESIS..... *Injection Phase-Locking*

Properties of Microwave IMPATT
Diode and Gunn Diode Oscillators

UNIVERSITY..... *of ALBERTA*

DEGREE FOR WHICH THESIS WAS PRESENTED..... *Ph. D.*

YEAR THIS DEGREE GRANTED..... *1971*

Permission is hereby granted to THE NATIONAL LIBRARY
OF CANADA to microfilm this thesis and to lend or sell copies
of the film.

The author reserves other publication rights, and
neither the thesis nor extensive extracts from it may be
printed or otherwise reproduced without the author's
written permission.

(Signed)..... *Beung C. So*

PERMANENT ADDRESS:

#11, 10945-84 ST.
EDMONTON
ALTA

DATED... *Jan. 2* 1971

THE UNIVERSITY OF ALBERTA

INJECTION PHASE-LOCKING PROPERTIES OF
MICROWAVE IMPATT DIODE AND GUNN DIODE OSCILLATORS,
WITH SYSTEM APPLICATIONS

by



Beung Chai So

A THESIS

SUBMITTED TO THE FACULTY OF GRADUATE STUDIES
IN PARTIAL FULFILMENT OF THE REQUIREMENTS FOR THE DEGREE
OF DOCTOR OF PHILOSOPHY

DEPARTMENT OF ELECTRICAL ENGINEERING

EDMONTON, ALBERTA

SPRING, 1971

UNIVERSITY OF ALBERTA
FACULTY OF GRADUATE STUDIES

The undersigned certify that they have read, and recommend to the Faculty of Graduate Studies for acceptance, a thesis entitled "Injection Phase-Locking Properties of Microwave IMPATT Diode and Gunn Diode Oscillators, with System Applications" submitted by Beung Chai So in partial fulfilment of the requirements for the degree of Doctor of Philosophy.

..... *Paul A. Gaud*
Supervisor

..... *B. S. ...*

..... *C. G. Englefield*

..... *D. ...*

..... *K. Kurukant*
External Examiner

Date. *29. December, 1970*

ABSTRACT

Injection phase-locking of microwave IMPATT diode and Gunn diode oscillators has been studied experimentally at X-band frequencies and has been analyzed qualitatively by the use of a "loading effect" method. In this method the external locking signal is taken to have an effect equivalent to an admittance whose phase depends on the relative amplitudes of, and the phase difference between, the oscillator and the external locking signals.

The theory is applied to a number of examples to indicate the properties of an injection phase-locked oscillator. The results obtained show that the injection locked IMPATT diode and Gunn diode oscillators may be suitable for certain system applications: e.g. (1) a self-excited oscillator containing a certain amount of noise can, when injection-locked to an external FM signal, be used as a broad-band and high-gain F.M. amplifier with good noise characteristics, (2) when a bias-modulated oscillator is injection-locked to a CW signal, an entire frequency pulling yields a practical phase-modulation scheme, while partial pulling properties permit the oscillator to be sideband-locked, achieving up-conversion with gain and frequency-stability, and (3) when the oscillator diode is used simultaneously for quasi-stationary injection-locking and detection, linear operation of the microwave frequency demodulation is obtained in a simple configuration.

ACKNOWLEDGEMENTS

The author wishes to express his appreciation for the assistance of many people during the course of this research:

To Dr. P.A. Goud for his advice and encouragement during the supervision of this work.

To Dr. C.G. Englefield, Professor Y.J. Kingma, Dr. H.J. Seguin, and Dr. S. Woods for serving on the doctoral committee.

To Mr. J. Fearn who contributed greatly to this work by his technical assistance throughout the project.

To members of the Microwave Electronics Laboratory at the University of Alberta, who were closely involved with this research, for their helpful discussions, understanding, and encouragement.

To members of the staff of the Department of Electrical Engineering, in particular members of the Microwave Power and the Radio Telescope Laboratories, and Mr. N. Burtch for their cooperation in lending me certain testing equipment during this project.

The author also thanks his wife, Jungil for her patience, encouragement, and help.

The author is also indebted to the following organizations:

To the National Research Council of Canada for continued support of the research and for provision of a research assistantship.

To the University of Alberta for a dissertation fellowship.

TABLE OF CONTENTS

	Page
-I	INTRODUCTION 1
1-1	Purposes of this Investigation 1
1-2	The Nature of Injection Phase-Locking in One-Port Microwave Oscillators 1
1-3	History and Applications of Injection Phase-Locking 5
1-4	Organization of Thesis 6
II	MICROWAVE IMPATT DIODE OSCILLATORS AND GUNN DIODE OSCILLATORS, A REVIEW 7
2-1	IMPATT Diode Oscillator Operation 7
2-2	Gunn Diode Oscillator Operation 9
2-3	Noise Performance 13
2-4	Description of Oscillators Tested 14
III	THEORETICAL ANALYSIS OF INJECTION PHASE-LOCKED OSCILLATORS 23
3-1	Introduction 23
3-1-1	Adler's Method 23
3-1-2	Second-Order Nonlinear Differential Equation Method 27
3-2	Loading Effect Method 28
3-2-1	Equivalent Circuit of Injection Locked-Oscillator 28
3-2-2	Effective Load Admittance due to Locking Signal 36
3-2-3	Locking Equation 44
3-3	Locking Relationships 46
3-3-1	Steady-State Phase Angle and Locking Time 46
3-3-2	Locking Range 50
3-3-3	Transient Phase Angle 51

	Page
3-3-4 Locking Figure of Merit	61
3-4 Locking to an FM Signal	63
3-5 Pulling Phenomenon Beyond Locking Range	73
3-5-1 An Analysis of Driven Oscillators	73
3-5-2 Output Spectra of Driven Oscillators	75
3-6 Phase Modulation Noise Improvement of Injection Phase-Locked Oscillators	77
IV EXPERIMENTAL STUDY OF BASIC INJECTION PHASE-LOCKING PROPERTIES OF OSCILLATORS	80
4-1 Introduction	80
4-2 Measurement of Locking Range	80
4-2-1 Description of Experimental Setup	81
4-2-2 Output Spectra of Locked Oscillators	85
4-2-3 Locking Range Variation with Power Ratio	88
4-2-4 Oscillator Quality Factor Derived from Locking Bandwidth	91
4-2-5 Interpretation of the Locking Signal Effect as the Change in Load Admittance	92
4-3 Measurement of Phase Angle Difference between the Locked Oscillator Output and the Locking Signal	95
4-3-1 Description of Experimental Setup with a Sensitive Microwave Phase Detector	95
4-3-2 Phase Angle Variation with Initial Frequency Difference	97
4-4 Injection Phase-Locked Oscillators with Relatively Large Locking Power Level	100
4-5 Intermodulation of Injection Phase-Locked Oscillators	106
4-5-1 Experimental Arrangement	107

4-5-2	Effect of Interfering Signal on Desired Signal	107
4-6	Self Injection Phase Locking	111
V	INJECTION PHASE-LOCKING OF BIAS-MODULATED OSCILLATORS	117
5-1	Introduction	117
5-2	Angle Modulation of Injection Phase-Locked Oscillators	118
5-2-1	Modulation Theory	118
5-2-2	System Applications	123
5-2-3	PM Noise Performance	131
5-3	Injection Phase Locking of a Sideband to the Locking Signal, a Theoretical and Experimental Analysis	135
VI	DEMODULATION BY INJECTION PHASE-LOCKED OSCILLATORS	148
6-1	Introduction	148
6-2	Injection Phase-Locked FM Reception	150
6-3	Experimental Performance of Frequency Demodulation	157
VII	SUMMARY AND CONCLUSIONS	162
	REFERENCES	167
APPENDIX-A	Some Characteristics of IMPATT Diodes and Gunn Diodes	175
A-1	Static Characteristics of IMPATT Diode	175
A-2	Dynamic Characteristics of IMPATT Diode	177
A-3	Bulk Differential Negative Conductance of n-type GaAs	182
APPENDIX-B	General Solution to the Locking Equation	186
APPENDIX-C	An Approximate Solution to the Differential Equation of A Locked Oscillator for the following cases (1) Locking Signal is Frequency-Modulated. (2) Self-Excited Oscillator is Frequency Modulated	191
APPENDIX-D	Effect of Additive DC Potential on Average Frequency Shift	198

	Page
APPENDIX-E Microwave Phase Detector	200
APPENDIX-F Injection Phase-Locking of a Nonlinear Conductance Diode Oscillator	203

LIST OF TABLES

	Page
TABLE 4.1: SOME ELECTRICAL CHARACTERISTICS FOR IMPATT DIODE OSCILLATORS TESTED.....	81
TABLE 4.2: SOME ELECTRICAL CHARACTERISTICS FOR GUNN DIODE OSCILLATORS TESTED.....	81
TABLE 4.3: LOCKING PERFORMANCE.....	94

LIST OF FIGURES

		Page
Fig 1.1:	BASIC INJECTION PHASE-LOCKING BLOCK DIAGRAM	3
Fig. 2.1:	X-BAND OSCILLATORS TESTED (a) SYA-3200 IMPATT DIODE OSCILLATOR..... (b) CL-8370 GUNN DIODE OSCILLATOR.....	15
Fig. 2.2:	CROSS-SECTIONAL VIEW OF SYA-3200 IMPATT DIODE OSCILLATOR.....	16
Fig. 2.3:	IMPURITY CONCENTRATION PROFILE OF SI IMPATT DIODE.....	17
Fig. 2.4:	BASIC CHARACTERISTICS OF A TYPICAL IMPATT DIODE OSCILLATOR (SYA-3200-3).....	18
Fig. 2.5:	A CROSS-SECTIONAL VIEW OF CL-8370 GUNN DIODE OSCILLATOR.....	20
Fig. 2.6:	CHARACTERISTICS OF GUNN DIODE OSCILLATOR USED (CL-8370-2).....	21
Fig. 3.1:	(a) NEGATIVE CONDUCTANCE OSCILLATOR MODEL..... (b) CURRENT VECTOR DIAGRAM OF Fig. 3.1a.....	24
Fig. 3.2:	HYPOTHETICAL CIRCUIT FOR LOCKING OF O_l BY IDEAL SOURCE O_s	30
Fig. 3.3:	OSCILLATOR-CIRCULATOR COMBINATION FOR LOCKING OF O_l BY O_s	30
Fig. 3.4:	EQUIVALENT CIRCUIT OF A LOCKED OSCILLATOR.....	34
Fig. 3.5:	A SIMPLIFIED EQUIVALENT CIRCUIT OF A LOCKED OSCILLATOR.....	34
Fig. 3.6:	EFFECTIVE SUSCEPTANCE VERSUS $ \Gamma $	39
Fig. 3.7:	NORMALIZED LOAD CONDUCTANCE AS A FUNCTION OF REFLECTION COEFFICIENT.....	41

	Page
Fig. 3.8:	LOCUS OF LOAD ADMITTANCE
	(a) LOCUS OF EFFECTIVE NORMALIZED LOAD ADMITTANCE.....
	(b) LOCUS OF SUPPLEMENTARY ADMITTANCE FROM Fig. 3.8a.....
	43
Fig. 3.9:	STEADY-STATE PHASE ANGLE VS. INITIAL FREQUENCY DIFFERENCE FOR Q_{ext} OF 100.....
	47
Fig. 3.10:	VARIATIONS OF θ WITH TIME FOR ZERO INITIAL FREQUENCY DIFFERENCE.....
	49
Fig. 3.11:	LOCKING RANGE VS. EFFECTIVE RETURN LOSS.....
	52
Fig. 3.12:	TRANSIENT RESPONSE OF A LOCKED OSCILLATOR FOR $Q_{ext} = 100$, $ \Gamma = 40$ DB, AND $\Delta\omega_o = 1.26 \times 10^6$ RAD/SEC.....
	55
Fig. 3.13:	TRANSIENT RESPONSE OF A LOCKED OSCILLATOR FOR $Q_{ext} = 100$, $ \Gamma = 20$ DB, AND $\Delta\omega_o = 200 \times 10^6$ RAD/SEC.....
	56
Fig. 3.14:	TRANSIENT RESPONSE OF A LOCKED OSCILLATOR FOR $ \Gamma = 40$ DB, $\theta_o = -100^\circ$, AND $Q_{ext} = 100$
	57
Fig. 3.15:	TRANSIENT RESPONSE OF A LOCKED OSCILLATOR FOR $ \Gamma = 40$ DB, $\theta_o = -100^\circ$, AND $Q_{ext} = 50$
	58
Fig. 3.16:	TRANSIENT RESPONSE OF A LOCKED OSCILLATOR FOR $ \Gamma = 30$ DB, $\theta_o = -100^\circ$, AND $Q_{ext} = 100$
	59
Fig. 3.17:	TRANSIENT RESPONSE OF A LOCKED OSCILLATOR FOR $ \Gamma = 30$ DB, $\theta_o = -100^\circ$, AND $Q_{ext} = 50$
	60
Fig. 3.18:	CONSERVATION FACTORS VS. MODULATING FREQUENCY...
	68
Fig. 3.19:	NONLINEAR PHASE CHARACTERISTICS OF INJECTION PHASE-LOCKING AND ITS ASSOCIATED TIME DELAY.....
	72
Fig. 3.20:	REDUCTION OF BEAT FREQUENCY DUE TO LOCKING.....
	76
Fig. 3.21:	TYPICAL BEAT-NOTE WAVEFORMS.....
	76
Fig. 3.22:	NOISE POWER SUPPRESSION FACTOR VERSUS NOISE FREQUENCY.....
	79
Fig. 4.1:	EXPERIMENTAL SETUP FOR MEASURING LOCKING RANGE..
	82
Fig. 4.2:	FOUR-PORT CIRCULATOR CHARACTERISTICS.....
	84

	Page
Fig. 4.3: OUTPUT SPECTRA OF THE LOCKED OSCILLATOR (IMPATT-SYA-3200-1).....	86
Fig. 4.4: BEAT FREQUENCIES VS. INITIAL FREQUENCY DIFFERENCE.....	87
Fig. 4.5: LOCKING RANGE AS A FUNCTION OF POWER GAIN.....	90
Fig. 4.6: MAXIMUM CHANGE IN FREQUENCY WITH RETURN LOSS OF LOAD.....	93
Fig. 4.7: EXPERIMENTAL SETUP FOR MEASURING STEADY-STATE PHASE ANGLE.....	96
Fig. 4.8: STEADY-STATE PHASE ANGLE VS. INITIAL FREQUENCY DIFFERENCE FOR AN IMPATT DIODE OSCILLATOR.....	98
Fig. 4.9: STEADY-STATE PHASE ANGLE VS. INITIAL FREQUENCY DIFFERENCE FOR A GUNN DIODE OSCILLATOR.....	99
Fig. 4.10: THE MAXIMUM POWER OUTPUT VS. THE VOLTAGE GAIN FOR AN IMPATT DIODE OSCILLATOR.....	104
Fig. 4.11: THE MAXIMUM POWER OUTPUT VS. THE VOLTAGE GAIN..	104
Fig. 4.12: FREQUENCY PUSHING FOR HIGH POWER INJECTION (SYA-3200-3).....	105
Fig. 4.13: EXPERIMENTAL SETUP FOR MEASURING INTERMODULATION PRODUCTS OF LOCKED OSCILLATORS.....	108
Fig. 4.14: RELATIVE OUTPUT POWERS AT VARIOUS FREQUENCIES OF THE INTERMODULATION PRODUCTS OF AN IMPATT DIODE OSCILLATOR FOR TWO INPUT CASE.....	109
Fig. 4.15: RELATIVE OUTPUT POWERS AT VARIOUS FREQUENCIES OF THE INTERMODULATION PRODUCTS OF AN IMPATT DIODE OSCILLATOR FOR THREE-INPUT CASE.....	110
Fig. 4.16: EXPERIMENTAL SETUP OF THE SELF-INJECTION-LOCKED OSCILLATOR.....	113
Fig. 4.17: OSCILLATION CHARACTERISTICS OF AN IMPATT DIODE OSCILLATOR.....	114
Fig. 4.18: EXTERNAL Q OF THE SELF-LOCKED OSCILLATOR.....	114
Fig. 4.19: OSCILLATION OUTPUT SPECTRA OF AN IMPATT DIODE OSCILLATOR FOR BIAS CURRENT OF 14 mA.....	116
Fig. 5.1: BLOCK DIAGRAM OF EXPERIMENTS FOR THE PHASE- CONTROL OF A LOCKED OSCILLATOR.....	124

	Page
Fig. 5.2: BREAKS OF PHASE-LOCKING AT THE PEAK MODULATION CYCLE.....	126
Fig. 5.3: RELATIVE DETECTOR OUTPUT VOLTAGE AS A FUNCTION OF MODULATING SIGNAL CURRENT OR VOLTAGE.....	128
Fig. 5.4: RELATIVE DETECTOR OUTPUT VOLTAGE AS A FUNCTION OF LOCKING POWER.....	129
Fig. 5.5: VARIATION OF PHASE DEVIATION WITH LOCKING POWER FOR THE CASE OF AN IMPATT DIODE OSCILLATOR (SYA-3200-1).....	133
Fig. 5.6: VARIATION OF PHASE DEVIATION WITH LOCKING POWER FOR THE CASE OF A GUNN DIODE OSCILLATOR (CL-8370-2).....	134
Fig. 5.7: FREQUENCY SPECTRA OF THE SIDEBAND-LOCKED OSCILLATOR WITH THE BIAS-MODULATION SIGNAL.....	137
Fig. 5.8: THE OUTPUT SPECTRA OF INJECTION-LOCKED OSCILLATOR WITH BIAS-MODULATION OF MULTIPLE-FREQUENCY SIGNAL.....	142
Fig. 5.9: LOCKING RANGE OF FIRST SIDEBANDS.....	144
Fig. 5.10: FREQUENCY SPECTRA OF SIDEBAND LOCKED IMPATT DIODE OSCILLATOR (SYA-3200-3) (a) AND (d) NO LOCKING SIGNAL IS APPLIED.....	145
(b) AND (e) PARTIALLY PULLING OF UPPER SIDEBAND TOWARD THE SIGNAL.....	145
(c) AND (f) LOCKING OF SIDEBAND TO THE SIGNAL...	145
Fig. 5.11: FREQUENCY SPECTRA OF SIDEBAND LOCKED GUNN DIODE OSCILLATOR (CL-8370-2) (a) AND (d) NO LOCKING SIGNAL IS APPLIED.....	146
(b) AND (e) PARTIALLY PULLING OF UPPER SIDEBAND TO THE SIGNAL.....	146
(c) AND (f) LOCKING OF SIDEBAND TO THE SIGNAL...	146
Fig. 6.1: AN EXPERIMENTAL SETUP FOR INJECTION PHASE-LOCKED FM RECEPTION.....	151
Fig. 6.2: DEMODULATOR CHARACTERISTICS SHOWING THE BEATS OCCURRING OUTSIDE LOCKING BANDWIDTH.....	159
Fig. 6.3: OSCILLOSCOPE DEMODULATOR CHARACTERISTICS (a) AND (b); FOR AN IMPATT DIODE OSCILLATOR.....	159
(c) AND (d); FOR A GUNN DIODE OSCILLATOR.....	159
Fig. 6.4: DEMODULATOR OUTPUT VOLTAGE VS. MAXIMUM FREQUENCY DEVIATION FOR A MODULATING FREQUENCY OF 100 KHz WHEN THE LOCKING GAIN IS 20 dB.....	161

	Page
Fig. A.1:	(a) READ DIODE ($p^+n_1n^+$)..... 176
	(b) ABRUPT p-n JUNCTION (p^+nn^+)..... 176
Fig. A.2:	(a) MODEL OF READ DIODE WITH AVALANCHE REGION, DRIFT REGION, AND INACTIVE REGION..... 179
	(b) EQUIVALENT CIRCUIT OF THE AVALANCHE REGION.... 179
	(c) EQUIVALENT CIRCUIT OF READ DIODE FOR SMALL TRANSIT ANGLE..... 179
Fig. A.3:	SCHEMATIC DIAGRAM SHOWING THE ELECTRON DENSITY VERSUS WAVE NUMBER IN THE REGION OF THE CONDUCTION BAND VALLEYS FOR n-TYPE GaAs..... 184
Fig. A.4:	AVERAGE VELOCITY VS. ELECTRIC FIELD FOR n-TYPE GaAs..... 184
Fig. D.1:	PLOT OF $\Delta_o \langle \sin\theta \rangle$ AS A FUNCTION OF $\Delta\omega_o$ 198
Fig. E.1:	MICROWAVE PHASE DETECTOR..... 200
Fig. E.2:	EQUIVALENT CIRCUIT OF Fig. E.1..... 200
Fig. E.3:	A PHASE DETECTOR WITH 3 DB COUPLER..... 202
Fig. F.1:	AN EQUIVALENT CIRCUIT OF THE INJECTION PHASE- LOCKED OSCILLATOR OF NONLINEAR CONDUCTANCE DIODE..... 204

CHAPTER I

INTRODUCTION

In many electronic systems employing microwave oscillators it is necessary to synchronize the frequency and phase of the oscillator signal to a reference signal. One way of achieving this end is by injecting the reference signal directly into the oscillator to be controlled. Under suitable conditions, the oscillator is then locked to the reference signal both in frequency and phase, and the oscillator is then referred to as being injection phase-locked.

Injection phase-locking has taken on increased importance with the development of solid-state microwave oscillators. Injection phase-locking presents possibilities for accomplishing amplification, modulation, demodulation and phase-control.

1-1 Purposes of this Investigation

For many applications involving injection phase-locking, it is necessary to have a detailed knowledge of the locking properties of the oscillator. The purposes of this investigation are 1) to study the basic locking properties of IMPATT diode and of Gunn Diode oscillators from the point of view of the loading effect of the reference signal on the oscillator. The analysis is to present a clear physical conception of locked oscillator operation at microwave frequencies. 2) to investigate system applications, both experimentally and theoretically, of injection phase-locking of oscillators.

1-2 The Nature of Injection Phase-Locking in One-Port Microwave Oscillators

If certain conditions are met, a one-port microwave oscillator may be phase-locked by the injection of a controlling signal into the oscillator. At microwave frequencies, the combination of a one-port oscillator and a circulator makes possible the separation of the oscillator output from the locking signal (see Fig.1.1).

The incident power wave of the locking signal passes from Port 1 to Port 2 of the circulator and impresses a signal on the oscillator. The output power of the oscillator passes from Port 2 to Port 3 of the circulator to the matched load. If the input signal has sufficient amplitude, and if its frequency is sufficiently close to the initial matched-load frequency ω_0 , the oscillator frequency will change to that of locking signal. At this new oscillation frequency the RF operating conditions will have changed. If the locking signal frequency is changed, the frequency of the oscillator signal will track this change until the initial frequency difference becomes too large, at which time the oscillator drops out of synchronism.

The mechanism of the injection phase-locking process depends upon the following:

- 1) the initial frequency difference between the oscillator signal and the reference signal.
- 2) the power ratio of the oscillator and the reference signal.
- 3) the oscillator circuit parameters.

Injection phase-locking is thus a technique whereby a small amplitude locking signal can be used to control the frequency and phase of a large amplitude oscillator signal.

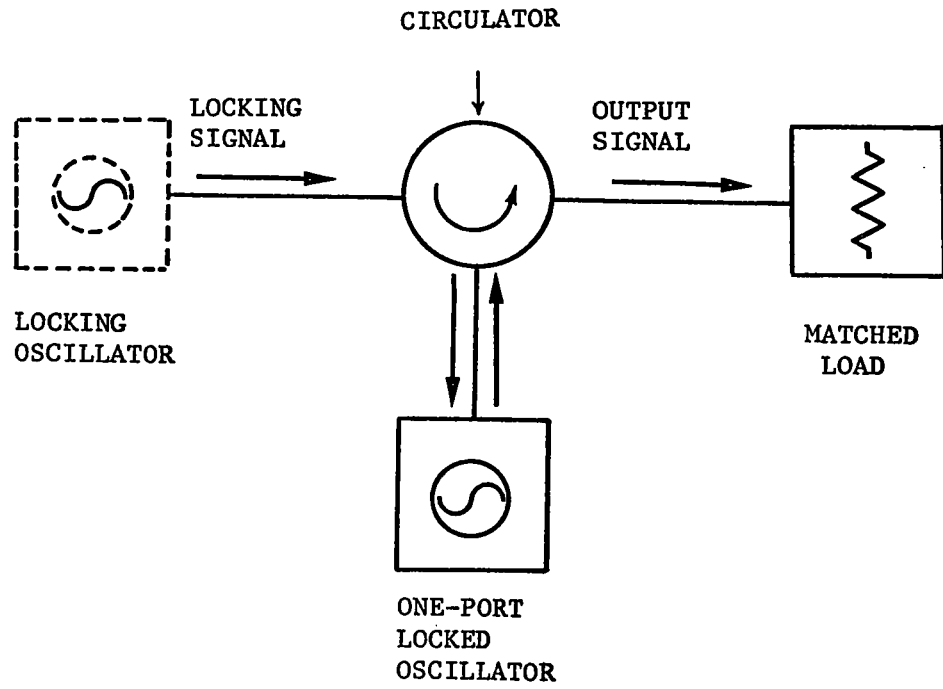


Fig.1-1 BASIC INJECTION PHASE-LOCKING BLOCK DIAGRAM.

1-3 History and Applications of Injection Phase-Locking

A number of investigations have been made into the subject of synchronization of oscillators. In 1927, van der Pol published a pioneering study on free-running oscillators that are capable of being synchronized to an external signal¹. There has since been a continually growing literature on this subject, great attention being given to the use of an oscillator as a synchronous-amplifier limiter, in an FM demodulation²⁻⁴.

In 1946, Adler⁵ obtained a differential equation, largely on the basis of intuitive reasoning, whose solution accounts for many of the observed phenomena of phase-locking. Theoretical and experimental treatments of oscillator synchronization have been concerned with the internal synchronization mechanism of a two-port oscillator with feedback; Huntoon and Weiss⁶ generalized the theory and extended the scheme used by Adler, in a manner which does not involve the particular oscillator.

The same approach as Adler's was applied to the magnetron, in a slightly different form, by Slater⁷. David⁸ experimentally verified Slater's theory with pulsed magnetrons. Khokhlov⁹ described a sinusoidal self-oscillation with simpler, so-called shortened equations by deriving the locking equation from the differential equation of an oscillator with a single-tuned circuit. If a more complex circuit were considered for the oscillator, the solution of the nonlinear differential equation would be considerably more difficult than that for this simple case.

Mackey¹⁰ showed that Adler's model describes the phase-locking phenomena in reflex klystron oscillators and he investigated the

transient response of the oscillator in order to obtain an estimate of the maximum modulation rate possible for the locking signal. In 1965 the locking behaviour of tunnel diode oscillators was experimentally studied by Stover and Shaw¹¹. One year later, Fukui¹² reported that he had successfully combined the output power from eight separate IMPATT diode oscillators by means of resistive hybrids; the finite isolation of the hybrids provided sufficient interaction between the oscillators for mutual phase-locking so that the powers combined phase-coherently. At nearly the same time, Hakki et al.¹³ succeeded in phase-locking a Gunn diode oscillator to a microwave signal and raised some questions about the relationship between the locking range and the oscillator circuit parameters and about the output spectrum of the unlocked driven oscillators.

As regards noise, the influence of noise originating inside the circuit, especially from the active elements needs to be considered. Such noise components influence the phase or frequency stability of the oscillators. Recently, the improvement of noise performance by controlling the oscillation frequency with a stable signal has been investigated¹⁴.

Past investigations of phase-locking phenomena, both theoretical and experimental, have dealt primarily with the stability of the locked state and with oscillator behaviour when operating near the synchronism range. There will be particular interest in the latter with regard to possible applications of injection locked oscillators. Furthermore, the available work needs to be extended by developing locking relations which are valid for higher relative power levels of locking signal.

1-4 Organization of Thesis

A brief description of static and dynamic characteristics of IMPATT diodes and of the theory of the Gunn diodes is presented in Appendix-A.

The most relevant mathematical relations used here are presented in Appendices B to F.

In Chapter II a review of the microwave IMPATT diode oscillator and of the Gunn diode oscillator is presented.

The fundamental locking equations for phase and amplitude of oscillator output are derived and solved in Chapter III, by using a "mismatched loading effect" point-of-view. Important relations among the various parameters of locked oscillators are obtained for later use.

In Chapter IV detailed experimental results for injection phase-locked IMPATT diode and Gunn diode oscillators are compared with the theoretically predicted values from Chapter III.

For system applications, FM amplification is already covered in the first four chapters. Chapter V treats phase modulation and sideband locking of bias modulated oscillators, while Chapter VI describes demodulation properties of injection phase-locked oscillators.

A summary of this work and its conclusions is given in Chapter VII.

1-4 Organization of Thesis

A brief description of static and dynamic characteristics of IMPATT diodes and of the theory of the Gunn diodes is presented in Appendix-A.

The most relevant mathematical relations used here are presented in Appendices B to F.

In Chapter II a review of the microwave IMPATT diode oscillator and of the Gunn diode oscillator is presented.

The fundamental locking equations for phase and amplitude of oscillator output are derived and solved in Chapter III, by using a "mismatched loading effect" point-of-view. Important relations among the various parameters of locked oscillators are obtained for later use.

In Chapter IV detailed experimental results for injection phase-locked IMPATT diode and Gunn diode oscillators are compared with the theoretically predicted values from Chapter III.

For system applications, FM amplification is already covered in the first four chapters. Chapter V treats phase modulation and sideband locking of bias modulated oscillators, while Chapter VI describes demodulation properties of injection phase-locked oscillators.

A summary of this work and its conclusions is given in Chapter VII.

CHAPTER II

MICROWAVE IMPATT DIODE OSCILLATORS AND GUNN DIODE OSCILLATORS - A REVIEW

Two important solid-state devices for generating microwave power are IMPATT (IMPact ionization and Avalanche Transit Time) diodes and Gunn diodes.

When a suitable p-n junction is biased into avalanche breakdown we obtain, under proper circuit conditions, a combined avalanche transit time effect which generates microwave energy. On the other hand, the Gunn diode is a bulk effect solid-state device; it does not consist of any p-n junction nor of any interfaces excepting ohmic contacts. The "Gunn effect" occurs in certain solid-state materials under conditions when a high electric field is applied; a differential negative conductance arises from an intervalley-transfer of charge carriers from a high mobility conduction band to a lower mobility higher energy band.

IMPATT diode and Gunn diode oscillators are well-suited for injection phase-locking applications.

In this chapter, we shall consider the microwave oscillations of an IMPATT diode and of a Gunn diode and some electrical characteristics of oscillators used in the course of this work will be discussed.

2-1 IMPATT Diode Oscillator Operation

Microwave energy may be extracted from almost any p-n junction if it is imbedded in a suitable rf circuit and reverse-biased into avalanche breakdown. This phenomenon was first predicted theoretically by Shockley¹⁶.

In 1958, Read¹⁷ proposed a high-frequency semiconductor diode consisting of an avalanche region at one end of a relatively high resistance region, serving as the drift space for the generated charge carriers (i.e. $p^+n_{in}^+$ or $n^+p_{ip}^+$ structures).

The first IMPATT operation¹⁸, reported by Johnston et al., however was obtained from a simple p-n junction. Read's work was followed closely by Lee et al.¹⁹ This indicated that, in addition to the particular doping profile proposed by Read, there are other classes of structure which also exhibit a negative resistance due to their IMPATT properties. From the small-signal theory developed by Misawa²⁰, it was confirmed that the negative conductance property of the IMPATT can be possessed by a junction diode with almost any doping profile.

From the small-signal point-of-view, when an RF voltage is applied to an IMPATT diode, an increase in differential current results. The current is retarded in phase with respect to the voltage applied by two effects: (1) carriers are generated by avalanche multiplication in a narrow avalanche region and injected into an adjacent drift region. The diode is biased so that the field in the avalanche region is high enough to cause breakdown during the positive half of the RF voltage cycle, but is below the critical field required for breakdown during the negative part of the voltage cycle. As a result, the carrier population builds up toward a new level with a delay time characteristic of the avalanche. In other words, the carrier current generated in the avalanche region increases during the positive half of the superimposed RF voltage cycle and decreases during the negative half. Therefore, the carrier current reaches its maximum value one quarter of a cycle after the voltage; i.e.,

the carrier current lags the voltage by 90° .

(2) the effect on the external terminals, i.e., the terminal current, is further delayed because of the transit time T_t during which the carriers are collected by the electrodes. During the entire RF cycle, the electric field in the drift region is kept high enough to cause the injected carriers to travel at limiting drift velocity. If the delay in the current is a quarter cycle by selecting an appropriate length of drift region, the in-phase component of the current becomes negative; that is, the external current lags the carrier current by 90° , and therefore the phase difference between the superimposed RF voltage and the fundamental Fourier component of the external current is 180° . In other words, the diode acts as a negative conductance, and in an appropriate circuit the device may therefore oscillate spontaneously.

Misawa²⁰ has considered the case of the "uniformly avalanching" diode in which impact ionization produces carriers at a uniform rate throughout the active region. Such a diode can be represented by a parallel connection of the depletion capacitance, a negative electronic conductance, and an electronic inductive susceptance. It is found that the electronic admittance is approximately proportional to the bias current, and the resonance frequency is proportional to the square root of the bias current. A similar expression has been obtained by Gilden and Hines²¹. (For more details see Appendix-A).

2-2 Gunn Diode Oscillator Operation

Gunn diodes exhibit electrical characteristics that are significantly different from the IMPATT devices.

In 1961, Ridley and Watkins²² suggested the possibility of obtaining bulk negative conductance in certain semiconductors by the transfer of electrons energized by high electric fields from high-mobility low energy bands to lower mobility higher energy bands. Detailed calculations by Hilsum²³ in 1962 showed that GaAs was a good candidate for exhibiting such a bulk negative conductance through these transferred electron effects. The first experimental evidence of this bulk negative resistance was achieved for GaAs by Gunn in 1963²⁴. He found that a relatively short sample would oscillate coherently at microwave frequencies if the bias was increased beyond an intensity of about 3 KV/cm. The frequency of oscillation was close to the reciprocal of the transit time of electrons through the sample.

An explanation of this observed phenomenon was advanced by Kroemer²⁵ in 1964, when he linked it with the Ridley-Watkins-Hilsum mechanism^{22,23}. The phenomenon of current oscillation was theoretically predicted by Ridley²⁶ for materials exhibiting voltage controlled differential negative conductance. It was found that spontaneous instability in a diode biased in the negative conductance region will give rise to the formation of a high field domain. This domain nucleates at some site of irregularity, grows and consumes more voltage until the rest of the diode becomes biased below threshold. At the same time the domain drifts along with the carrier stream towards the anode where it disappears, causing the nucleation mechanism to repeat itself, etc. The current circuit fluctuates with a frequency equal to the reciprocal of the transit time taken by the domain to traverse the interelectrode spacing.

McCumber and Chynoweth²⁷ theoretically investigated both current oscillation and microwave amplification. For the analysis, the energy

transport equation was numerically integrated for a GaAs device. The solution for the velocity-field characteristics of bulk GaAs was found to possess a region of differential negative conductance at electric fields higher than threshold.

The bulk negative conductance device can be made to oscillate in resonant circuits, the frequency of the oscillation being determined to a great extent by the circuit parameters.

Of the semiconducting materials having the electron transfer mechanism, n-type GaAs is the best understood and used for producing useful amounts of microwave power. In order for the electron-transfer mechanism to give rise to the negative-conductance effects, the material must satisfy the following conditions: (1) the lattice temperature must be low enough so that, in the absence of an applied electric field, most of the carriers are in the lower-conduction band, (2) in the lower-conduction band valley, the carriers must have small effective mass, which leads to high mobility and a low density of states, (3) in the subsidiary conduction-band valleys the carriers must have a large effective mass, and hence low mobility and a high density of states, (4) energy separation between valleys must be considerably less than that between the conduction and valence bands, so that the negative-conductance effect can be obtained at moderate electric fields, i.e., much lower than avalanche breakdown conditions. GaAs satisfies the above criteria and has exhibited many modes of operation³³ when biased above the critical field. (For more details see Appendix-A).

Various bulk modes of operation have been studied, depending on operating conditions and material parameters. These modes of operation are not fundamentally different from each other since all depend on the

mechanism of inter-valley carrier transport. We can determine a criterion for the formation of strong space-charge instabilities. From Kroemer's argument³⁴, an important boundary separating the various modes of operation in GaAs is the (carrier concentration)(sample length) product, $n_0 L = 10^{12} \text{cm}^{-2}$.

When the $n_0 L$ product is between 10^{11} and 10^{12}cm^{-2} , the sample can not support traveling dipole domains but can support growing space-charge waves, and can be operated as a stable small-signal amplifier. When the $n_0 L$ product is greater than 10^{12}cm^{-2} , the device is unstable because of the cyclic formation of either the accumulation layer or the high field domain. Samples with $n_0 L > 10^{12} \text{cm}^{-2}$ and connected to a constant voltage circuit are capable of supporting fully developed traveling dipole domains and operate in the Gunn, or transit-time mode of operation in which the frequency of oscillation is determined by the drift velocity of the carriers and the length of the sample. If a sample with $n_0 L > 10^{12} \text{cm}^{-2}$ is connected to a resonant circuit, three basic modes of operation are possible: the transit time domain mode, the quenched domain mode in which fully developed dipole domains are quenched before they reach the anode, and the inhibited domain mode in which the start of domain formation is delayed. Under the condition of very small doping fluctuations across the device or of a very small space charge accumulation, the electric field can effectively remain uniform across the device. The sample will then appear to the circuit as a true negative conductance whose mode is called the limited-space-charge-accumulation (LSA)³².

2-3 Noise Performance

A basic theory for the RF noise spectrum of oscillators was given by Edson³⁵ and Mullen³⁶. Noise affects the behaviour of oscillators in at least two ways. During sustained oscillation, noise creates unintended perturbations or modulation in both the amplitude and the phase of the output. Thus, an unintended change in frequency or phase will be described as FM or PM noise and an unintended change in amplitude will be described as AM noise.

Several workers^{37,38} have investigated the noise phenomena associated with a p-n junction under avalanche breakdown. According to their work, the noise in an IMPATT diode arises mainly from the statistical nature of the generation rates of electron-hole pairs in the avalanche region. Both the AM noise and the FM noise of IMPATT diode oscillators can be quite high³⁹, the noise output of germanium diode oscillators being significantly lower than that of silicon diode oscillators⁴⁰ for comparable doping profiles. From a noise analysis of IMPATT diode oscillators, it is found that the mean-square noise current varies inversely as the direct current density, and that a lower noise measure is obtained in a semiconductor possessing higher ionization coefficients.

The AM and FM noise in the output of typical Gunn diode oscillators⁴¹ is about 30 dB higher than that for a good reflex klystron when measured in a 70 Hz wide band spaced 1 KHz away from the carrier, but it falls off at a rate of about 9 dB per octave over the range 1 KHz to 100 KHz away from the carrier. Therefore, the Gunn diode oscillator can compete favourably against a reflex klystron. Hobson⁴² has developed

a theory that accounts for the FM noise in the output from a Gunn diode oscillator. He attributes it to jitter in the triggering times of the domains due to Johnson noise⁴³ in the nucleating region.

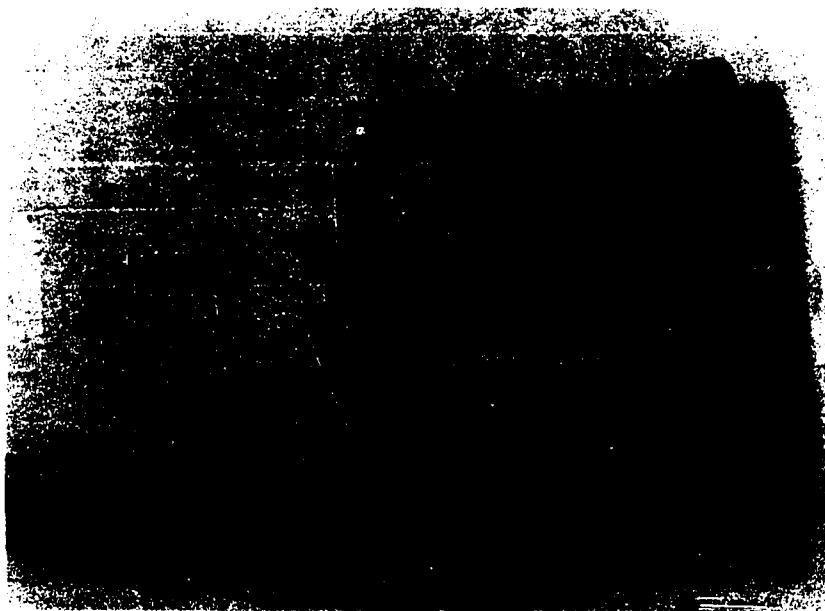
2-4 Description of Oscillators Tested

All the experimental work reported here has been conducted at X-band frequencies, using IMPATT diode oscillators containing Si epitaxial one-sided abrupt p-n junctions (Sylvania SYA-3200) and Gunn diode oscillators, employing GaAs epitaxial Gunn diodes (Mullard CL-8370). The standard pill-type package with two prongs is employed in both oscillators. The X-band oscillators tested are shown in Fig. 2.1.

(a) IMPATT diode oscillators

The IMPATT diode is mounted in a coaxial cavity as shown in Fig.2.2. The diode doping profile is shown in Fig.2.3. The oscillator cavity is slot-coupled to the end-wall of the WR-90 waveguide. The free-running oscillator frequency can be tuned mechanically by changing the end-loading capacitance of the cavity by means of a screw. Electronic frequency tuning is obtained by varying the bias current.

Fig.2.4 shows the basic characteristics of a typical IMPATT diode oscillator. This oscillator gives a power output of 24 mW at 9.79 GHz when operated at 20.5 mA. With this oscillator, it can be seen that the oscillation frequency increases by 40 MHz as the bias current is raised from the oscillation threshold to 23 mA at a fixed mechanical tuning point. The slope of the oscillation frequency versus bias current curve is about +3 MHz/mA.

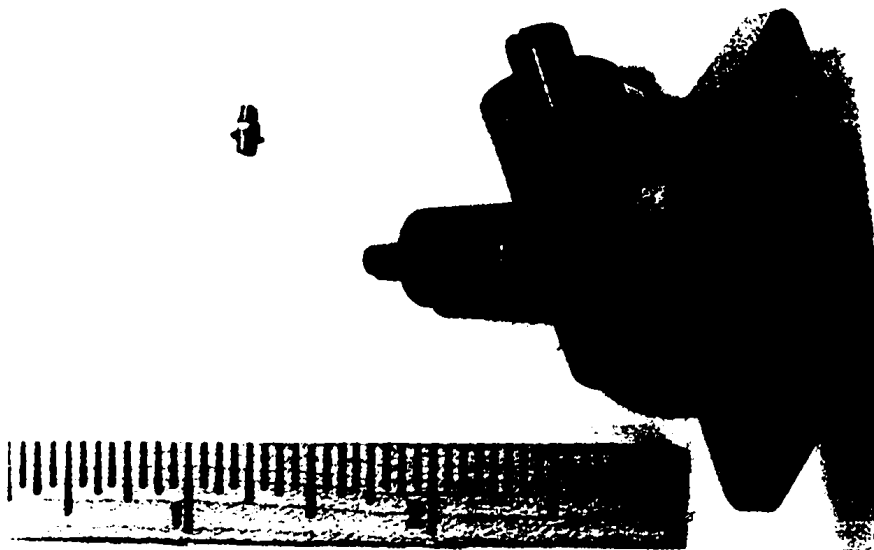


(a) SYA-3200 IMPATT DIODE OSCILLATOR

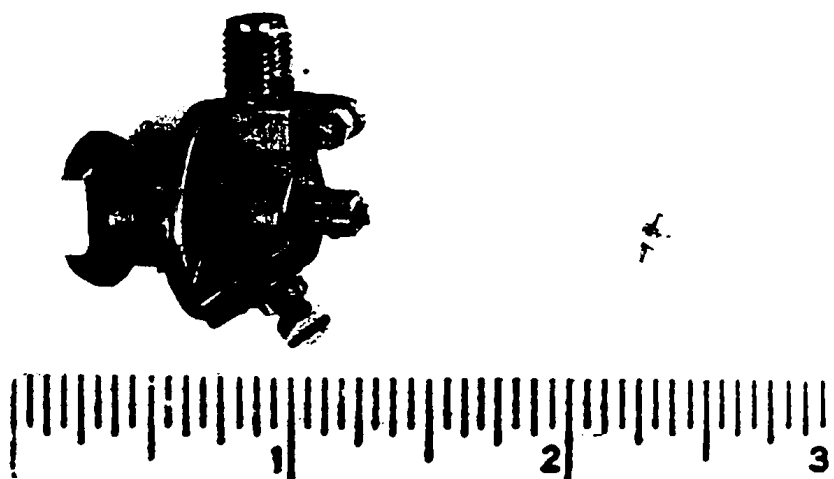


(b) CL-8370 GUNN DIODE OSCILLATOR

Fig.2-1 X-BAND OSCILLATORS TESTED



(a) SYA-3200 IMPATT DIODE OSCILLATOR



(b) CL-8370 GUNN DIODE OSCILLATOR

Fig.2-1 X-BAND OSCILLATORS TESTED

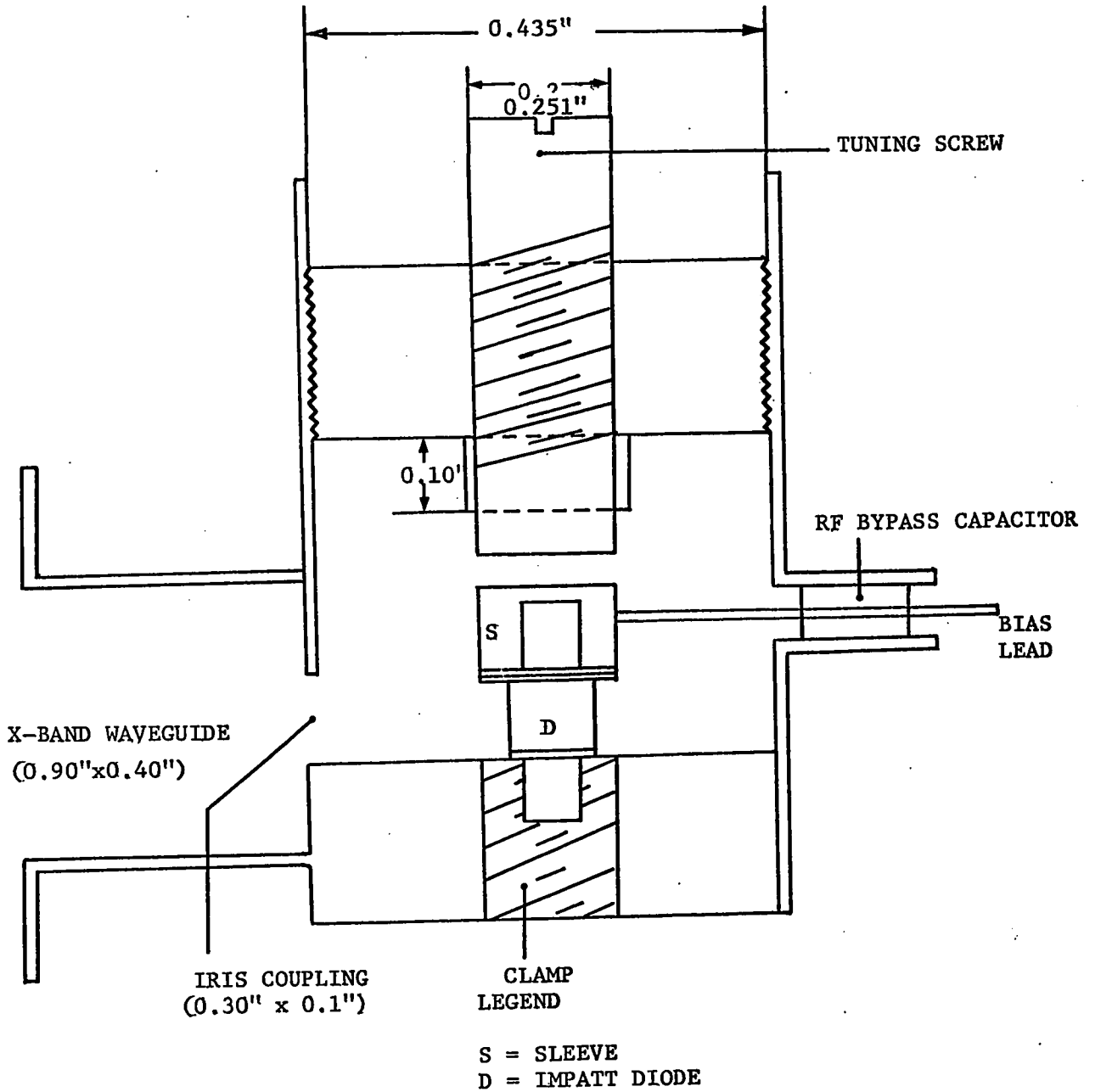


Fig.2-2 CROSS-SECTIONAL VIEW OF SYA-3200 IMPATT DIODE OSCILLATOR

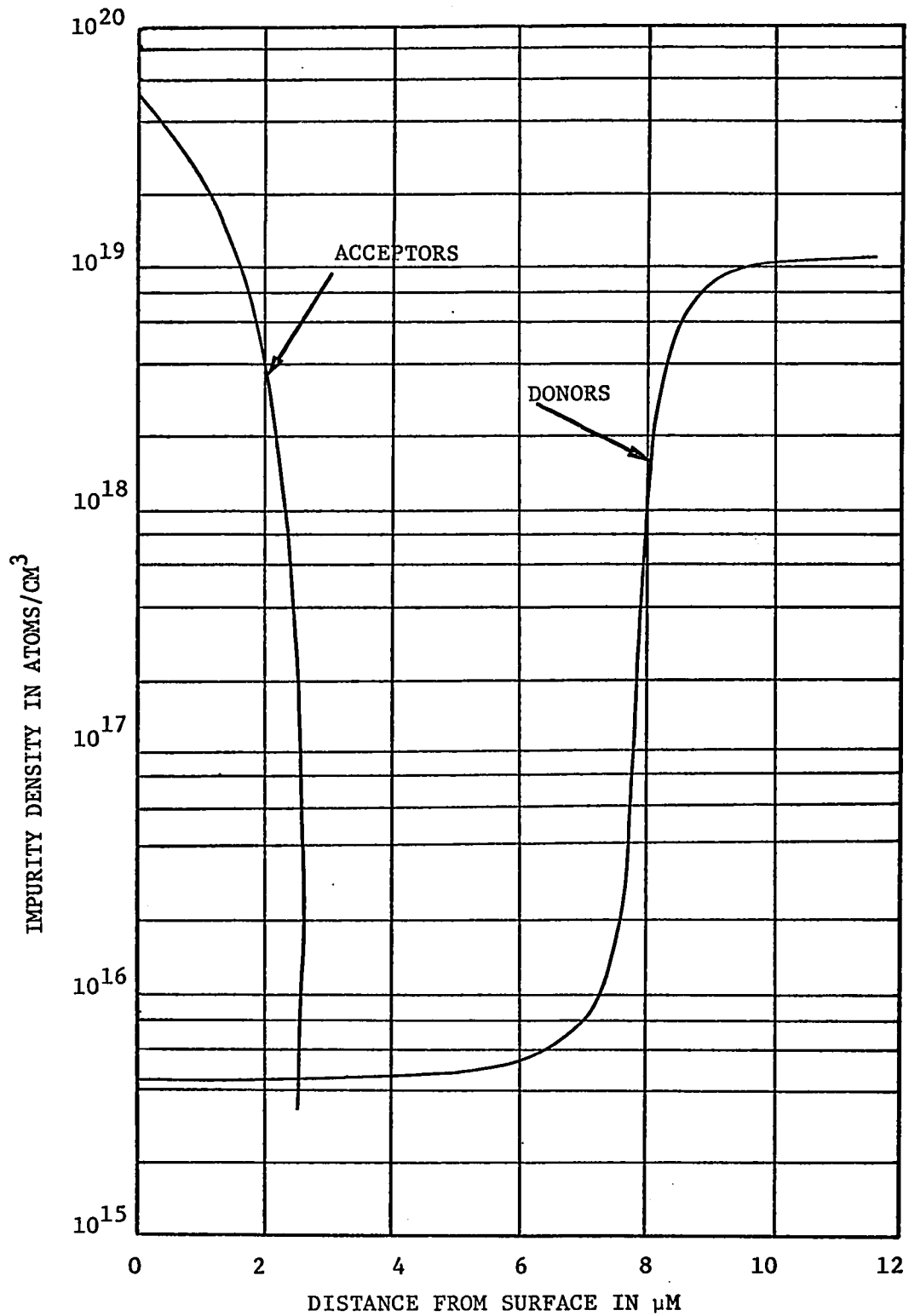


Fig.2-3 IMPURITY CONCENTRATION PROFILE OF Si IMPATT DIODE

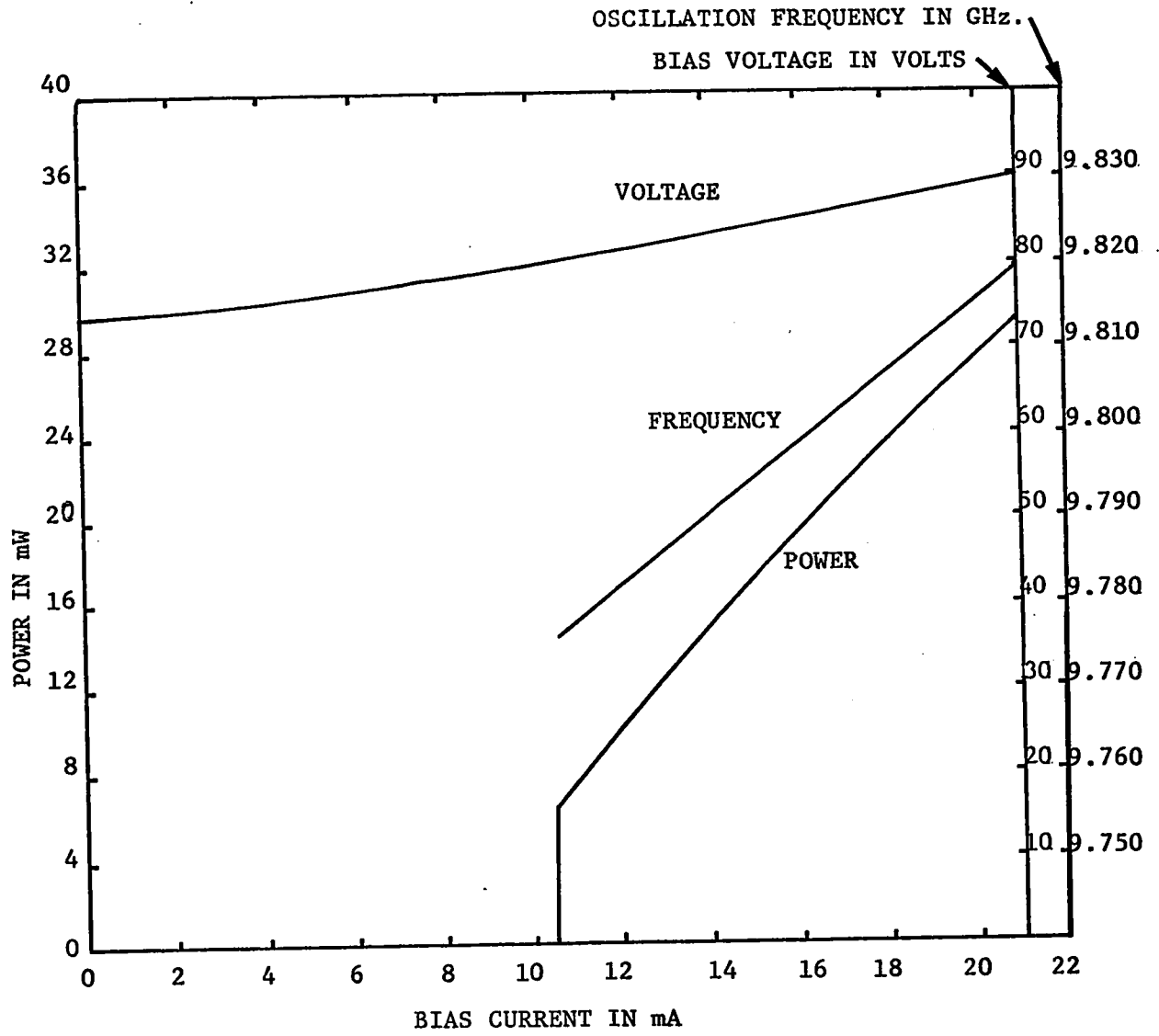


Fig.2-4 BASIC CHARACTERISTICS OF A TYPICAL IMPATT DIODE OSCILLATOR
(SYA -3200-3)

(b) Gunn Diode Oscillators tested

The Gunn diode was mounted in a coaxial cavity, shorted at the middle of the outer conductor which is divided into two discs and isolated from each other by a thin teflon sheet to form an RF by-pass capacitor, as shown in Fig.2.5. The bias was applied to the Gunn diode through this by-pass capacitor. An O.S.M. coaxial output connector is used and coupled to the cavity by means of a capacitive probe. Mechanical frequency tuning is accomplished by means of a tuning screw whose length can be varied in the cavity, and electronic tuning is obtained by directly varying the bias voltage.

Fig.2.6 shows the basic characteristics of the oscillator. This oscillator gives a power output of 6.2 mW at 9.22 GHz when operated at 7 volts. With this oscillator it can be seen that the oscillation frequency decreased by 20.7 MHz as the bias voltage across it is raised from the oscillation threshold to 5.2 volts, that is, the slope of the oscillation frequency versus bias voltage curve is negative. It is seen from the experimental results the frequency decreased with voltage by about 7.4 MHz/volt. The frequency shift observed is the resultant of the two effects, namely the true shift due to the voltage change and an effect due to the temperature change which follows a change in input power. The dependence of power output on voltage was very complex, since mode jumping often occurred as the bias voltage was increased. It should be stressed that no adjustments were made to the cavity during this experiment. Optimizing the cavity setting at each different bias voltage results in appreciably more microwave power.

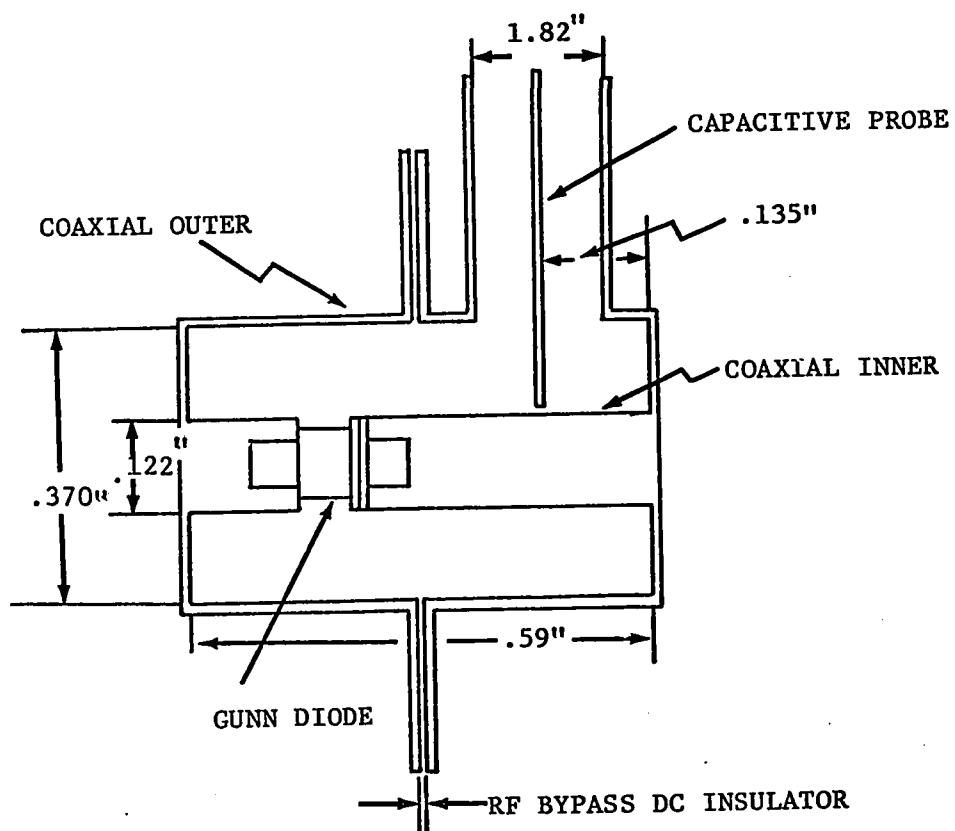


Fig.2-5 A CROSS-SECTIONAL VIEW OF CL-8370 GUNN DIODE OSCILLATOR

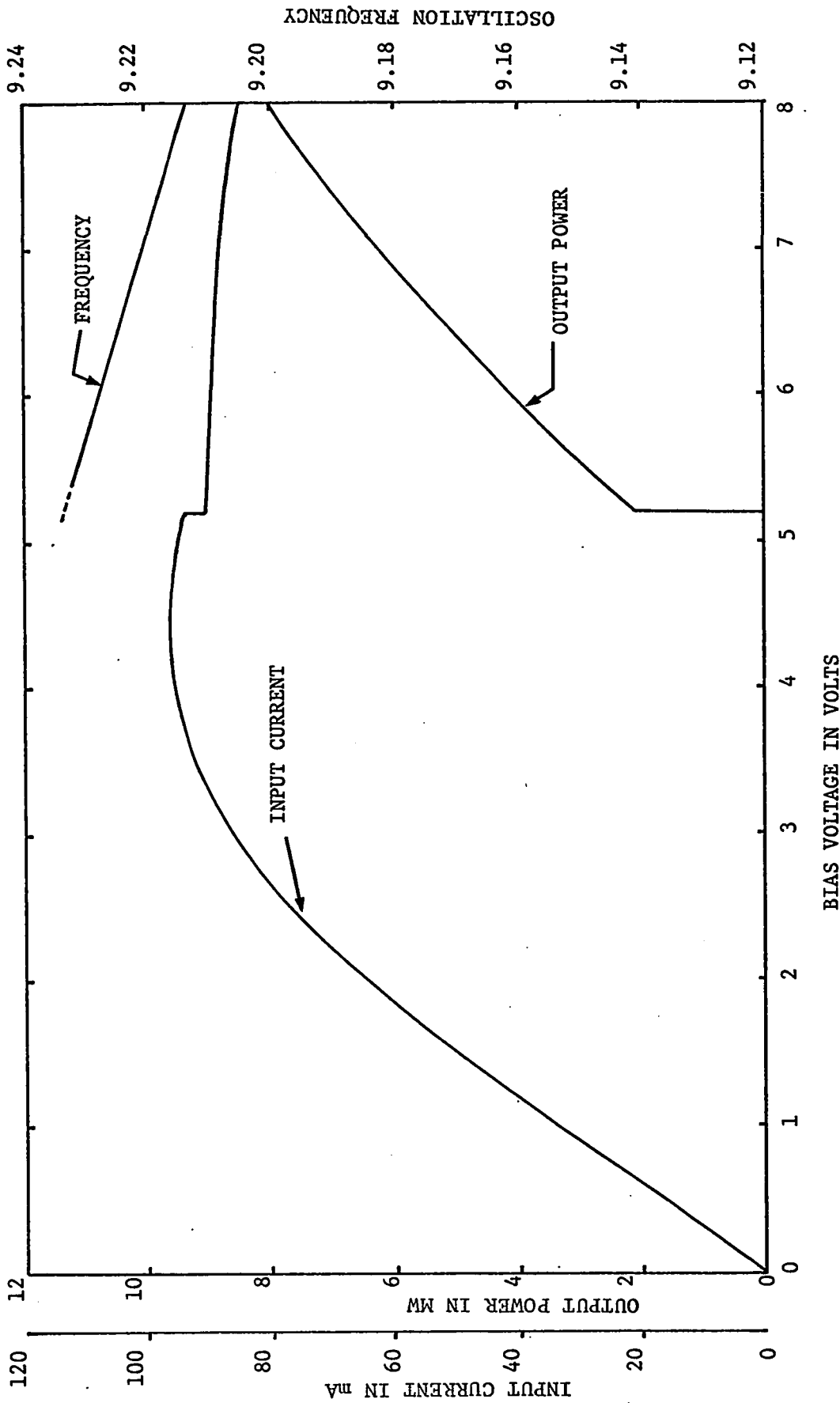


Fig.2-6 CHARACTERISTICS OF A TYPICAL GUNN DIODE OSCILLATOR (CL-8370-2)

It appears from these experiments that the IMPATT diode and Gunn diode oscillators may operate in modes where bias condition changes alter either the frequency or amplitude of the oscillations separately, or both together.

CHAPTER III

THEORETICAL ANALYSIS OF INJECTION PHASE-LOCKED OSCILLATORS

In this chapter, the injection phase-locking relations which will be required are presented. Previous work describing phase-locking phenomena is reviewed briefly, and then, by considering the loading effect of the locking signal on the microwave oscillator to be locked, the locking properties will be analyzed.

3-1 Introduction3-1-1 Adler's Method

Adler⁵ investigated locking phenomena in oscillators based on the model in Fig.3.1a for lower frequency oscillators of the lumped constant circuit type. He has given a derivation of the locking equation which gives a good physical picture of the phenomena.

The oscillator circuit consists of a negative conductance, $-G(e)$ and a resonant circuit G_r, L_r, C_r . The output voltage is e and the input locking signal current is $i_s(t)$. For a free-running oscillator, $i_s(t) = 0$, the oscillator output is assumed to be sinusoidal when operating in a steady state with output voltage e . Power is dissipated in the conductance G_r , and the voltage across the nonlinear negative conductance $-G(e)$ causes a current $i(e)$ to be returned to the circuit from the negative conductance that is just sufficient to maintain the constant amplitude of E .

The total current of the resonant circuit is the vector sum of the injected current i_s and the current i returned from the negative conductance due to the voltage e across it, as shown in Fig.3.1b. In the analysis, the following assumptions were made.

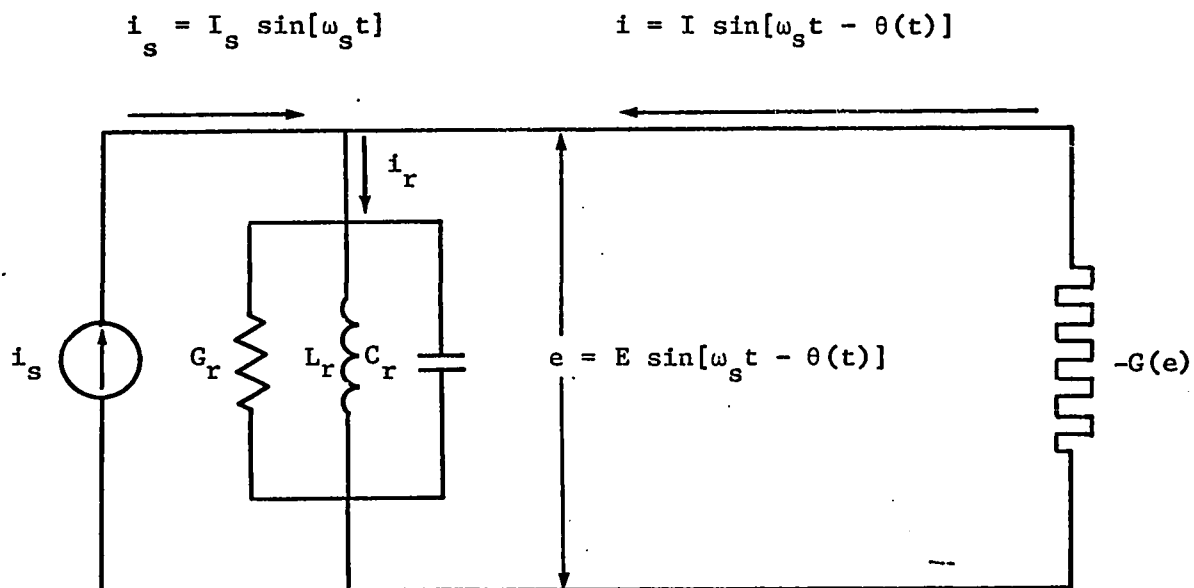


Fig.3-1a A NEGATIVE CONDUCTANCE OSCILLATOR MODEL.

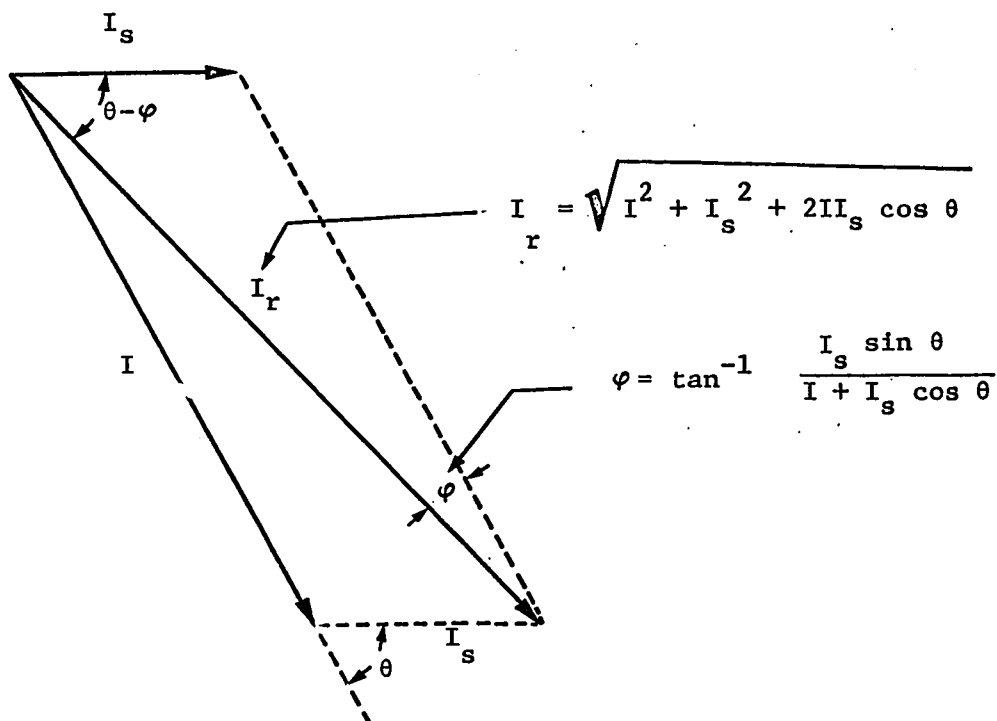


Fig.3-1b CURRENT VECTOR DIAGRAM OF Fig.3-1a.

- 1) The locking frequency is near the middle of the passband of the tuned circuit.
- 2) The time constant of the amplitude regulation process must be much shorter than the time constant of the passive circuit.
- 3) The locking signal must be much smaller than the output signal.

Let the input locking signal have the form:

$$i_s = I_s \sin \omega_s t \quad (3.1)$$

and let the output current, returned from the negative conductance due to the voltage across it, be of the form:

$$i = I \sin [\omega_s t - \theta(t)]. \quad (3.2)$$

Then, the magnitude of the total current is

$$I_r = \sqrt{I^2 + I_s^2 + 2II_s \cos \theta} \quad (3.3)$$

and the phase angle between two currents is

$$\varphi = \tan^{-1} \frac{I_s \sin \theta}{I + I_s \cos \theta}. \quad (3.4)$$

Consequently, the total current in the resonant circuit can be written as:

$$i_r = \sqrt{I^2 + I_s^2 + 2II_s \cos \theta} \cdot \sin(\omega_s t - \theta + \tan^{-1} \frac{I_s \sin \theta}{I + I_s \cos \theta}). \quad (3.5)$$

By assuming that $I_s \ll I$, the tuned circuit current i_L is nearly sinusoidal and is related to the voltage across it. The limiting action of the nonlinear conductance maintains the voltage of a constant.

Let us consider the condition when the oscillator is operating normally at a frequency determined by the tuned circuit. The current of

i must be in phase with the current of i_r for oscillation to be maintained at the resonant frequency of the tuned circuit. Oscillation at any other frequencies is prohibited by a phase shift introduced by the tuned circuit.

When a locking signal of slightly different frequency is applied to the oscillator, the current i combines with i_s producing i_r . A phase shift θ between the locking and oscillator signals is required to maintain oscillation at the locking signal. The necessary phase θ is introduced by the tuned circuit.

From Fig.3.1a, an approximate expression of the phase shift produced by the single-tuned passive circuit for a frequency ω is given by

$$\varphi = \tan^{-1} \frac{2Q(\omega - \omega_o)}{\omega_o} \quad (3.6)$$

where $Q = \frac{\omega_o C}{G_r}$ (the loaded Q) and $\omega_o = \frac{1}{\sqrt{L_r C_r}}$ (the resonance frequency of the tuned circuit).

The instantaneous frequency of the oscillator output is the time derivative of the instantaneous phase angle of $(\omega_s t - \theta)$ in Eq.3.2:

$$\omega = \omega_s - \frac{d\theta}{dt} \quad (3.7)$$

Equating Eq. 3.4 to 3.6, and using Eq. 3.7, we get

$$\frac{d\theta}{dt} + \frac{\omega_o}{2Q} \frac{I_s}{I} \frac{\sin\theta}{I + I_s/I \cos\theta} = \omega_s - \omega_o \quad (3.8)$$

Under the condition that $I_s \ll I$, the oscillator output current is equal to the free-running oscillator current. Then a more approximate locking equation, referred to as Adler's equation, is given by

$$\frac{d\theta}{dt} + \frac{\omega_o}{2Q} \frac{I_s}{I} \sin\theta = \omega_s - \omega_o \quad (3.9)$$

Adler's work verified previously obtained experimental results on low-frequency phase locked oscillators.

Mackey¹⁰ showed that Eq. 3.9 accurately described injection locking phenomena in reflex klystron oscillators.

3-1-2 Second-Order Nonlinear Differential Equation Method

Let us consider the second-order nonlinear differential equation method. The approach here is to derive the locking equation directly from the current equation of the oscillator circuit of Fig.3.1a:

$$C_r \frac{de}{dt} + G_r e + \frac{1}{L_r} \int e dt - i - i_s = 0. \quad (3.10)$$

Introducing $i_s = I_s \sin \omega_s t$ into the above equation, and taking the time derivative, we obtain

$$\frac{d^2 e}{dt^2} - 2\delta(e) \frac{de}{dt} + \omega_o^2 e = \frac{I_s}{I} \cos \omega_s t \quad (3.11)$$

where $\omega_o = \frac{1}{\sqrt{L_r C_r}}$, the natural frequency, and

$$\delta(e) = [G(e) - G_r] / 2C_r.$$

In order to obtain an approximate solution to this differential equation, a solution of the following form is considered:

$$e = E(t) \sin[\omega_s t - \theta(t)] \quad (3.12)$$

The amplitude $E(t)$ and the phase angle $\theta(t)$ are assumed to be slowly varying functions of time which do not change appreciably over one rf cycle. Let us further apply the Adler's assumptions. Then, under the above conditions, two first-order differential equations describing $E(t)$ and $\theta(t)$ can be derived from Eq. 3.12, as follows:

$$\frac{dE}{dt} = -\frac{E}{2} \delta[E \sin(\omega_s t - \theta)] + \frac{I_s}{2C_r} \cos\theta \quad (3.13)$$

$$\frac{d\theta}{dt} = -\frac{I_s}{2C_r E} \sin\theta + (\omega_s - \omega_o) \quad (3.14)$$

The two first-order differential equations are commonly known as the "shortened equations".⁹ At the oscillation frequency $E = I/G_r$, and by noting that $Q = \omega_o C_r / G_r$, Eq. 3.14 can be written

$$\frac{d\theta}{dt} + \frac{\omega_o}{2Q} \frac{I_s}{I} \sin\theta = \omega_s - \omega_o \quad (3.15)$$

which is identical to Adler's equation (Eq. 3.10).

In addition, it can be shown that the locking properties of the phase-locked loop are also described by the same differential equation. Recognition of this similarity ties together the extensive literature on each of these locking techniques and will generate many new applications.

If a more complex passive circuit were considered for the oscillator, the derivation of the differential equation could be considerably more difficult than the simple examples given here. Moreover, since the concept of an incident wave and a reflected wave is more convenient than that of voltage and current at microwave frequencies, the application of a "loading effect" on the power wave is desirable.

3-2 Loading Effect Method

3-2-1 Equivalent Circuit of Locked Oscillators

Under fixed dc bias conditions, the frequency and output power

of a microwave oscillator are uniquely specified by the load presented to the diode.

Further, if the output frequency is to be modified by the application of an external signal, its effect must be to change the reflection coefficient. The purpose of the following analysis is to determine the variations of this coefficient as a function of magnitude, frequency, and phase of the externally applied signal. These variations of the reflection coefficient with the locking power will be used to describe the locked operation of the oscillator.

Consider a microwave oscillator operating into a matched load. Its output power and frequency are specified by this particular load at which the reflection coefficient is zero. Suppose now, that a signal of frequency ω_s is introduced into the oscillator output line. If the signal is of sufficient amplitude, and ω_s is not greatly different from the initial matched-load frequency ω_o , the oscillator will change its frequency to ω_s . At this new frequency of oscillation, its power output and r-f conditions will have changed. Its d-c bias current will, however, remain the same, since it is determined by the d-c power supply. As ω_s is changed, the operating frequency of the oscillator will track this change, until the frequency separation becomes too large, at which time the oscillator loses synchronism. We are concerned here with the change of operating conditions as the oscillator tracks the locking signal frequency.

Consider the circuit shown in Fig.3.2. O_l represents the oscillator to be locked by a signal supplied from the "ideal" injection source O_s . The characteristics of this ideal source are: (1) the

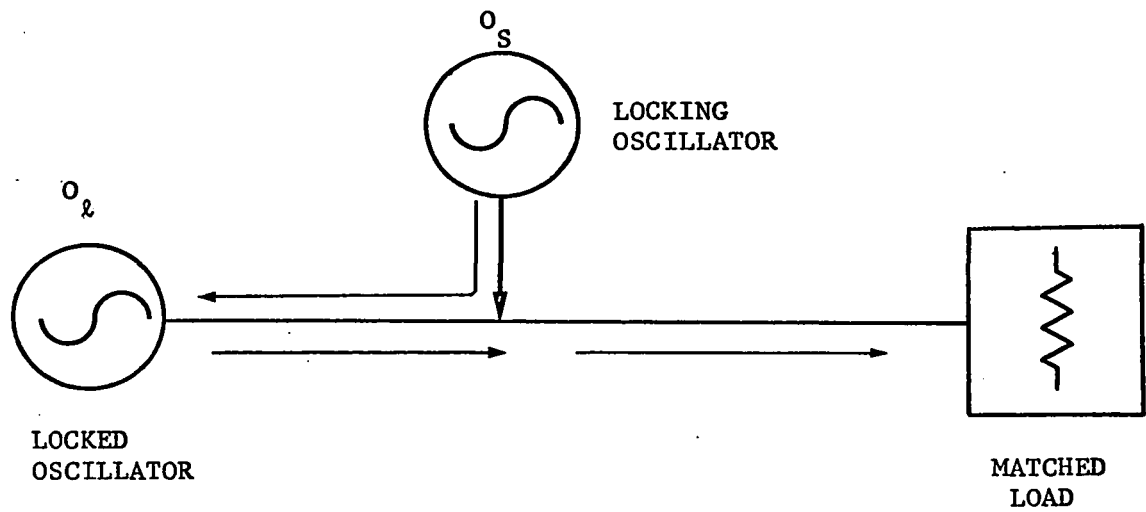


Fig.3-2 HYPOTHETICAL CIRCUIT FOR LOCKING OF O_l BY IDEAL SOURCE O_s

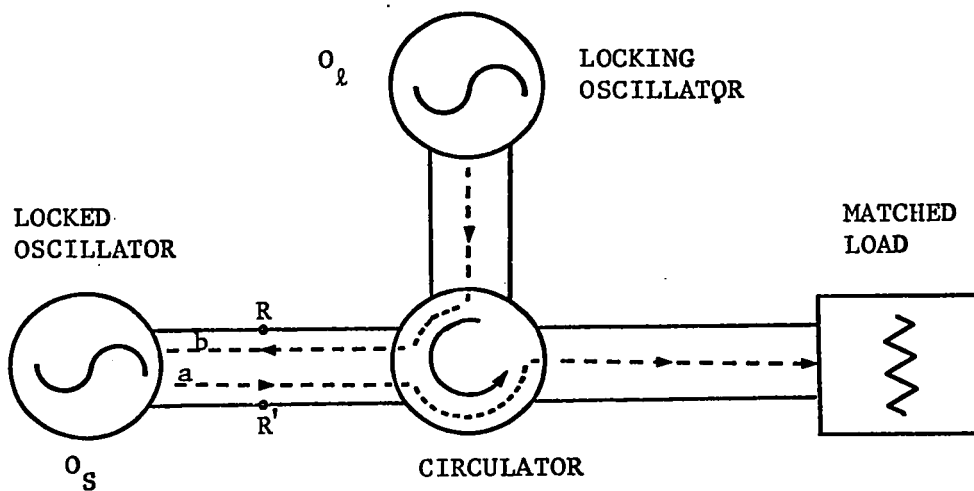


Fig.3-3 OSCILLATOR-CIRCULATOR COMBINATION FOR LOCKING OF O_l BY O_s

locking signal propagates only toward the oscillator to be locked;

(2) the oscillator output is isolated from the locking signal input;

(3) the amplitude, phase, and frequency of the injection signal may be varied independently, and are all independent of the operation of the locked oscillator. A circuit for this ideal injection case may be approximated in practice by using a well-matched circulator at microwave frequencies. The combination of a one-port oscillator and a circulator, as shown in Fig.3.3, makes possible the isolation of the oscillator output from the locking signal output.

The injection phase-locking properties of the microwave oscillator can be determined qualitatively by using the concepts of a "normalized phase locking wave", b , and a "normalized output wave", α , which are convenient scalar complex quantities whose magnitudes are, respectively, proportional to the locking and output transverse E-field magnitudes and whose phases are those of the locking and output E-fields.

The normalization basis is taken so that $bb^* = |b|^2$ is equal to the power flow into the oscillator whereas $\alpha\alpha^* = |\alpha|^2$ represents the power flow out of the oscillator.

The locking power is considered to be a reflected power due to an equivalent mismatched load at the reference plane RR' ; the plane of detuned short. The output power of the oscillator is the power incident towards this load. Since the reflection coefficient is defined as the ratio of the reflected transverse electric intensity to the incident transverse electric intensity, the reflection coefficient seen looking towards the matched circulator at the reference plane RR' is the ratio of the locking transverse electric intensity to the output transverse electric intensity:

$$\Gamma = \frac{b}{a} e^{j\theta} = \sqrt{\frac{P_s}{P_i}} e^{j\theta} \quad (3.16)$$

where P_s = locking power,

P_i = oscillator output power, and

θ = phase angle between the external signal and the oscillator output.

Whenever the locking signal is applied, the reflection coefficient has a value greater than zero. This change of reflection coefficient reveals the mechanism of oscillator locking; when locking to an external signal, the oscillator assumes a phase and power output for which the resulting reflection coefficient as given by Eq. 3.16 specifies the frequency ω_s . As ω_s is changed, therefore, the reflection coefficient varies in a manner determined by the load characteristic of the oscillator.

Therefore, the effect of the locking signal can be interpreted as a change in the load admittance presented by the locked oscillator. This change causes a frequency shift. Consequently, the behaviour of the oscillator under locked condition may be analyzed in terms of this loading effect.

The analysis of properties of the injection phase-locked oscillator is substantially simplified by incorporating in the equivalent circuit of the oscillator a nonlinear electronic admittance. Fig.3.4 shows a simplified equivalent circuit of a locked oscillator, in the form of a parallel tuned circuit. Although a microwave resonator is not a simple resonant circuit, in the vicinity of a resonant frequency it can ordinarily be represented by a parallel combination of constant lumped inductance, capacitance, and conductance having admittance $G_t + jB_t$.

The active device admittance is represented by $-G_e + jB_e$, and the load admittance due to the locking signal by Y_1 . The electronic conductance G_e and susceptance B_e are functions of the rf voltage and the d-c parameters associated with the oscillator:

$$\begin{aligned} G_e &= F_1 (V_{rf}, V_{dc}) \\ B_e &= F_2 (V_{rf}, V_{dc}). \end{aligned} \quad (3.17)$$

The explicit form of Eqs. 3.17 is determined by the dynamics of the electric discharge, and the derivation of these equations is, in general extremely difficult. An ideal transformer⁴⁴, having an n:1 turns ratio, is taken to couple the diode to a transmission line of characteristic admittance Y_0 . At the reference plane R-R' the electronic admittance and tuned circuit admittance are transformed to the transmission line in the forms of a conductance \bar{G} and a susceptance \bar{B} which consists of an inductance \bar{L} and a capacitance \bar{C} . It is desirable to introduce the equivalent circuit of Fig.3.5 since all measurements are taken along the transmission line between the oscillator output port and the circulator.

Relationships among those various parameters are, respectively, at the reference plane RR'

$$\begin{aligned} \bar{G} &= (-G_e + G_t) \\ \bar{C}\omega - \frac{1}{\bar{L}\omega} &= \frac{1}{n^2} (B_e + B_t) \end{aligned} \quad (3.18)$$

where ω is the oscillation frequency.

The normalized admittance of the circuit Fig 3.5 is

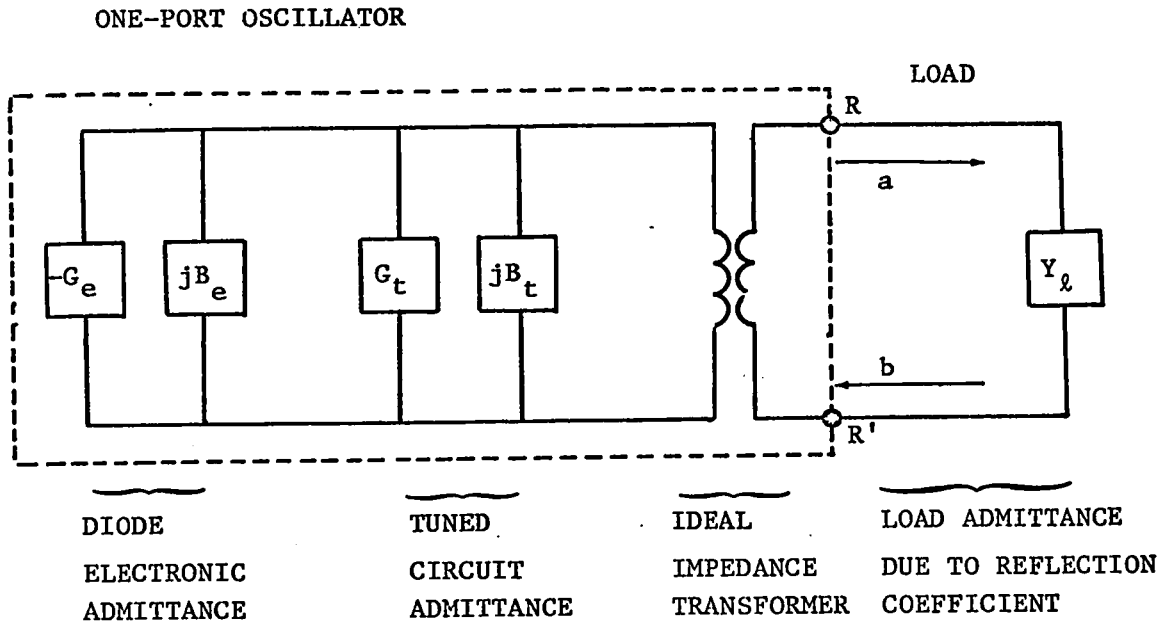


Fig.3-4 EQUIVALENT CIRCUIT OF A LOCKED OSCILLATOR.

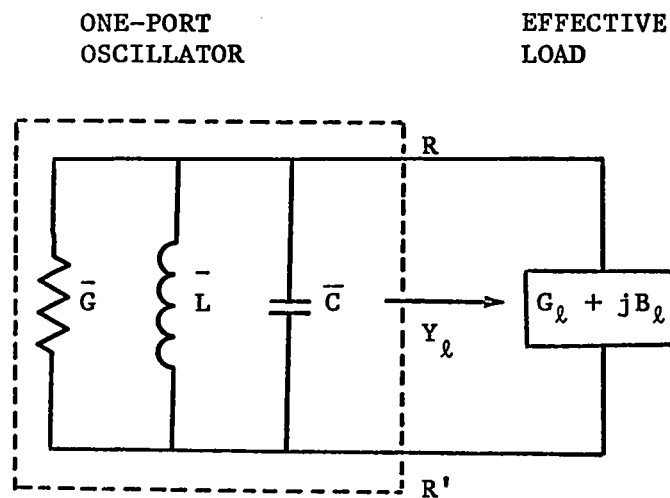


Fig.3-5 A SIMPLIFIED EQUIVALENT CIRCUIT OF A LOCKED OSCILLATOR.

$$\bar{y} = \frac{1}{Y_0} [G + j(\bar{C}\omega - \frac{1}{\bar{L}\omega})] = \bar{g} + j \bar{b}. \quad (3.19)$$

Assuming \bar{G} , \bar{C} , and \bar{L} are frequency-independent, a plot of \bar{y} on the admittance plane is a straight line which intersects the real axis at the resonant frequency ω_0 such that

$$C\omega_0 - \frac{1}{L\omega_0} = 0$$

or

$$\omega_0 = \frac{1}{\sqrt{LC}}. \quad (3.20)$$

In terms of ω_0 , the normalized susceptance \bar{b} becomes

$$b = Q_{\text{ext}} \left(\frac{\omega}{\omega_0} - \frac{\omega_0}{\omega} \right) \quad (3.21)$$

where $Q_{\text{ext}} = \frac{\omega_0 \bar{C}}{Y_0}$; the external Q of the oscillator.

In the vicinity of ω_0 , we thus can write the approximate expression;

$$\bar{b} = Q_{\text{ext}} \frac{2\Delta\omega}{\omega_0} \quad (3.22)$$

where $\omega = \omega_0 + \Delta\omega$.

Thus, in the neighbourhood of ω_0 , susceptance is a linear function of frequency.

As discussed in Eq. 3.16, since the reflection coefficient is greater than zero when a locking signal is applied, the equivalent load

seen by the oscillator is under these conditions no longer a matched load. Let the resultant load admittance

$$Y_{\ell} = G_{\ell} + j B_{\ell} .$$

The equivalent circuit then becomes that of Fig. 3.4, in which the effective load admittance Y_{ℓ} is dependent on locking power and frequency.

Finally, under steady-state conditions, we can write a relation between the oscillator circuit and the load as follows:

$$\bar{g} + j \bar{b} + g_{\ell} + j b_{\ell} = 0. \quad (3.23)$$

Eq.3.23 expressed the operational dependence of the oscillator upon the load. When the d-c conditions are fixed, then Eq. 3.23 defines the operation of the oscillator into a particular load admittance.

3-2-2 Effective Load Admittance due to a Locking Signal

Let us now analyze the effect of the locking signal on the equivalent load in detail. As shown in Fig.3.5, the effective load admittance seen looking toward the circulator at the reference plane RR' is given by

$$Y_{\ell} = G_{\ell} + jB_{\ell} = Y_0 \left(\frac{1 - \Gamma}{1 + \Gamma} \right) \quad (3.24)$$

Substituting Eq. 3.16 into Eq. 3.24, we obtain the effective load susceptance due to the power waves. Normalizing these with respect to the characteristic admittance Y_0 , we get

$$g_{\ell} = \frac{G_{\ell}}{Y_0} = \frac{1 - |\Gamma|^2}{1 + |\Gamma|^2 + 2|\Gamma|\cos\theta} \quad (3.25)$$

$$b_{\ell} = \frac{B_{\ell}}{Y_0} = \frac{-2|\Gamma|\sin\theta}{1 + |\Gamma|^2 + 2|\Gamma|\cos\theta} \quad (3.26)$$

where g_{ℓ} is the "effective normalized load conductance", and b_{ℓ} is the "effective normalized load susceptance". We may now substitute these expressions into Eq. 3.23 and write it in two parts, the real and imaginary parts of the equation, obtaining

$$-\bar{g} = \frac{1 - |\Gamma|^2}{1 + |\Gamma|^2 + 2|\Gamma|\cos\theta} \quad (3.27)$$

$$\bar{b} = \frac{2|\Gamma|\sin\theta}{1 + |\Gamma|^2 + 2|\Gamma|\cos\theta} \quad (3.28)$$

Let us consider the case where the oscillator is locked to the incoming signal, so that θ is a constant independent of time. In this case Eq. 3.28, when solved for frequency, indicates a frequency differing from the value which we should have without the locking signal by the amount $\left(\frac{2|\Gamma|\sin\theta}{1 + |\Gamma|^2 + 2|\Gamma|\cos\theta}\right)$. That is, using Eq. 3.21, we have

$$\frac{2|\Gamma|\sin\theta}{1 + |\Gamma|^2 + 2|\Gamma|\cos\theta} = Q_{\text{ext}} \left(\frac{\omega}{\omega_0} - \frac{\omega_0}{\omega} \right) \quad (3.29)$$

where ω_0 is the frequency at which the oscillator would operate in the absence of an external signal. But if θ is to be a constant, this means that the frequency ω of operation must be the same as the frequency ω_s of the external signal. In other words, Eq. 3.29 determines $\sin\theta$, or the phase angle between oscillator output and locking signal, in terms of the initial frequency difference $(\omega_s - \omega_0)$ between the locking signal

and the free-running frequency of the oscillator output, and $|\Gamma|$, the relative amplitude of the signal. We may differentiate Eq. 3.26 with respect to θ and solve for a maximum value of \bar{b}_ℓ . This occurs when

$$\cos\theta = -\frac{2|\Gamma|}{1+|\Gamma|^2}.$$

Substituting this into Eq. 3.26 we obtain

$$|b_\ell|_{\max} = \frac{2|\Gamma|}{1-|\Gamma|^2}. \quad (3.30)$$

This maximum value of b_ℓ fixes a maximum value for the frequency difference between the locking signal and the free-running frequency, beyond which locking cannot occur.

Eq. 3.26 can be plotted as a function of magnitude of the reflection coefficient, as shown in Fig.3.6. For $|\Gamma| \ll 1$, susceptance is approximately proportional to the magnitude of the reflection coefficient. In other words, locking range here increases linearly with the magnitude of the locking voltage wave in accordance with Eq. 3.22. When $|\Gamma|$ is close to unity, effective load susceptance is no longer proportional to $|\Gamma|$. Therefore the linear approximation is limited to the low locking power level case, in which the load susceptance has the maximum value of $2|\Gamma|$ when $\theta = 90^\circ$. This fixes a locking range under locked conditions.

The injection phase-locking behaviour can thus be simulated by an effective variable susceptance which is a finite positive or negative susceptance added in parallel to the equivalent circuit of the locked one-port oscillator, which dynamically counteracts any phase shift of the locked oscillator and the locking signals under locked conditions. This

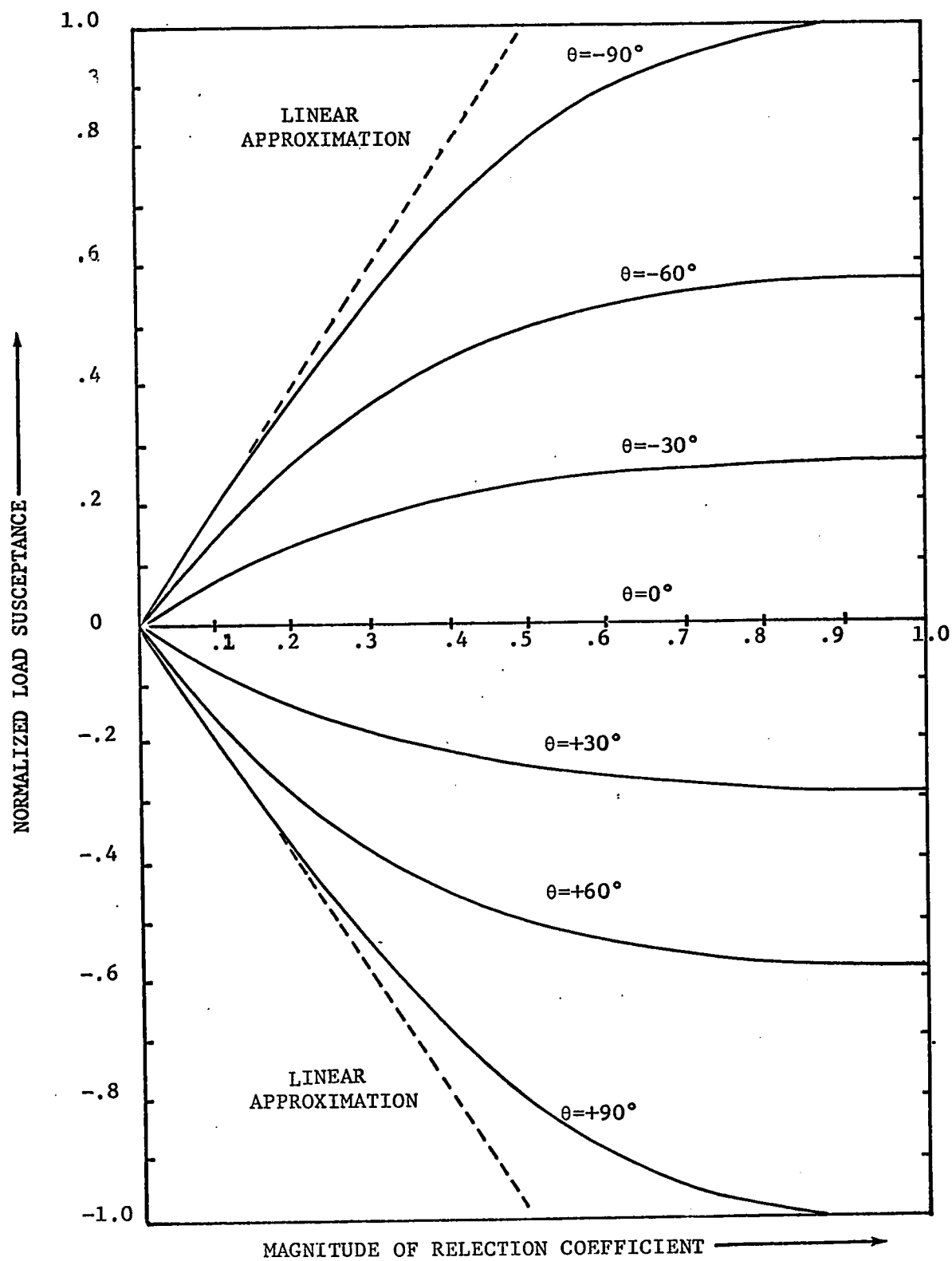


Fig.3-6 EFFECTIVE SUSCEPTANCE VERSUS $|\Gamma|$

susceptance is the physical means by which the phase of the oscillator converges towards that of the impressed signal.

Let us consider next the normalized load conductance variation with reflection coefficient. Eq. 3.25 shows that the effective conductance decreases monotonically from 1 to zero (open circuit) as $|\Gamma|$ increases from zero to unity for all values of θ within the locking range as illustrated in Fig.3.7.

In order to determine the effect of the locking signal on the load conductance, let the matched load be the reference. Then a "supplementary" conductance can be defined as

$$g' = g_{\ell} - 1 \quad \text{or} \quad G' = G_{\ell} - Y_0 \quad (3.31)$$

By substituting Eq. 3.31 into Eq. 3.27 we obtain

$$g' = \frac{-2(|\Gamma|^2 + |\Gamma|\cos\theta)}{1 + |\Gamma|^2 + 2|\Gamma|\cos\theta} \quad (3.32)$$

Consequently, the resulting value of θ in Eq. 3.32 leads to a conductance contribution of the locking signal to the load, when θ is determined from Eq. 3.29, which will result in a modified rf voltage and power. Since the sign of g' is negative the locking signal acts like a negative conductance, i.e. the negative sign represents a power flow from the locking signal into the oscillator. This term is a maximum when $\omega_s = \omega_o$ and approaches zero when $\omega_s - \omega_o$ is at its extreme limit.

Fig.3.7 shows how the supplementary conductance varies with reflection coefficient. When $|\Gamma| \ll 1$, g' is approximately zero, or g_{ℓ} is unity. That is, the oscillator sees an almost matched load, which

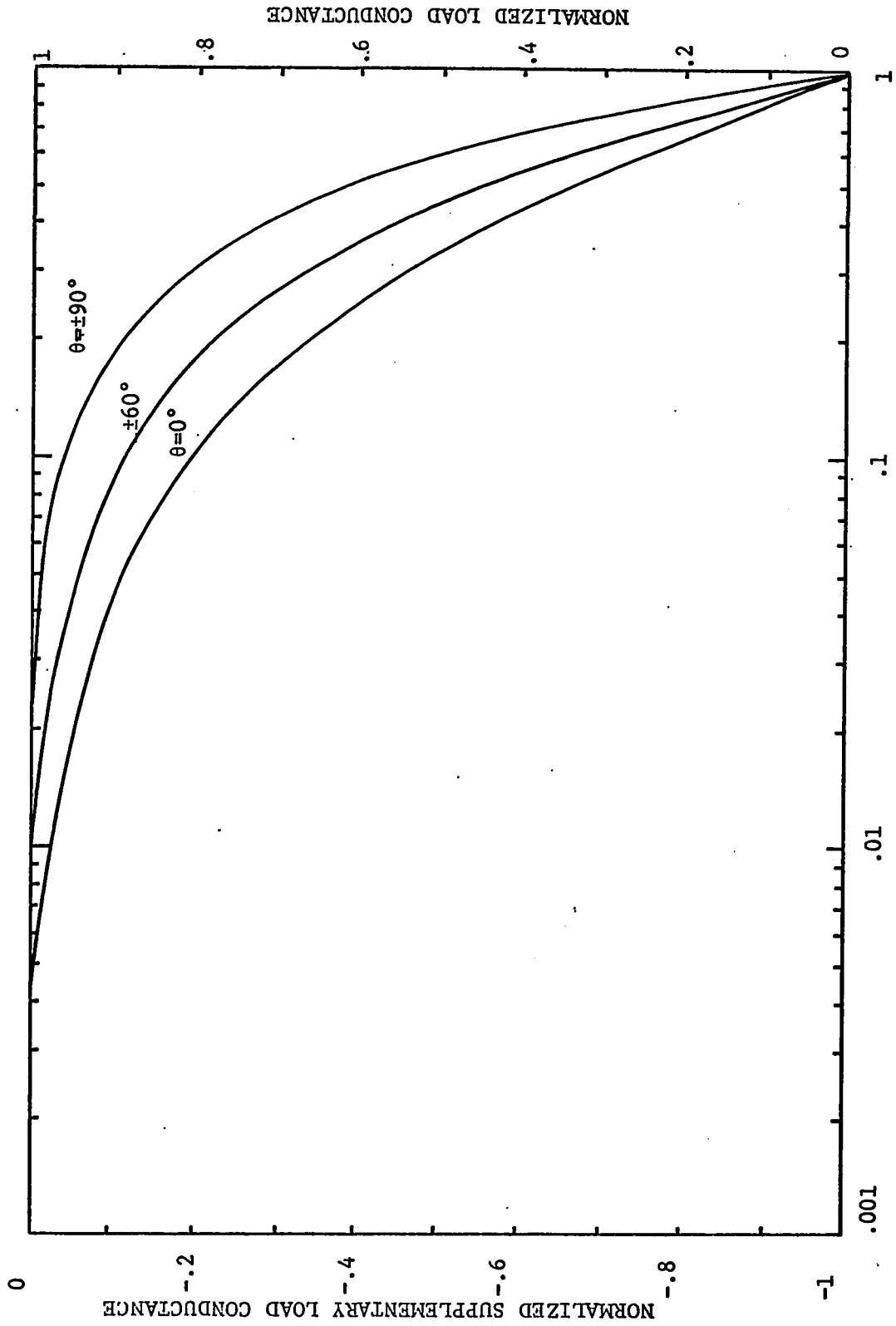


Fig.3-7 NORMALIZED LOAD CONDUCTANCE AS A FUNCTION OF REFLECTION COEFFICIENT.

means the oscillator produces the same power as the free-running power. This problem will be discussed in detail in Chapter IV.

Let us discuss the locus of the points of g_ℓ and b_ℓ when the magnitude of the reflection coefficient is constant and the phase angle is allowed to vary. From Eq. 3.25 and Eq. 3.26, we obtain

$$\left(g_\ell - \frac{1 + |\Gamma|^2}{1 - |\Gamma|^2}\right)^2 + b_\ell^2 = \left(\frac{2|\Gamma|}{1 - |\Gamma|^2}\right)^2 \quad (3.33)$$

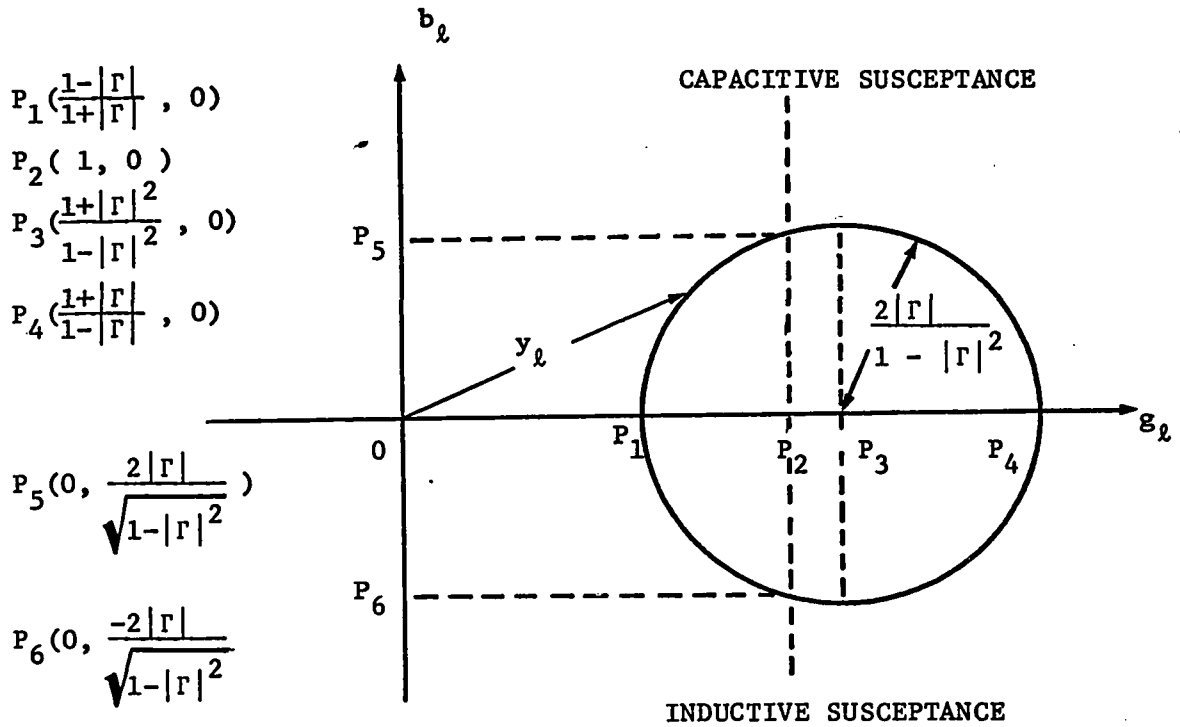
which can be plotted as shown in Fig.3.8a. The center of the circle is located at the point $\left(\frac{1 + |\Gamma|^2}{1 - |\Gamma|^2}, 0\right)$, and the radius of the circle is given by $\frac{2|\Gamma|}{1 - |\Gamma|^2}$. In order to clearly know the conductive contribution of the locking signal to the load, we may substitute Eq. 3.31 into Eq. 3.33, obtaining

$$\left(g' - \frac{2|\Gamma|^2}{1 - |\Gamma|^2}\right)^2 + b_\ell^2 = \left(\frac{2|\Gamma|}{1 - |\Gamma|^2}\right)^2 \quad (3.34)$$

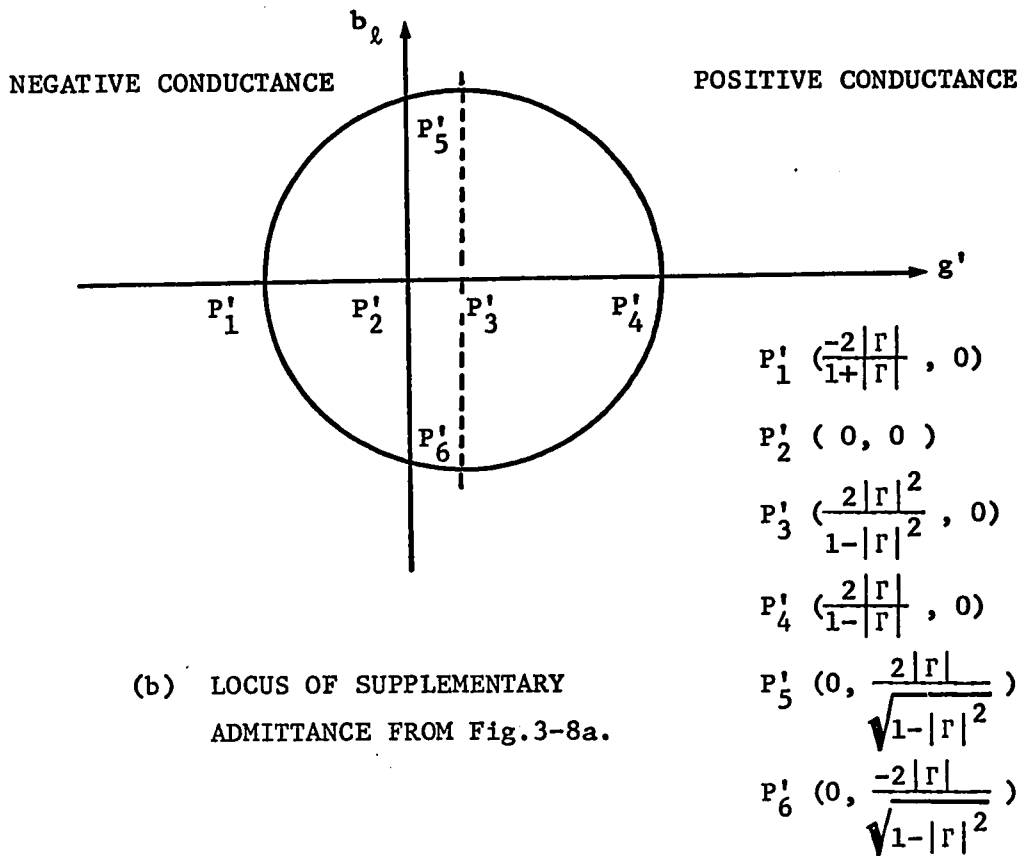
which can be plotted as shown in Fig.3.8b. It is obviously seen that the locking signal contributes a negative conductance to the load on the left of the b-axis. However, at the portion between $g' = 0$ and $g' = \frac{2|\Gamma|^2}{1 - |\Gamma|^2}$, the positive conductance contribution is obtained, which is arbitrarily reduced to zero by making $|\Gamma|$ much smaller than unity.

It is very interesting to note that the phase angle of the reflection coefficient at the turning point of the load conductance can be written as

$$\theta_m = \pm \left(\tan^{-1} \frac{2|\Gamma|}{1 - |\Gamma|^2} + \sin^{-1} \frac{1 + |\Gamma|^2}{\sqrt{1 + 3|\Gamma|^2}} \right) \quad (3.35)$$



(a) LOCUS OF EFFECTIVE NORMALIZED LOAD ADMITTANCE.



(b) LOCUS OF SUPPLEMENTARY ADMITTANCE FROM Fig. 3-8a.

Fig. 3-8 LOCUS OF LOAD ADMITTANCE.

where $|\Gamma| \ll 1$, $\theta_m \approx \pm 90^\circ$.

3-2-3 Locking Equation

The loading effect method discussed above will be used to obtain the locking equation in this section. From the locking equation, many important locking relationships can be derived, as will be discussed in the section 3-3.

An oscillator can be locked to an external signal injected into the oscillator if the locking signal frequency is near the normal operating frequency of the oscillator.

If a locking signal having exactly the same frequency as that of free-running oscillator is applied to the oscillator the locking signal cannot be distinguished from a reflected wave. It will then simulate a correction to the reflection coefficient of unity, or to the matched load admittance in accordance with Eqs. 3.28 and 3.21. If, originally, the oscillator is operating at a different frequency from the reference signal, this signal can pull the oscillator into synchronism, and into a definite phase relationship with it, provided there is some phase for which the reactive effect of the simulated admittance of the signal (see Eq. 3.26) is large enough to provide the necessary frequency pulling. As soon as the locking signal is present, the phase angle between the locking signal and oscillator will begin to approach the required value to produce this frequency pulling, and after a short time the oscillator will have settled down to a steady-state, synchronous with the locking signal, and with a constant phase angle between them. Therefore, there must be a time-dependent term, in Eq. 3.29, varying with the phase angle between the

oscillator and the external signal, which would depend on the frequency difference $(\omega - \omega_s)$ if the reference signal had frequency ω_s , and the oscillator frequency ω .

Therefore, we may substitute Eq. 3.22 into Eq. 3.29, obtaining

$$\frac{\omega_o |\Gamma| \sin\theta}{Q_{\text{ext}} (1 + |\Gamma|^2 + 2|\Gamma| \cos\theta)} = \omega - \omega_o \quad (3.36)$$

Consequently, if the locking signal is suddenly impressed, the phase θ will adjust itself to the proper value in Eq. 3.36, with a time constant which will be discussed in the next section. As a result in Eq. 3.36, $\omega - \omega_o = \omega_s - \omega_o - (\omega_s - \omega)$ where $\omega_s - \omega_o$ is the initial frequency difference $\Delta\omega_o$ and $\omega_s - \omega$ is the instantaneous frequency difference $\frac{d\theta}{dt}$. By making these substitutions and rearranging Eq. 3.36, the locking equation is obtained:

$$\frac{d\theta}{dt} + \frac{\omega_o |\Gamma| \sin\theta}{Q_{\text{ext}} (1 + |\Gamma|^2 + 2|\Gamma| \cos\theta)} = \Delta\omega_o \quad (3.37)$$

The above differential equation describes the process of injection phase-locking. This equation is useful even for higher relative levels of locking signal, a case often encountered in practice. It is interesting to note that, for relatively low levels of locking signal, Eq. 3.37 is identical to the Adler's equation⁵.

For many system applications, the level of locking signal is relatively small compared to the oscillator output, so that Eq. 3.37 can be reduced to

$$\frac{d\theta}{dt} + \Delta_o \sin\theta = \Delta\omega_o \quad (3.38)$$

where Δ_o is the maximum initial frequency difference at which locking can occur for a given ratio of locking signal and the oscillator output voltage waves. We may use Eq. 3.16 obtaining

$$\Delta_o = \frac{\omega_o}{Q_{\text{ext}}} \sqrt{\frac{P_s}{P_i}} \quad (3.39)$$

3-3 Locking Relationship

3-3-1 Steady-State Phase Angle and Locking Time

For stable locking, the instantaneous frequency difference $d\theta/dt$ must be zero. In other words the phase angle θ must be constant. Let this constant be θ_{ss} , which is called the steady-state phase angle. Then, the steady-state solution to Eq. 3.37 is given by:

$$\theta_{\text{ss}} = \sin^{-1} \left(\frac{1+|\Gamma|^2}{2|\Gamma|} \sqrt{1 + \left(\frac{\frac{\Delta\omega_o}{\omega_o}}{2Q_{\text{ext}}} \right)^2} \cdot \frac{\frac{\Delta\omega_o}{\omega_o}}{2Q_{\text{ext}}} \right) + \sin^{-1} \left(\frac{1}{\sqrt{1 + \left(\frac{\frac{\Delta\omega_o}{\omega_o}}{2Q_{\text{ext}}} \right)^2}} \cdot \frac{\frac{\Delta\omega_o}{\omega_o}}{2Q_{\text{ext}}} \right) \quad (3.40)$$

The steady-state phase angle of Eq. 3.40 is plotted in Fig.3.9. This steady-state value of the phase angle can also be obtained by letting $t = \infty$ in the general solution of Eq. 3.37, which will be derived in the Appendix-B. It is very interesting to investigate Eq. 3.40 for special cases. Suppose that the reflection coefficient is small

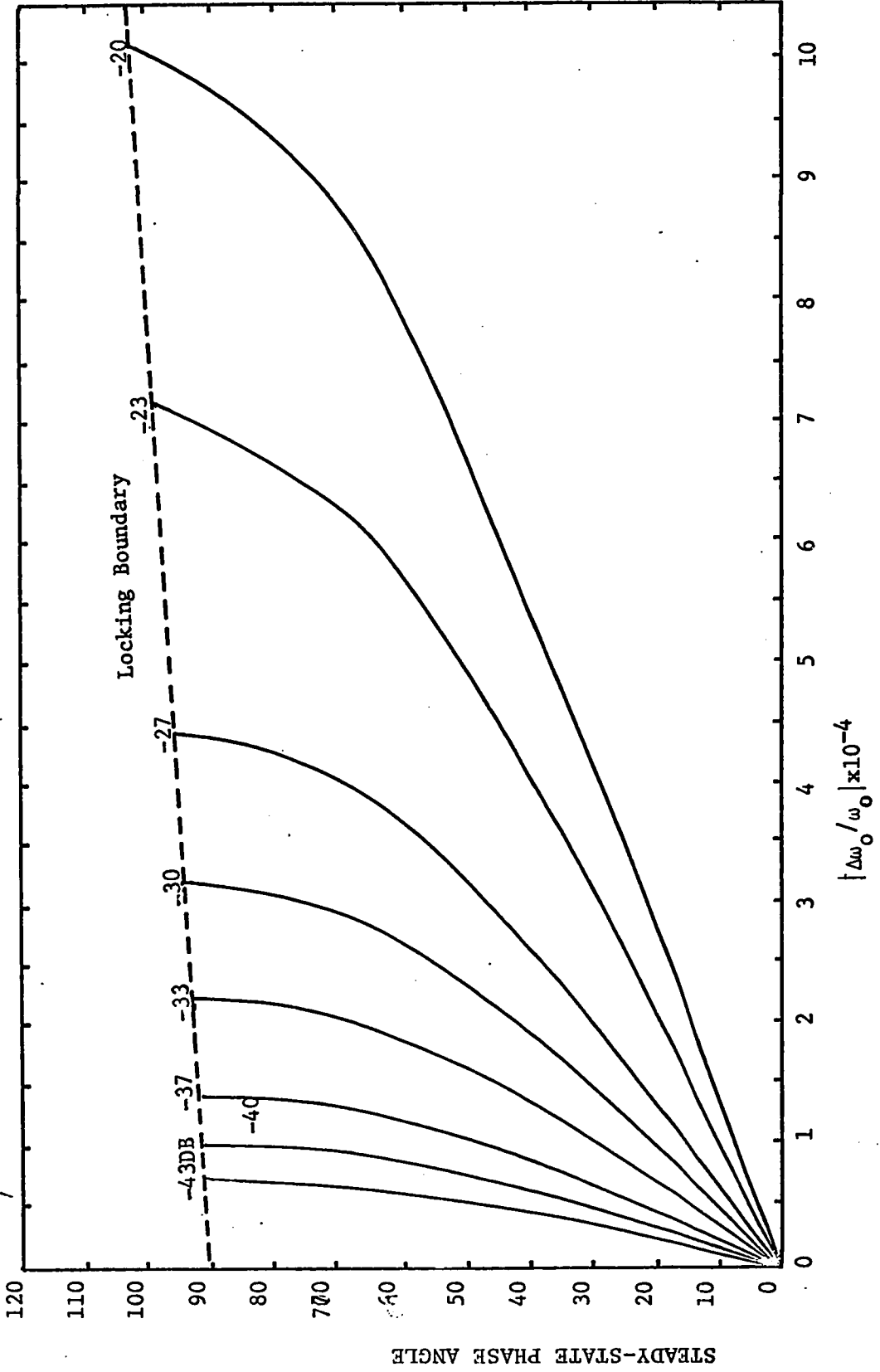


Fig. 3-9 STEADY-STATE PHASE ANGLE VS. FRACTIONAL INITIAL FREQUENCY DIFFERENCE

FOR Q_{ext} of 100.

compared to unity. Then Eq. 3.40 becomes

$$\theta_{ss} = \sin^{-1} \left(\frac{\Delta\omega_o}{\Delta_o} \right) \quad (3.41)$$

which can also be derived from Eq. 3.38 for the steady-state case.

Under the above assumptions, the transient response of the phase angle for the case $\Delta\omega_o = 0$ is written as

$$\theta = 2 \tan^{-1} \left(e^{-\Delta_o t} \tan \frac{\theta_o}{2} \right) \quad (3.42)$$

which is plotted in Fig. 3.10. The curves of Eq. 3.42 are symmetrical about $\theta = 0$. It is seen that, for low values of initial phase angle, the transient phase angle θ approaches zero exponentially.

For small values of initial phase θ_o , the transient phase angle $\theta(t)$, from Eq. 3.42 becomes

$$\theta(t) \approx \theta_o e^{-\Delta_o t} \quad (3.43)$$

To be consistent with the conventional definition of "time constant" for transient circuits, let us define a locking time constant T_l , to be the time required for the phase angle between the oscillator being locked and the locking signal to reduce to $1/e$ of the initial phase difference θ_o , in the above case,

$$T_l = 1/\Delta_o = \frac{Q_{ext}}{\omega_o} \sqrt{\frac{P_i}{P_s}} \quad (3.44)$$

It is seen from Eq. 3.43 that the phase difference approaches the final value approximately exponentially at a rate determined by the locking time constant $1/\Delta_o$.

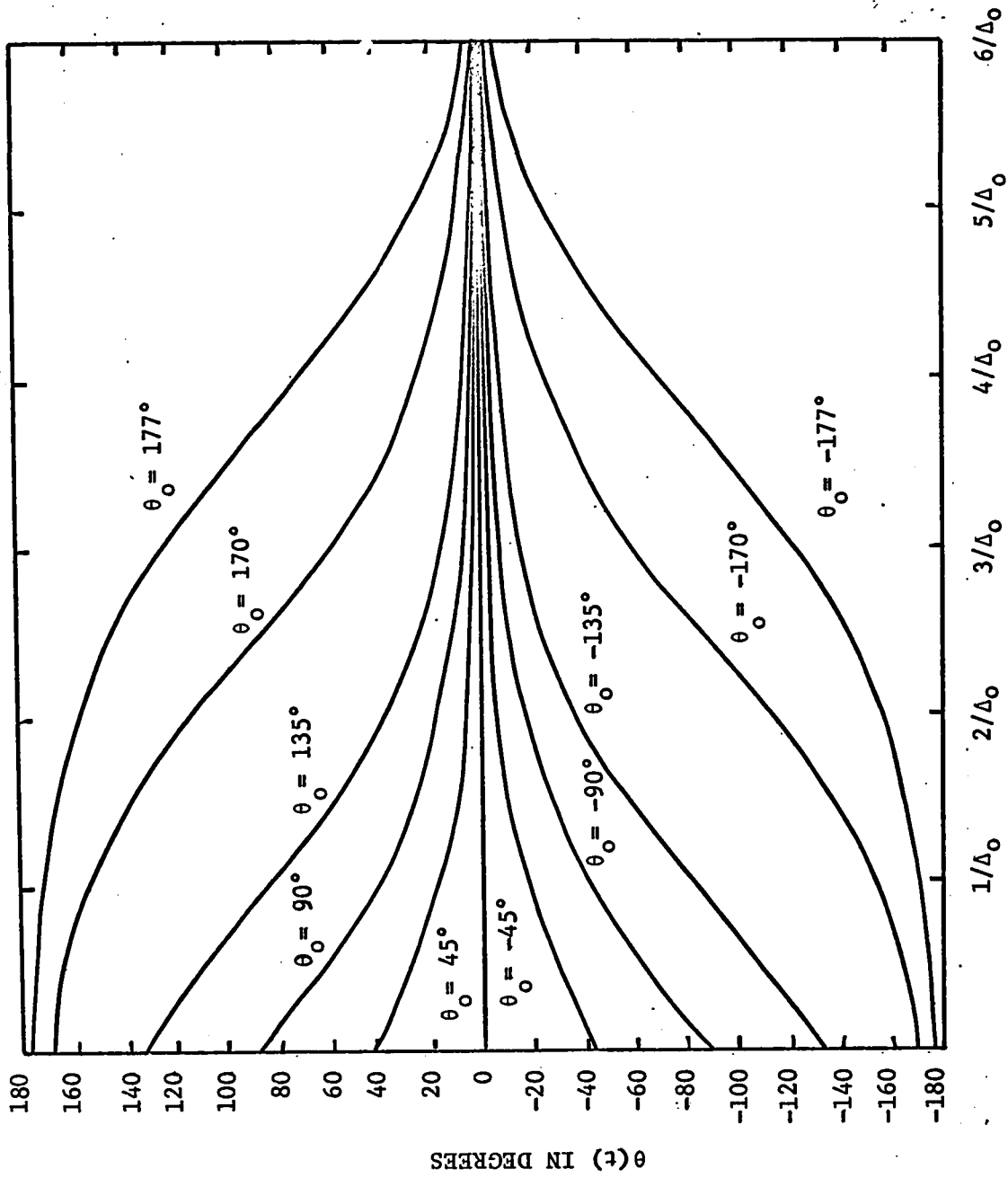


Fig. 3-10. VARIATIONS OF θ WITH TIME FOR LOW INITIAL PHASE ANGLE.

3-3-2 Locking Range

The locking range may be defined as the maximum initial frequency difference at which locking can take place for a given ratio of locking power to oscillator power. When the initial frequency difference is larger than the locking range, the oscillator cannot be locked.

Since $d\theta/dt$ in Eq. 3.37 must be zero for stable injection phase-locking, the relationship between steady-state phase angle and initial frequency difference can be found as follows:

$$\Delta\omega_o = \frac{\omega_o |\Gamma| \sin\theta}{Q_{\text{ext}} (1 + |\Gamma|^2 + 2|\Gamma| \cos\theta)} \quad (3.45)$$

We may differentiate the above equation with respect to θ and solve for a maximum. This occurs under the following condition;

$$\theta = \cos^{-1} \left(-\frac{2|\Gamma|}{1 + |\Gamma|^2} \right) \quad (3.46)$$

It is worth while to note that the condition of Eq. 3.46 is identical to that of the effective load susceptance for a maximum value, as we expected (Eq. 3.30). Locking range is a function of the locking signal amplitude, oscillation frequency, and circuit. The greater the amplitude of the locking signal the greater will be the locking range. High oscillator frequencies and circuits with low Q also result in large locking range.

Substituting this value of θ into Eq. 3.46, we obtain the maximum initial frequency, or the "locking range";

$$\Delta_1 = \frac{|\Gamma|}{Q_{\text{ext}} (1 - |\Gamma|^2)} \omega_o \quad (3.47)$$

As a result, for low level injection locking, the locking range is proportional to $|\Gamma|$ or the square root of the locking power ratio to the oscillator output. Under this condition, Δ_1 is equal to Δ_o in Eq. 3.39.

Eq. 3.47 is plotted in Fig. 3.11 where Eq. 3.47 can be easily compared with Eq. 3.39. As discussed in the section 3-2, it is interesting to note that, from the magnitude of the reflection coefficient in Eq. 3.16, the effective return loss in dB can be evaluated, which is essentially the same as the gain of the locked oscillator;

$$G(\text{dB}) = 20 \log_{10} \frac{1}{|\Gamma|} \quad (3.48)$$

3-3-3 Transient Phase Angle in General

The general solution of Eq. 3.37 specifies time as a function of phase. From it, phase can be calculated as a function of time, which will show its transient response.

We may integrate Eq. 3.37, as given in the Appendix-B subject to the condition

$$|\Delta\omega_o| < \Delta_1$$

which means that the initial frequency difference is smaller than the locking range. For the sake of simplicity, let

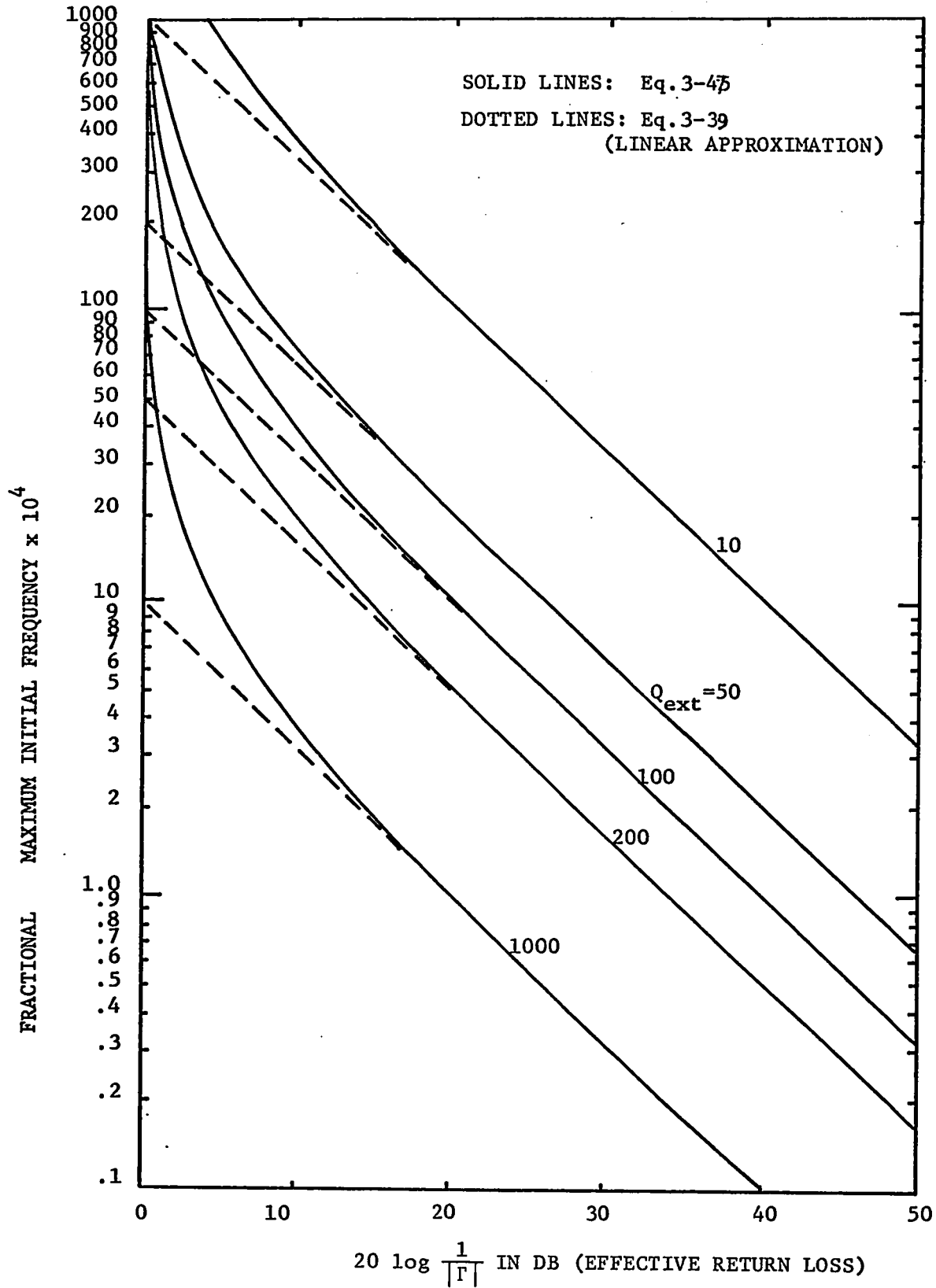


Fig.3-11 LOCKING RANGE VS. EFFECTIVE RETURN LOSS.

$$\xi_1 = \frac{\omega_o}{2Q_{\text{ext}}} \frac{2|\Gamma|}{1 + |\Gamma|^2} \quad (3.49)$$

and

$$\xi_2 = \frac{\omega_o}{2Q_{\text{ext}}} \quad (3.50)$$

Then, the solution with the initial condition $\theta(o) = \theta_o$ is

$$\begin{aligned} & \frac{1}{\sqrt{1 - \left(\frac{\Delta\omega_o}{\Delta_1}\right)^2}} \log \frac{\left\{ \left(\frac{\Delta\omega_o}{\xi_1} - \frac{\Delta\omega_o}{\xi_2}\right) \tan \frac{\theta}{2} - 1 - \sqrt{1 - \left(\frac{\Delta\omega_o}{\Delta_1}\right)^2} \right\} \left\{ \left(\frac{\Delta\omega_o}{\xi_1} - \frac{\Delta\omega_o}{\xi_2}\right) \tan \frac{\theta_o}{2} - 1 + \sqrt{1 - \left(\frac{\Delta\omega_o}{\Delta_1}\right)^2} \right\}}{\left\{ \left(\frac{\Delta\omega_o}{\xi_1} - \frac{\Delta\omega_o}{\xi_2}\right) \tan \frac{\theta}{2} - 1 + \sqrt{1 - \left(\frac{\Delta\omega_o}{\Delta_1}\right)^2} \right\} \left\{ \left(\frac{\Delta\omega_o}{\xi_1} - \frac{\Delta\omega_o}{\xi_2}\right) \tan \frac{\theta_o}{2} - 1 - \sqrt{1 - \left(\frac{\Delta\omega_o}{\Delta_1}\right)^2} \right\}} \\ & + \frac{\frac{\Delta\omega_o}{\xi_2} (\theta - \theta_o)}{\frac{\xi_2}{\xi_1}} - \frac{\xi_1}{\xi_2} \log \left(\frac{\frac{\Delta\omega_o}{\xi_1} + \frac{\Delta\omega_o}{\xi_2} \cos \theta - \sin \theta}{\frac{\Delta\omega_o}{\xi_1} + \frac{\Delta\omega_o}{\xi_2} \cos \theta_o - \sin \theta_o} \right) \\ & = \xi_1 \left\{ 1 + \left(\frac{\Delta\omega_o}{\xi_2}\right)^2 \right\} t \end{aligned} \quad (3.51)$$

if $|\Delta\omega_o| < \Delta_1$.

Fig.3.12 is a plot of Eq. 3.51 for $|\Gamma| = 40$ dB, $Q_{\text{ext}} = 100$, and $\Delta\omega_0 = 1.26 \times 10^6$ rad/sec. As locking time increases, the phase angle approached the steady-state value of 11.766° . When $\Delta\omega_0 = 0$ the curves are symmetric about the $\theta = \theta_{\text{ss}} = 0$ but as $\Delta\omega_0$ increases the curves become increasingly asymmetric as shown in Fig.3.12. However, when the locking signal power level is higher than before the curves are more symmetric about the $\theta = \theta_{\text{ss}}$ even if $\Delta\omega_0$ is increased, as shown in Fig. 3.13.

Now let us plot Eq. 3.51 as a parameter of $\Delta\omega_0$. Fig.3.14 is for $|\Gamma| = 40$ dB, $\theta_0 = -100^\circ$, and $Q_{\text{ext}} = 100$. Fig.3.15 is for $|\Gamma| = 40$ dB, $\theta_0 = -100^\circ$, and $Q_{\text{ext}} = 50$. The curves of Fig.3.15 approach the steady-state values faster than Fig.3.14 because the locking range in the case of Fig.3.15 is larger than that of Fig.3.14.

Let us consider cases with a higher locking power level than the above cases. Fig.3.16 is for $|\Gamma| = 30$ dB, $\theta_0 = -100^\circ$, and $Q_{\text{ext}} = 100$, while Fig.3.17 is for $|\Gamma| = 30$ dB, $\theta_0 = -100^\circ$, and $Q_{\text{ext}} = 50$. From Figs. of 3.16 and 3.17 it is seen that a higher locking power makes the oscillator approach faster the steady-state phase angle with reference to the locking signal. In addition, it is also seen that a smaller frequency difference results in faster phase-approaching the steady-state value of the oscillator. For all cases above, the free-running frequency is taken at 10 GHz. Suppose that the magnitude of reflection coefficient $|\Gamma|$ is relatively small, thus making

$$\Delta_1 = \Delta_0 = \xi_1$$

and that the initial difference frequency is far less than the free-running frequency, thus making

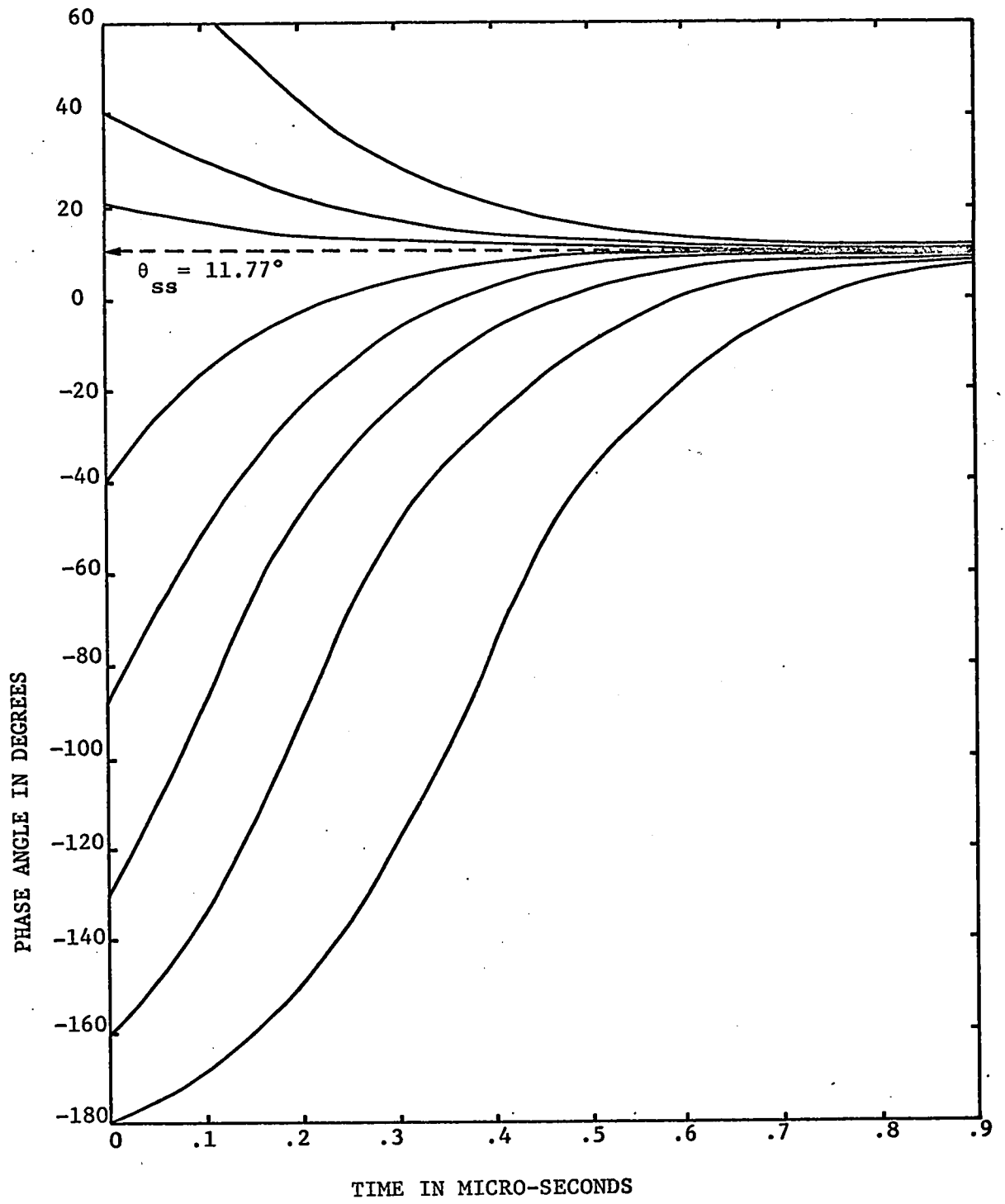


Fig.3-12 TRANSIENT RESPONSE OF A LOCKED OSCILLATOR FOR $Q_{ext} = 100$,
 $|\Gamma| = 40$ DB, and $\Delta\omega_o = 1.26 \times 10^6$ RAD/SEC.

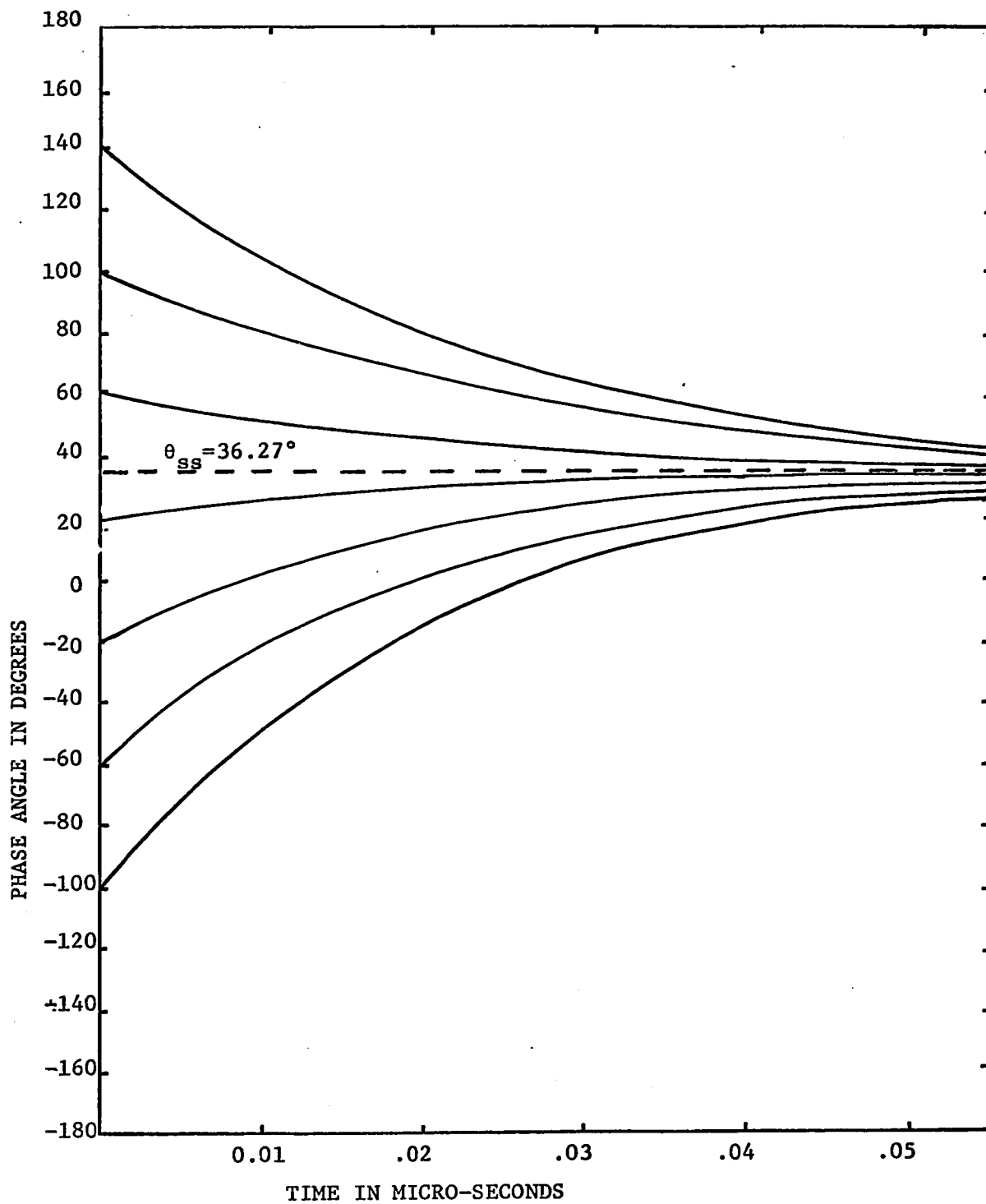


Fig.3-13 TRANSIENT RESPONSE OF A LOCKED OSCILLATOR FOR $Q_{ext} = 100$,
 $|\Gamma| = 20$ DB, AND $\Delta\omega_0 = 200 \times 10^6$ RAD/SEC.

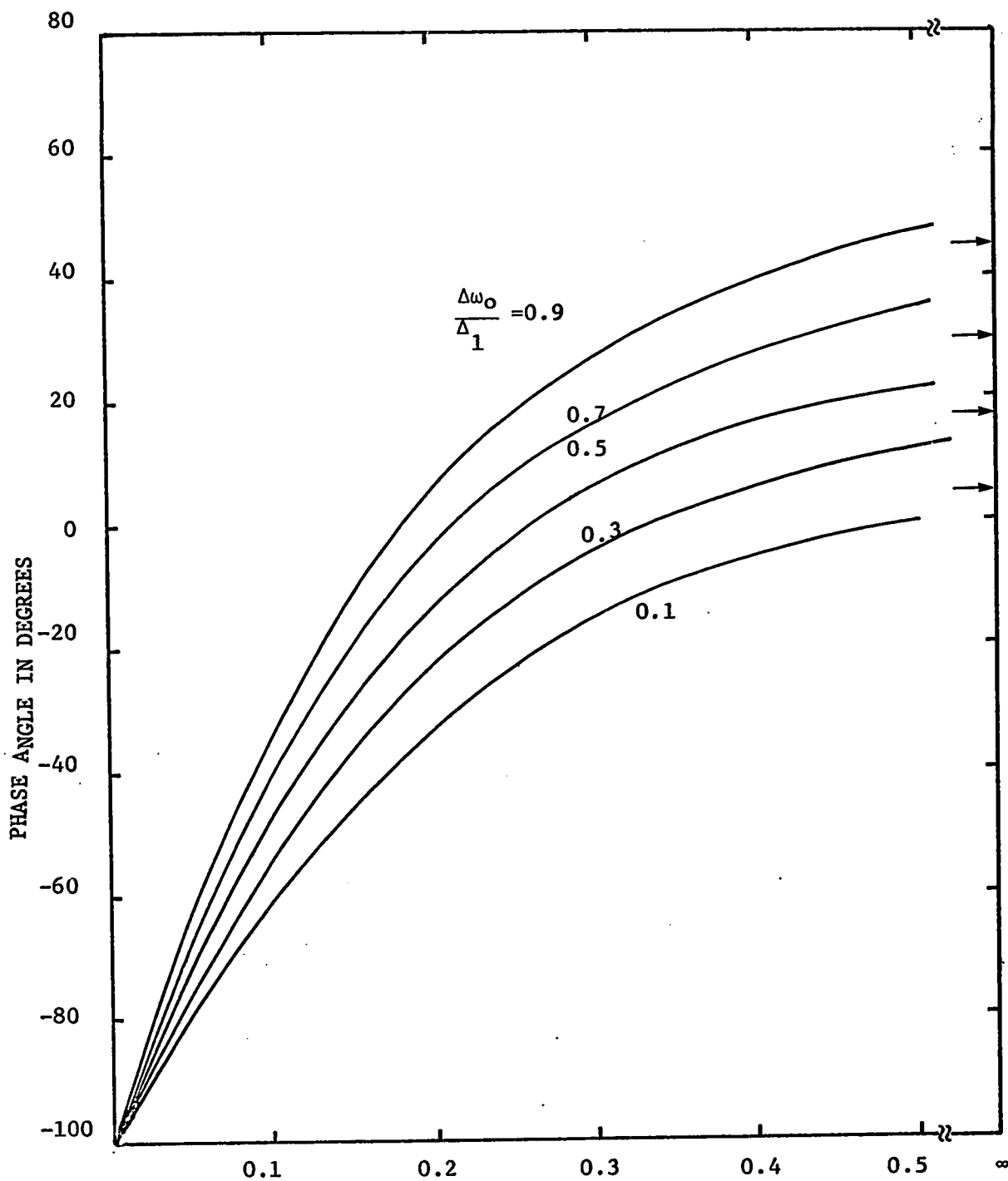


Fig.3-14 TRANSIENT RESPONSE OF A LOCKED OSCILLATOR
FOR $|\Gamma|=40\text{DB}$, $\theta_o = -100^\circ$, AND $Q_{\text{ext}} = 100$.

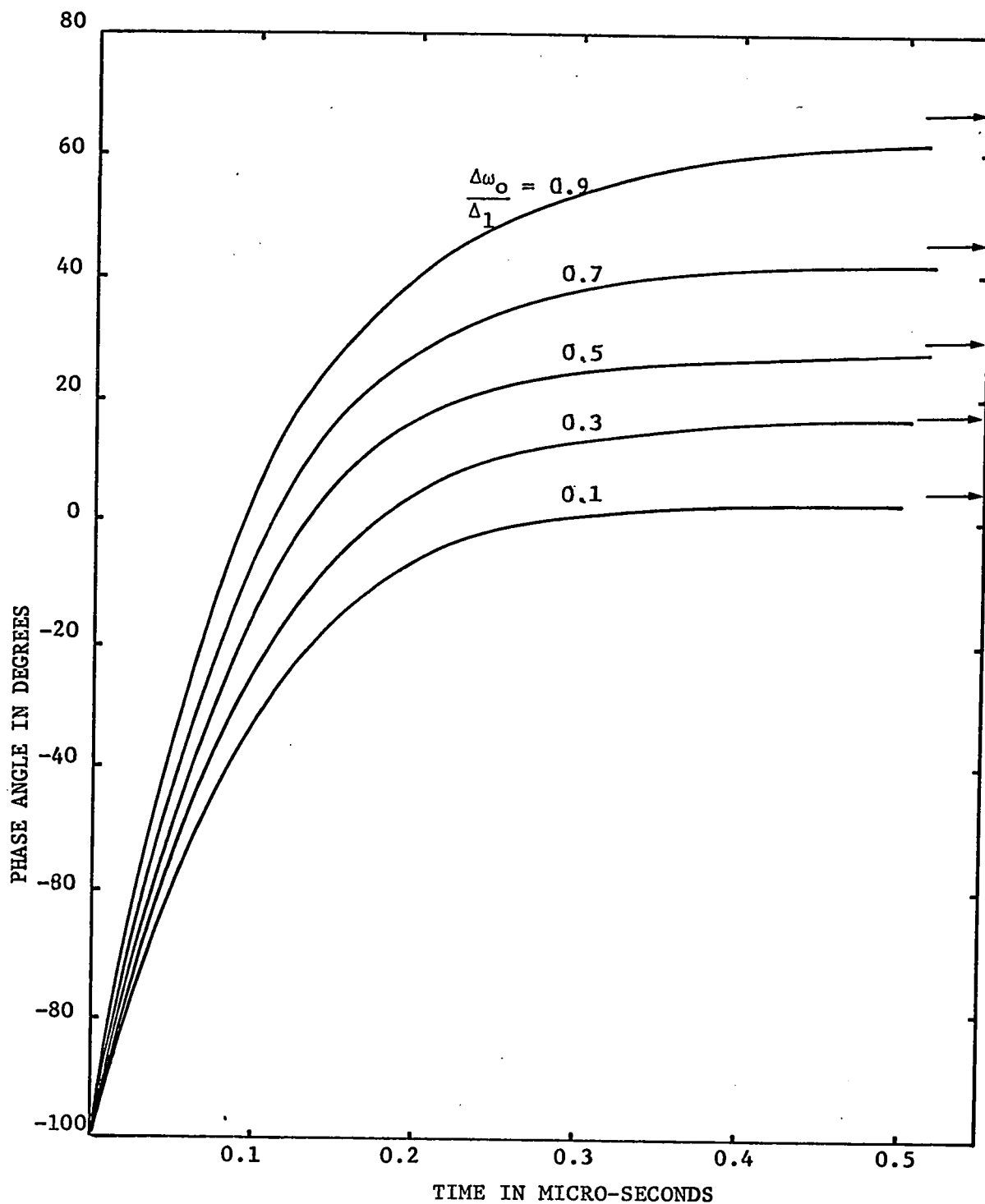


Fig.3-15 TRANSIENT RESPONSE OF A LOCKED OSCILLATOR FOR
 $|\Gamma| = 40$ DB, $\theta_0 = -100^\circ$, AND $Q_{\text{ext}} = 50$

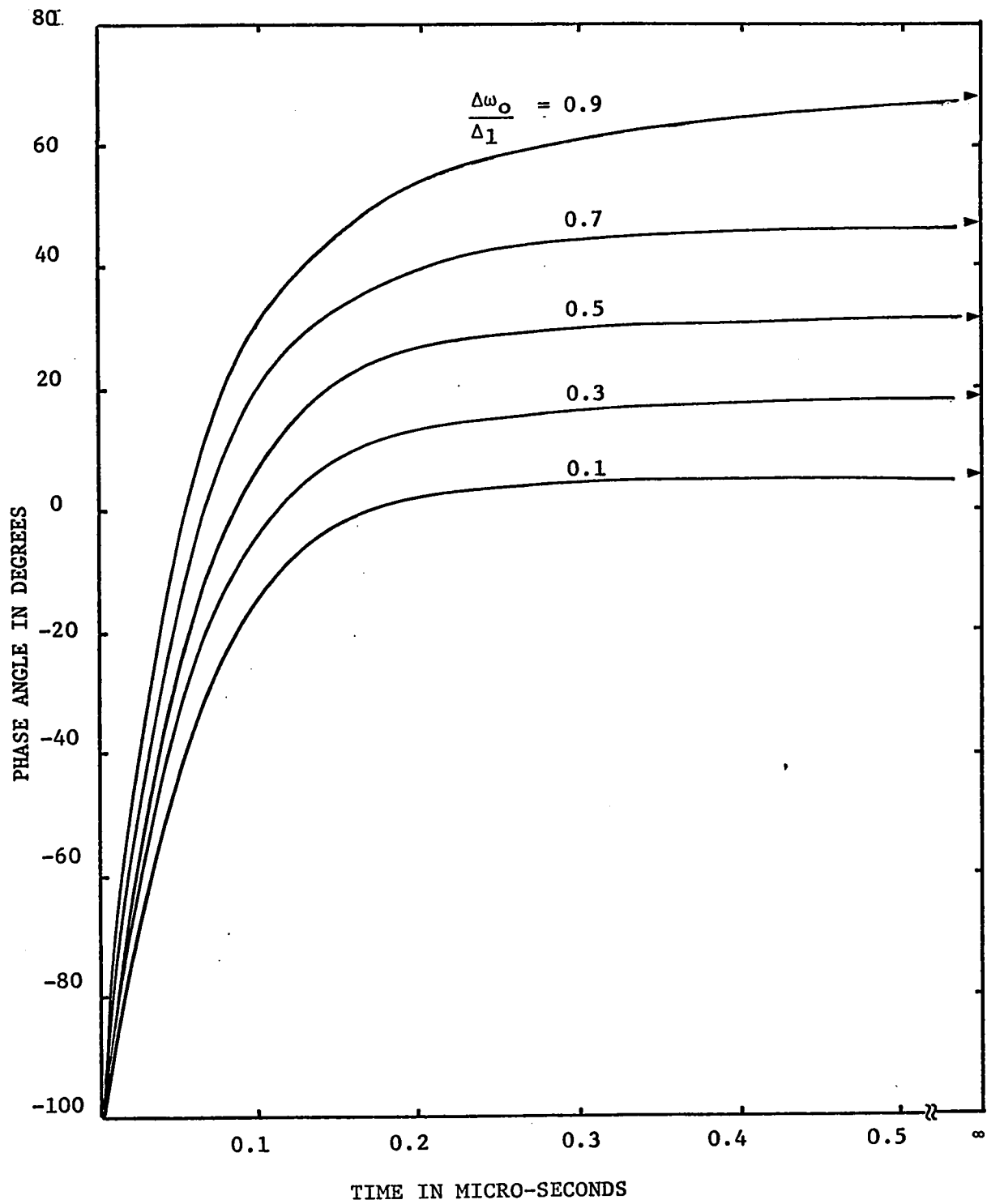


Fig.3-16 TRANSIENT RESPONSE OF A LOCKED OSCILLATOR FOR
 $|\Gamma|=30$ DB, $\theta_0 = -100^\circ$, AND $Q_{\text{ext}} = 100$.

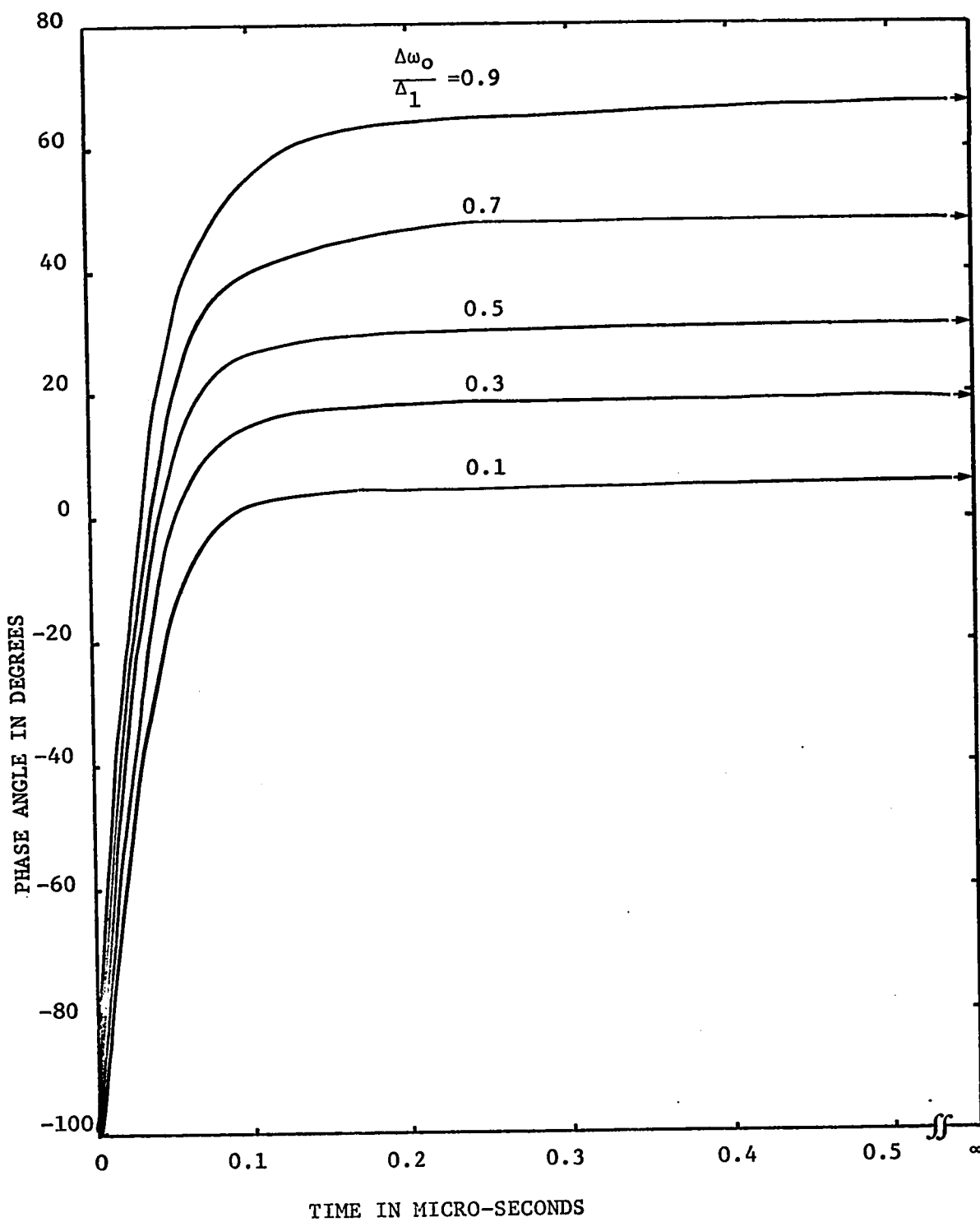


Fig.3-17 TRANSIENT RESPONSE OF A LOCKED OSCILLATOR FOR $|\Gamma|=30\text{DB}$, $\theta_o = 100^\circ$, AND $Q_{\text{ext}} = 50$.

$$|\Delta\omega_o| \ll \omega_o / 2Q_{\text{ext}} \quad \text{or} \quad |\Delta\omega_o / \epsilon_2| \ll 1$$

Then we obtain from Eq. 3.51:

$$\frac{1}{\sqrt{1 - \left(\frac{\Delta\omega_o}{\Delta_o}\right)^2}} \log \frac{\left\{ \frac{\Delta\omega_o}{\Delta_o} \tan \frac{\theta}{2} - 1 - \sqrt{1 - \left(\frac{\Delta\omega_o}{\Delta_o}\right)^2} \right\} \left\{ \frac{\Delta\omega_o}{\Delta_o} \tan \frac{\theta_o}{2} - 1 + \sqrt{1 - \left(\frac{\Delta\omega_o}{\Delta_o}\right)^2} \right\}}{\left\{ \frac{\Delta\omega_o}{\Delta_o} \tan \frac{\theta}{2} - 1 + \sqrt{1 - \left(\frac{\Delta\omega_o}{\Delta_o}\right)^2} \right\} \left\{ \frac{\Delta\omega_o}{\Delta_o} \tan \frac{\theta_o}{2} - 1 - \sqrt{1 - \left(\frac{\Delta\omega_o}{\Delta_o}\right)^2} \right\}} = \Delta_o t \quad (3.52)$$

In this case, by using Eq. 3.41 the transient phase angle can be obtained in terms of the steady-state and initial phase angles:

$$\theta = 2 \tan^{-1} \left\{ \csc \theta_{ss} - (\cot \theta_{ss}) \left[\frac{\cot \frac{\theta_{ss}}{2} - \tan \frac{\theta_o}{2} + (\tan \frac{\theta_{ss}}{2} - \tan \frac{\theta_o}{2}) e^{-(\Delta_o \cos \theta_{ss}) t}}{\cot \frac{\theta_{ss}}{2} - \tan \frac{\theta_o}{2} - (\tan \frac{\theta_{ss}}{2} - \tan \frac{\theta_o}{2}) e^{-(\Delta_o \cos \theta_{ss}) t}} \right] \right\} \quad (3.53)$$

It is seen from Eq. 3.53 that the transient terms decrease exponentially with time.

The transient response of the locked oscillator is of great interest, as it places a limit on the useable modulation rates of the locking signal. If the modulation rate is not too high, locked oscillators may be used as amplifiers of angle modulation signals and as angle modulators.

3-3-4 Locking Figure of Merit

It is seen from Eq. 3.39 that the total locking bandwidth about the free-running frequency for a small locking power is equal to $2\Delta_o$ which is approximately proportional to the ratio of the locking signal

and the oscillator output voltage waves. Therefore the normalized locking bandwidth can be written as

$$\frac{2\Delta_o}{\omega_o} = \eta \sqrt{\frac{P_s}{P_i}}$$

where η is a proportionality constant:

$$\eta = \frac{2\Delta_o}{\omega_o} \sqrt{\frac{P_i}{P_s}} = \frac{2}{Q_{\text{ext}}} \quad (3.54)$$

Now it is interesting to note that the locking signal is attenuated or partially reflected so that not all of the available locking signal is effective in locking the oscillator.

It is thus apparent η serves as a figure of merit of the injection phase-locked oscillator which characterizes the locking efficiency of an oscillator. The η is equal to a gain-bandwidth product and will be diminished by signal losses; thus, the larger η , the greater the normalized locking bandwidth that can be obtained for a given locking signal power.

The high locking figure of merit indicates that the locking signal is being used efficiently in locking the oscillator; hence, relatively little of the locking signal energy is attenuated or reflected.

Since the locking figure of merit is equal to twice the inverse of the external Q of the oscillator, the locking figure of merit is dependent only upon the oscillator circuit. Consequently, it can be suggested that a method for Q measurement by injection phase-locking offers a simpler, and more accurate measurement of oscillator circuit Q

than a conventional method at microwave frequencies.

3-4 Locking to an FM Signal

As discussed, it is possible to apply an external signal to an oscillator, of frequency very close to that at which the oscillator would normally operate, and by means of this external signal to cause the oscillator to produce power whose phase is determined by the external signal, as long as the signal frequency is within the locking range. Thus the oscillator operating in this way takes on some of the properties of an amplifier.

The transient response of the locked oscillator is of interest as it places a limit on the useable modulation rates of the locking signal. The locked oscillator may be used to amplify signals that are angle modulated if the modulation rates are not too high.

Eq. 3.52 describes the oscillator response when the locking signal is suddenly switched on with an initial phase difference θ_0 with respect to the free-running oscillator. The solution also describes the case of a step change of phase of the locking signal by an initial amount θ_0 .

By use of hyperbolic functions, for convenience, Eq. 3.52 can be written as:

$$\theta(t) = 2 \tan^{-1} \left[\frac{1}{k} - \frac{\sqrt{1-k^2}}{k} \tanh \Delta_0 \frac{\sqrt{1-k^2}}{2} (t-C) \right] \quad (3.55)$$

where $k = \Delta\omega_0/\Delta_0$, $C =$ integration constant. The integration constant C permits us to fit the equation to the initial phase difference θ_0 which exists when the external signal is switched on:

$$C = \frac{2}{\Delta_0 \sqrt{1-k^2}} \tanh^{-1} \left(\frac{\tan \frac{\theta_0}{2} - \frac{1}{k}}{\frac{1}{k} + \sqrt{\frac{1-k^2}{k^2}}} \right) \quad (3.56)$$

Since the function \tanh approaches unity with increasing argument, the steady-state will be reached when

$$\tanh \frac{\Delta_0 \sqrt{1-k^2}}{2} (t-C) \approx 1 \quad (3.57)$$

For the special case $\Delta\omega_0 = 0$, let us consider the curves of Fig.3.10. It is seen that the steady state is essentially reached at time t_1 equal to $6/\Delta_0$.

For analysis purposes, the input FM signal will be taken as

$$e_1(t) = A_1 \cos[\omega_c t + \phi(t)] \quad (3.58)$$

where $e_1(t)$ = applied FM wave

A_1 = constant amplitude of FM

ω_c = carrier frequency in radian/second

ϕ_t = angle modulation in radians

The locked output with an additional phase modulation can be expressed as follows;

$$e_2(t) = A_2 \cos[\omega_c t + \phi(t) - \theta(t)] \quad (3.59)$$

where $\theta(t)$ is the additional phase modulation.

From Eq. 3.58, the instantaneous frequency of the input FM signal is

$$\omega_s(t) = \omega_c + \phi'(t) \quad (3.60)$$

For convenience, by using Eqs. 3.59 and 3.38 we obtain an expression for $\theta'(t)$;

$$\theta'(t) = (\omega_c - \omega_o) + \phi'(t) - \Delta_o \sin\theta(t) \quad (3.61)$$

where $\theta'(t)$ is the time derivative of $\theta(t)$ and $\phi'(t)$ is the instantaneous frequency deviation in radian/second. For the case where the modulating signal is a single frequency sinusoid, $\phi'(t)$ can be written as:

$$\phi'(t) = \Delta\omega \sin \omega_m t \quad (3.62)$$

or

$$\phi = -\frac{\Delta\omega}{\omega_m} \cos \omega_m t$$

where $\Delta\omega$ is the maximum frequency deviation.

Substituting of Eq. 3.62 into Eq. 3.61 gives

$$\theta'(t) = \omega_c - \omega_o + \Delta\omega \sin \omega_m t - \Delta_o \sin\theta \quad (3.63)$$

It is seen from Eq. 3.63 that the additional phase $\theta(t)$ is a function of $(\omega_c - \omega_o)$, $\Delta\omega$, and ω_m , provided that Δ_o is constant.

Let us consider the symmetric case, $\omega_c = \omega_o$. Then we have

$$\theta'(t) = \Delta\omega \sin \omega_m t - \Delta_o \sin \theta \quad (3.64)$$

With some assumptions, we can obtain an approximate solution to Eq. 3.64, which is adequate to analyze the distortion of the FM-locked oscillator.

First, let us assume that the maximum frequency deviation is much less than the locking range of the oscillator:

$$\Delta\omega \ll \Delta_o$$

In Appendix-C, a solution of Eq. 3.64 has been obtained by a piecewise linearization. From Eq.C.23, we can write ;

$$\theta(t) = \frac{\frac{\Delta\omega}{\Delta_o} \sin(\omega_m t - \tan^{-1} \frac{\omega_m}{\Delta_o})}{\sqrt{1 + (\frac{\omega_m}{\Delta_o})^2}}. \quad (3.65)$$

From Eqs. 3.59, 3.62 and 3.65, we obtain the instantaneous phase deviation of the locked oscillator with respect to the carrier:

$$\alpha(t) = \theta(t) - \phi(t) = \frac{\frac{\Delta\omega}{\omega_m}}{\sqrt{1 + (\frac{\omega_m}{\Delta_o})^2}} \sin(\omega_m t + \tan^{-1} \frac{\omega_m}{\Delta_o}). \quad (3.66)$$

Therefore the modulation index ratio of the output to input, defined as the modulation suppression factor, can be obtained from the peak phase deviation ratio of the locked output to the original input FM signal:

$$S_1 = \frac{1}{\sqrt{1 + (\frac{\omega_m}{\Delta_o})^2}}. \quad (3.67)$$

Isobe and Tokita⁴⁵ have studied the response of the FM-locked oscillator output with the aid of an analog computer. Eq. 3.67 is in good agreement with their results. For the case of small modulation indexes the frequency modulation index of the locked output is not noticeably affected, when the self-excited oscillator is injection phase-locked with an external FM locking signal. However, as the modulation frequency of the input FM signal is increased injection phase-locking has more effect on the modulation index of the oscillator output. Consequently, it is worthwhile to have an "upper modulating" frequency

limit" up to which the locked oscillator can reproduce the input frequency deviation without any noticeable distortion.

In other words, if an FM signal is applied to the oscillator the output of the locked oscillator should have the same "quality" as the input signal. However, the locked output will be distorted from the input signal. As a consequence the modulation index ratio of the oscillator output to $\Delta\omega/\omega_m$, modulation index of the input signal, is a measure of the degree of conservation (reverse of suppression).

It has been shown⁴⁶ that a noise power suppression factor of the oscillator, injection phase-locked with a noisy signal, characterizes the locked resultant FM spectra. In this case it is assumed that both the locking signal and the locked oscillator are phase-modulated by the small signals of noise spectra; there is no AM-PM conversion and vice-versa.

Let us use Eq. 3.64 in order to determine the upper modulation frequency limit permissible on the locking signal. Then we may define a modulation power conservation factor of an FM injection phase-locked oscillator:

$$C_1 = 1 + \left(\frac{\omega_m}{\Delta_o}\right)^2 \quad (3.68)$$

This conservation factor in dB is plotted in Fig.3.18. It is seen from Fig.3.18 that the power spectra, when ω_m is less than $0.35\Delta_o$, are conserved without any noticeable suppression; when

$$\omega_m = 0.35\Delta_o \quad (3.69)$$

then the conservation factor is only about -0.5 dB. For example; if $f_o = 10$ GHz, $|\Gamma| = 20$ dB, and $Q_{\text{ext}} = 100$, then $f_m = 3.5$ MHz. Fig.3.18

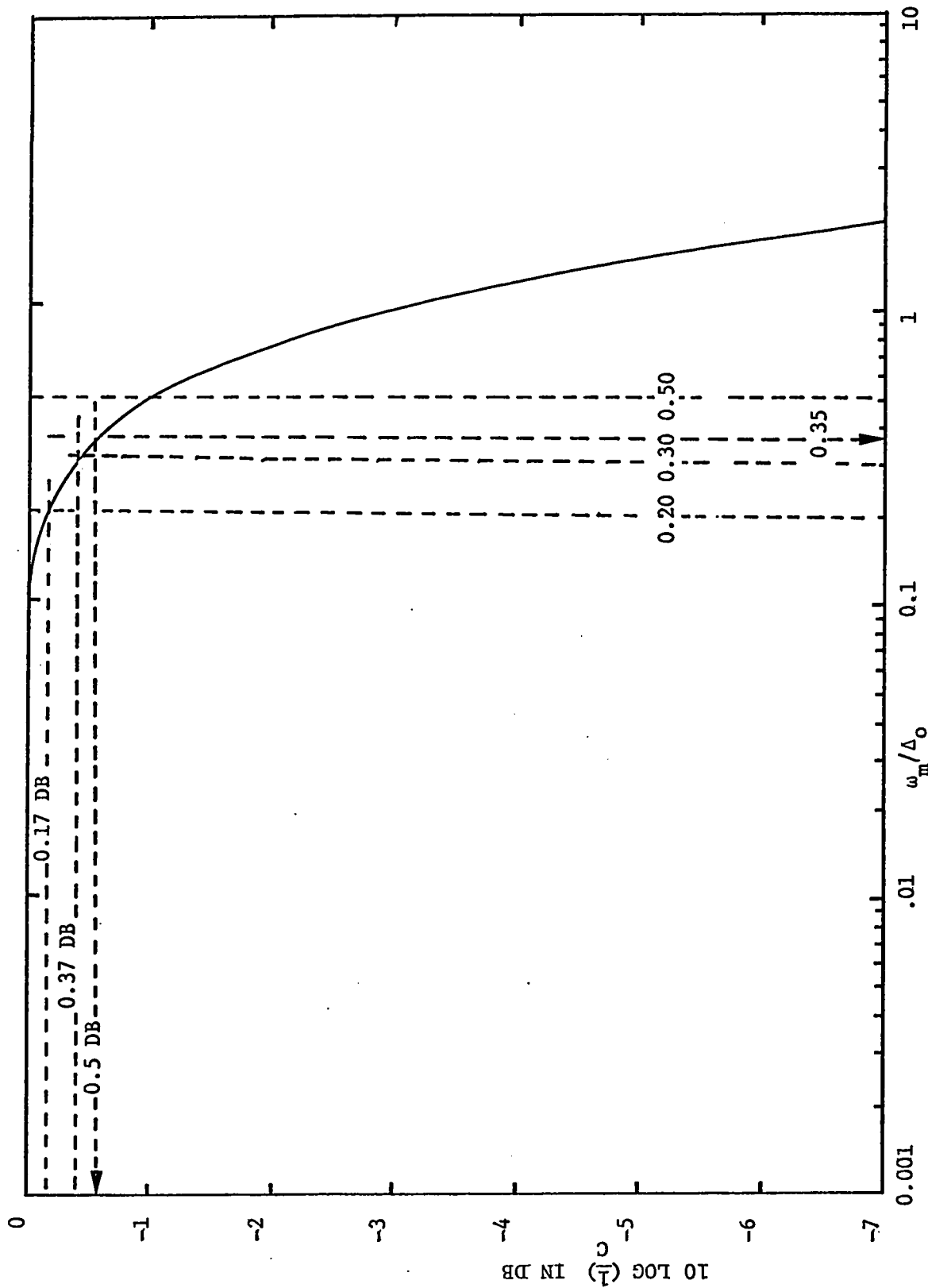


Fig. 3-18 CONSERVATION FACTORS VS. MODULATING FREQUENCY

also indicates that at the ω_m/Δ_o of 0.5 the conservation factor is reduced by 1.0 dB, while at the ω_m/Δ_o of 0.35 the factor is only -0.5 dB.

From the above discussion, the upper modulation frequency component of an FM locking signal seems to be well conserved for injection phase-locking at which the conservation factor is less than -0.5 dB.

So far we considered the distortion associated with the modulation frequency. However, even if the modulation frequency is very small compared to the locking range, changes in input frequency result in nonlinear changes in the phase relationships that exist in the locked oscillator, because the steady-state phase angle is an inverse sine function of the locking frequency deviation. Therefore, changes in modulation frequency introduce indirect frequency modulation: as a result distortion will be introduced by the phase locking. In this case, phase modulation is a consequence of the additional resultant phase shift, which varies throughout the modulating cycle. Since the deviation due to phase modulation is increased with the change in phase angle, the distortion will also increase with the frequency deviation.

For the purposes of this distortion analysis concerned with the frequency deviation of the input signal, the nonlinear phase response of Eq. 3.41 may be used.

Let us assume that the modulating frequency is very small compared to the locking range and frequency deviation. Then the distortion is concerned mainly with the group delay or envelope delay distortion due to nonlinear phase shape.

Delay time measures the time required to propagate a change

in the envelope of the actual information bearing part of the signal through the locking system. If the $\theta(t)$ is proportional to frequency the delay time will be constant for all frequencies and there will be no distortion of the transmitted signal.

For our case, $\theta(\omega)$ is not linear but instead includes higher order terms;

$$\theta(\omega) = \sin^{-1} \frac{\omega - \omega_0}{\Delta_0} = \frac{\omega - \omega_0}{\Delta_0} + \frac{1}{2 \cdot 3} \left(\frac{\omega - \omega_0}{\Delta_0} \right)^3 + \frac{1 \cdot 3}{2 \cdot 4 \cdot 5} \left(\frac{\omega - \omega_0}{\Delta_0} \right)^5 + \frac{1 \cdot 3 \cdot 5}{2 \cdot 4 \cdot 6 \cdot 7} \left(\frac{\omega - \omega_0}{\Delta_0} \right)^7 + \dots \quad (3.70)$$

Ignoring the linear phase component, $\theta(\omega)$ can be written as;

$$\theta(\omega) = \frac{1}{6} \left(\frac{\omega - \omega_0}{\Delta_0} \right)^3 + \frac{3}{40} \left(\frac{\omega - \omega_0}{\Delta_0} \right)^5 + \frac{5}{112} \left(\frac{\omega - \omega_0}{\Delta_0} \right)^7 + \dots \quad (3.71)$$

The envelope delay distortion of our phase locking characteristics, which is defined as the delay time or the derivative of the phase angle with respect to angular frequency due to the nonlinear terms of the phase angle equation, can be written as;

$$D = \frac{1}{2\Delta_0} \left(\frac{\omega - \omega_0}{\Delta_0} \right)^2 + \frac{3}{8\Delta_0} \left(\frac{\omega - \omega_0}{\Delta_0} \right)^4 + \frac{5}{16\Delta_0} \left(\frac{\omega - \omega_0}{\Delta_0} \right)^6 + \dots \quad (3.72)$$

It is seen from Eq. 3.72 that the most serious form of distortion occurs in the parabolic delay distortion. However, if the locking range is assumed to be larger than the peak frequency deviation, the higher order terms are negligible.

The nonlinear phase characteristic of injection phase-locking

and its associated time delay response are showed in Fig.3.19. It is interesting to note from Fig.3.19 that the locking system introduces a phase shift proportional to frequency around the free-running frequency. The time delay within the deviation of $0.68\Delta_o$ is almost constant. In this range , the phase characteristic does not introduce any appreciable delay distortion so the time delay is nearly constant for all components of the FM signal. At $0.68\Delta_o$, the ratio of the linear portion to the actual phase angle becomes;

$$\left. \frac{\frac{\Delta\omega}{\Delta_o}}{\sin^{-1} \frac{\Delta\omega}{\Delta_o}} \right] \frac{\Delta\omega}{\Delta_o} = 0.68 \quad \approx 90\% \quad (3.73)$$

In conclusion, if the angular frequency deviation of the input FM signal is less than about $0.68\Delta_o$ injection phase-locking does not introduce any appreciable distortion because the time delay ($d\theta/d\omega$) is almost constant of the F.M. signal for all components.

Let us consider another source of distortion. If the input carrier of the FM signal is not centered exactly on ω_o , the parabolic delay distortion yields a linear delay distortion which is serious in communication system.

To show this, let the parabolic delay be evaluated about ω_1 instead of about ω_o :

$$D_2 = \frac{1}{2\Delta_o^3} (\omega - \omega_1)^2 \quad (3.74)$$

Let

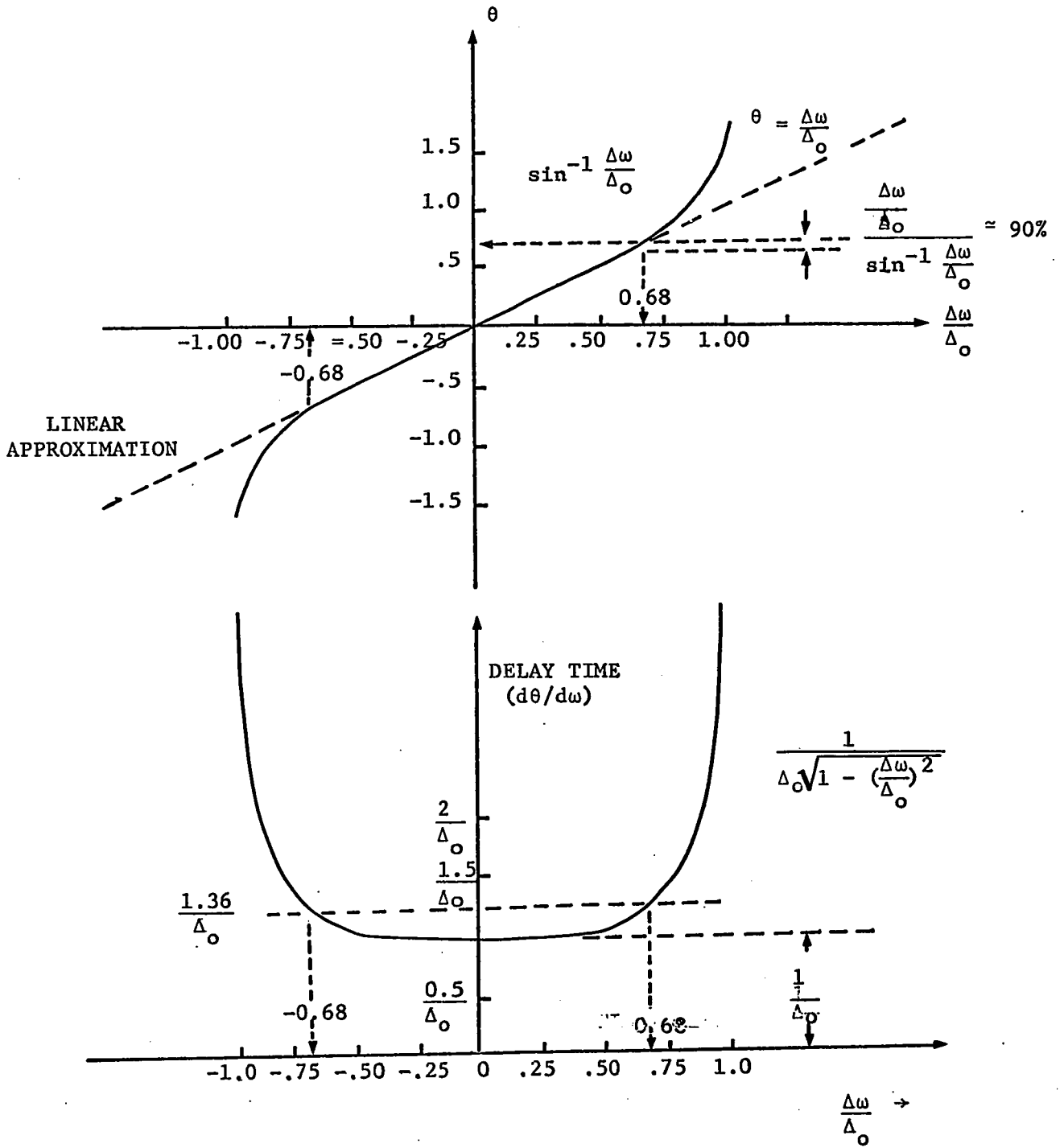


Fig.3-19 NONLINEAR PHASE CHARACTERISTICS OF INJECTION PHASE-LOCKING AND ITS ASSOCIATED TIME DELAY.

$$\omega_1 - \omega_o = \Delta\omega_1 \quad \text{or} \quad \omega_1 = \omega_o + \Delta\omega_1 \tag{3.75}$$

By substituting Eq. 3.75 into Eq. 3.74, we can obtain

$$D_2 = \frac{1}{2\Delta_o^3} [(\omega - \omega_o)^2 - 2\Delta\omega_1(\omega - \omega_o) + (\Delta\omega_1)^2] \tag{3.76}$$

It is interesting to note that the delay distortion of Eq. 3.76 has a parabolic component of unchanged magnitude plus a linear component of magnitude $\frac{\Delta\omega_1}{\Delta_o^3}$. Consequently, the analysis illustrates that in an FM locked oscillator, the baseband distortion depends also upon the location of the carrier frequency with respect to the oscillator free-running frequency. As a result, it is important to maintain the free-running frequency equal to the center frequency of the information bandwidth. The bias voltage tunability of oscillators would be useful for this purpose.

3-5 Injection Phase-Locking Phenomena Outside the Locking Range

3-5-1 An Analysis of Driven Oscillators

Outside the locking range, $|\Delta\omega_o| > \Delta_1$, the general solution to Eq. 3.37 under this condition is, as given in the Appendix-2,

$$\frac{2}{\sqrt{\left(\frac{\Delta\omega_o}{\Delta_1}\right)^2 - 1}} \left\{ \tan^{-1} \left[\frac{\left(\frac{\Delta\omega_o}{\xi_1} - \frac{\Delta\omega_o}{\xi_2}\right) \tan \frac{\theta}{2} - 1}{\sqrt{\left(\frac{\Delta\omega_o}{\Delta_1}\right)^2 - 1}} \right] - \tan^{-1} \left[\frac{\left(\frac{\Delta\omega_o}{\xi_1} - \frac{\Delta\omega_o}{\xi_2}\right) \tan \frac{\theta_o}{2} - 1}{\sqrt{\left(\frac{\Delta\omega_o}{\Delta_1}\right)^2 - 1}} \right] \right\}$$

$$+ \frac{\Delta\omega_o}{\xi_2} (\theta - \theta_o) - \frac{\xi_1}{\xi_2} \log \left[\frac{\frac{\Delta\omega_o}{\xi_1} + \frac{\Delta\omega_o}{\xi_2} \cos\theta - \sin\theta}{\frac{\Delta\omega_o}{\xi_1} + \frac{\Delta\omega_o}{\xi_2} \cos\theta_o - \sin\theta_o} \right] = \xi_1 \left[1 + \left(\frac{\Delta\omega_o}{\xi_2}\right)^2 \right] t \tag{3.77}$$

if $|\Delta\omega_o| > \Delta_1$.

Because the solution of Eq. 3.77 is unwieldy and difficult to understand physically, let us consider the case of small locking power.

Then we obtain

$$\frac{\sqrt{\left(\frac{\Delta\omega_o}{\Delta_o}\right)^2 - 1}}{2} \Delta_o t = \tan^{-1} \left(\frac{\frac{\Delta\omega_o}{\Delta_o} \tan \frac{\theta}{2} - 1}{\sqrt{\left(\frac{\Delta\omega_o}{\Delta_o}\right)^2 - 1}} \right) \Bigg|_{\theta_o}^{\theta} \quad (3.78)$$

Eq. 3.78 represents a periodic variation characterized by its wave form and its fundamental frequency, which will be found a little later.

It is seen from Eq. 3.78 that the periodic relationship between $\sin\theta$ and t shows that the character of the beat-note is nonsinusoidal.

The period of Eq. 3.78, T_b , is such that t increases by T_b when θ increases by 2π , and is found from the following relation:

$$\frac{\sqrt{\left(\frac{\Delta\omega_o}{\Delta_o}\right)^2 - 1}}{2} \Delta_o T_b = \pi \quad (3.79)$$

when $\Delta\theta = 2\pi$, therefore

$$T_b = \frac{2\pi}{\sqrt{(\Delta\omega_o)^2 - \Delta_o^2}} \quad (3.80)$$

Consequently the average beat-note frequency can be written as

$$\overline{\Delta\omega_b} = \sqrt{1 - \left(\frac{\Delta_o}{\Delta\omega_o}\right)^2} \Delta\omega_o \quad (3.81)$$

$\frac{\overline{\Delta\omega_b}}{\Delta\omega_o}$ approaches unity for large values of $\Delta\omega_o$, far from the point where locking occurs; but it drops toward zero when $\Delta\omega_o$ approaches the value

of Δ_o , as shown in Fig.3.20.

The implicit form of Eq. 3.78 is cumbersome and does not provide much insight into the problem. However, a plot of typical waveforms, as in Fig.3.21 is very revealing and the nonsinusoidal character of the beat-note is evident. Moreover, the positive and negative excursions are obviously unequal in area, and therefore the diode must contain some additional amount of dc potential over the dc bias potential which is initially applied, even before lock is obtained.

The average dc potential developed at the diode in this case is given in Appendix-D.

Since this property is very important in the case of injection phase-locking of bias modulated oscillators, the detailed analysis on this phenomenon will be done in Chapter V.

3-5-2 Output Spectrum of Driven Oscillators

We have obtained the general solution to Eq. 3.37 in the preceding section, but the solution in its exact form is not as clear for a spectral analysis as some approximate solutions. Stover⁴⁷ has found that a third-order solution is sufficient to yield the significant physical trends.

The Fourier decomposition of Eq. 3.78 is given by

$$\theta(t) = \sqrt{1 - \left(\frac{\Delta_o}{\Delta\omega_o}\right)^2} \Delta\omega_o t + 2 \sum_{n=1}^{\infty} \frac{K^n}{n} \sin(n \sqrt{1 - \left(\frac{\Delta_o}{\Delta\omega_o}\right)^2} \Delta\omega_o t) \quad (3.82)$$

$$\text{where } K = \left(\frac{\Delta\omega_b}{\Delta\omega_o} - 1\right) / \left(\frac{\Delta\omega_b}{\Delta\omega_o} + 1\right) \quad \text{and } \Delta\omega_b = \sqrt{1 - \left(\frac{\Delta_o}{\Delta\omega_o}\right)^2} \Delta\omega_o.$$

Thus, $\theta(t)$ is a complex periodic function whose fundamental frequency

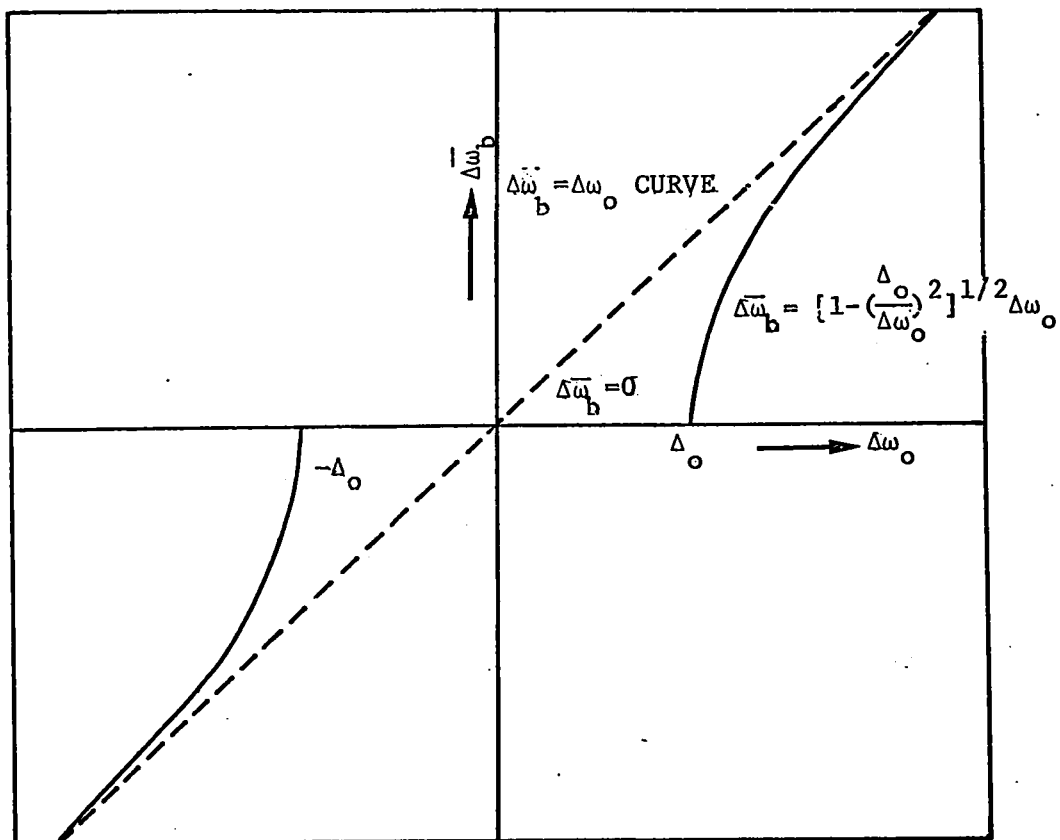


Fig.3-20 REDUCTION OF BEAT FREQUENCY DUE TO LOCKING

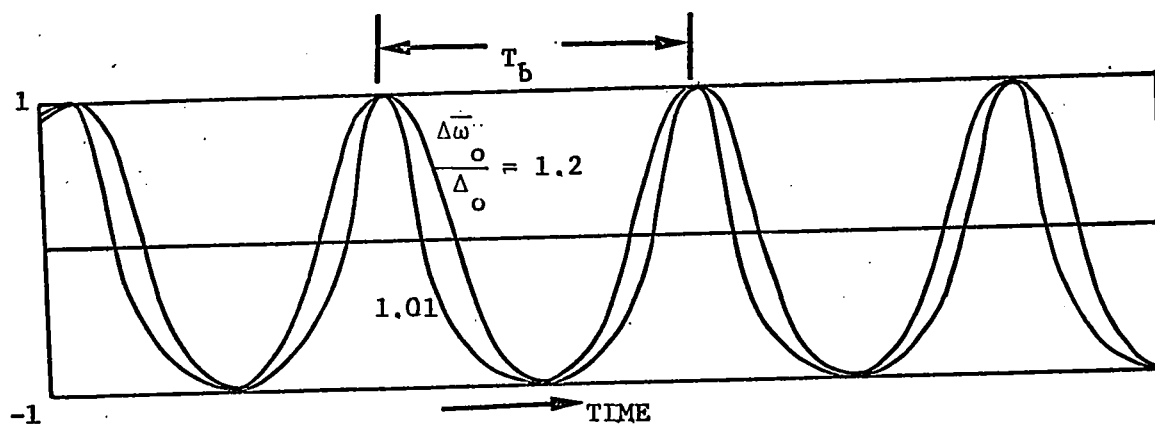


Fig.3-21 TYPICAL BEAT-NOTE WAVEFORMS

is the modified beat frequency $\Delta\omega_b$.

Eqs. 3.27 and 3.28 in conjunction with Eq. 3.82 imply that the forced oscillation is subject to simultaneous amplitude and frequency modulation on a time scale $2\pi/\Delta\omega_b$ about the free-running oscillations of amplitude and frequency.

The simultaneous amplitude and frequency modulation by a complex function in Eq. 3.82 represents a case of multitone modulation, which can produce an extremely complicated frequency spectrum. However, under typical experimental conditions $k \ll 1$, and only the Fourier components of θ corresponding to the first few values of n need be considered.

It has been shown^{47,48} that, under appropriate conditions, cancellation of one-sideband can occur, the non vanishing sideband lying on the far side of ω_0 from the locking frequency.

3-6 P.M. Noise Improvement in Injection Phase-Locked Oscillators

Generally in oscillators there is influence of noise originating inside the circuit, especially from the active elements. Such noise component may influence the phase or frequency stability of the oscillators. Particularly it is known that there is such noise component in the solid-state diode oscillators^{35-40,49-51}. One way to improve the noise performance is to control the oscillator frequency by injecting a stable locking signal.^{12,15,45.}

The effect of the noise component on the free-running oscillation and the action of a stable locking signal can be analyzed by means of bias modulation and then injection phase-locking the oscillator at the same

microwave frequencies. This approach is taken in Chapter V.

Consider a hypothetical case in which the locking signal is noise free and the oscillator to be locked, is noisy.

Let it be assumed that the oscillation frequency ω_o is sinusoidally bias modulated by a baseband noise tone of frequency ω_m . Then the noise power suppression factor, which characterizes the locked resultant PM power spectra under an injection phase-locked state for two oscillators of the same average frequency with the locking signal noise free and the oscillator noisy, is given in Appendix-C.

$$S_2 = \frac{1}{1 + \left(\frac{\Delta_o}{\omega_m}\right)^2} \quad (3.83)$$

Eq. 3.83 is plotted in Fig.3.22. It is seen from Fig.3.22 that noise near the carrier will be attenuated as the noise power suppression factor S_2 tends to zero, or $10 \log \frac{1}{S_2}$ tends to infinity, for low ω_m ; noise far away from the carrier will be unattenuated as S_2 will go to the value of unity, or $10 \log \frac{1}{S_2}$ tends to zero, for large ω_m .

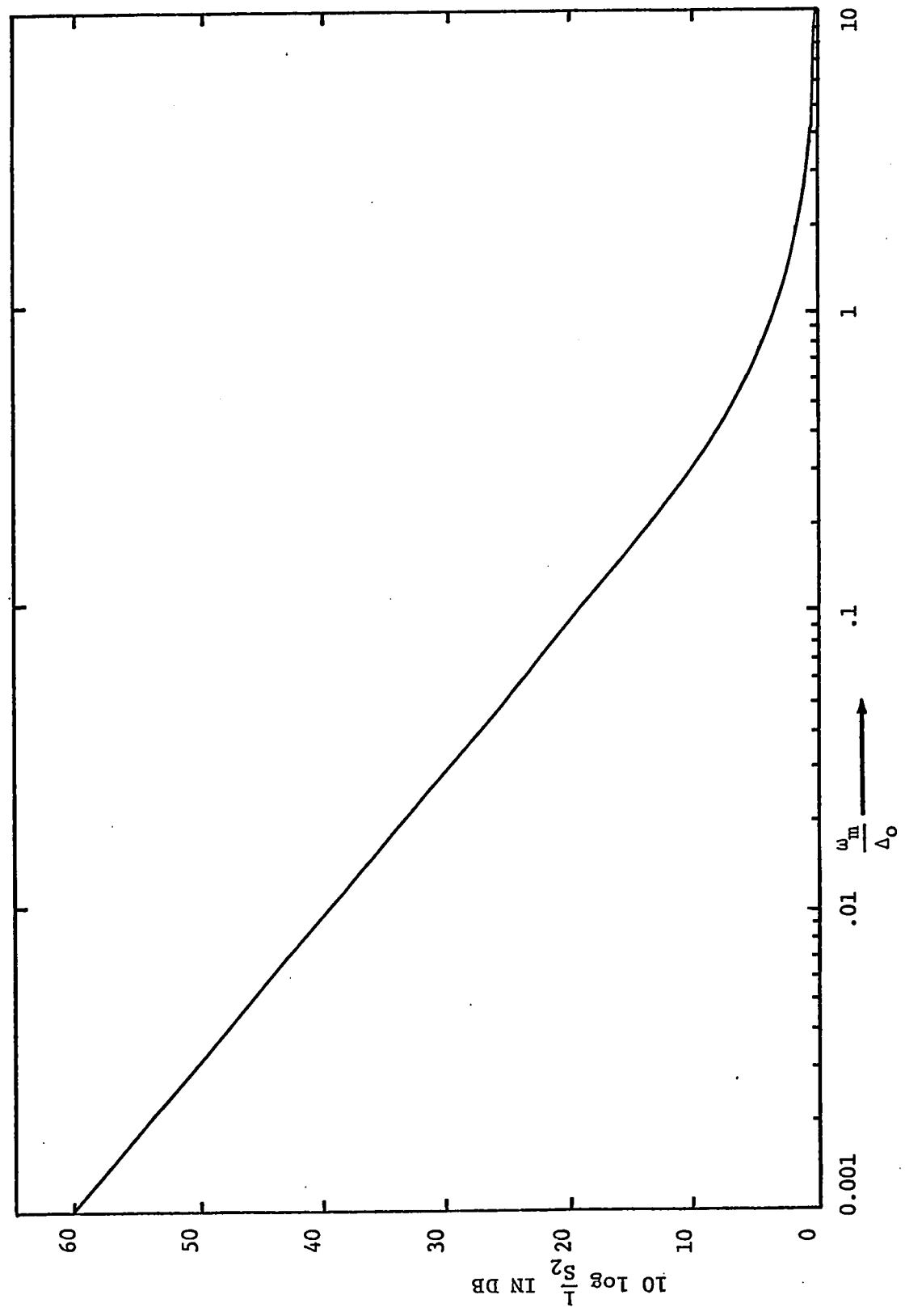


Fig. 3-22 NOISE POWER SUPPRESSION FACTOR VERSUS NOISE FREQUENCY

CHAPTER IV

EXPERIMENTAL STUDY OF BASIC INJECTION PHASE-LOCKINGPROPERTIES OF OSCILLATORS4-1 Introduction

This chapter describes a detailed systematic experimental study of the basic locking behaviour of injection phase-locked IMPATT diode oscillators and Gunn diode oscillators.

The experimental study includes:

- 1) Measurement of locking range as a function of the locking power ratio to the oscillator output.
- 2) Measurement of phase angle difference between the locked power oscillator output and the locking signal as a function of the initial frequency difference.
- 3) Phase-locking measurement of multi-signal injected oscillators.
- 4) Measurements for frequency stabilization.

In addition, the results are compared to those from the variable load experiments.

This experimental work covers the study of four IMPATT diodes (Table 4.1) and four Gunn diodes (Table 4.2). All measurements were made at X-band frequencies. The experimental results are in good accord with the theories developed in Chapter 3 and indicate that IMPATT diode oscillators and Gunn diode oscillators may be used as amplifiers for angle modulated signals.

4-2 Measurement of Locking Range

4-2-1 Description of Experimental Setup

Table 4.1 SOME ELECTRICAL CHARACTERISTICS FOR IMPATT DIODE
OSCILLATORS TESTED.

IMPATT DIODE OSCILLATOR	NORMAL DC OPERATION		NORMAL RF OUTPUT	
	CURRENT IN mA	VOLTAGE IN VOLTS	RF POWER IN mW	RF FREQUENCY IN GHz
SYA-3200-1	19.0	82.1	27.0	9.800
SYA-3200-2	19.0	80.3	29.0	9.800
SYA-3200-3	23.0	93.2	30.0	9.800
SYA-3200-4	19.0	83.9	35.0	9.800

Table 4.2 SOME ELECTRICAL CHARACTERISTICS FOR GUNN DIODE
OSCILLATORS TESTED

GUNN DIODE OSCILLATOR	NORMAL DC OPERATION		NORMAL RF OPERATION	
	CURRENT IN mA	VOLTAGE IN VOLTS	RF POWER IN mW	RF FREQUENCY IN GHz
CL-8370-1	115.0	7.1	7.1	9.300
CL-8370-2	118.0	7.0	6.2	9.400
CL-8370-3	120.0	6.5	6.7	9.300
CL-8370-4	119.0	6.2	5.0	9.400

The experimental setup for measuring the locking range is shown in Fig. 4.1 The locking signal from a stabilized reflex klystron oscillator was impressed on the IMPATT diode oscillator or on the Gunn diode oscillator through a precision attenuator, a 20 dB directional coupler, and path 1-2 of a four-port circulator. The locking signal

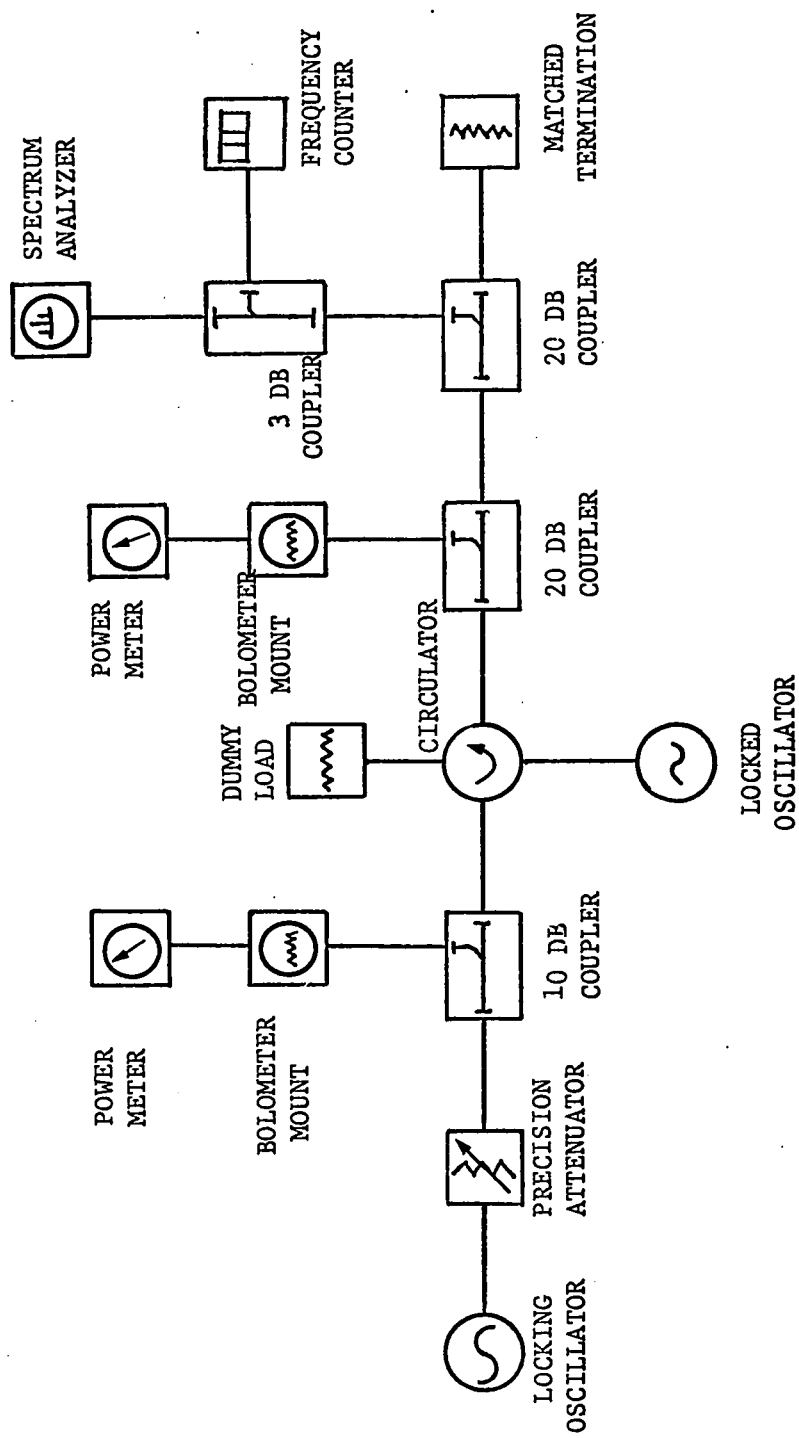


Fig. 4-1 EXPERIMENTAL SETUP FOR MEASURING LOCKING RANGE

power was calibrated for a particular attenuator setting, and monitored by means of a power meter connected to the auxiliary arm of a directional coupler. Path 1-2 of the circulator had a return loss of the order of 40 dB. Therefore, the locking signal oscillator was adequately isolated from the rest of the system. The locked oscillator output signal was dissipated in a matched load, passing through the circulator path 2-3, and two 20 dB directional couplers. Any power reflected from the output circuit is passed through the circulator path 3-4 and is dissipated in a matched load connected to port 4. Actually, the circulator path 1-4 provided isolation of the order of 52 dB. The insertion losses of the circulator path 1-2 and 2-3 were about 0.2 dB. The loss of the circulator is plotted as a function of frequency in Fig.4.2. The frequency and the oscillator output power were measured by means of two directional couplers fitted with a power meter, and a frequency counter.

Two different methods for measuring the locking range were used, but the same experimental setup was used.

First, the locking signal was swept in frequency, while holding the amplitude of the locking signal constant and a direct reading frequency counter was used to determine the locking range over which the IMPATT diode oscillator or the Gunn diode oscillator was locked. During every experiment, the locking signal amplitude was kept constant. The oscillator output was displayed on a spectrum analyzer after transmission through directional couplers. Actually a very small portion of the oscillator output was sufficient to be analyzed, as shown in Fig. 4.1.

The locking range measurements were made by presenting the oscillator output on the spectrum analyzer and by observing the locking frequency, on the frequency counter, required to just pull the oscillator

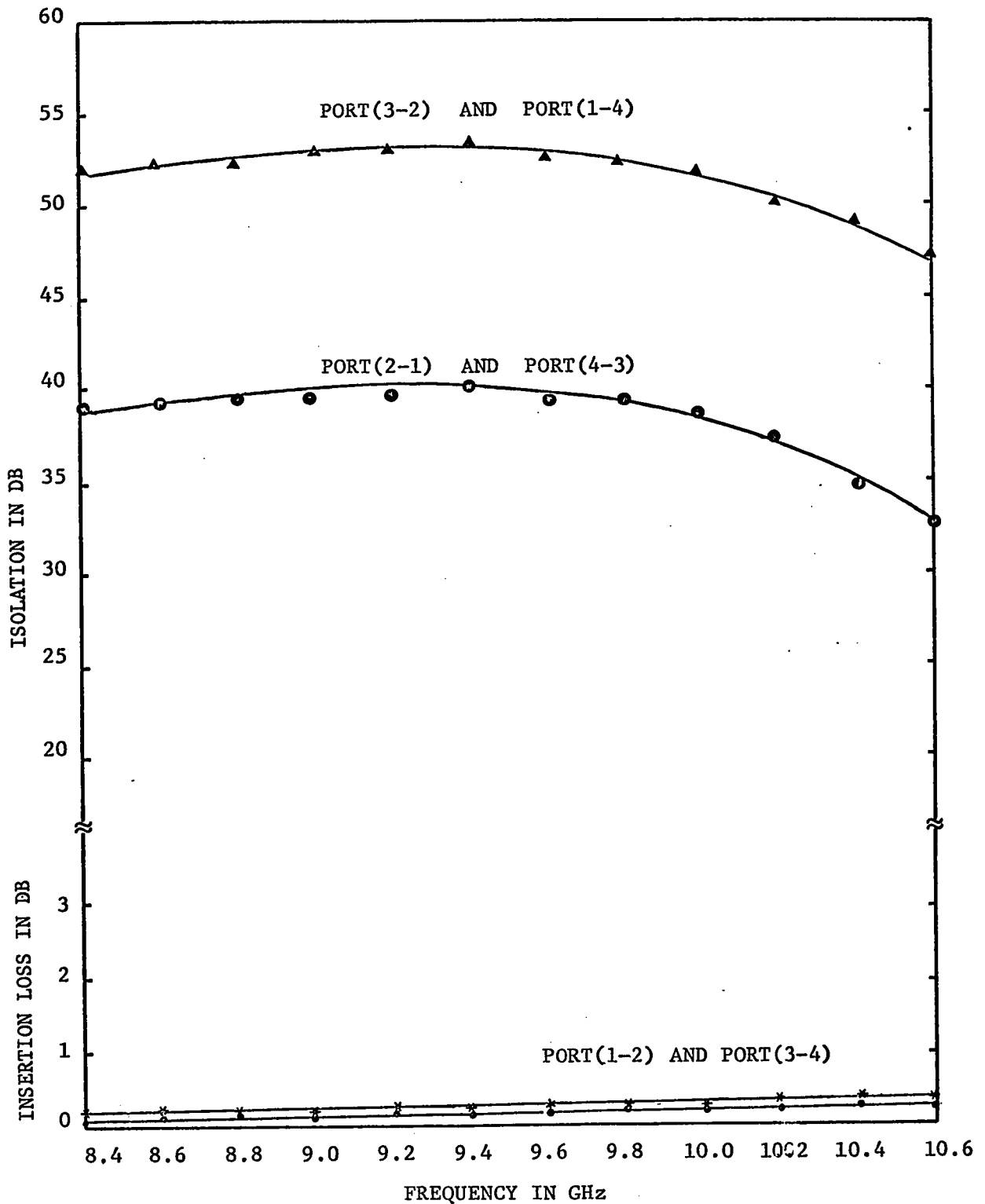


Fig.4-2 FOUR-PORT CIRCULATOR CHARACTERISTICS.

into lock at a given locking power ratio to the oscillator output. When the locking signal frequency was very far from the free-running frequency of the oscillator only two or three spectral lines were seen on the spectrum. Then the signal frequency was slowly swept from the far side of ω_0 while the locking signal power was held constant. As the frequency came close to ω_0 , complicated spectral lines were seen. In this case, the spectral line at ω_s is growing as ω_s is near to ω_0 . At a certain frequency all spectra except that at ω_s disappeared. This distinct frequency gave us the locking range.

Second, another method of measuring locking range entailed holding the signal frequency ω_s constant while its power was varied. This method is a very sensitive way to measure the end points of the locking range. The output spectra observed will be treated in the next section.

4-2-2 Output Spectra of Locked Oscillators

When no locking signal was injected, only a single line at ω_0 is present. When a locking signal at a fixed frequency ω_s was admitted to the oscillator, several spectral lines at frequencies ω_s , $\omega_s + \Delta\omega_0$, appear where $\Delta\omega_0$ is defined as in Eq. 3.81. As the power of the locking signal was increased, the following phenomena occurred as seen in the sequence of Fig.4.3:

- 1) The line at ω_s increased in amplitude.
- 2) The line which had been at ω_0 was pulled toward the line at ω_s , and decreased in amplitude.
- 3) Several other short lines appeared, these components were principally on the opposite side of the oscillator output line from the locking signal frequency.

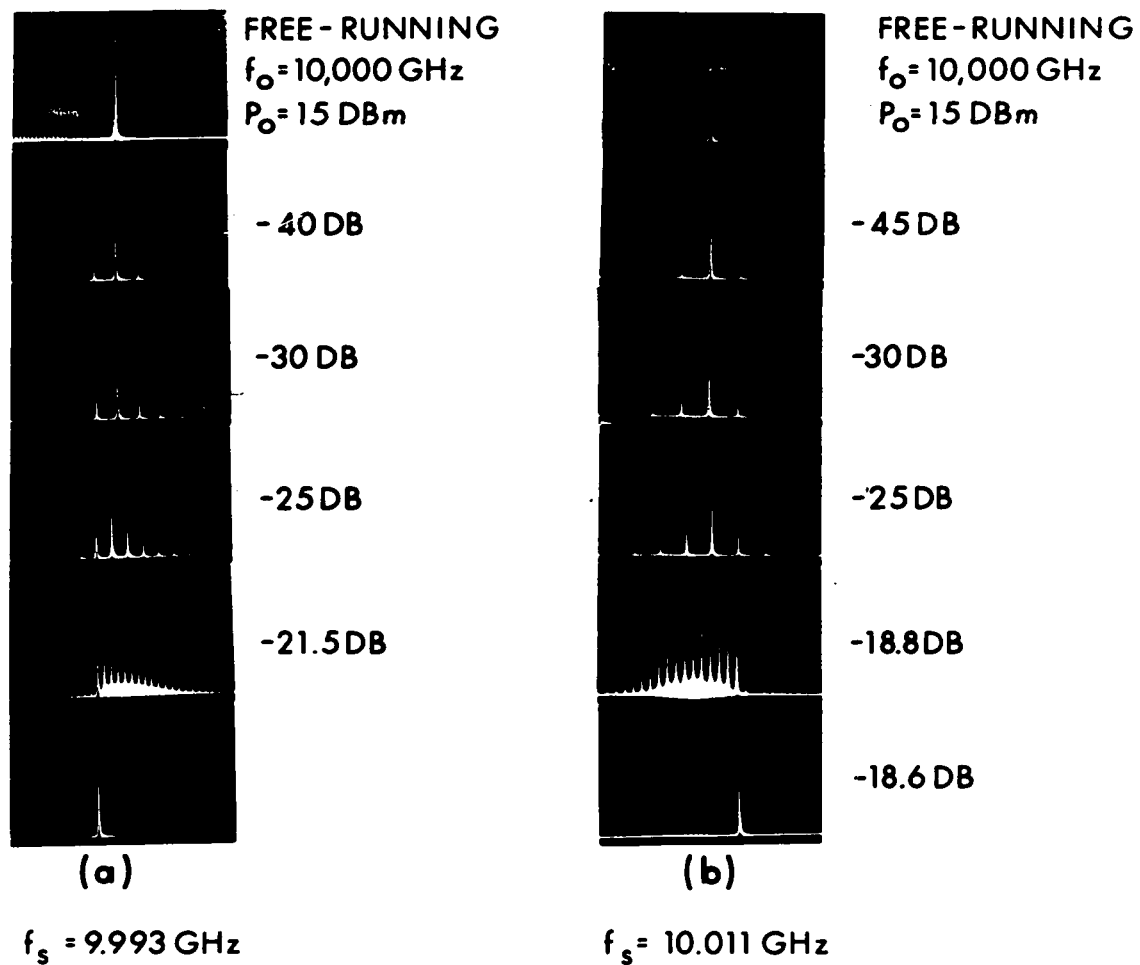


Fig. 4-3 OUTPUT SPECTRA OF THE LOCKED OSCILLATOR
 (IMPATT-SYA - 3200-1) VER.; 10 dB/div. HOR.; 10 MHz/div.

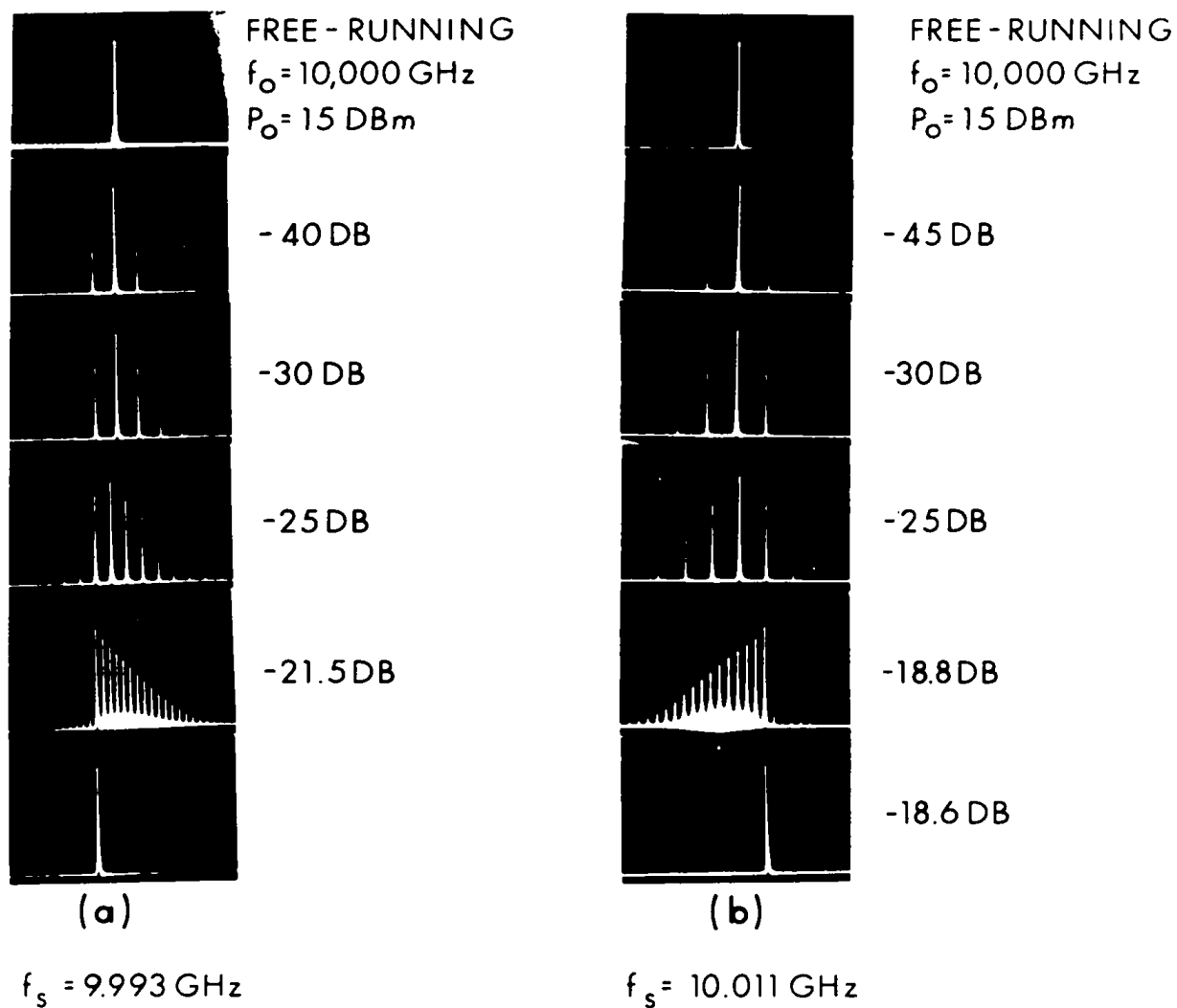


Fig. 4-3 OUTPUT SPECTRA OF THE LOCKED OSCILLATOR
 (IMPATT-SYA-3200-1) VER.; 10dB/div. HOR.; 10MHz/div.

- 4) As locking power level was increased further, the beat-note frequency continued to decrease toward zero, the amplitude of the line at the modified oscillation frequency continued to diminish in size, and the amplitude of the spectral line at ω_s continued to grow.
- 5) As the locking power was increased still further, the line at ω_s became almost as large as the free-running oscillator output line had been. The components other than the locking signal became very small in amplitude but were crowded together in frequency.
- 6) As the locking signal power was increased still more, all of the lines except the one at ω_s suddenly disappeared at a very sharp and distinct point. The output power at ω_s was still essentially equal to the free-running oscillator power; the locking signal power at ω_s was still much less than the oscillator output power. These properties are in good agreement with theories developed in chapter 3.

Fig.4.4 shows plots of measured beat frequency $\overline{\Delta\omega_b}$ as a function of the initial difference frequency at a given power ratio, which are in excellent agreement with the theoretical curve of Fig.3.20.

4-2-3 Locking Range Variation with Power Ratio

Fig.4.5 shows the measured upper side locking range as a function of maximum initial frequency difference. It is seen that the locking power needed to injection phase-lock increased at the rate of 20 dB/decade of the locking range, which is derived from the theory of Eq. 3.39, in case of small locking power. However, as the locking power increases, the locking range is no longer proportional to the ratio between the locking signal and the oscillator output voltage waves (see Eq.3.47). In addition, the oscillator circuit parameters, including the coupling parameter at the oscillator output port, became a function of frequency

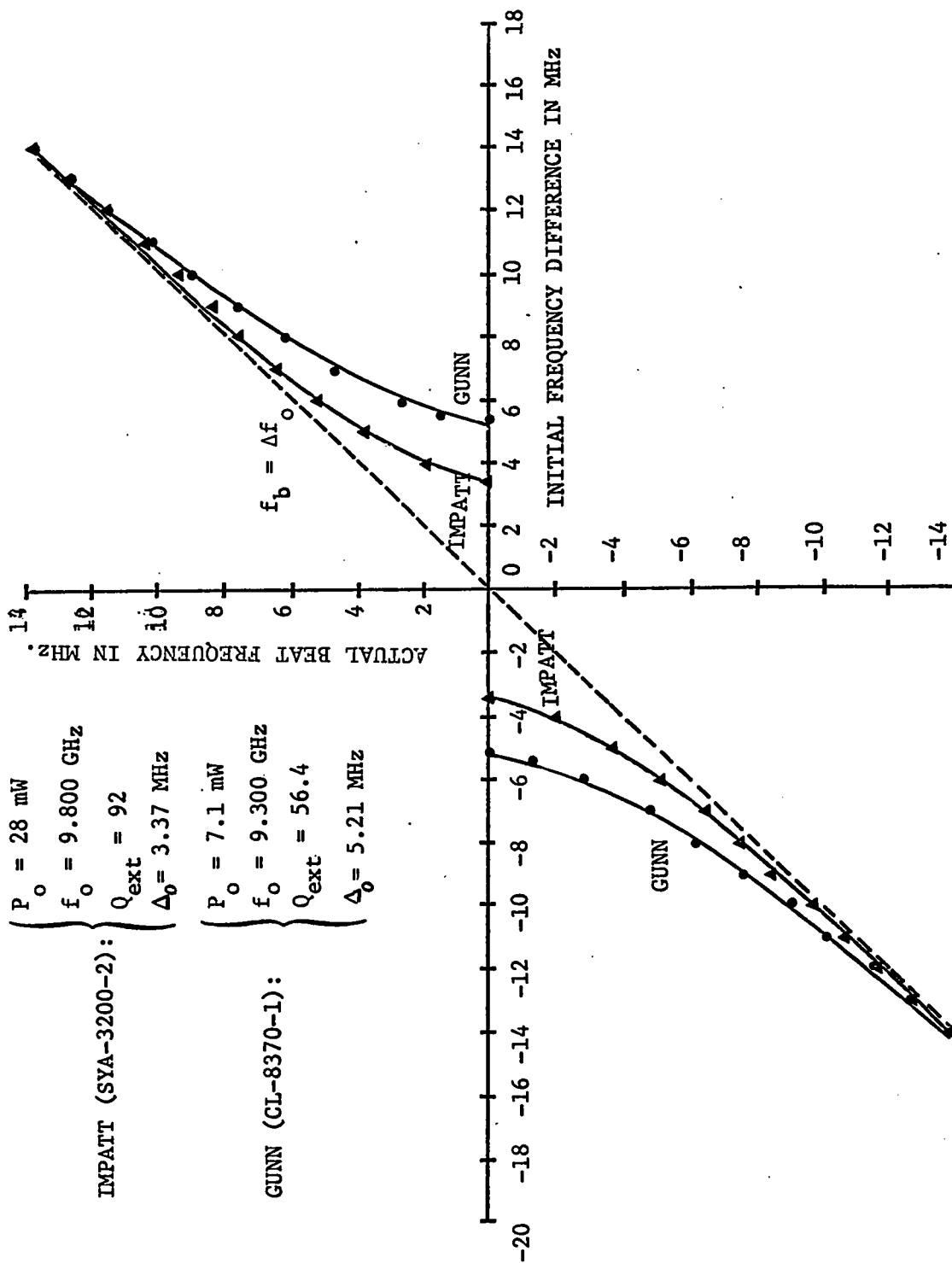


Fig. 4-4 BEAT FREQUENCIES VS. INITIAL FREQUENCY DIFFERENCE

over the broad locking bandwidth. Assuming frequency independent parameters, the locking range increases much faster with large injected power than is the case for small locking power, in accordance with Eq. 3.47. In Fig.4.5, for a given locking range, the IMPATT diode oscillator is injection phase-locked at higher locking powers than the Gunn diode oscillator. The typical IMPATT diode oscillator (SYA-3200) had a locking range of 10 MHz when the locking signal was 20.2 dB below the oscillator output while the typical Gunn diode (CL-8370) had a locking range of the same value as the IMPATT when the locking signal was 25.0 dB below the oscillator output.

As seen in Fig.4.2, the reflections from the circulator port-2 may be comparable with the locking power when the power gain is higher than 45 dB. As a result, data taken with a very small locking signal (power gain 45 dB) are considered to be less reliable points.

As predicted from the theory, the experimental points are in good agreement with the theoretical straight line.

The same diode, when tuned to different frequencies, had the same locking range properties.

Experimental data were taken for some other free-running frequencies by inserting a tuning screw. The locking range properties were much the same for all of those cases. This means that the locking figure of merit is an inherent parameter of the locked oscillator. The locking range characteristic will be solved by considering the locking figure of merit.

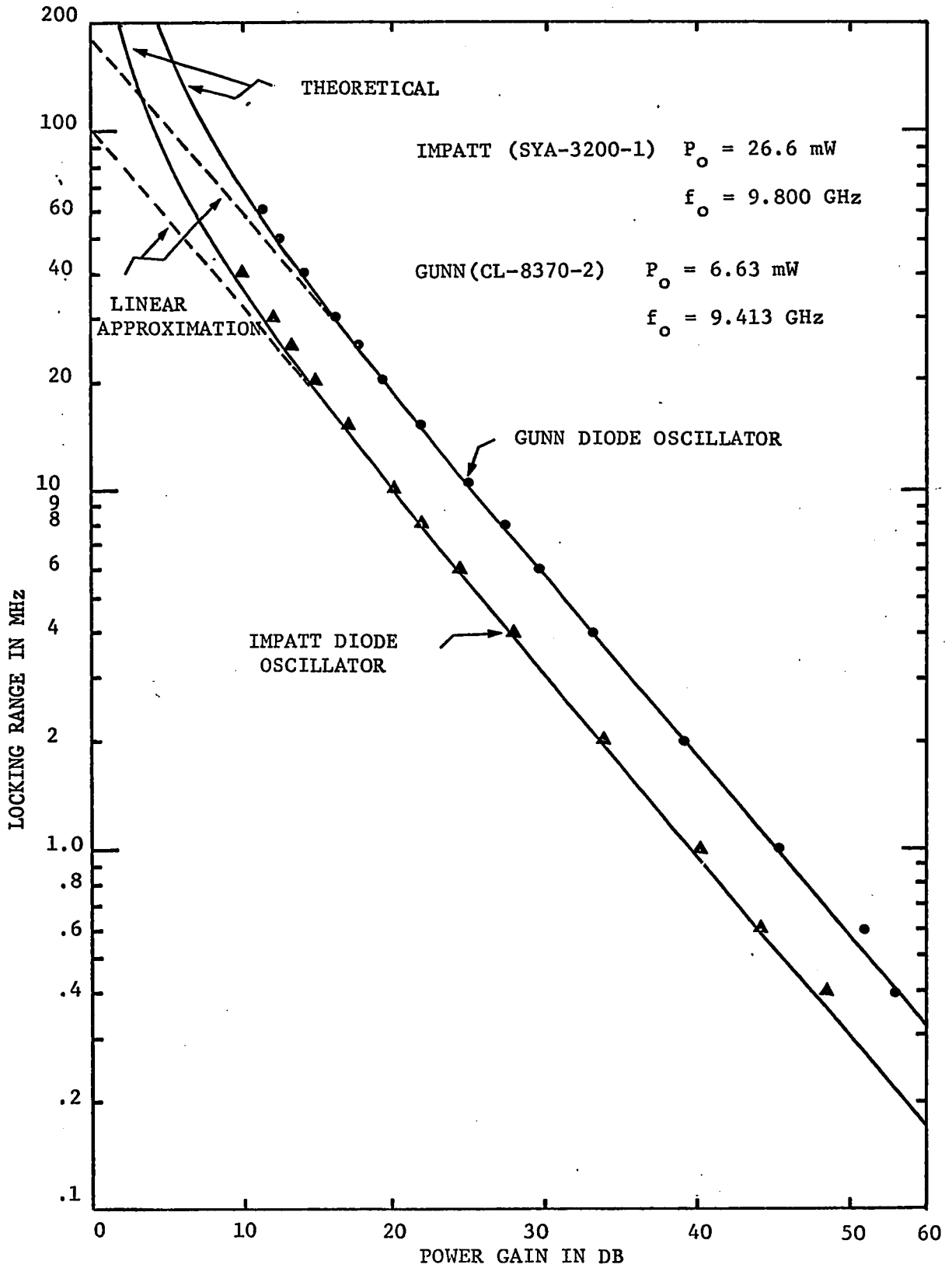


Fig.4-5 LOCKING RANGE AS A FUNCTION OF POWER GAIN.

4-2 -4 Oscillator Quality Factor Derived from Locking Bandwidth

It was shown in Chapter III that the normalized locking bandwidth is proportional to the ratio of the locking power to the oscillator output power. Therefore, the locking figure of merit can be calculated by measuring the locking range, the free-running frequency, the locking power, and the oscillator output power, independently, and by using Eq. 3.54. Accordingly, the external Q of the oscillator can be obtained by

$$Q_{\text{ext}} = \frac{2}{\eta} \quad (4.1)$$

As seen in Fig.4.5, typical values of the locking figure of merit are:

$\eta = 0.0204$ for the IMPATT diode oscillator and

$\eta = 0.0382$ for the Gunn diode oscillator.

Therefore, typical values of the external Q are:

$Q_{\text{ext}} = 98.1$ for the IMPATT diode oscillator and

$Q_{\text{ext}} = 52.3$ for the Gunn diode oscillator.

Table 4-3 shows the values of locking figure of merits tested. From Tables 4-1, 4-2, and 4-3, it may be seen that the better the RF power (efficiency) is matched from the diode circuit to the external load circuit, the better the external locking signal matches into the diode.

The values of the external Q will be compared to those measured in an experiment, in which the "real" load admittance was varied, described in the next section.

4-2-5 Interpretation of the Locking Signal Effect as the Change in Load Admittance

The oscillator was coupled to a length of wave-guide of appropriate admittance and facilities were provided for measuring the frequency and power transmitted along it.

In order to interpret the locking signal's effect on the oscillator, we inserted an adjustable post, mounted on a movable carriage, which penetrates a short distance into the wave-guide so as to give rise to a reflected wave whose phase at the oscillator depends on a position of the post along the wave-guide. The reflection coefficient $|\Gamma|$ of the post was moved along the line while frequency as well as output power were measured. For each given value of the reflection coefficient, the maximum change in frequency was observed. From these results, Fig.4.6 was obtained, where the return loss in dB calculated from the measured reflection coefficient is equivalent to the power gain in dB;

$$20 \log \frac{1}{|\Gamma|} = 10 \log \frac{P_i}{P_s} \quad (4.2)$$

Therefore, it is very easy to experimentally interpret the locking signal's effect on the oscillator as a change in load admittance presented to the oscillator, as shown in Fig.4.6.

In addition, the external Q of the oscillator was also measured from the maximum frequency change and from the reflection coefficient due to a change in load admittance:

$$Q_{\text{ext}} = |\Gamma| \frac{\omega_0}{\Delta_0} \quad (4.3)$$

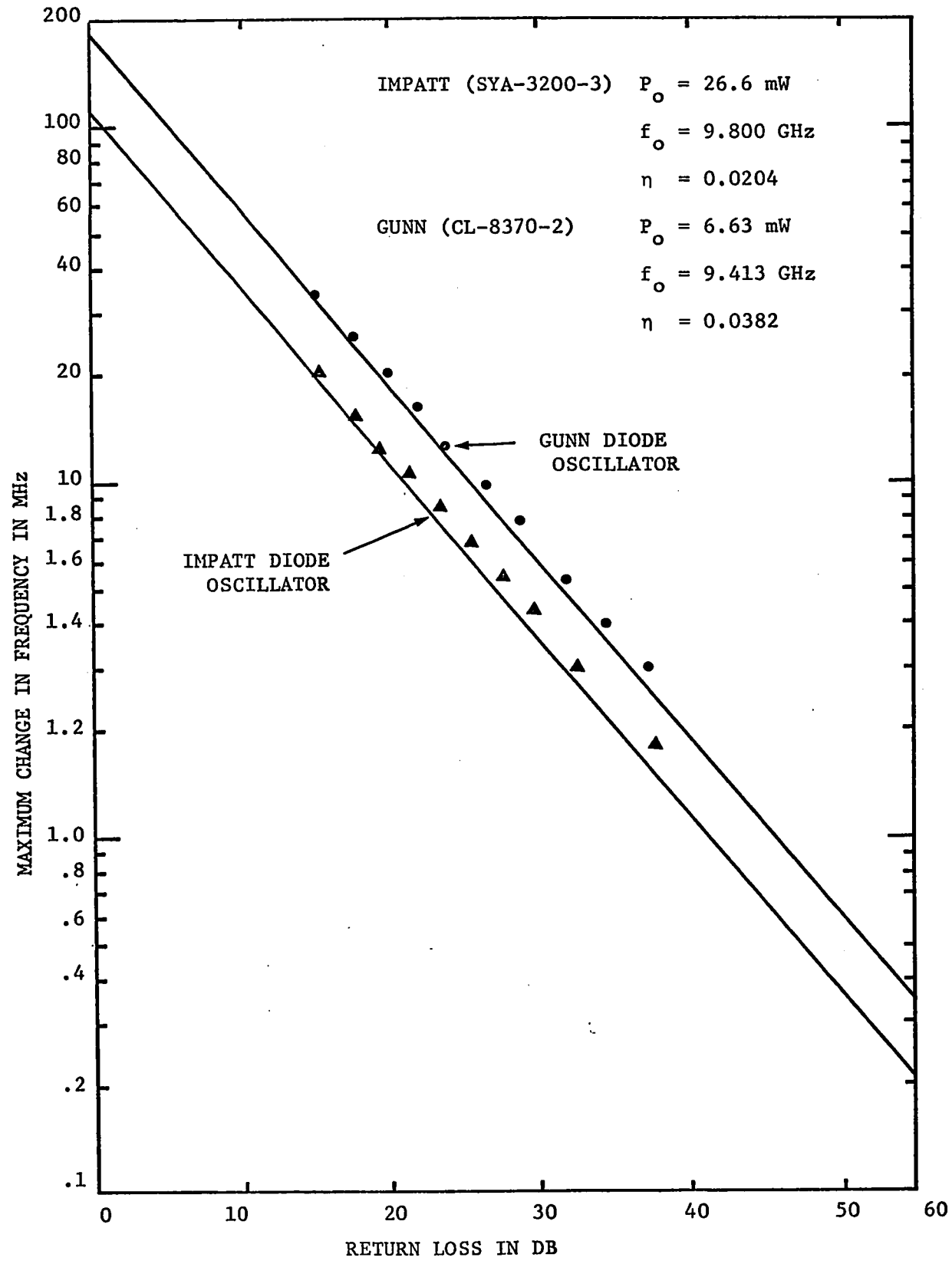


Fig.4-6 MAXIMUM CHANGE IN FREQUENCY WITH RETURN LOSS OF LOAD.

which is equivalent to Eq. 3.39 and Eq. 3.51. The values are very close to those obtained in section 4-2-3.

Table 3. LOCKING PERFORMANCE

OSCILLATOR	LOCKING FIGURE OF MERIT	EXTERNAL Q
SYA-3200-1	0.0204	98.1
SYA-3200-2	0.0217	92.0
SYA-3200-3	0.0170	117.8
SYA-3200-4	0.0211	95.0
CL-8370-1	0.0397	50.4
CL-8370-2	0.0382	52.3
CL-8370-3	0.0392	51.0
CL-8370-4	0.0378	53.0

On the other hand, let us consider the locked operation of an oscillator. When the locking signal is applied, the oscillator shifts frequency from the free-running frequency to the locking signal. Since the DC current condition has remained fixed, the operation point of the oscillator on the loading diagram has to be shifted to a new frequency line, when the reflection coefficient has a value of greater than zero. This value of reflection coefficient has been given in Eq. 3.16. This change of reflection coefficient reveals the mechanism of oscillator synchronization; when locking to an external signal, the oscillator assumes a phase and power output for which the resulting reflection

coefficient specifies the frequency of operation, which is equal to that of the external signal. As the frequency of the external signal is changed, accordingly, the reflection coefficient varies in a manner determined by the load characteristic of the oscillator. Therefore, the effect of the locking signal can be interpreted as a change in the load admittance presented to the oscillator. As a result, an analysis of this type is applicable to any microwave oscillator.

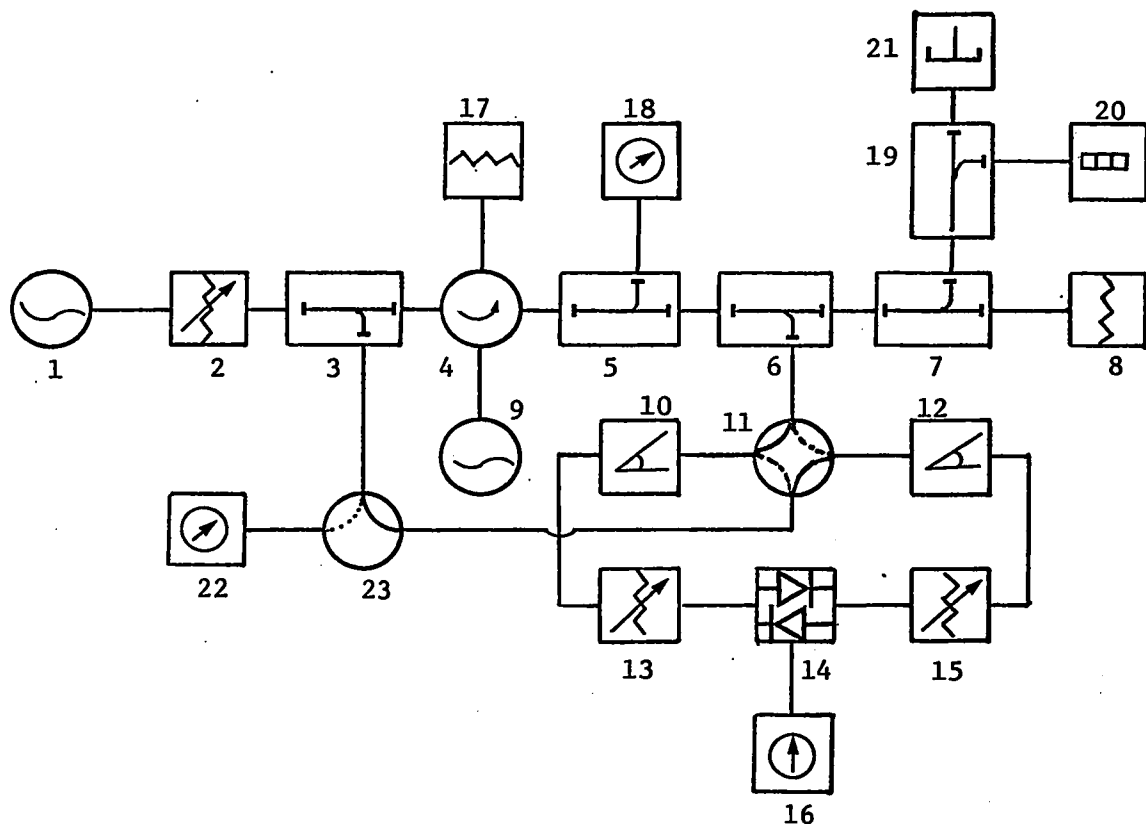
4-3 Measurement of Phase Angle Difference between the Locked Oscillator and the Locking Signal

4-3-1 Description of Experimental Setup Employing a Sensitive Microwave Phase Detector

The experimental setup for measuring the phase angle between two signals is shown in Fig.4.7. A sensitive microwave phase detector is added to the setup in Fig. 4.1.

A phase detector⁵²⁻⁵⁹ consisting of two diode detectors fed from a hybrid junction (a magic tee) was used. The two diodes are mounted in the coplanar arms, and connected in series-opposition. A centered-zero dc null meter was connected to the balanced detectors.

The stabilized locking signal and the locked output are each monitored by a suitable directional coupler; these are connected to a magic tee phase sensitive detector system. We can compensate for any phase shift caused by nonequal transmission line lengths by means of an adjustable phase shifter. It is desirable that the amplitudes of two signals fed to the square law detectors are set equal by means of variable attenuators. The operation of the microwave phase detector is



LEGEND

- | | | | |
|----|---------------------------|----|---------------------------|
| 1 | LOCKING SIGNAL OSCILLATOR | 13 | PRECISION ATTENUATOR |
| 2 | PRECISION ATTENUATOR | 14 | BALANCED PHASE DETECTOR |
| 3 | 10 DB DIRECTIONAL COUPLER | 15 | PRECISION ATTENUATOR |
| 4 | 4-PORT CIRCULATOR | 16 | DC NULL METER |
| 5 | 20 DB DIRECTIONAL COUPLER | 17 | MATCHED TERMINATION |
| 6 | 20 DB DIRECTIONAL COUPLER | 18 | POWER METER AND BOLOMETER |
| 7 | 20 DB DIRECTIONAL COUPLER | 19 | 3DB DIRECTIONAL COUPLER |
| 8 | MATCHED TERMINATION | 20 | FREQUENCY COUNTER |
| 9 | LOCKED OSCILLATOR | 21 | SPECTRUM ANALYZER |
| 10 | PRECISION PHASE SHIFTER | 22 | POWER METER AND BOLOMETER |
| 11 | WAVEGUIDE SWITCH | 23 | WAVEGUIDE SWITCH |
| 12 | PRECISION PHASE SHIFTER | | |

Fig.4-7 EXPERIMENTAL SETUP FOR MEASURING STEADY-STATE PHASE ANGLE

treated in Appendix-D. The detector output is a sinusoidal function of phase difference between the two inputs.

When the locking signal is exactly out-of-phase with the locked oscillator output, the output of the detector reaches a null. When the phase of the locked oscillator output changes, the balance which produces the null is upset. Since this null balance was found to be very sharp and since the transmission lines of the two channels have frequency-dependent characteristics, the balance has to be recalibrated for every different measurement.

4-3-2 Phase Angle Variation with Initial Frequency Difference

Fig. 4.8 and Fig. 4.9 show how the steady-state phase angles of locked oscillators vary with the initial frequency difference for given locking power ratios and it may be seen that the experimental measurements are in excellent agreement with theory for the high gain cases.

During the experiment, it was sometimes difficult to maintain a balance; the oscillator tended to jump inward, out of lock, at the locking boundary. Consequently, the experimental points near the locking boundary tend to have an uncertainty, as seen in the figures.

Because the null balance depends upon the amplitude and frequency of both the locked oscillator and of the locking signal, its stability demonstrates the degree of stability in amplitude and frequency of both the locked oscillator and the locking oscillator. In this experiment the null balance was very good, which indicates that the amplitude and the frequency of the locked oscillator were very stable when applying a stabilized locking signal.

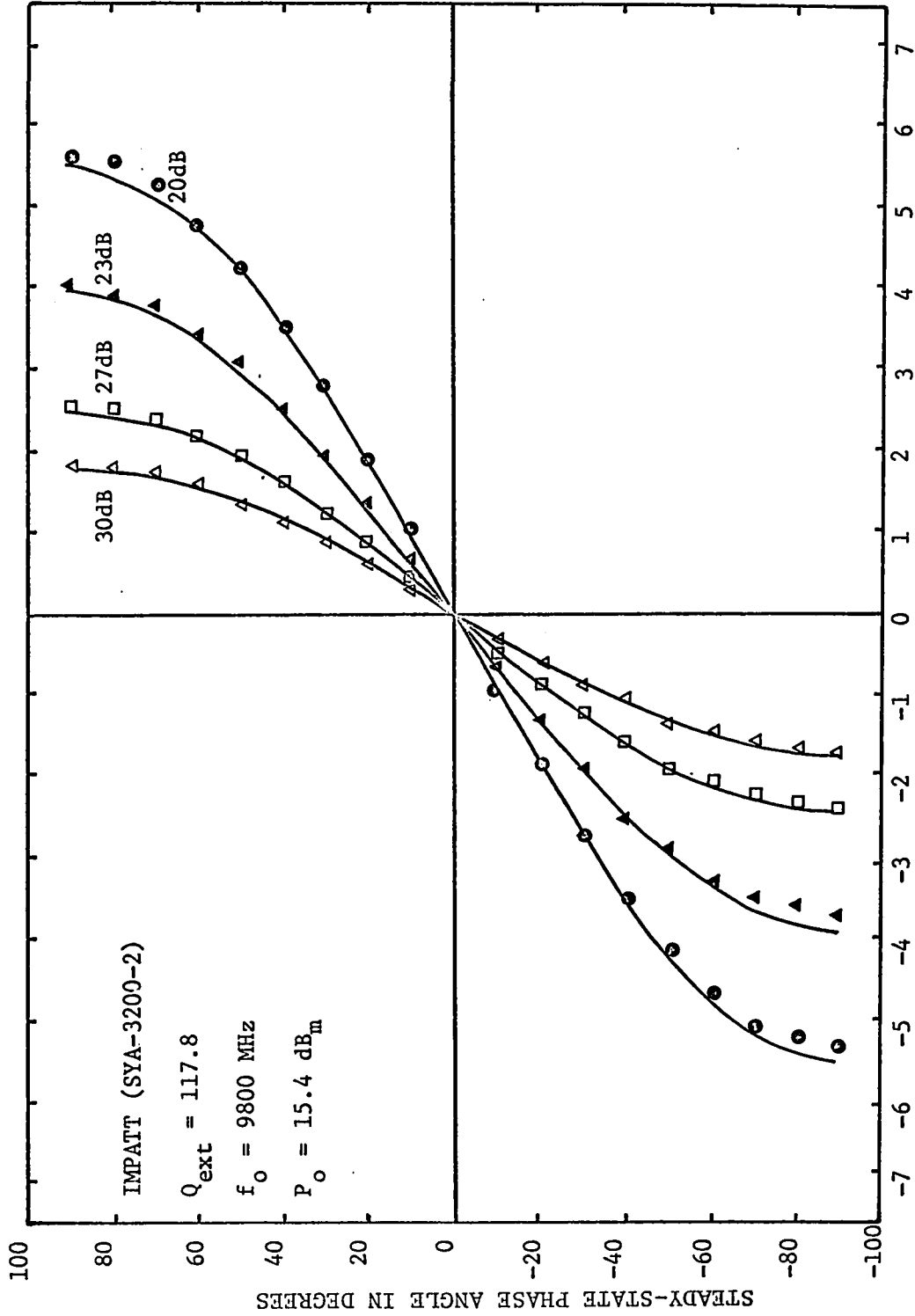


Fig.4-8 STEADY-STATE PHASE ANGLE VS. INITIAL FREQUENCY DIFFERENCE

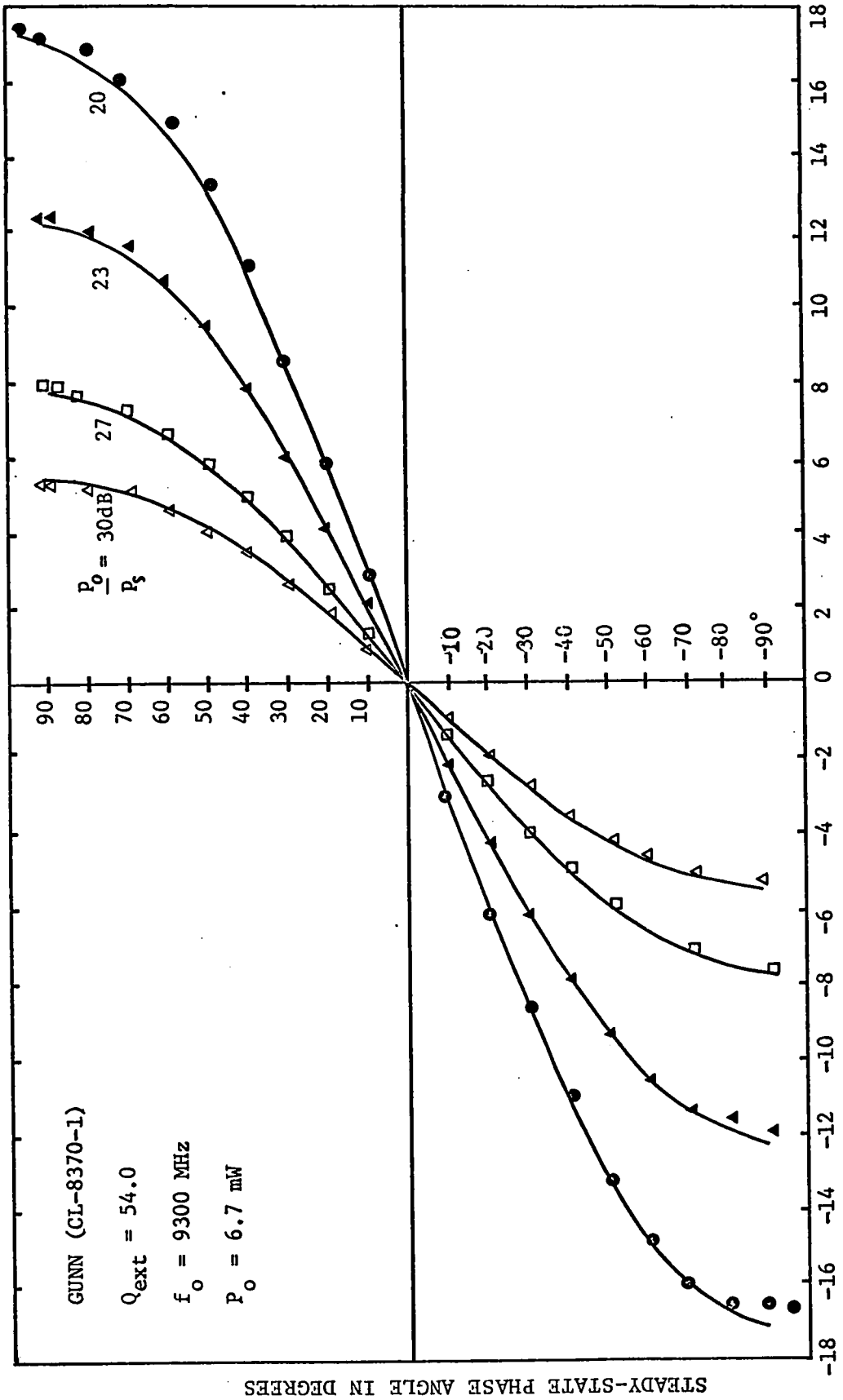


Fig.4-9 STEADY-STATE PHASE ANGLE VS. INITIAL FREQUENCY DIFFERENCE

Besides the above measurements, the phase angle between the two signals can be observed as a function of i) oscillator bias current ii) ambient temperature, and iii) the voltage applied to a varactor tuning diode or the current drive applied to YIG, coupled into the locked oscillator. Phase control by means of bias voltage or current will be treated theoretically and experimentally in Chapter V.

4-4 Injection Phase-Locked Oscillators with Relatively Large Locking Power

The theory developed in Chapter III assumes that the oscillator is characterized by an equivalent circuit with linear elements and that the reflected wave of the locking signal from the oscillator does not appreciably affect the output wave of the oscillator. However, at saturation, both the IMPATT diode oscillator and the Gunn diode oscillator are nonlinear elements^{17,60-67}. In addition, the portion of the locking signal reflected from the oscillator appreciably affects the total output power wave. In other words, the net amplitude of the two interfering signals emerging from the oscillator toward the circulator is the vector sum of the locked oscillator output and the reflected signal.

First, let us consider the van der Pol type equation with an injected current term, which describes the locked oscillator with a nonlinear conductance. The nonlinear conductance postulated is voltage-dependent, and the current through the nonlinear element may be expressed (Appendix-F) as

$$i_g = a_1 e + a_3 e^3 \quad (4.4)$$

where a_1 is the small-signal negative diode conductance and a_3 is positive constant.

As shown in Appendix-F, we can obtain, under some assumptions, solutions to the van der Pol-type circuit equation with the injected current term. From Eq. F.20, we obtain for the output voltage of the locked oscillator, when the free-running oscillator is tuned for maximum power output:

$$E^2 = E_o^2 \left(1 + \frac{E_e}{E} \cos\theta \right) \quad (4.5)$$

where E_o is the free-running optimum output obtained for the optimum load conductance, E is the locked oscillator output, E_e is the effective amplitude of the locking signal, and θ is the phase angle between the locking and locked oscillator signals.

Huntoon and Weiss⁶ have shown that the amplitude and frequency deviation of the locked oscillator are functionally related and that the maximum value of the locked oscillator amplitude can be given by

$$E = E_o + K_a E_e \quad (4.6)$$

where K_a is much less than E_o/E_e and is an amplitude change coefficient derived from the oscillator amplitude change when a small supplementary admittance is added to the original load admittance due to the injected voltage. More recently, by using the power concept, Kurokawa¹⁴ has shown that the locked oscillator output power at microwave frequencies can become larger or smaller than the free-running oscillator power and that the locked oscillator power approaches the free-running oscillator power as the locking frequency moves away from the free-running frequency.

In addition, let us take into account the effect of the reflected part of the locking signal from the reference oscillator on the total output power. Due to interference between the reflected portion of the locking signal and the locked oscillator output the total power emerging from the oscillator output line toward the circulator is modified. If the locking frequency is swept across the locking bandwidth of the oscillator there will be a minimum-and a maximum power point, respectively. From our experimental results, it has been observed that the output power from a locked oscillator may decrease or increase with an increase in locking signal, depending upon the oscillator and the operating conditions. To experimentally check this behavior, let us choose the case of constructive interference, which results in maximum power points. If the reflected part of the locking signal is taken to be the principal cause of the low locking figure of merit, we may assume that the effective locking signal voltage and the reflected locking voltage are approximately ηE_s and $(1-\eta)E_s$, respectively.

As mentioned above, let us assume that, at the maximum power point, the reflected locking signal and the generated oscillator output wave interfere constructively. As a result, the actual constructive output E_m emerging from the oscillator may then be expressed as:

$$E_m^2 = [E + (1 - \eta)E_s]^2 \quad (4.7)$$

Substitution of Eqs.4.5 and 4.6 into Eq.4.7 and first-order approximation yield, for the maximum output power P_m emerging from the oscillator,

$$P_m = P_o \left[1 + (2 - \eta) \frac{E_s}{E_o} - K_a \eta^2 \left(\frac{E_s}{E_o} \right)^2 \right] \quad (4.8)$$

If E_s is small compared to E_o , then the actual maximum power

can be approximately expressed as

$$P_m \approx P_o \left[1 + (2-\eta) \frac{E_s}{E_o} \right] \quad (4.9)$$

Figs. 4.10 and 4.11 show how the estimated maximum power compares with the measured maximum power. It is seen from the figures that the reflection hypothesis used in conjunction with the van der Pol oscillator theory appears to explain the observed amplitude variation reasonably well for the case of relatively small η .

The analysis above has been concerned only with nonlinear conductance. However, nonlinear susceptance effects are normally present also. Consequently, for practical locked oscillators, we need a better theoretical understanding and a full experimental characterization of the nonlinear behaviour to determine the variations of conductance and susceptance with amplitude.

A nonlinear susceptance study for the IMPATT diode has been published by Read¹⁷, Blue⁶², Gummel and Scharfetter⁶³, Evans and Haddad⁶⁴, and Glance⁶⁵. Nonlinear analysis of the Gunn diode has been carried out by Peterson and Knight⁶⁶.

As the locking power increases, the nonlinear susceptance effects cause the locked oscillator to have an asymmetric distribution about the free-running frequency. It has been shown experimentally that the upper side locking range is larger than its lower side counterpart for both the IMPATT and Gunn diode oscillators. It is believed that this is caused by nonlinear susceptance in the diode.

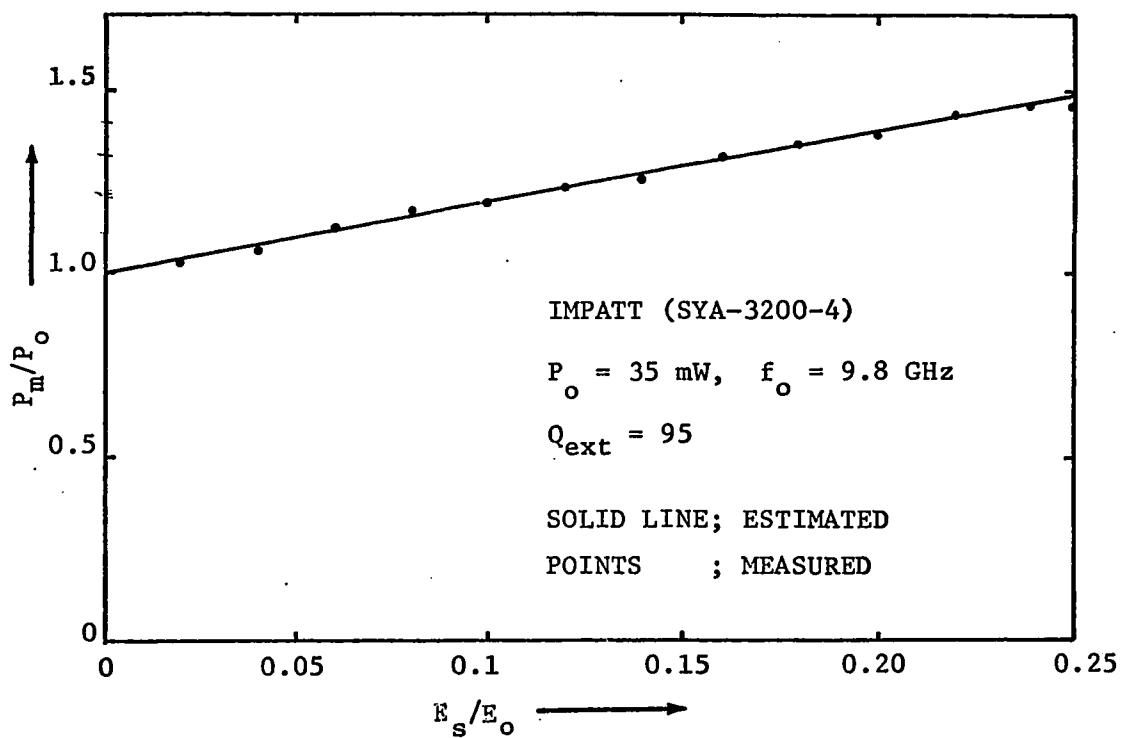


Fig.4-10 THE MAXIMUM POWER OUTPUT VS. THE VOLTAGE GAIN

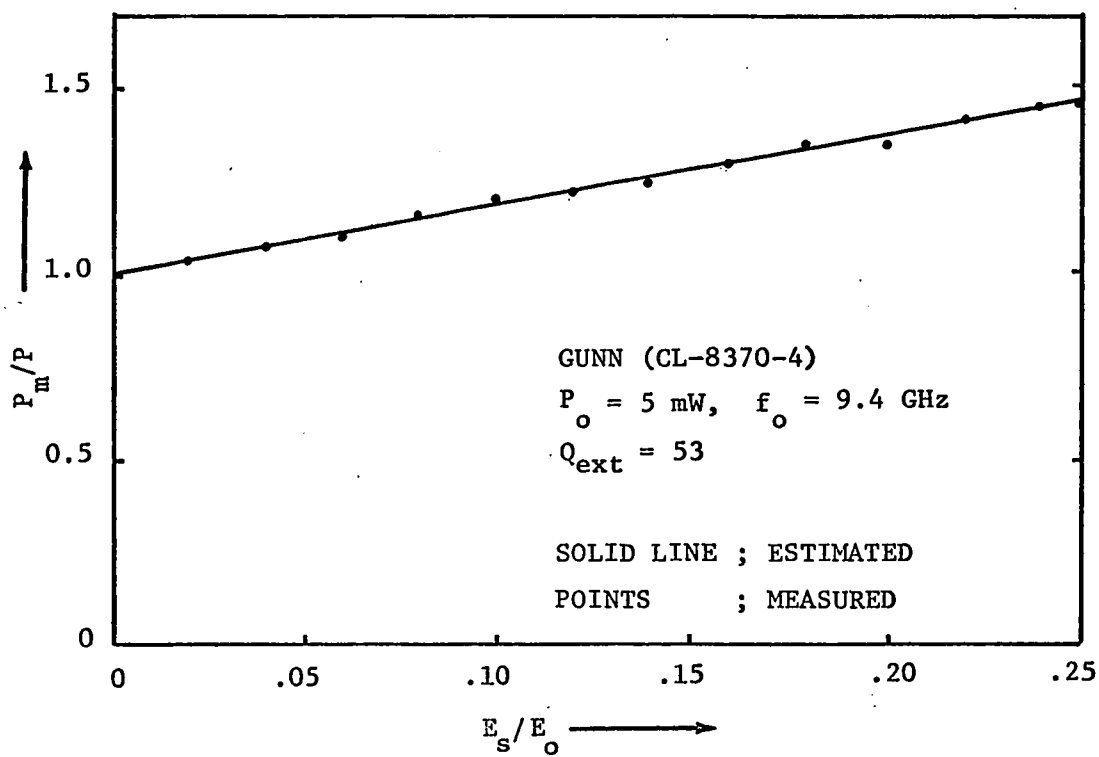
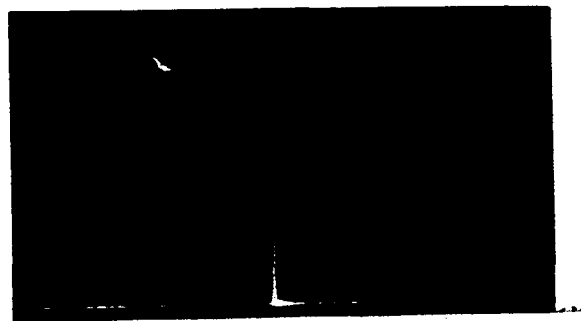
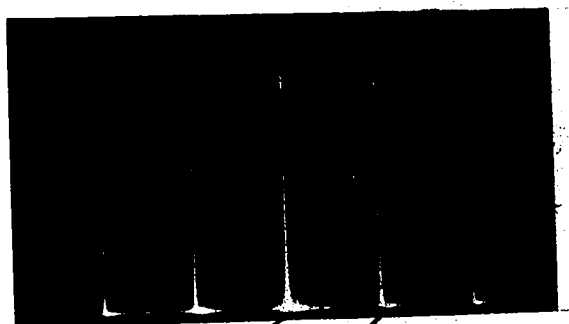


Fig.4-11 THE MAXIMUM POWER OUTPUT VS. THE VOLTAGE GAIN



$f_0 = 9.800 \text{ MHz}$

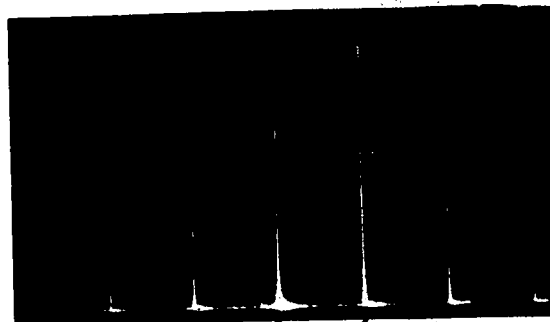
FREE-RUNNING (f_0)



$f_{S1} = 9.857 \text{ GHz}$

$f_{C1} = 9.806 \text{ GHz}$

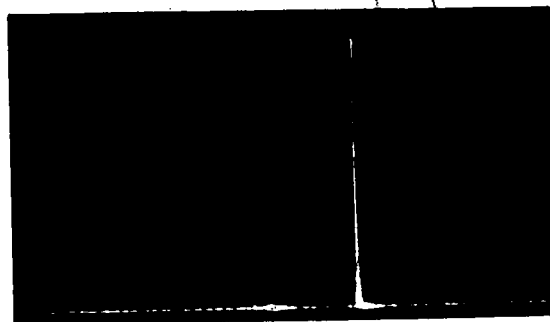
CARRIER f_{C1} DRIVER f_{S1}



$f_{S2} = 9.848 \text{ GHz}$

$f_{C2} = 9.799 \text{ GHz}$

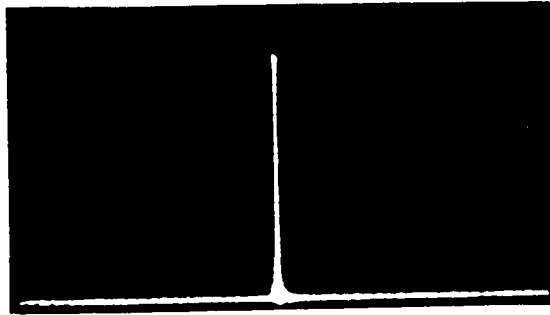
CARRIER f_{C2} DRIVER f_{S2}



$f_{S3} = 9.844 \text{ GHz}$

LOCKED (f_{S3})

Fig.4-12 FREQUENCY PUSHING FOR RELATIVELY HIGH POWER INJECTION (SYA-3200-3)
Vertical; 10 DB/div, Horizontal; 30 MHz/div.



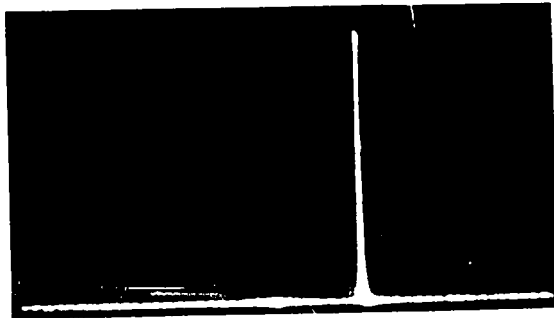
DRIVE RUNNING (0.1)



CARRIER 1.01 DRIVER 1.51



CARRIER 1.01 DRIVER 1.51



It must be mentioned that we have observed an abnormal frequency pushing phenomenon for larger frequency separations. As discussed in Section 4-2, injection phase-locking phenomena were obtained only for small frequency separations, giving the typical injection locking spectrum with sidebands and frequency pulling effects, as shown in Fig.4.3. For larger frequency separations, the carrier frequency component was pushed away from the locking frequency. In addition, as the locking frequency approached the previous free-running frequency, the carrier moved away from the locking frequency and decreased in amplitude. Fig.4.12 illustrates this phenomenon for different values of locking signal frequency. It is believed as a result that the resonant circuit is not single-tuned, as originally assumed, but multi-tuned, causing the "abnormal behaviour".

The microwave power available from solid-state sources can be significantly increased by combining^{68,69} the output powers of several devices. Particularly, it is very interesting to note that the output power of separate sources can be combined by mutual injection phase-locking in conjunction with hybrids⁷⁰⁻⁷³ for the purpose of power combining and splitting. We can utilize the good performance of injection phase-locking for stabilized microwave power.

4-5 Intermodulation Products of Injection Phase-Locked Oscillators.

This section deals with an experimental study of the intermodulation products appearing at the output of the locked oscillator.

In order to know what performance of input noise the injection phase-locking provides, we can see the effect that the noise in the locking source has on the intermodulation products of the locked oscillators. We

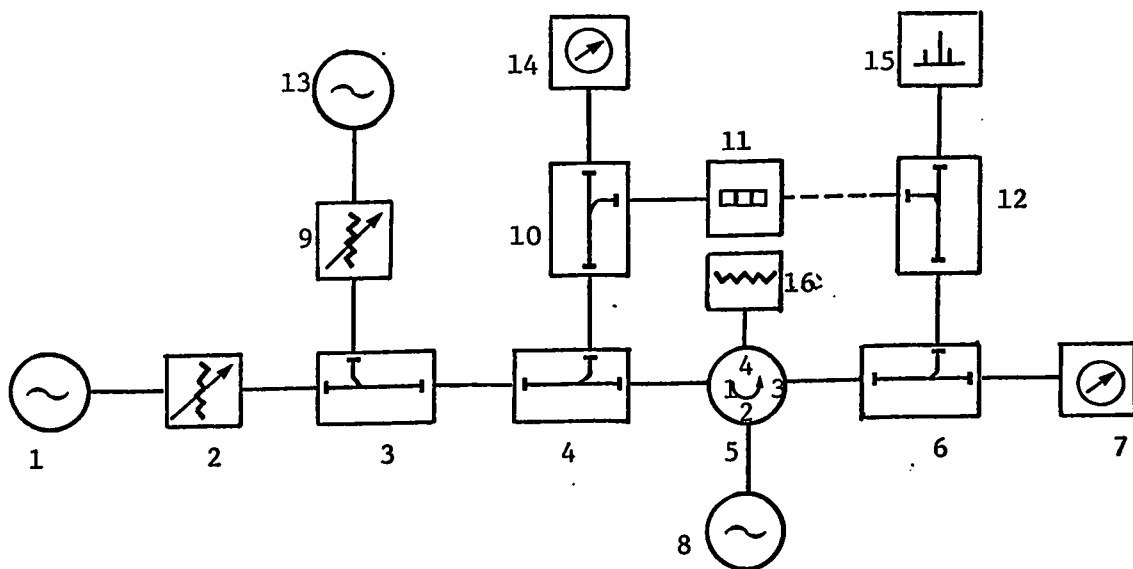
may simplify the discussion by taking interfering signal component combining it with a desired locking signal, and observing the effect on the output of the locked oscillator. Since random noise consists of almost equal amplitudes, we can even select one of these for our single noise-frequency component.

4-5-1 Experimental Arrangement

The experimental setup used to measure the intermodulation products is shown in Fig.4.13. Two input locking sources are fed into the oscillator through directional couplers and attenuators. With the different signal sources set at the desired level, the output of the system is displayed on a spectrum analyzer and is searched for various frequency components. The spectrum analyzer is calibrated for various frequencies within the bandwidth. By use of the calibration curve, the output amplitudes are recorded for different frequency and amplitude combinations.

4-5-2 Effect of Interfering Signal on Desired Signal

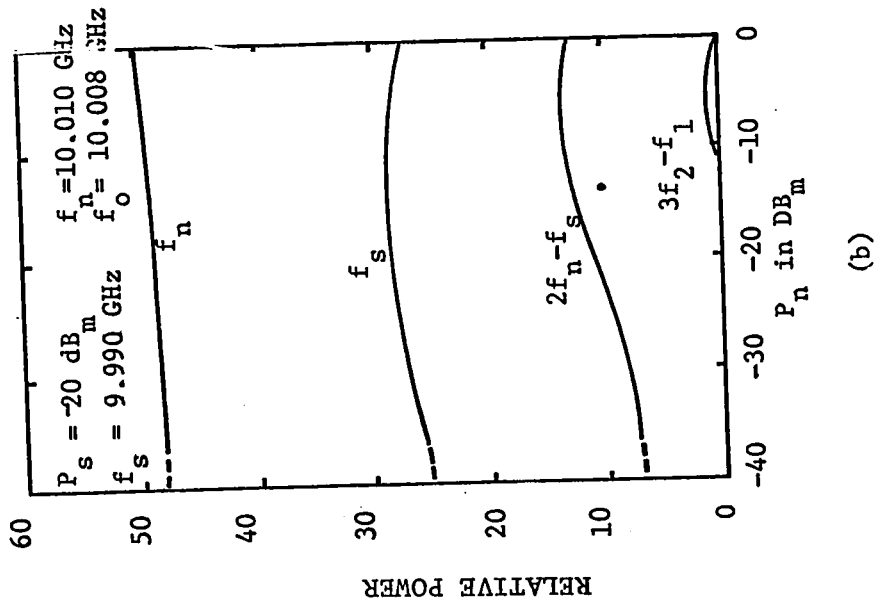
Some typical results are plotted in Figs.4.14 and 4.15. The relative power levels of the various components of the products are plotted as a function of the power level of the interfering input signal. In Fig.4.14 the results of a two-input signal consisting of the interfering signal and the desired signal are presented. For the case of Fig.14(a) since the interfering signal frequency ω_n is far removed from the free-running frequency ω_o and since the desired signal frequency ω_s is close enough to ω_o , the oscillator is locked to ω_s . Let us increase the relative power of the interfering signal from low value to 0 dB_m which is considered sufficient power for locking to occur. In the output signal of the locked



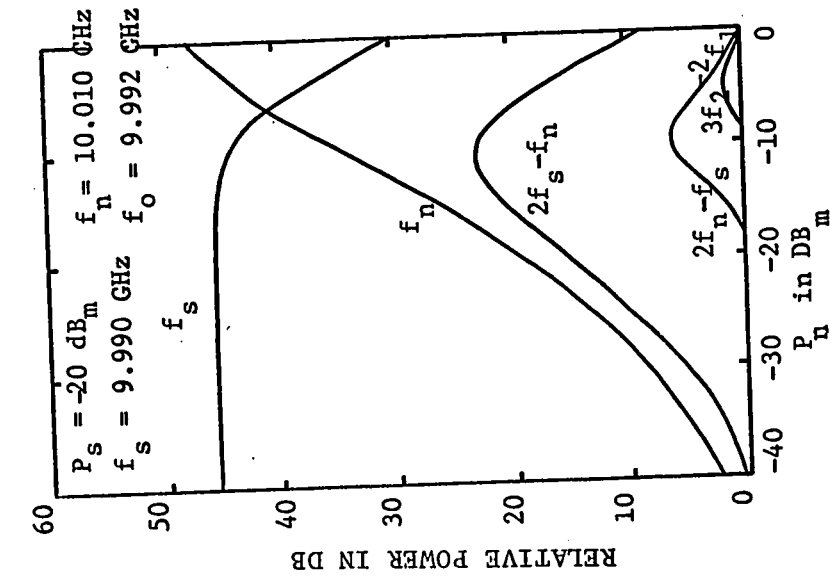
LEGEND

- | | | | |
|---|---------------------------|----|-------------------------|
| 1 | LOCKING SIGNAL OSCILLATOR | 9 | PRECISION ATTENUATOR |
| 2 | PRECISION ATTENUATOR | 10 | 3 DB COUPLER |
| 3 | 10 DB DIRECTIONAL COUPLER | 11 | FREQUENCY COUNTER |
| 4 | 20 DB DIRECTIONAL COUPLER | 12 | 3 DB COUPLER |
| 5 | FOUR-PORT CIRCULATOR | 13 | LOCKING OSCILLATOR |
| 6 | 20 DB DIRECTIONAL COUPLER | 14 | POWER METER & BOLOMETER |
| 7 | POWER METER & BOLOMETER | 15 | SPECTRUM ANALYZER |
| 8 | LOCKED OSCILLATOR | 16 | DUMMY LOAD |

Fig.4-13 EXPERIMENTAL SETUP FOR MEASURING INTERMODULATION PRODUCTS OF LOCKED OSCILLATORS



(a)



(b)

Fig. 4-14 RELATIVE OUTPUT POWERS AT VARIOUS FREQUENCIES OF THE INTERMODULATION PRODUCTS OF AN IMPACT DIODE OSCILLATOR (SYA-3200-4) FOR TWO-INPUT CASE.

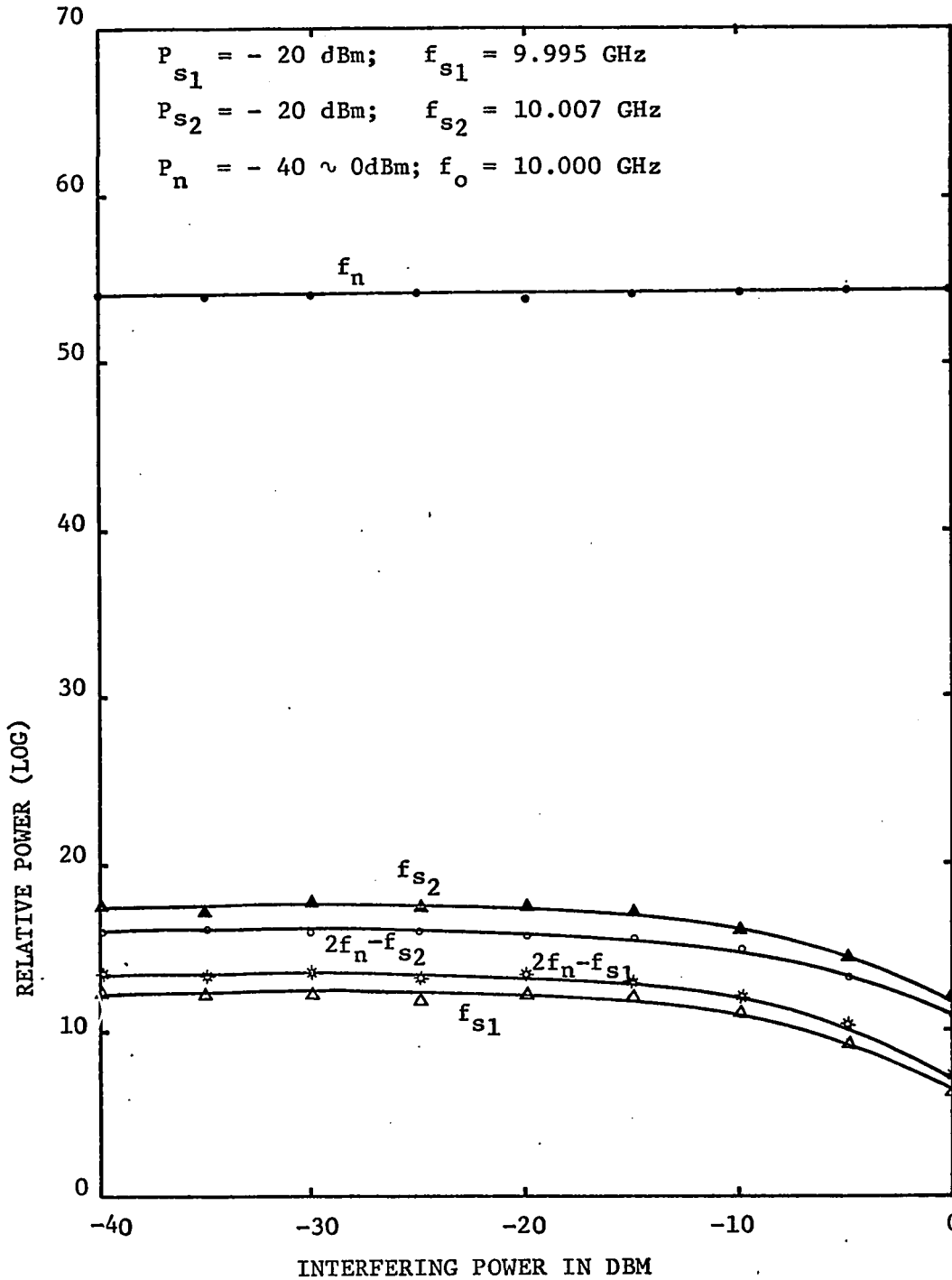


Fig.4-15 RELATIVE AMPLITUDES OF THE OUTPUT POWERS AT VARIOUS FREQUENCIES OF THE INTERMODULATION PRODUCTS OF AN IMPATT DIODE OSCILLATOR (SYA-3200-4) FOR THREE-INPUT CASE

oscillator, the interfering signal level is below the level of the desired signal and most power resides at ω_s . This means that noise far away from the carrier frequency is actually attenuated by injection phase-locking. On the other hand, since the desired signal of Fig.4.14(b) is far from ω_o and since ω_n is very close to ω_o , the oscillator is locked to ω_n and most of the output power resides at ω_n . As a result the interfering signal component of the output is predominant. This means that noise near the carrier is unattenuated. These experimental results agree with the theory discussed in section 3-4.

It is also interesting to note the decrease in power of the desired signal at ω_s as the power of the interfering signal at ω_n is increased, which means a loss in gain of desired signal when a high level interfering signal is presented. $2f_n - f_s$, $2f_s - f_n$, $4f_s - 3f_n$, and $4f_n - 3f_s$ also appear in the output due to the higher order terms of nonlinearity.

Fig.4.15 shows the results of a three-input case. Here two inputs f_{s1} and f_{s2} are kept constant while an interfering signal at ω_n is varied in power level. The interfering signal frequency ω_n is set to almost coincide with ω_o , so the oscillator is locked to ω_n and most of the output power resides at this frequency. This explains the same property as discussed before.

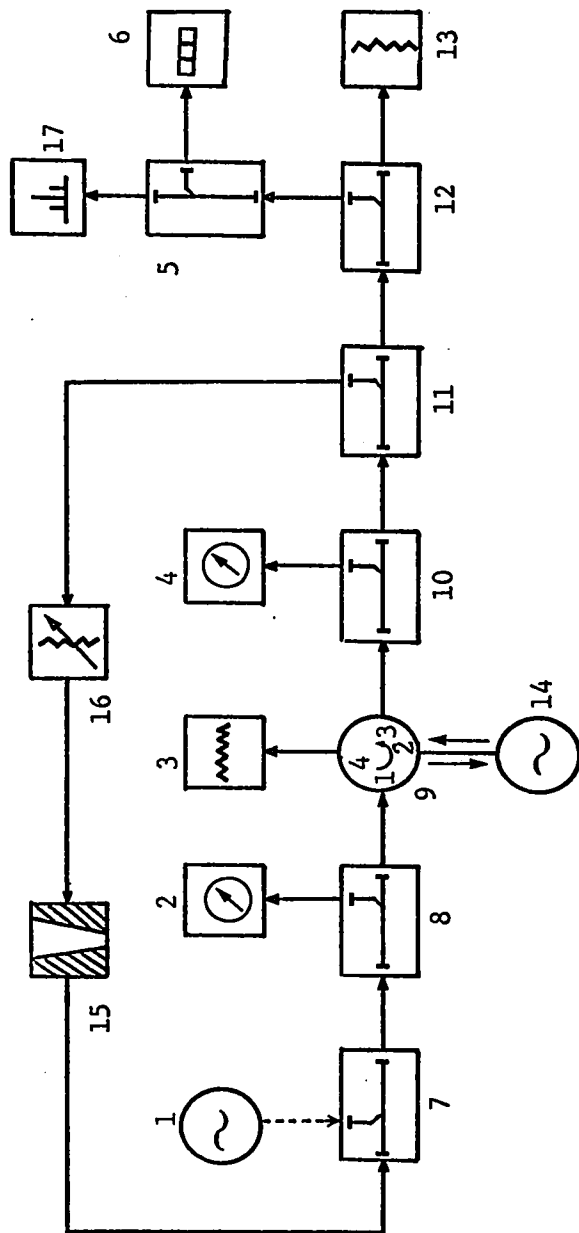
4-6 Self Injection Phase Locking

Frequency stabilization of a self-excited oscillator can be obtained by means of an external resonant circuit⁵⁴⁻⁵⁷, by impressing a small portion of the oscillator output back upon the oscillator through

a high Q resonator tuned to the desired frequency. Self injection phase-locking can be used for desirable purpose.

Fig.4.16 shows the experimental setup of the self-injected oscillator. A part of the output power can be coupled by means of a directional coupler and fed back to the oscillator through a high Q transmission cavity. The output power can be measured by means of a directional coupler and a power meter at circulator output port 3. The feedback ratio is controlled by a precision attenuator. The frequency and the spectrum of the output of the oscillator are monitored by a frequency counter and a spectrum analyzer, respectively, as seen in Fig.4.16. The power fed through the high Q cavity serves as the locking signal. The noise component of this feedback signal is greatly diminished by passing the signal through the cavity. As a result, this self-injection locking can provide a considerable noise reduction or frequency stabilization.

A change in frequency of operation is produced either by a change in electronic susceptance or by tuning of the resonant cavity. If the oscillator frequency is tuned slightly off the frequency of the stabilizing resonator, the resonator susceptance takes on such a large value that the frequency pulling resulting from this susceptance pulls the frequency of the oscillator back to the resonator frequency. Consequently, variation of the oscillation frequency with bias current, under condition of self-injection back to the oscillator, will demonstrate properties of these locked oscillators. Fig.4.17 shows the frequency variation of a self-injection locked IMPATT diode oscillator with dc bias current. It is clearly seen from Fig.4.17 that the oscillation frequency does not vary appreciably with bias current.



LEGEND

- | | | | |
|---|---------------------------|----|---------------------------|
| 1 | LOCKING SIGNAL | 9 | FOUR-PORT CIRCULATOR |
| 2 | POWER-METER & BOLOMETER | 10 | 20 DB DIRECTIONAL COUPLER |
| 3 | MATCHED TERMINATION | 11 | 10 DB DIRECTIONAL COUPLER |
| 4 | POWER METER & BOLOMETER | 12 | 20 DB DIRECTIONAL COUPLER |
| 5 | 3 DB DIRECTIONAL COUPLER | 13 | MATCHED TERMINATION |
| 6 | FREQUENCY COUNTER | 14 | LOCKED OSCILLATOR |
| 7 | 10 DB DIRECTIONAL COUPLER | 15 | HIGH Q CAVITY |
| 8 | 20 DB DIRECTIONAL COUPLER | 16 | PRECISION ATTENUATOR |
| | | 17 | SPECTRUM ANALYZER |

Fig. 4-16 EXPERIMENTAL SETUP OF THE SELF-INJECTION-LOCKED OSCILLATOR

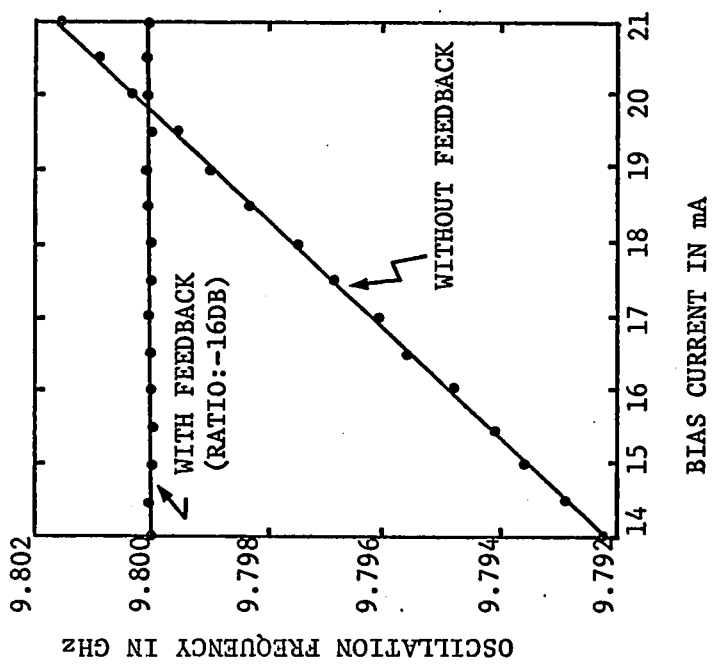


Fig.4-17 OSCILLATION CHARACTERISTICS OF AN IMPATT DIODE OSCILLATOR (SYA-3200-4)

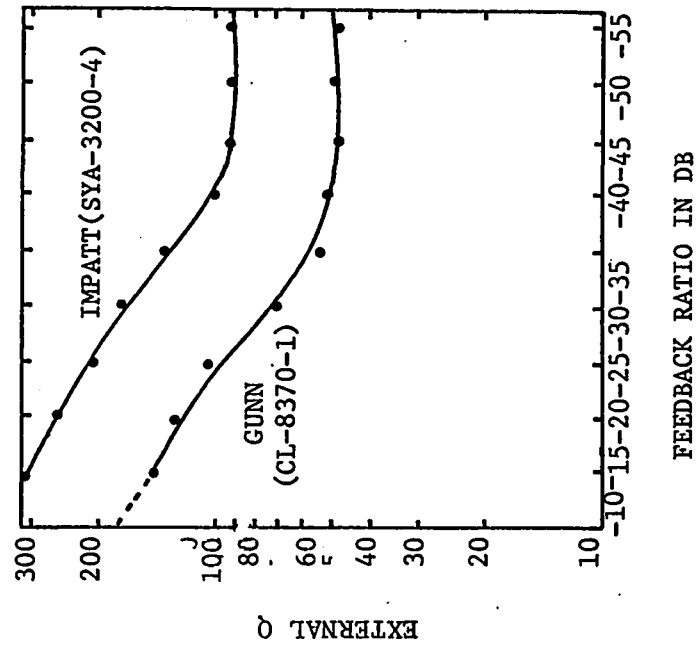
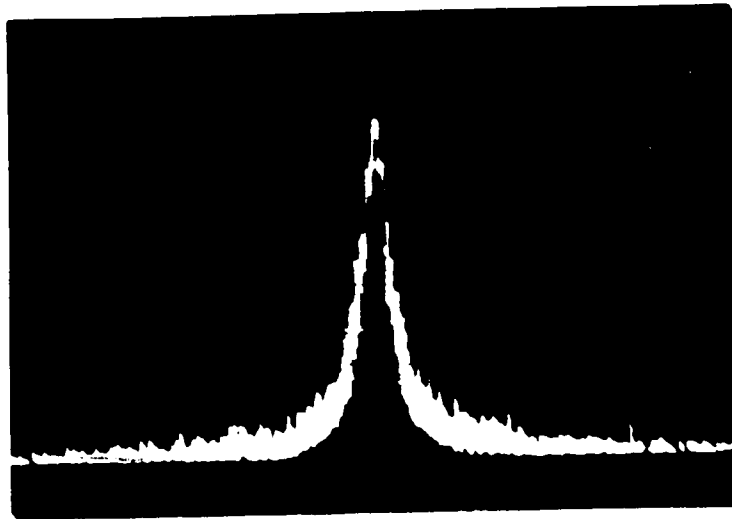


Fig.4-18 EXTERNAL Q OF SELF-LOCKED OSCILLATOR

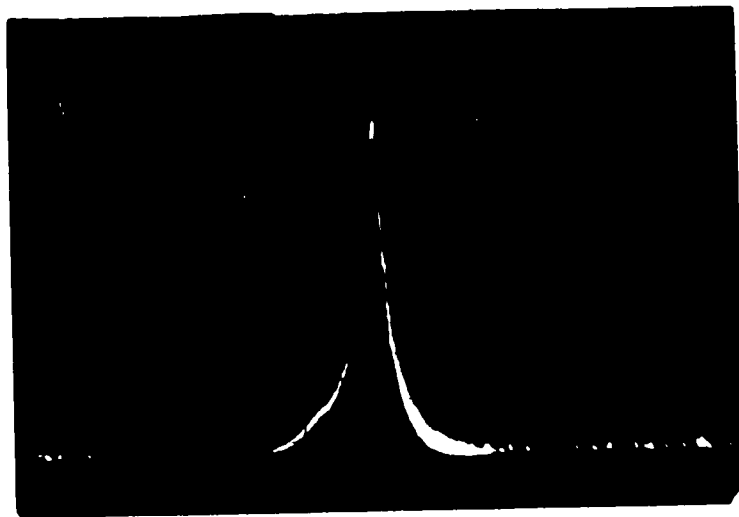
It is further interesting to note that the actual external Q of the oscillator circuit is heightened by self-injection phase-locking. The external Q measurement can be carried out using injection phase-locking techniques, as discussed in section 4-2-4. In other words, the actual Q_{ext} of the self-injection locked oscillator may be measured by simply applying an external locking signal, denoted by the dotted line in Fig.4.16, and using some formulas derived in chapter 3. Fig.4.18.6 shows the measured Q_{ext} as a function of feedback ratio at a bias current of 14 mA.

According to the well-known noise theory of the negative conductance oscillator, the rms frequency deviation from the carrier is inversely proportional to the external Q . Consequently by increasing the Q_{ext} of the oscillator, noise can be improved. That is, applying self-injection locking to a microwave oscillator with poor noise characteristics yields good noise suppression.

Fig.4.19(a) shows the output spectrum of the IMPATT diode oscillator when no self-injection is applied. Fig.4.19(b) shows the output spectrum when self-injection is applied with a feedback ratio of - 16 dB. The spectrum of self-injection locked oscillator is much better than the original spectrum of the oscillator without self-injection. Therefore, this self-injection locking is considered to be a kind of injection phase-locking.

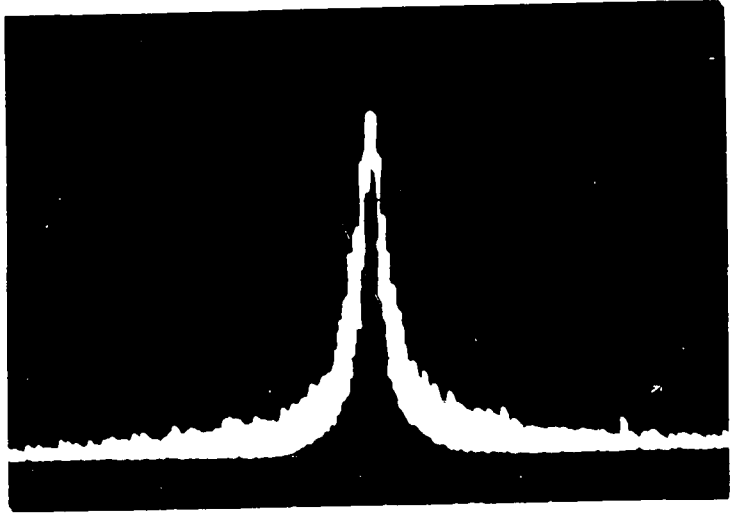


(a) NO FEEDBACK IS APPLIED

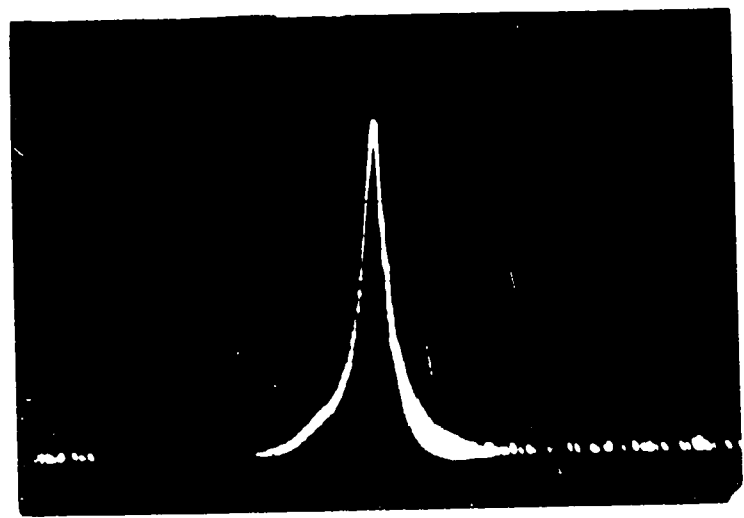


(b) FEEDBACK (-16 DB) IS APPLIED

Fig.4-19 OSCILLATION OUTPUT SPECTRA OF AN IMPATT DIODE OSCILLATOR (SYA-3200-4) FOR BIAS CURRENT OF 14MA.



(1) NO FEEDBACK IS APPLIED



(2) FEEDBACK IS APPLIED

Figure 1 shows the spectrum of the signal when no feedback is applied. The spectrum is very narrow and sharp, indicating a high resolution. Figure 2 shows the spectrum of the signal when feedback is applied. The spectrum is slightly broader and the baseline is noisier, indicating a lower resolution and higher noise level.

CHAPTER V

INJECTION PHASE-LOCKING OF BIAS MODULATED OSCILLATORS

5-1 Introduction

This chapter describes the results of a theoretical and experimental study of the injection phase-locking properties of some Impatt and Gunn oscillators, in which a modulating signal is also applied to the bias circuit.

The problems considered in this chapter are: (1) to study phase modulation properties of injection-locked oscillators, and to utilize injection phase-locking to obtain a P.M. microwave source suitable for system applications. Further, to demonstrate the frequency stabilization or the suppression of P.M. noise by means of bias-modulation and injection phase-locking, (2) to describe the operation of an injection phase-locked oscillator acting simultaneously as a suitable upconverter with gain. This mode of operation is obtained by modulating the bias current, while at the same time injecting a stable microwave signal whose frequency lies within one of the induced sidebands.

Two types of phase control of the oscillator are achieved by the injection of energy from a reference signal into the oscillator. Firstly, there can be an entire frequency pulling of the oscillator, provided that certain locking signal amplitude and frequency conditions are satisfied. Secondly, the phase angle of the oscillator can be a complex function whose fundamental frequency is the modified beat frequency and whose Fourier decomposition can be obtained for analysis.

General approaches, applicable to any microwave oscillator, are outlined, and system applications are included for possible carriers of information.

It is assumed throughout this chapter that the locking signal level is very small compared to the oscillator output level.

5-2 Angle Modulation of Injection Phase-Locked Oscillators

5-2-1 Modulation Theory

It is seen from Eq. 3.41 that the steady-state phase angle between the locked oscillator output and the locking signal is a function of free-running frequency, assuming the other parameters are constant. If the free running frequency is slowly time-variant, then the oscillator phase is also time-variant:

$$\theta(t) = \sin^{-1} \left[\frac{\omega_s - \omega_o(t)}{\Delta_o} \right] \quad (5.1)$$

If the locking signal amplitude and frequency are independent of time, it is seen from Eq. 5.1 that the phase θ is a function of ω_o , which is the oscillation frequency in the absence of the locking signal. So far as the phase angle between the locking signal and the locked output is concerned, a positive change in the locking frequency is equivalent to an equal negative change of ω_o . As a result, if the frequency ω_o is time-variant, the oscillator phase θ will be time-modulated. In this analysis, the locked output power P_i is assumed to be constant while the frequency is changed with time. Otherwise the oscillator phase is also dependent upon the locking range Δ_o according to Eqs. 3.39 and 5.1.

Electronic tuning of IMPATT diode oscillators has been treated explicitly by Gilden and Hines²¹. The dependence of Gunn diode oscillators on the bias voltage has been observed by Hakki and Knight⁷⁴, Bott et al.⁷⁵ and many other investigators⁷⁶⁻⁷⁸. This tuning effect is attributed to the variations of the electronic susceptance with bias current or voltage. Both the electronic conductance and susceptance of the diodes, as well as the RF voltage of the oscillators are functions of the DC operating conditions. If these parameters change, both the free-running frequency and the output power are modified. Therefore, the output RF voltage of the bias-voltage tuned oscillators inevitably varies with bias voltage, resulting in AM distortion. However, AM distortion can be minimized by proper tuning of the circuit, if the modulation index is small.

If the oscillator operates with a DC bias current or voltage, A_o , and a superimposed sinusoidal bias current or voltage whose amplitude and frequency are A_m and ω_m , respectively, the total bias current or voltage can be assumed to be modulated in a manner such that

$$A = A_o(1 + m \sin \omega_m t) \quad (5.2)$$

where $m = A_m/A_o \ll 1$. The operating frequency of the oscillator is simultaneously modulated⁷⁹. The output frequency of the oscillator can be expressed as a linear function of the bias modulating condition, for low modulation index:

$$\omega_o(t) = \omega_c + \Delta\omega \sin \omega_m t \quad (5.3)$$

where ω_c is the center frequency of the oscillator and $\Delta\omega$ is the maximum

frequency deviation from ω_c due to the superimposed AC bias current;
thus

$$\Delta\omega = k A_m \quad (5.4)$$

where k is a constant. This process varies the instantaneous frequency of the oscillator in synchronism with, and in direct proportion to, the amplitude of a modulating signal.

Let us apply a locking signal, whose frequency is not greatly different from the center frequency, to the bias-modulated oscillator. Then the dynamic phase angle is

$$\theta(t) = \sin^{-1} \left(\frac{\omega_s - \omega_c}{\Delta_o} - \frac{\Delta\omega}{\Delta_o} \sin \omega_m t \right) \quad (5.5)$$

Eq. 5.5 shows that the phase of the locked oscillator is modulated by the modulating signal. It is also seen from Eq. 5.5 that for stable injection locking, $|\omega_s - \omega_c \pm \Delta\omega|$ must be smaller than the locking range Δ_o . If this condition is not satisfied, the injection locking is interrupted.

For a symmetrical modulation characteristic, let the locking frequency equal the center frequency of the oscillator. Then, from Eq. 5.5 the phase of the locked oscillator becomes

$$\theta(t) = - \sin^{-1} \left(\frac{\Delta\omega}{\Delta_o} \sin \omega_m t \right) \quad (5.6)$$

where $|\theta| \leq \frac{\pi}{2}$ and $|\frac{\Delta\omega}{\Delta_o}| \leq 1$.

Thus, the phase θ in Eq. 5.6 is varied in accordance with the modulating signal. Consequently, the instantaneous output voltage of the locked

oscillator, with the modulating signal of frequency ω_m , can be obtained by use of Eqs. 5.6 and 3.12:

$$e(t) = E \sin(\omega_s t + \sin^{-1} \frac{\Delta\omega}{\Delta_o} \sin \omega_m t) \quad (5.7)$$

It is seen from Eq. 5.7 that this is not the usual type of phase-modulation; here, the sine of the phase, rather than the phase itself, is proportional to the modulating signal. Therefore, the frequency spectra produced in this system differ from the usual case.

However, as discussed in the Appendix-E, a typical microwave phase detector output is a sine function of input phase difference:

$$v = M_2 \sin \theta(t)$$

Substituting Eq.5.5 into Eq.E-9 of Appendix-E yields the time-dependent output voltage of the detector:

$$v(t) = M_2 \left(\frac{\omega_c - \omega_s}{\Delta_o} + \frac{\Delta\omega}{\Delta_o} \sin \omega_m t \right) \quad (5.8)$$

where M_2 is a constant. Eqs. 5.6 and 5.8 show that the detector output has a real value only when

$$|\omega_c - \omega_s \pm \Delta\omega| < \Delta_o$$

If the above condition is not satisfied, in other words, if the phase-locking does not take place, the detector is not able to reproduce the modulating signal. When the locking frequency ω_s is not equal to the carrier frequency ω_c , the detector output contains a DC component:

$$V_{DC} = \frac{M_2}{\Delta_o} (\omega_c - \omega_s)$$

This DC component gives the direction and magnitude of the frequency difference. The magnitude is proportional to the frequency difference. Therefore, it is possible for the oscillator to be tuned automatically to the locking frequency by using the DC component to control a suitable oscillator parameter.

When the locking frequency ω_s is made equal to the center frequency of the bias-modulated oscillator ω_c , the detector output is directly proportional to the time-varying term in Eq. 5.6:

$$v = M_2 \frac{\Delta\omega}{\Delta_o} \sin \omega_m t \quad (5.9)$$

As a result, the phase-modulated signal studied here can be very easily demodulated by means of a conventional microwave phase detector. Therefore, this angle modulation scheme in conjunction with a receiver should be very attractive at the higher microwave frequencies, where conventional microwave receivers are difficult to build.

On the other hand, the linear approximation of the phase can be obtained by making Δ_o relatively large. Then the PM output voltage may be written as

$$e(t) = E \sin(\omega_s t + \Delta\theta \sin \omega_m t) \quad (5.10)$$

where $\Delta\theta = \frac{\Delta\omega}{\Delta_o} = k_\theta A_m$; the maximum phase deviation.

Thus, when the locking range is held constant, Eq. 5.10 is an expression of a normal PM carrier because $\Delta\theta$ is directly proportional to the amplitude of the modulating signal.

It is worthwhile to note that the instantaneous frequency for the PM signal is given by

$$\omega_i = \omega_s + \Delta\omega \left(\frac{\omega_m}{\Delta\omega} \right) \cos \omega_m t$$

Thus, as seen above, the maximum incidental frequency is $\Delta\omega \left(\frac{\omega_m}{\Delta\omega} \right)$. Since for practical cases $\omega_m \ll \Delta\omega$, the effective transmission band-width of the PM signal is therefore reduced by injecting the locking signal, at the rate of $\omega_m / \Delta\omega$. The smaller transmission bandwidth also presents an advantage of the phase-modulation scheme of injection phase-locked oscillators.

The above analysis is based on the assumptions that the modulation frequencies involved are low enough so that quasi-steady-state conditions exist and that the oscillator output does not appreciably vary with the modulating signal.

5-2-2 System Application

The modulation theory discussed in the above section can be applied to modulation systems. Eqs. 5.3, 5.4 and 5.8 may be used to describe the circuit shown in Fig.5.1.

The oscillation frequency was modulated by direct modulation of the oscillator bias current through an appropriate capacitor, as shown in Fig.5.1. For the stage of the angle modulation experiment, measurements were made on the injection phase-locking behaviour of bias modulated oscillators. A stabilized locking signal from a reflex klystron is divided into two parts: One supplies a small locking signal to the IMPATT or Gunn diode oscillator while the other bypasses the oscillator and is

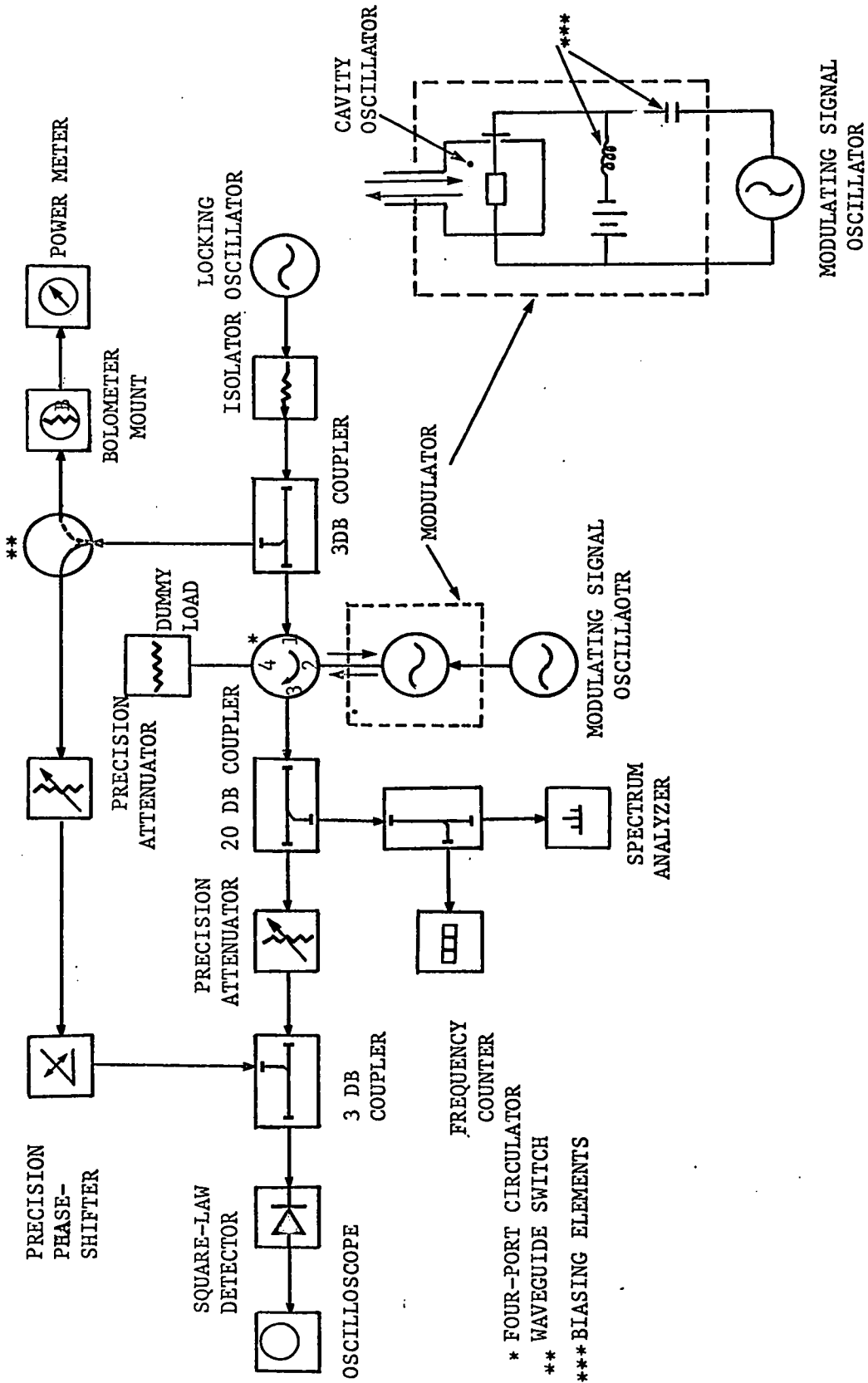


Fig. 5-1 BLOCK DIAGRAM OF EXPERIMENTS FOR THE PHASE-CONTROL OF A LOCKED OSCILLATOR

combined with the oscillator output by a second directional coupler, where the two signals interfere because of the phase difference introduced by the oscillator; a phase-sensitive, square-law detector is connected to this coupler. At the input to the detector, the PM signal is converted to an AM+PM signal whose AM is proportional to the modulating signal.

When the oscillator is locked to a locking signal which is equal to the center frequency of the modulated oscillation, the AC component of the detector output can be expressed as Eq. 5.9

$$v = M_2 \frac{\Delta\omega}{\Delta_o} \sin \omega_m t$$

It is seen from the above equation and from Eq. 5.5 that the output voltage has a real value only when the absolute value of $\Delta\omega$ is less than Δ_o . If $\Delta\omega$ is larger than Δ_o , entire locking is no longer maintained.

Fig. 5.2 shows phase patterns of the locked oscillator output. For the case of $\omega_s = \omega_o$, Fig. 5.2a shows that the oscillator is entirely locked to the locking signal, so that the phase of the output fully traces the bias modulating signal, when $\Delta\omega < \Delta_o$. In Fig. 5.2b, the sharp breaks at the sine-wave peaks indicate the unlocked portion of the cycle when $\Delta\omega$ is slightly larger than the locking range. This experimental result verifies Eq. 5.9.

On the other hand, for the case of $\omega_s \neq \omega_c$, the breaks can occur at the upper sine-wave peaks or at the lower ones. In Fig. 5.2c, the breaks at the upper peaks are of the case when $\omega_s < \omega_c$; the locking is now impossible at the lower peaks. This result verifies partially Eq. 5.8.

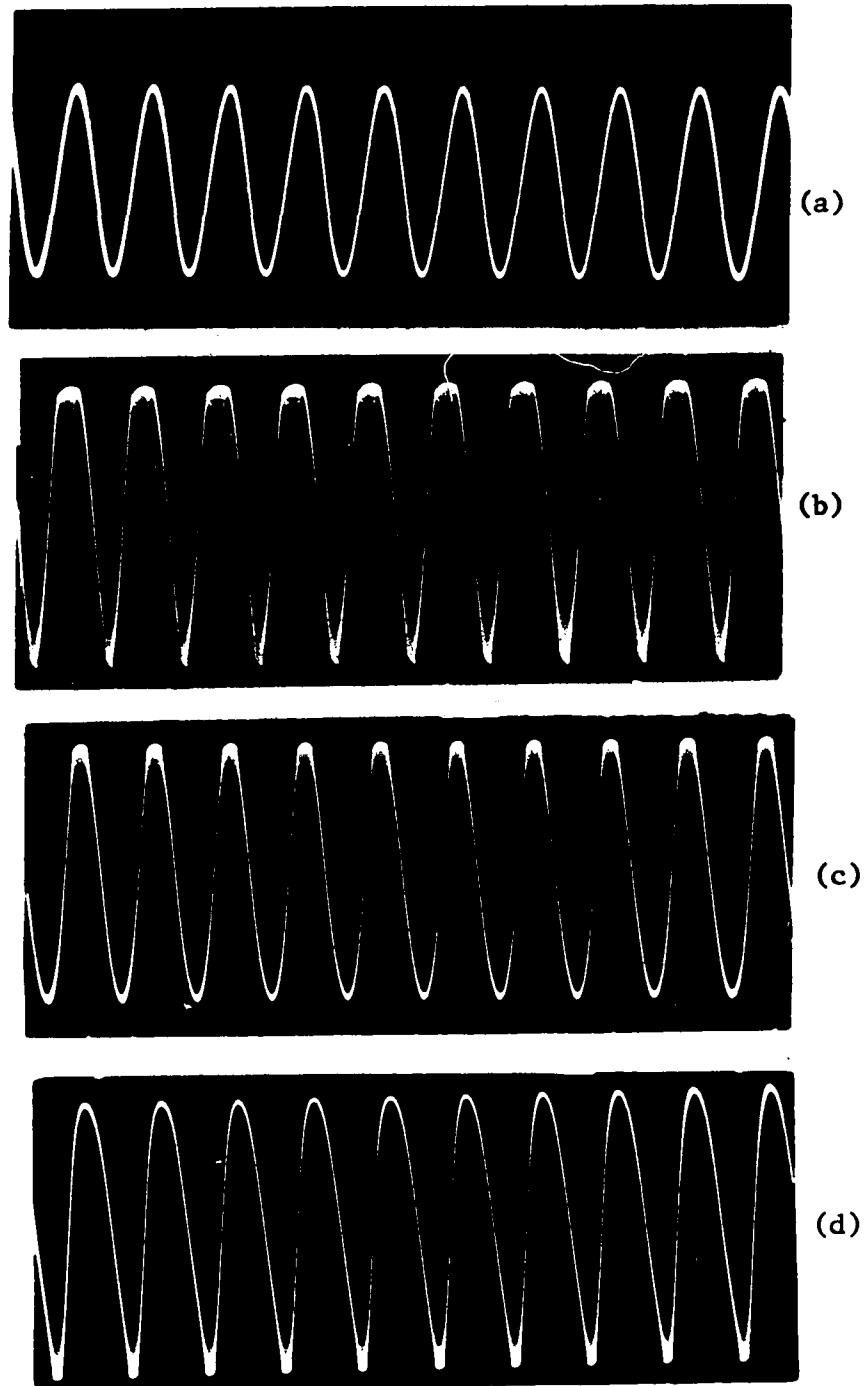
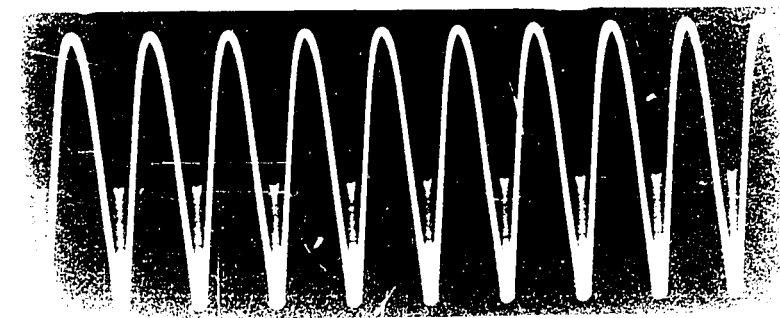
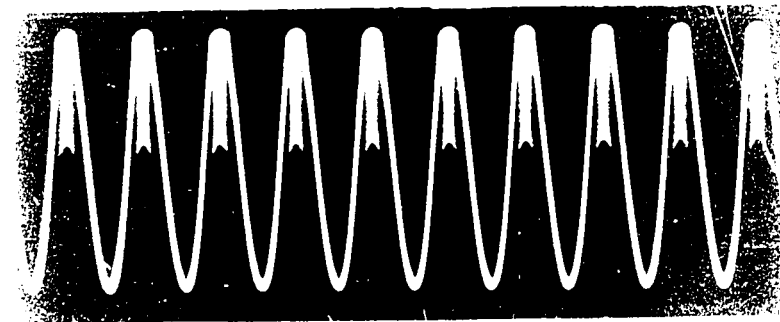
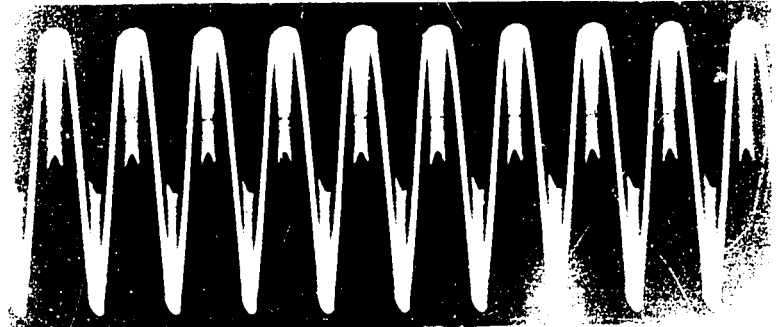
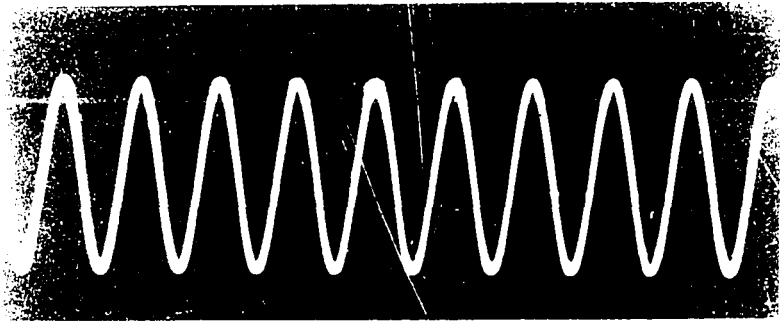


Fig.5-2 BREAKS OF PHASE-LOCKING AT THE PEAK MODULATION CYCLE.



In order to verify the above theory in more detail, we may substitute Eqs. 3.39 and 5.4 into Eq. 5.9. Then we obtain

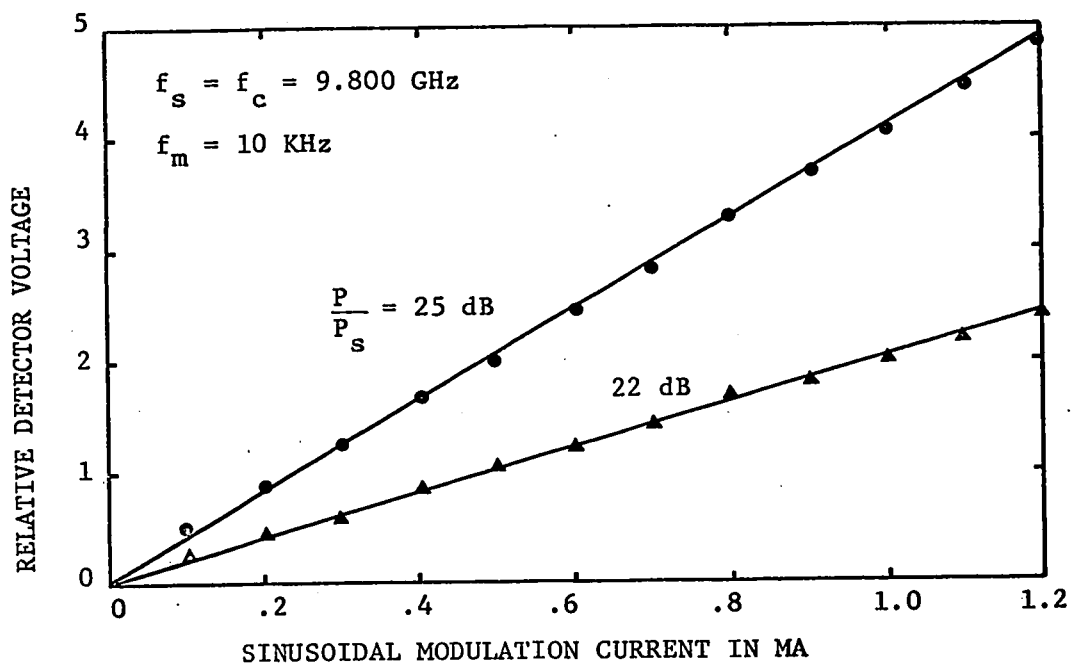
$$v = \frac{K_2}{|\Gamma|} A_m \sin \omega_m t \quad (5.11)$$

where K_2 can be made constant by holding the output of the oscillator and of the reference signal constant, respectively. Eq. 5.11 indicates that the detector output is directly proportional to the modulating signal when all other parameters are held constant. Fig.5.3 shows the experimental detector output as a function of modulation signal amplitude. The experimentally observed detector output is also seen to be proportional to the modulation signal. In this case, the modulation frequency was 10 KHz and the locking signal frequency was equal to the center frequency of the oscillator. For a unique value of detector conversion factor, the reference signal into the detector was made constant throughout the experiment.

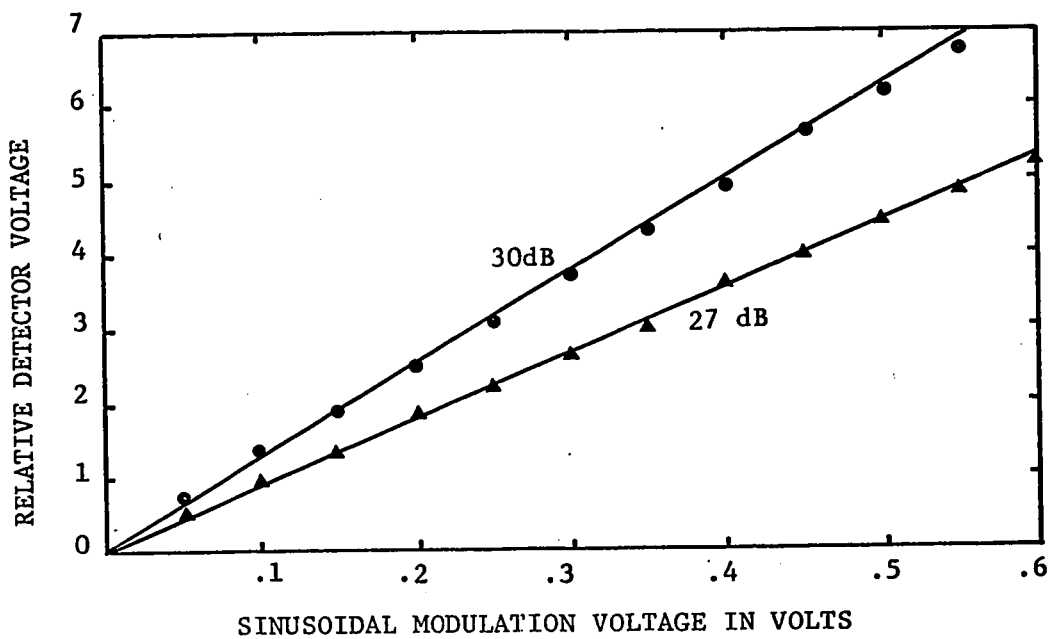
On the other hand, Eq. 5.11 also indicates that the detector output is inversely proportional to $|\Gamma|$ or to the square root of the locking power when all other parameters are held constant.

Fig. 5.4 shows the variation of the amplitude of the detector output with locking signal level, when the oscillator is bias-modulated with a 10 KHz-modulating signal. The experimental results are in good agreement with the theoretical values discussed in the Section 5-2-1.

For the case of an IMPATT diode oscillator (SYA-3200-1), there are no experimental points which are available for the values of $\sqrt{p_s/p_o}$ for less than 0.029, as seen in Fig.5.4a, because injection locking at the

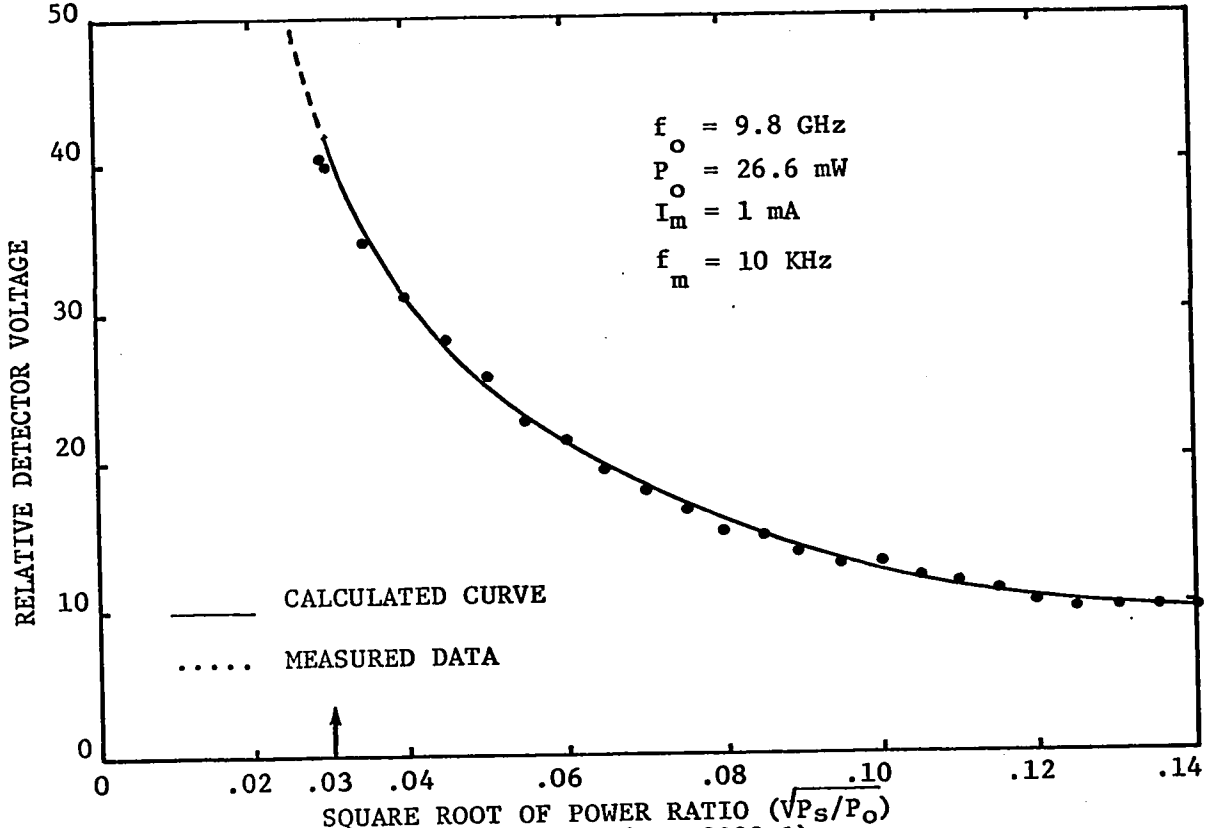


(a) AN IMPATT DIODE OSCILLATOR (SYA-3200-3)

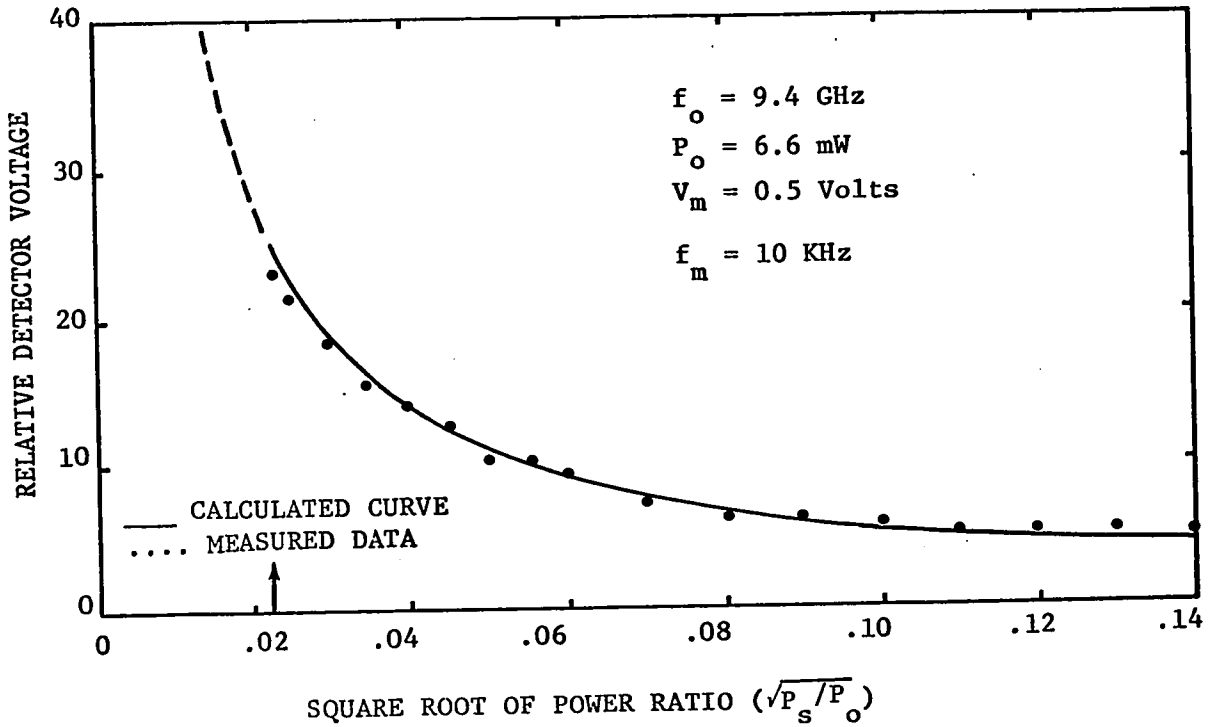


(b) A GUNN DIODE OSCILLATOR (CL-8370-2)

Fig.5-3 RELATIVE DETECTOR OUTPUT VOLTAGE AS A FUNCTION OF MODULATING SIGNAL CURRENT OR VOLTAGE



(a) AN IMPATT DIODE OSCILLATOR (SYA-3200-1).



(b) A GUNN DIODE OSCILLATOR (CL-8370-2)

Fig.5-4 RELATIVE DETECTOR OUTPUT VOLTAGE AS A FUNCTION OF LOCKING POWER.

peaks of the modulation cycle was no longer possible after the maximum frequency deviation $\Delta\omega$ had become larger than the locking range $\Delta\omega_0$. In this case, the oscillator was modulated with a modulation current of 1 mA-amplitude.

For the case of a Gunn diode oscillator (CL-8370-2), there are no experimental points available for the values of $\sqrt{p_s/p_o}$ less than 0.023, when modulated with modulation voltage of 0.5 volt-amplitude. It is indicated that the dynamic modulation sensitivity, which is determined by the injection phase-locking measurement, is equal to the static modulation sensitivity obtained from the electronic tuning characteristics.

It is very interesting to note that the locking boundary condition can be used to provide a quantitative check of Eq. 5.6. For the IMPATT diode oscillator (SYA-3200-1), the maximum frequency deviation $\Delta\omega$ from the center frequency can be approximately calculated from the frequency sensitivity 3 MHz/mA of the electronic tuning. At the locking boundary the deviation is approximately $\Delta\omega = (2\pi \times 3 \times 10^6 \text{ Hz/mA}) \times 1 \text{ mA}$. Then, we obtain the locking boundary condition:

$$\frac{\Delta\omega}{\Delta\omega_0} = \frac{\Delta\omega}{\omega_0} \leq \frac{1}{Q_{\text{ext}} |\Gamma|}$$

Therefore, $|\Gamma| \geq \frac{\Delta\omega}{\omega_0} Q_{\text{ext}} = 0.03$

The Gunn diode oscillator (CL-8370-2) has an approximate frequency sensitivity of 7.4 MHz/volt. Therefore, the maximum frequency deviation due to the amplitude of 0.5 volt is $2\pi \times 7.4 \times 10^6 \text{ (Hz/volt)} \times 0.5 \text{ volt}$. Finally, $|\Gamma| \geq \frac{\Delta\omega}{\omega_0} Q_{\text{ext}} = 0.022$. Our experimental points at the locking boundary are very close to these calculated values.

So far, we have discussed the angle modulation of an injection phase-locked oscillator, in which a modulating signal is simultaneously applied to the bias circuit. It is apparent that the phase modulation scheme used may be employed for communication purposes.

5-2-3 PM Noise Performance

Let us now consider how variations of the oscillator frequency affect the locking phase.

By differentiating Eq. 5.1 with respect to ω_o , the rate of change of the phase angle with ω_o can be expressed as

$$\frac{\partial \theta}{\partial \omega_o} = - \frac{[1 + \frac{\Delta \omega_o}{\omega_o}]}{\Delta_o \cos \theta}, \text{ or } \Delta \theta \approx - \frac{Q_{\text{ext}}}{\omega_o \cos \theta} \frac{\Delta \omega_o}{\sqrt{\frac{P_s}{P_o}}} \quad (5.12)$$

It is seen from the above equation that the phase deviation rates near the locking boundary approach quite large values even though the frequency deviation be small. The minimum rate of change of the phase deviation occurs at the center of the locking band, where $\theta = 0$ and $\omega_s = \omega_o$. Further, the phase deviation can be decreased by increasing the locking power because the locking range Δ_o increases with power.

However, since Δ_o is proportional to the square root of the locking power, increases of the locking power are relatively ineffective in reducing the phase deviation.

In chapter 3, we discussed the phase-modulation noise improvement of injection phase-locked oscillators. Consider the case of a locking signal that is comparatively noise-free, applied to an oscillator to

be locked, which is comparatively noisy. Let us assume that the free-running oscillation frequency ω_o is sinusoidally modulated by a baseband noise modulating signal of frequency ω_m . The effect of this noise component on the free-running oscillation, and the subsequent action of the stable locking signal may be analyzed by means of the theory for injection phase-locking of bias-modulated oscillators. Then, our purpose is to minimize the phase deviation of the noise-modulated oscillator by injection phase-locking with a stable locking signal.

Assuming that the amplitude of the noise component is kept constant throughout the locking range, we can draw curves of phase variation with locking signal power where frequency is a parameter.

Since, according to Eq. 5.6, the value of $(\sin \theta)$ is equal to $(\Delta\omega/\Delta_o)\sin \omega_m t$, the maximum value of the phase can be expressed as

$$\theta_\ell = \sin^{-1} \frac{K}{|\Gamma|} \quad (5.13)$$

where $K = \frac{Q_{\text{ext}} \Delta\omega}{\omega_o}$. Since the phase detector output is proportional to $\sin \theta$, it is experimentally possible to measure the maximum value of the phase. From Eq. 5.13, we may plot θ_ℓ as a function of $|\Gamma|$. Figs. 5.5 and 5.6 show how the measured and calculated values of the phase deviation compare for the IMPATT and Gunn diode oscillators tested respectively. In accordance with the theory, it is seen that the slope of the phase deviation decreases sharply towards zero as locking power increases. Thus, for power ratios beyond the "knee" of these curves, the locking power becomes increasingly less and less effective in further reducing the phase deviation caused by the bias modulating signal ω_m . The dotted line in Figs. 5.5 and 5.6 represents the locus of points at which the

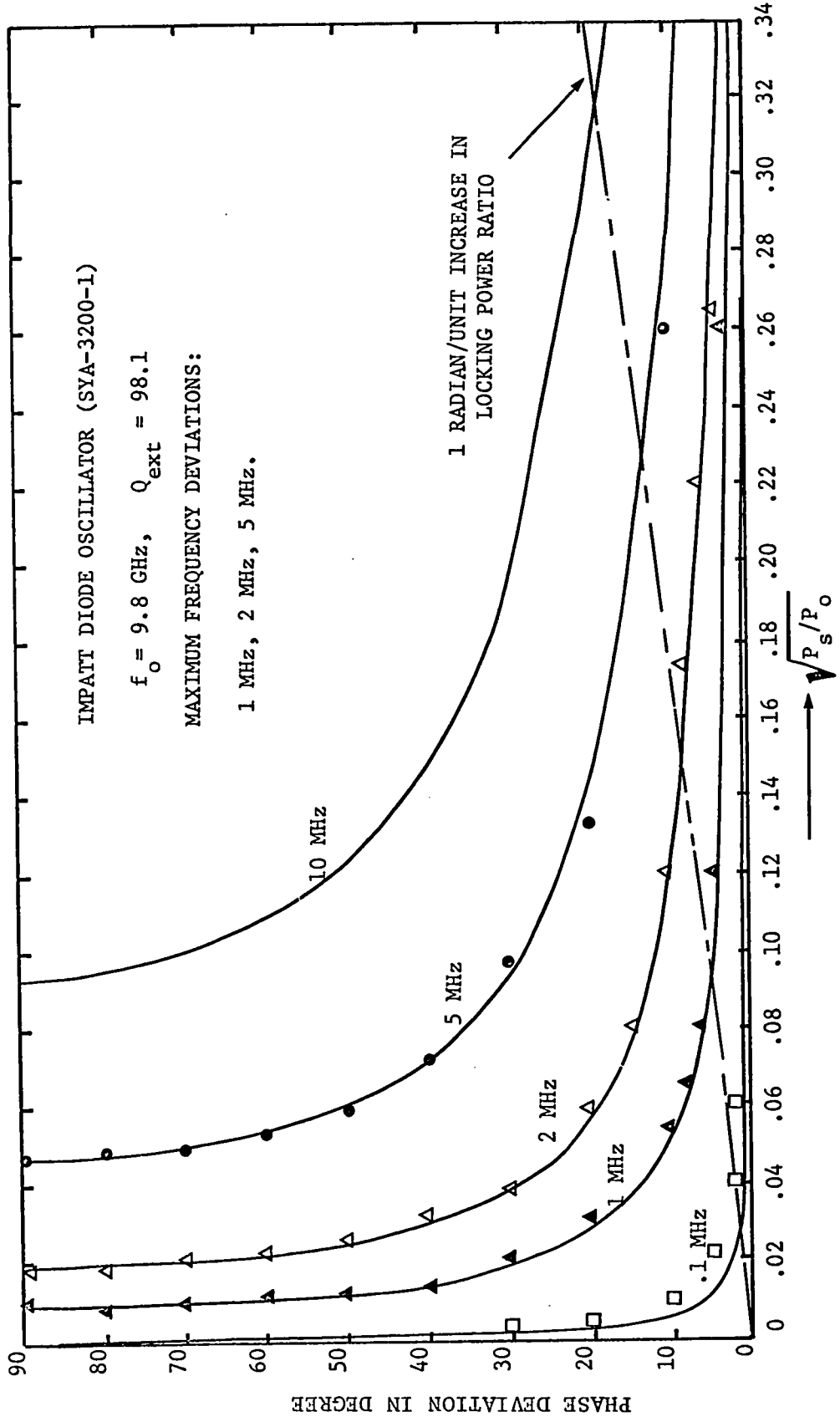


Fig.5-5 VARIATION OF PHASE DEVIATION WITH LOCKING POWER FOR THE CASE OF AN IMPATT DIODE OSCILLATOR (SYA-3200-1)

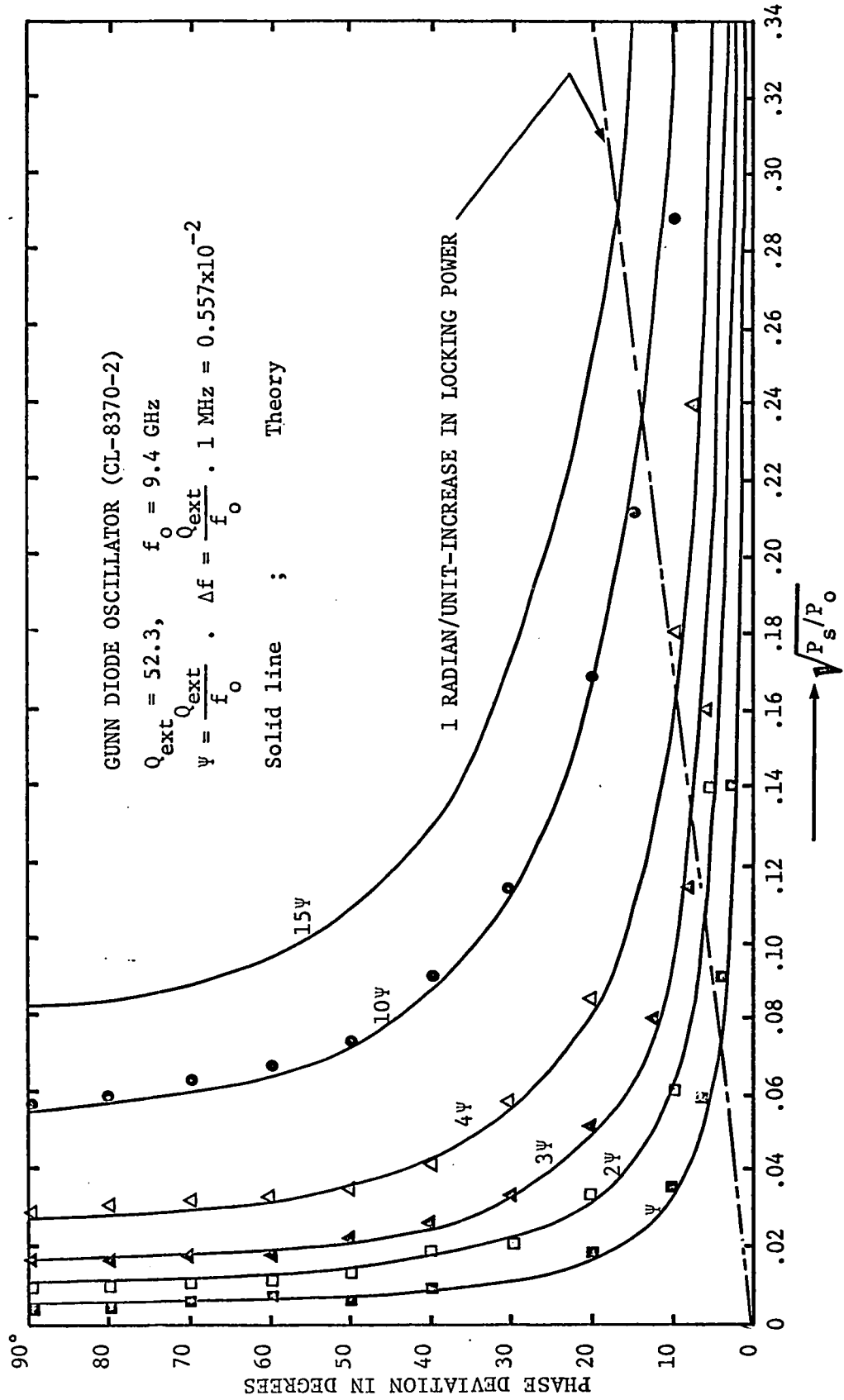


Fig. 5-6 VARIATION OF PHASE DEVIATION WITH LOCKING POWER FOR THE CASE OF A GUNN DIODE (CL-8370-2)

slope is one radian per unit-increase in the locking power. This line may mark the approximate boundary between efficient and inefficient phase deviation suppression. It is indicated that in the inefficient region the phase deviation is a rapidly increasing function of K which is equal to $(Q_{\text{ext}} \Delta\omega/\omega_0)$.

In addition it is also interesting to note that it is not always possible to reduce the interfering component close to the carrier to that of the locking signal, as shown in Figs. 5.5 and 5.6. It may be that the phase was modulated by hum from the power supply. In addition, the up-conversion noise⁸⁰⁻⁸² of the low frequency noise, excited by thermal generation and avalanche multiplication, may contribute to this additive phase deviation. A detailed study of the up-conversion noise would be very valuable. Although not covered in this thesis, the work is presently being done in this laboratory.

We may draw the conclusion that in the injection phase-locked oscillator power gain can be increased at the expense of phase stability by decreasing the locking power.

5-3 Injection Phase Locking of a Sideband to the Locking Signal, a Theoretical and Experimental Analysis

For an oscillator partially locked to the locking signal, a characteristic FM spectrum with an asymmetric distribution of sidebands has recently been investigated^{47-48,83-84}. When the oscillator is far from lock, when $|\omega_s - \omega_0| \gg \Delta_0$, it is clear from Eq. 3.38 that $d\theta/dt$ is nearly equal to $(\omega_s - \omega_0)$. Locking phenomena outside the locking range are discussed in Section 3-2. Eq. 3.81 explains how the beat frequency

varies with the locking range. We have shown in Chapter 4 that the experimental values of the beat frequencies agree with the theoretical ones.

Under the above conditions there would be FM sidebands of nearly equal amplitude at frequencies ω_s and $\omega_s - 2\Delta\bar{\omega}_b$ (upper sideband locking). Since the average beat frequency varies with ω_o , the stability of $\Delta\bar{\omega}_b$ is strongly dependent upon that of ω_o , as indicated in Eq. 3.81.

Now let us apply a modulating signal whose frequency ω_ℓ is nearly equal to the beat frequency $\Delta\bar{\omega}_b$. Then the average beat frequency can be controlled by this modulating signal. In other words, the beat-note wave shown in Fig.3.21 is synchronized to the modulating signal. In this case, one of sidebands generated by the modulating signal is located at the locking frequency ω_s , and the carrier frequency is thus shifted from $\omega_s - \Delta\bar{\omega}_b$ to $\omega_s - \omega_\ell$ (upper sideband locking) or from $\omega_s + \Delta\bar{\omega}_b$ to $\omega_s + \omega_\ell$ (lower sideband locking), as seen in Fig.5.7b.

Conversely, let us first apply the modulating signal through the bias circuit to the diode and then apply a stabilized locking signal, whose frequency is nearly at one of the first sideband frequencies. Then the sideband frequency is pulled and locked to the locking signal due to partial pulling. The sidebands are separated from the reproduced carrier, at frequency $(\omega_s + \omega_\ell)$ or $(\omega_s - \omega_\ell)$ by integral multiples of the modulating frequency ω_ℓ . These characteristics are illustrated in Fig.5.7c.

The oscillator output under these conditions has a frequency spectrum whose intervals correspond to the modulating frequency. It is noteworthy that the reproduced carrier signal is at a higher power level

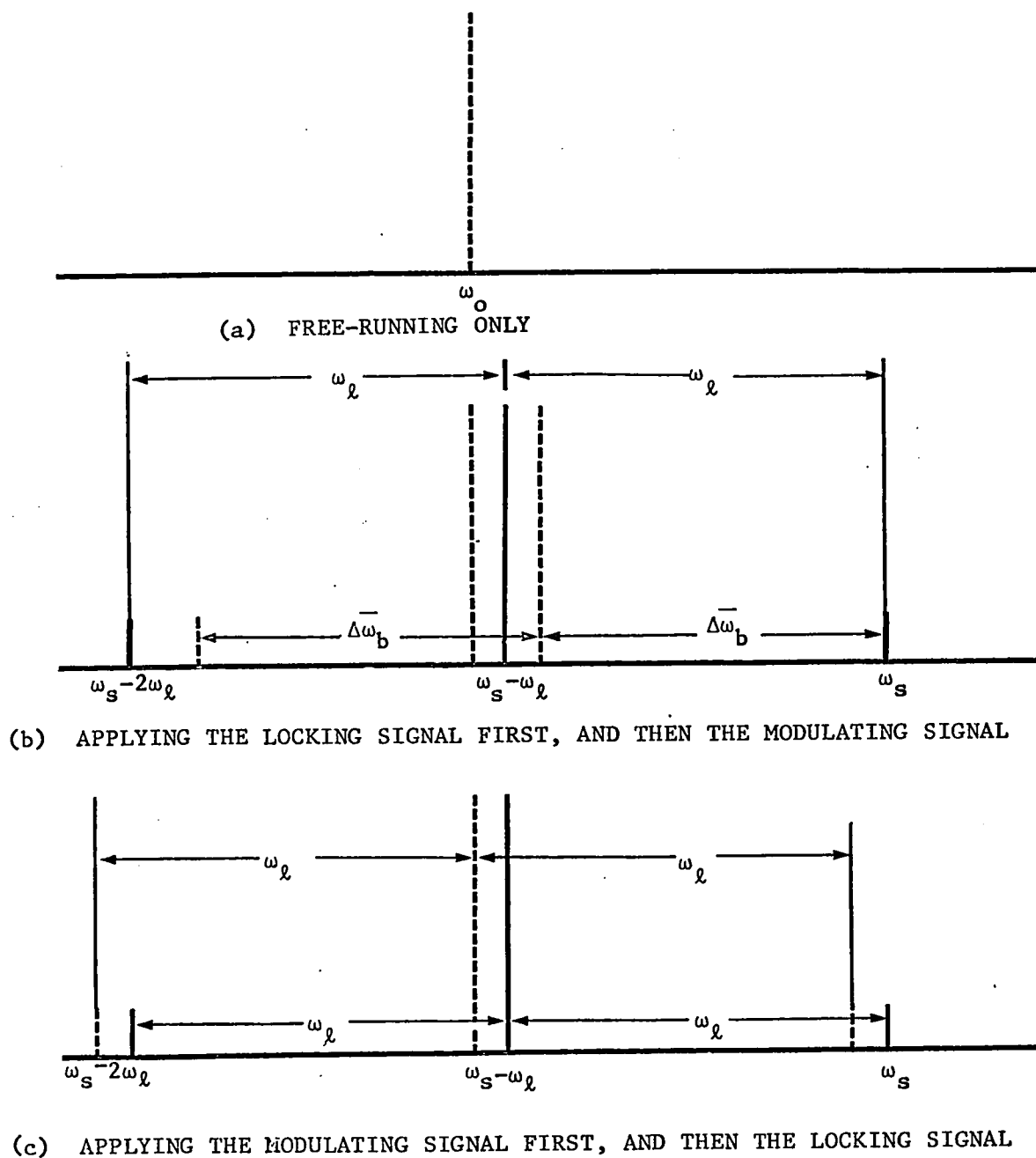


Fig.5-7 FREQUENCY SPECTRA OF THE SIDEBAND-LOCKED OSCILLATOR WITH THE BIAS-MODULATION SIGNAL

than the input modulating signal.

As a result, the oscillator output has a spectrum composed of lines whose intervals correspond to the modulating frequency ω_ℓ . For example, when the upper sideband frequency of the bias-modulated oscillator is locked to the locking frequency, the carrier frequency is then shifted to a new frequency:

$$\omega_o' + \omega_\ell = \omega_s \quad (5.14)$$

therefore, $\omega_o' = \omega_s - \omega_\ell$

It is seen from Eq. 5.14 that the reproduced carrier signal is taken at much higher frequency $\omega_s - \omega_\ell$ than ω_ℓ . In addition, the power of the reproduced carrier is delivered from the locked oscillator, whose power is much higher than the modulating signal. On the other hand the reproduced carrier frequency is not dependent on the original carrier frequency. Consequently, as long as the locking signal is stable, frequency stability will be imposed by the locking signal. In other words, up-conversion with gain and frequency stability is obtained in this way. This is due to the injection phase-locking properties.

The case of a single-frequency bias modulated signal can be extended to that of multiple-frequency signals. Let a one-tone FM signal, which will be applied to the diode of the oscillator through the bias circuit, be expressed as:

$$a_m(t) = A \sum_{n=-\infty}^{\infty} J_n(M) \sin(\omega_\ell + n\omega_m)t \quad (5.15)$$

where A = the peak amplitude of the FM wave

ω_c = the center frequency of the carrier

$M = \frac{\Delta\omega}{\omega_m}$ = the modulation index

$\Delta\omega$ = the maximum frequency deviation

ω_m = the modulating frequency of the FM wave

$J_n(M)$ = the Bessel function of the first kind of n'th order.

In practice, the amplitude of the spectral components of higher frequencies become negligible and hence almost all of the energy of the signal is contained in the spectral components lying within a finite bandwidth, $2\Delta\omega$. When this FM signal is applied directly to the diode of the oscillator through a bias circuit, the output of the oscillator will have complicated sidebands. Since the modulating signal has multi-frequency components, each of these components causes its own sidebands. In other words, when more than one modulating frequency is present in FM, sidebands are caused by all the sum and difference frequencies between the harmonics, as well as the harmonics themselves^{85, 86}. The output of the bias FM modulated oscillator may be expressed as:

$$a(t) = A' \sin[\omega_c t + mA \sum_{n=-\infty}^{\infty} \frac{J_n(M)}{\omega_c + n\omega_m} \sin(\omega_c + n\omega_m)t] \quad (5.16)$$

where A' = the peak amplitude of the oscillator output

ω_c = the center frequency of the oscillator

m = the electronic tuning sensitivity

From Eq. 5.16, it is clear that terms of the form

$$\sin[\omega_c \pm n_1(\omega_c \pm \omega_m) \pm n_2(\omega_c + 2\omega_m) \pm n_3(\omega_c + 3\omega_m) \pm \dots]t \quad (5.17)$$

for integral values of n_i will appear in the result. The actual carrying

out of the development is too tedious and is not sufficiently important to be set down here in detail. We are here interested in the case of a low modulation index. Therefore, the output of the oscillator is a narrow-band FM signal which occupies the effective transmission bandwidth $2(\omega_c + \Delta\omega)$ by Carson's rule. Thus for low modulation index, only the carrier and the first upper and lower sidebands are important, while the remainder are ignored. Accordingly from Expression 5.17, the frequency terms of the oscillator output can be expressed as follows:

$$\begin{aligned}\omega_c &= \text{carrier frequency} \\ \omega_c + (\omega_m \pm n\omega_m) &= \text{first upper sideband frequencies} \\ \omega_c - (\omega_m \pm n\omega_m) &= \text{first lower sideband frequencies}\end{aligned}$$

These characteristics are illustrated in Fig. 5.8a, which shows the spectrum of the multiple frequency modulated signal with low modulation index.

Let us next apply a locking signal, whose frequency is near the center of the first upper (or lower) sideband and whose amplitude is relatively sufficient for sideband locking to the oscillator through a circulator. Then, all the frequency components of the first sideband are locked to the single frequency ω_s of the locking signal. Under this condition, the carrier component must vary with the frequency of the modulating signal to maintain the corresponding frequency intervals from the locking signal frequency. Therefore, the carrier frequency spectra vary according to the following:

$$\omega'_c = \omega_s - (\omega_m \pm n\omega_m) \quad (5.18)$$

where the n are all integers within the transmission bandwidth. It is

seen from Eq. 5.14 and Eq. 5.1 that under the locked condition the carrier is of the same form as the signal to which the original FM signal is converted from ω_ℓ to $\omega_s - \omega_\ell$ in carrier frequency. Thus, the carrier component is frequency-modulated since the AC bias signal is frequency modulated. It is also noteworthy that the reproduced signal frequency components are not functions of the oscillation frequency. This means that sideband locking also establishes frequency stabilization.

In addition, since most of the power resides near the carrier component, the reproduced signal, to which the original FM signal is converted, is at a much higher power level than the original one, as shown in Fig.5.8b.

In order to utilize the amplified and stabilized FM signal, we may connect a microwave band-pass filter at the output port of the circulator to select only the desired signal.

The experimental arrangement for sideband locking is the same as shown in Fig.5.1, except for the phase detector portion.

For the experiments carried out to investigate these phenomena, a VHF modulating signal and DC bias voltage are admitted to the diode through a monitor tee. For the first stage of the experiment a single frequency VHF signal ($f_\ell = 50$ MHz) is applied to the diode in addition to the DC bias. The locking signal, which has a constant power, is swept in frequency for the measurement of the side-band locking range. The locking range variation of the first sideband with modulating power is plotted in Fig.5.9. As seen in the figure, the sideband locking range increases with an increase of modulating power level. This explains why

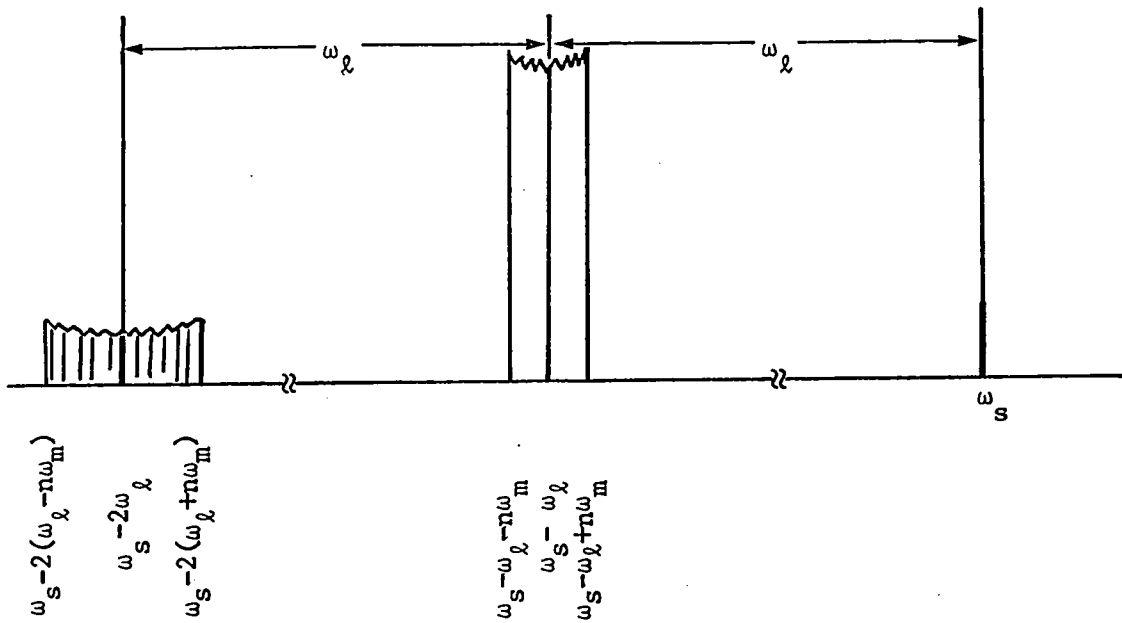
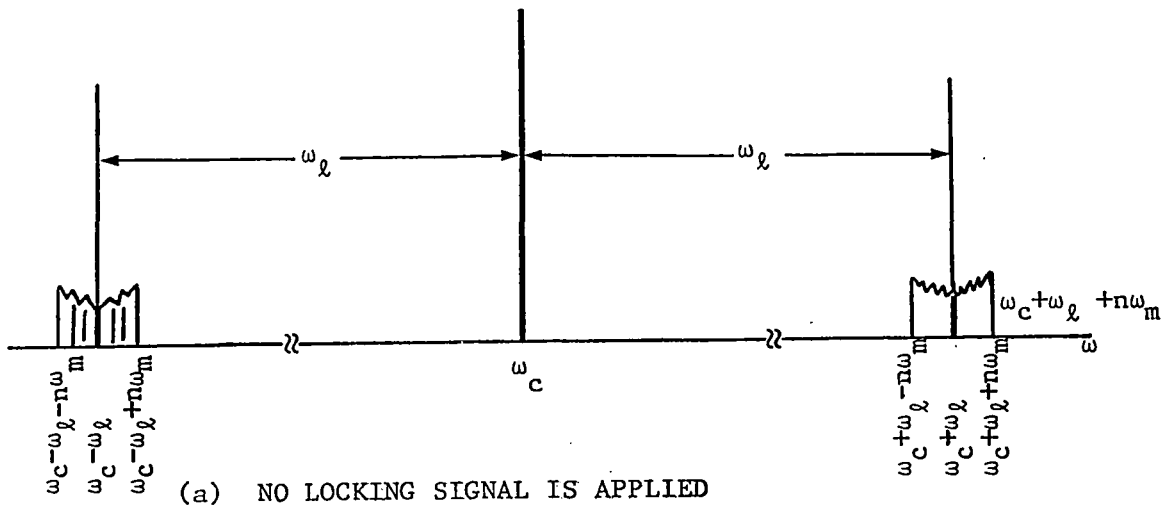


Fig.5-8 THE OUTPUT SPECTRA OF INJECTION LOCKED-OSCILLATOR WITH BIAS-MODULATION OF MULTIPLE-FREQUENCY SIGNAL.

the stronger modulating signal more powerfully controls the modified beat frequency. For the IMPATT diode oscillator, the upper sideband locking range is almost the same as the lower one, as shown in Fig.5.9a. However, for the Gunn diode oscillator, the upper sideband locking range is larger than the lower one. This deviation results from the inevitable amplitude modulation of the oscillator by the modulating signal, because the fundamental locking range is a function of the effective reflection coefficient. Consequently a varactor tuned Gunn oscillator would be suggested to be better than the bias-current tuned oscillator.

For the next stage of the experiments a VHF FM signal instead of a single frequency signal is applied to the diode and a microwave locking signal is admitted to the oscillator in the same way as before.

Figs.5.10 and 5.11 show the frequency spectra of an IMPATT diode oscillator and of a Gunn diode oscillator, respectively, during the process of the sideband injection phase-locking. The reproduced carrier spectra are seen in Figs.5.10 and 5.11(a), (b) and (c), while the first upper sideband spectra are seen in Figs.5.10 and 5.11 (d), (e), and (f). In the figures, (a) and (d) are the spectra of the carrier and first upper sideband, respectively, for the case of FM bias signal but no locking signal: (b) and (e) same as (a) and (d) respectively, but with locking signal near the first upper sideband. The injection ratio was 20 dB; (c) and (f) show the spectra of the carrier and the first upper sideband which are the same case as (b) and (e), respectively, but the locking signal frequency is decreased and the oscillators were upper sideband-locked entirely.

It is clearly seen that the reproduced carrier signal is the

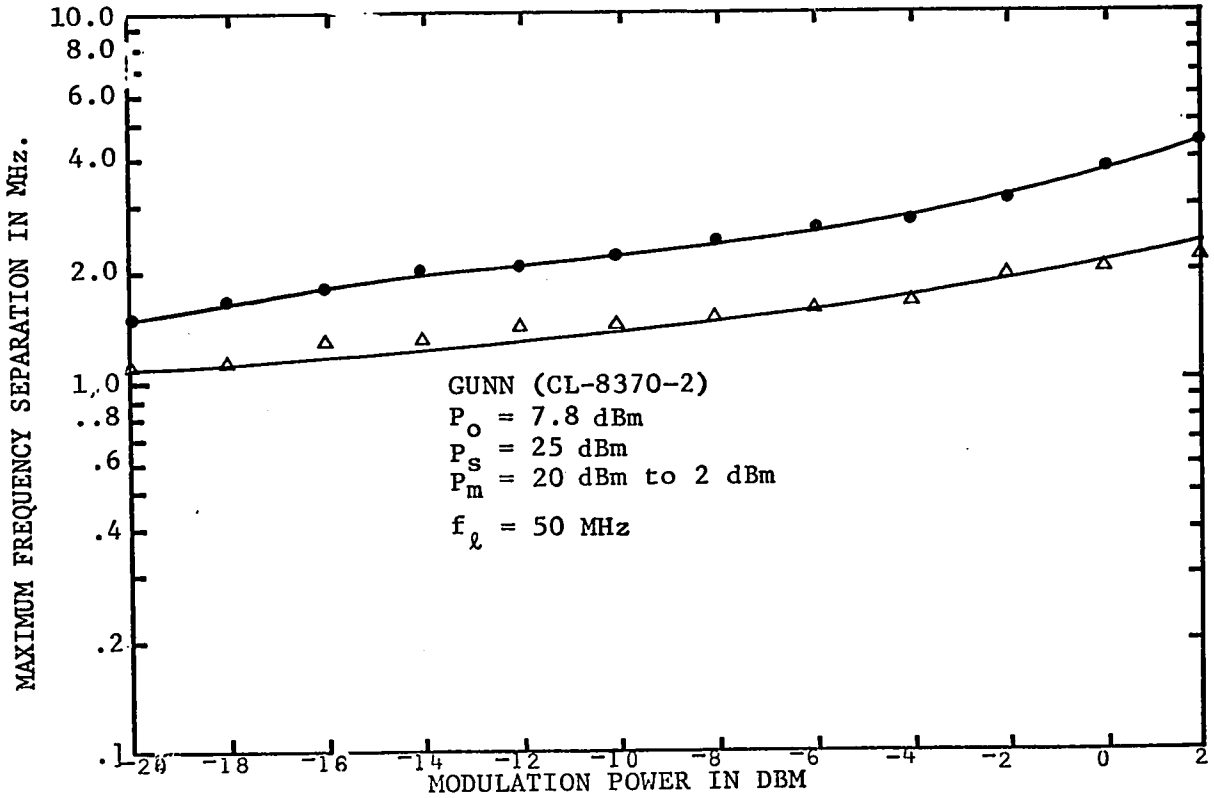
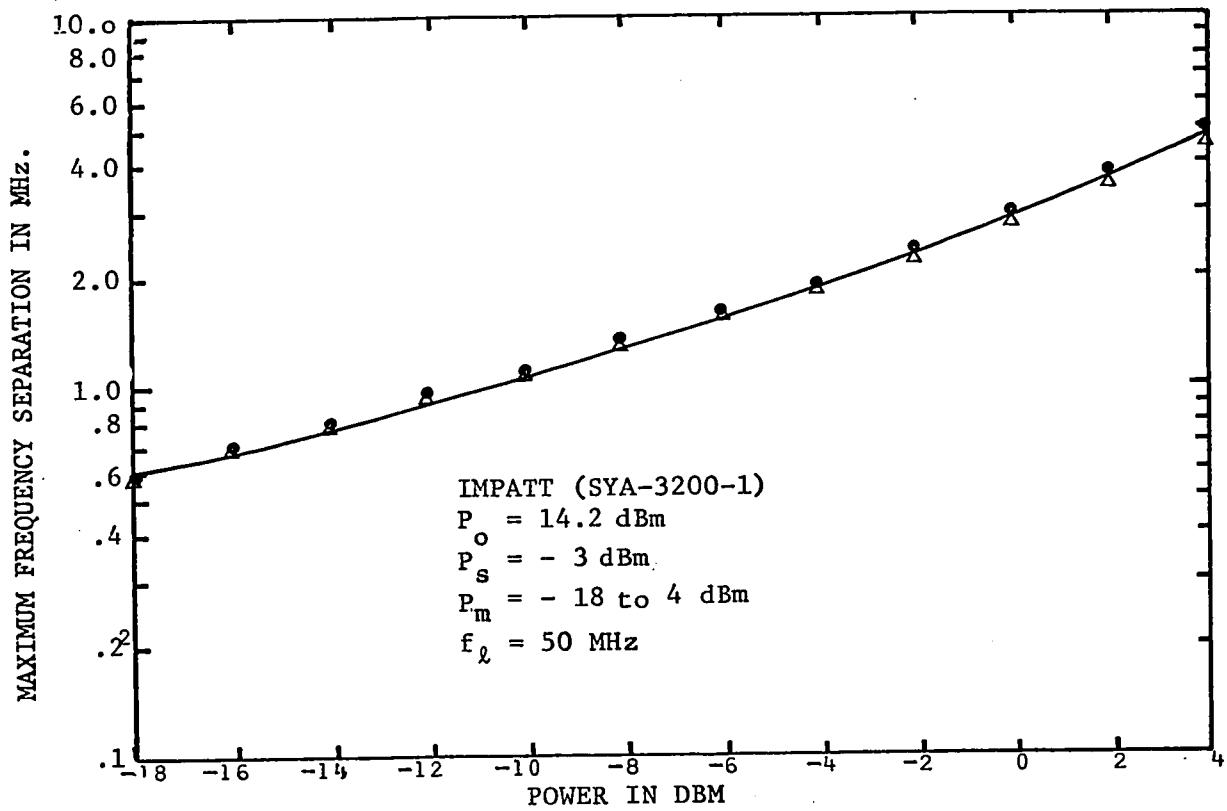


Fig.5-9 LOCKING RANGE OF FIRST SIDEBANDS

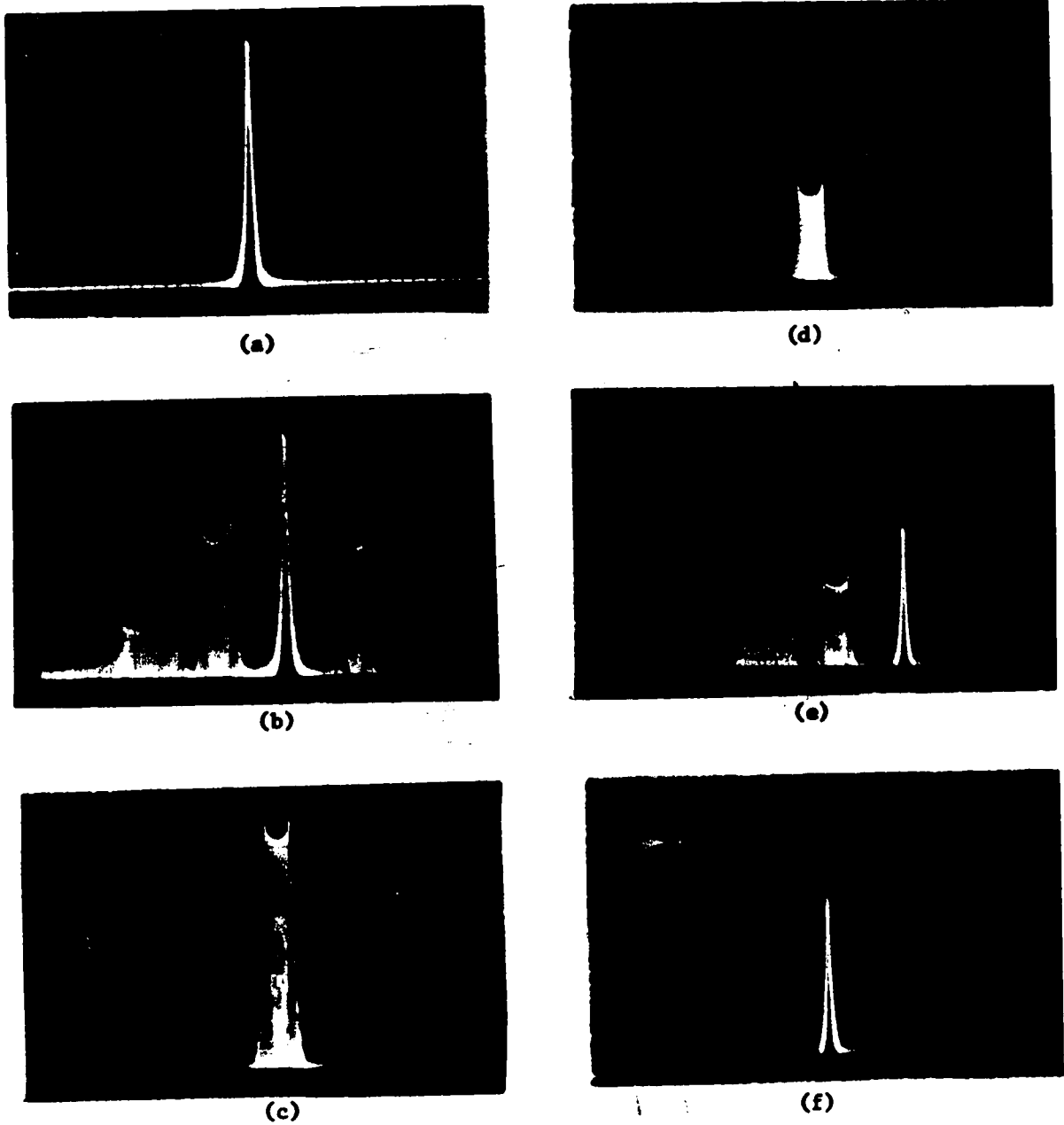


Fig.5-10 FREQUENCY SPECTRA OF SIDE-BAND LOCKED IMPATT DIODE OSCILLATOR (SYA-3200-3):

- (a) and (d); NO LOCKING SIGNAL IS APPLIED.
 (b) and (e); PARTIALLY PULLING OF UPPER SIDEBAND TOWARD THE SIGNAL.
 (c) and (f); LOCKING OF SIDEBAND TO THE SIGNAL.

Vertical Scale, 10 DB/div. Horizontal Scale, 3 MHz/div.

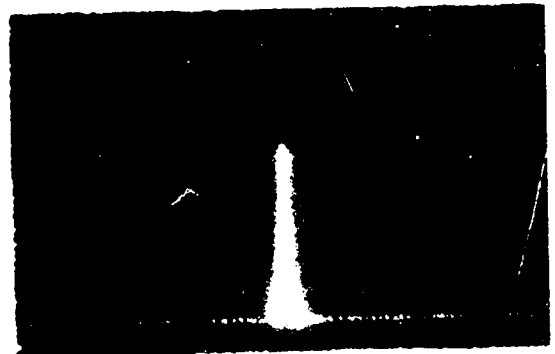
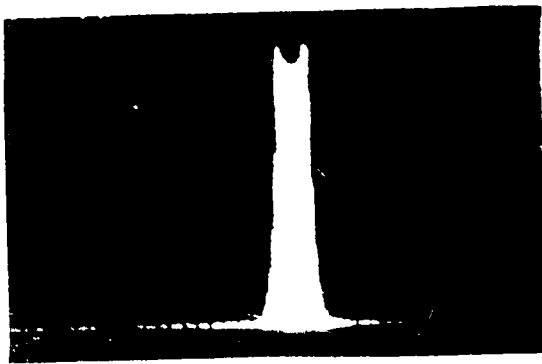
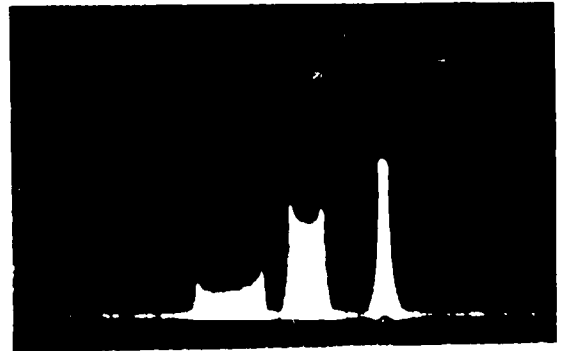
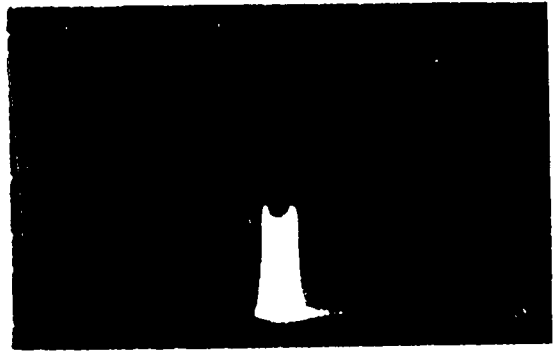
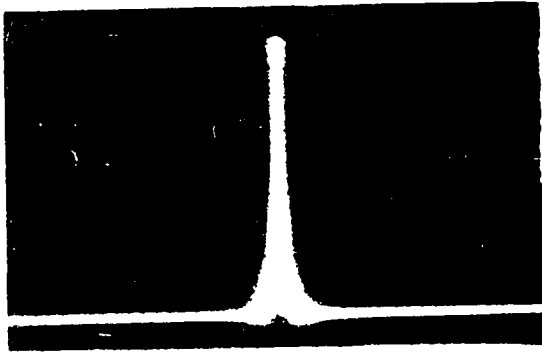


Figure 4. The NMR spectra of the polymer...

...

...

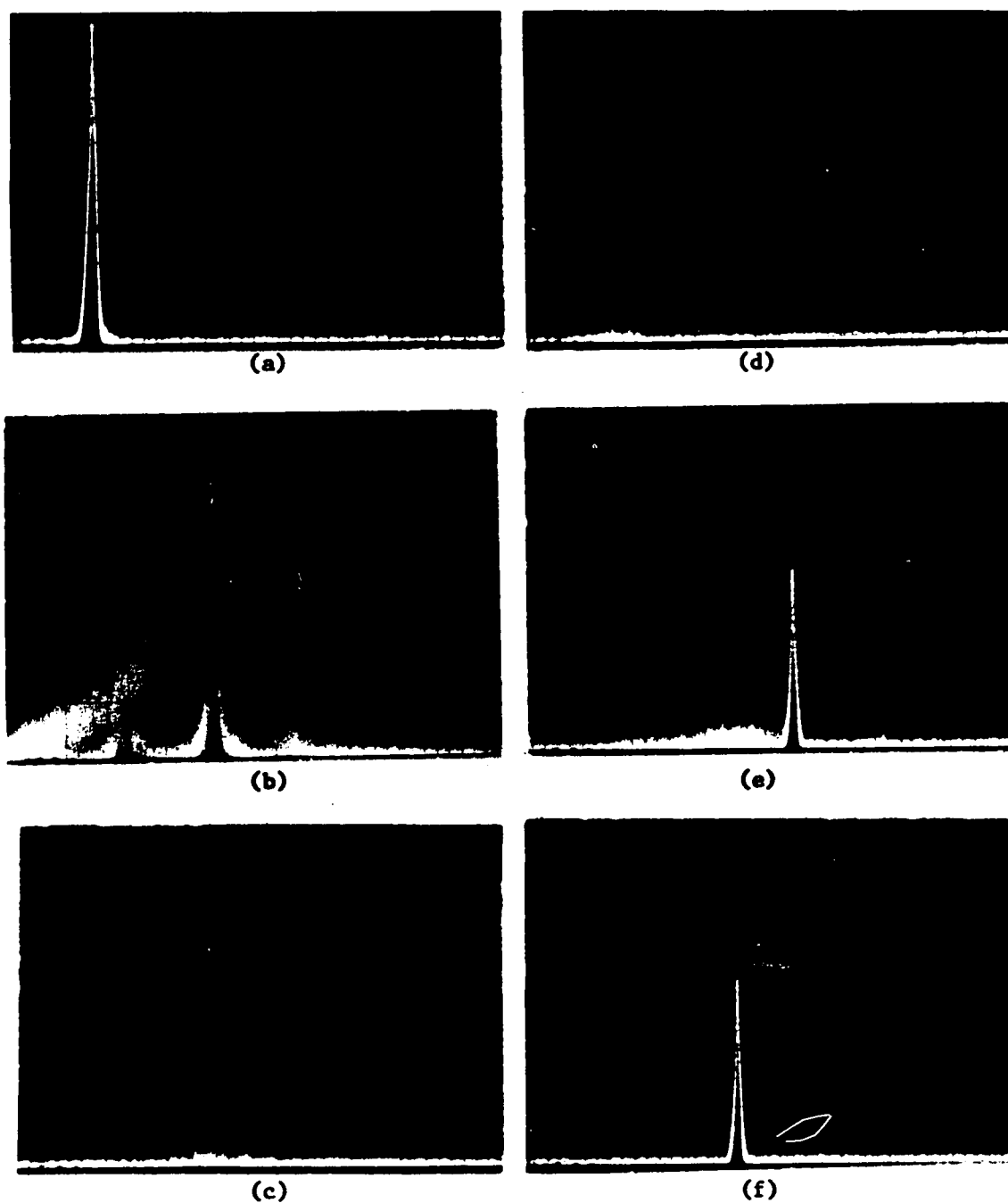
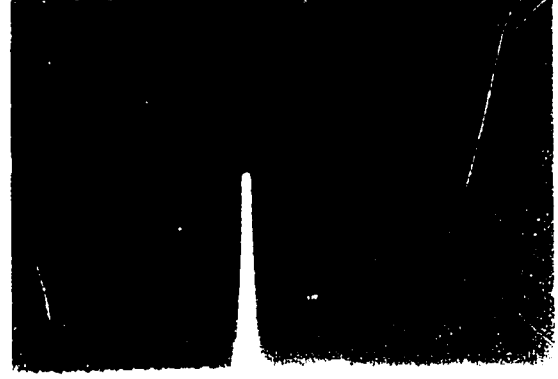
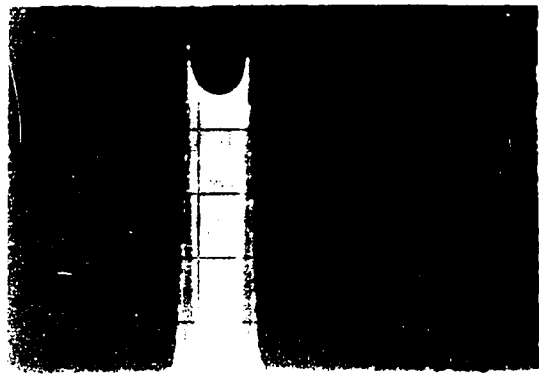
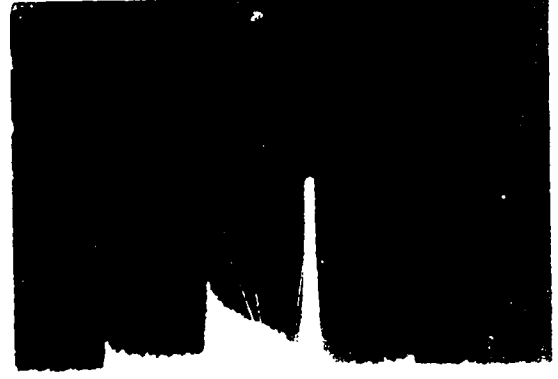
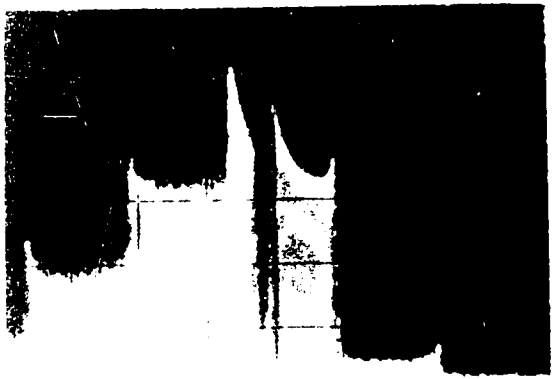
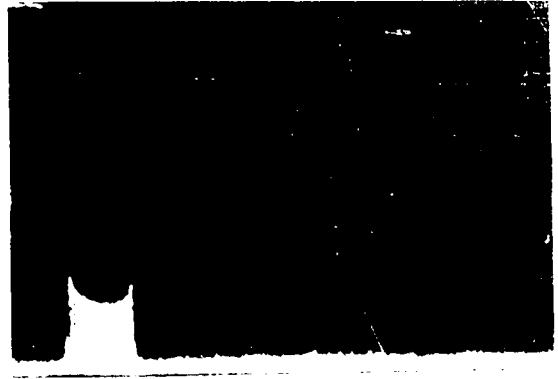
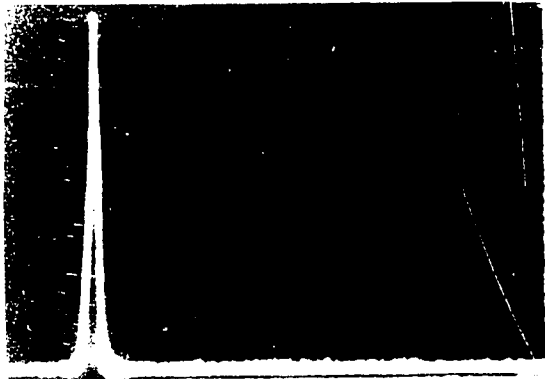


Fig.5-11 FREQUENCY SPECTRA OF SIDE-BAND LOCKED GUNN DIODE OSCILLATOR (CL8370-2):

- (a) and (d); NO-LOCKING SIGNAL IS APPLIED.
- (b) and (e); PARTIALLY PULLING OF UPPER SIDEBAND TO THE SIGNAL.
- (c) and (f); LOCKING OF SIDEBAND TO THE SIGNAL.

Vertical Scale, 10 DB/div. Horizontal Scale, 3 MHz/div.



amplified and up-converted VHF FM signal.

So far, two types of phase control of the IMPATT diode oscillator and of a Gunn diode oscillator by injection of energy from a reference signal into the oscillator have been discussed. An entire frequency pulling of the bias modulated oscillators yields a practical phase modulation scheme. Partial pulling properties permit the oscillators to be sideband-locked, achieving up-conversion with gain and frequency stability.

CHAPTER VI

FREQUENCY DEMODULATION BY INJECTION PHASE-LOCKING

6-1 Introduction

It has been shown⁸⁷⁻⁸⁸ that the locking properties of the phase-locked loop and of injection phase locked oscillators are described by the same differential equation. Recognition of this basic similarity can generate new applications. Since a phase-locked loop oscillator can be used as a frequency demodulator, in which application it has superior performance to a conventional discriminator, an injection locked oscillator can also be used as a frequency demodulator with good performance. This chapter deals with the properties of the injection locked oscillator in frequency demodulation.

Injection phase-locked oscillator frequency demodulators using vacuum tube oscillators have been built by Woodyard⁸⁹, Carnahn and Kalmus⁹⁰, Beers⁹¹, Bradley⁹², and Corrington⁹³ and good experimental results have been reported. Since the advent of microwave solid-state oscillators such as the IMPATT diode and Gunn diode, the application of injection phase-locking has become attractive at microwave frequencies due to the simplicity of the circuitry and the potential locking range of the locked oscillators. As a result, the FM receiver application of injection locked microwave oscillators using IMPATT diodes and Gunn diodes will become very interesting for microwave FM reception. We shall first give a general description of the circuitry and then consider the details.

The demodulation process makes use of two modes of operation. The first mode of operation occurs inside the diode of the locked oscillator. The second mode of operation occurs in a crystal detector where the input signal and the locked output signal are combined and mixed outside the locked oscillator.

The oscillator in FM reception is either locked in or it is not; there is no intermediate condition. If the incoming signal is too weak to lock in the oscillator for the full deviation, the oscillator may break out at the ends of the swing and cause distortion. The demodulator in the injection locked configuration must have sufficient sensitivity ahead of the locked oscillator to assure that the input to the oscillator is adequate to lock in the oscillator for all signals to be received. In other words, the baseband bandwidth of the injection locked frequency demodulator must be less than the locking range of the locked oscillator.

On the other hand, considerable attention has been given also to the possible use of microwave oscillators as regenerative mixers⁹⁴⁻¹⁰⁵. As discussed in Section 3-5, when the locking signal frequency is located outside of the locking range, the beat frequency is not exactly equal to the initial frequency difference: the beat frequency is less than the initial frequency difference and is dependent upon the injection level because of the partial locking phenomena.

As seen in Fig.4.3, the amplitude spectrum of the oscillator output at the locking frequency is increased as the locking frequency approaches the free-running frequency, and a complicated output spectrum occurs. As a result, the level and frequency of the beat note vary with the locking signal.

However, when the injection power level is small compared to that of the oscillator output, the oscillator diode can be used simultaneously as a self-oscillating regenerative mixer; a simple down-converter using a microwave oscillator as a mixer and local oscillator may be obtained. The oscillator is operated much the same way as for a detector, but with one major difference; the diode is permitted to oscillate while as a detector it is passive.

In addition for the case of the Gunn diode, not only the microwave signal but also the IF component can be amplified by the negative resistance¹⁰⁶ with a positive conversion gain. However, for the case of the IMPATT diode the IF signal cannot be amplified because the low frequency negative resistance found in Gunn Diodes does not appear. Nevertheless, it will be confirmed that the FM injected signal is amplified and demodulated by the IMPATT diode.

6-2 Injection Locked FM Reception

A circuit diagram of the injection-locked FM receiver is shown in Fig.6.1. The diode in the locked oscillator is used as a frequency demodulator. It can provide efficient limiting, FM demodulation within a single diode with no need for a complicated circuit. The input circuit can be connected directly. By itself, it can be used as a broad-band limiter followed by a wide-band detector and will provide excellent overall performance. The incoming microwave FM signal was injected into the diode of the oscillator through an isolator, attenuators, a coupler, and a waveguide rotary switch. The oscillator output power and frequency were measured by a power monitor and a frequency counter, respectively, through a waveguide rotary switch. The locked output was displayed on

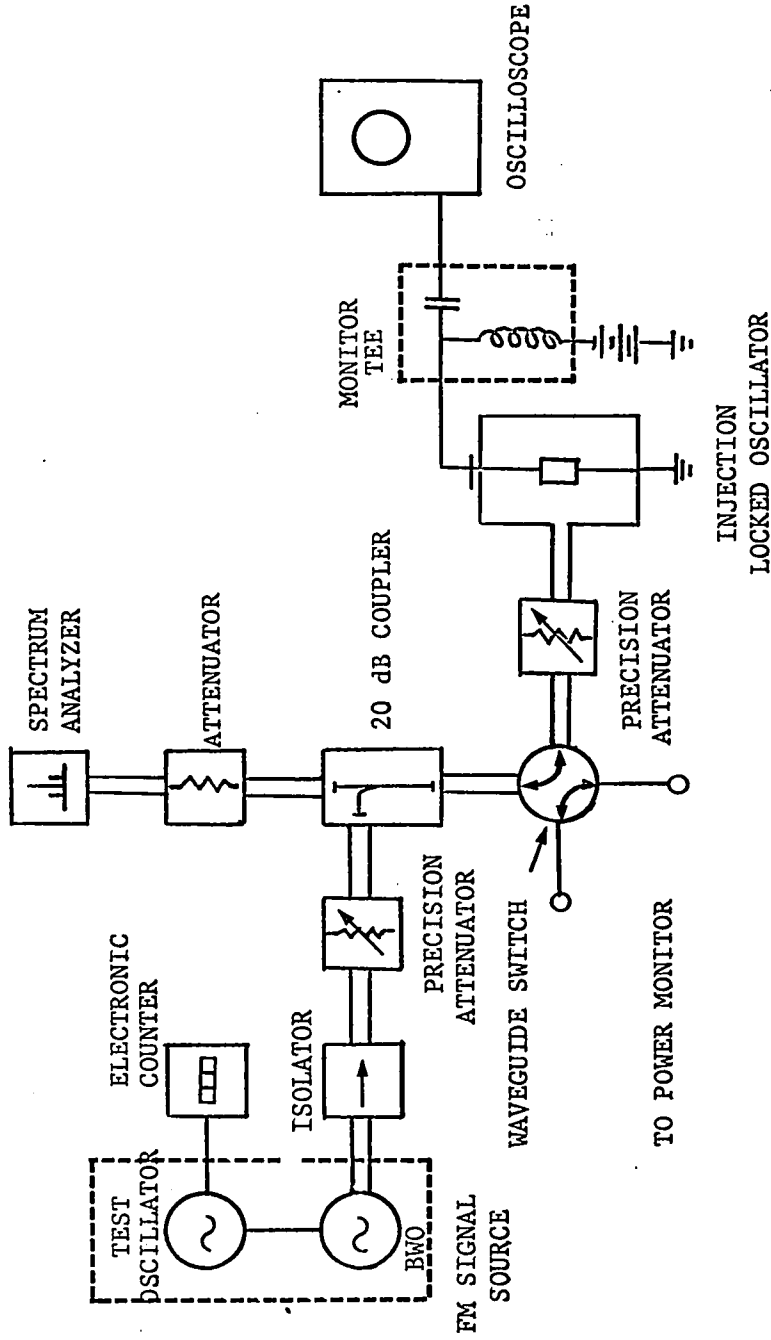


Fig.6-1 AN EXPERIMENTAL SETUP FOR INJECTION PHASE-LOCKED FM RECEPTION

the spectrum analyzer for monitoring the locking. The same circuit for the monitor tee as discussed in Section 5-2-2 was used. The detected output was coupled to the oscilloscope through the capacitor arm of the monitor tee.

Let us consider the condition when the oscillator is operating normally at a frequency determined by the tuned circuit. Oscillation at any other frequency is prohibited by phase shift introduced by the tuned circuit. When a locking signal of slightly different frequency is applied to the oscillator, the resultant voltage across the diode will be the vector sum of the locking signal and the output voltages. A phase shift between the locking and oscillator signals is required to maintain oscillation at the frequency of the locking signal.

As the locking signal deviates above and below the center frequency, the amplitude and the phase with respect to the carrier of the resultant voltage across the diode of the oscillator varies with the original FM. In other words, the locking signal is combined with the oscillator output in the diode where two signals interfere because of the phase difference introduced by the oscillator. Thus at the diode, the FM signal is converted to an AM-PM signal whose AM is linearly related to the frequency deviation of the original FM, over a bandwidth sufficient to accept a full frequency swing encountered in the FM signal.

If the carrier deviation extends beyond the locking range of the oscillator, the circuit will not be able to remain in step with the deviation of the input carrier. This results in a "breakout" condition,

which can be observed at the extremes of the demodulator characteristics. The breakout phenomena represent the modified beat frequency swings between the deviating carrier and the oscillating demodulator, as discussed in Section 3-4-1. Thus, if the carrier deviates beyond the locking range, the oscillator will not remain synchronized with the input carrier and will therefore oscillate in the unlocked but driven condition. So long as the carrier frequency deviations remain within the locking range, the oscillator circuit will be forced or pulled into step with the input signal.

The sensitivity is high since a relatively weak input signal can control relatively strong oscillations.

Its circuitry is very simple and its alignment is straightforward. Consequently, this type of demodulator is attractive at the higher microwave frequencies, where conventional demodulators are difficult to build.

Let us analyze the oscillating demodulator circuit. Let the input signal be an FM signal expressed as

$$e_s = E_s \sin\left(\omega_c t - \frac{\Delta\omega}{\omega_m} \cos \omega_m t\right) \quad (6.1)$$

where ω_c is the center frequency of the FM signal, $\Delta\omega$ is the maximum frequency deviation, and ω_m is the modulating frequency of the FM.

The output of the injection-locked oscillator can be, according to the locking theory described in Chapter III, expressed as

$$e = E \sin\left(\omega_c t - \frac{\Delta\omega}{\omega_m} \cos \omega_m t - \theta(t)\right) \quad (6.2)$$

where $\theta(t)$ is the instantaneous phase difference between the input and the output signal. The demodulator output is contained in $\theta(t)$.

It is well-known that any device with a nonlinearity in its voltage-current characteristic may be used as a detector. The IMPATT diode is such a device due to the space charge generated by the avalanche¹⁷, the Gunn diode is also such a device due to the growth of space-charge waves¹⁰⁶.

The demodulated output voltage may be (ref. Eq. D.9 of Appendix-D) expressed as

$$v_o(t) = M_1 E_s E \sin \theta(t) \quad (6.3)$$

where M_1 is the demodulator circuit constant.

The instantaneous phase in Eq. 6.2 can be determined from the basic locking equation discussed in Chapter III. With the input signal, expressed as Eq. 6.1, the locking equation of the locked oscillator may be, from Eq. 3.38, written as

$$\frac{d\theta}{dt} + \Delta_o \sin \theta = (\omega_c - \omega_o) + \Delta\omega \sin \omega_m t \quad (6.4)$$

where Δ_o is the maximum initial frequency difference of the locked oscillator at the given locking power level.

Let us assume that ω_m is low enough so that $d\theta/dt$ is negligible compared to Δ_o . Thus, under the quasi-state locked condition, we obtain from Eq. 6.4,

$$\sin \theta = \frac{\omega_c - \omega_o}{\Delta_o} + \frac{\Delta\omega}{\Delta_o} \sin \omega_m t \quad (6.5)$$

In order that Eq. 6.5 be a solution to Eq. 6.4 it is necessary that

$$\frac{d\theta}{dt} = \frac{\frac{\Delta\omega \omega_m}{\Delta_o} \cos \omega_m t}{1 + \left[\left(\frac{\omega_c - \omega_o}{\Delta_o} \right) + \frac{\Delta\omega}{\Delta_o} \sin \omega_m t \right]^2} \quad (6.6)$$

for all t . From Eq. 6.6 an excellent approximate solution can be obtained.

By substituting Eq. 6.5 into Eq. 6.3, we obtain

$$v_o(t) = \frac{M_1 E_s E}{\Delta_o} (\omega_c - \omega_o) + \frac{M_1 E_s E \Delta\omega}{\Delta_o} \sin \omega_m t \quad (6.7)$$

The first term of the right-hand side of the above equation represents a DC component due to the FM signal injection locking. The first term gives the direction of the frequency difference; its magnitude is proportional to that of the frequency difference. This DC component is responsible for the pull-in phenomena described in Chapter III; actually, variations of this component give rise to a change in effective susceptance which results in frequency synchronization to the center frequency of the FM signal.

According to the above analysis, a voltage and current curve can be plotted as a function of frequency in Fig. 6.2.

So far, we have discussed a quasi-state case. In the derivations

the tacit assumption has been made that the modulating frequency involved is low. As seen in Eq. 6.7, the modulating signal is ideally reproduced under the above condition. If this condition is not satisfied, we must solve the system differential equation in order to describe the phase more correctly.

In Ruthroff's paper¹⁰⁷ a solution of improved accuracy to Eq. 6.4 has been found by an iteration procedure:

$$\begin{aligned} \sin \theta(t) = & \left[\frac{\omega_c - \omega_o}{\Delta_o} + \frac{\Delta\omega}{\Delta_o} \sin \omega_m t \right] - \left[\frac{\omega_m \Delta\omega \cos \omega_m t}{\Delta_o^2} \right] \\ & - \left[\frac{\omega_m^2 \Delta\omega \sin \omega_m t}{\Delta_o^3} \right] + \left[\frac{\omega_m^3 \Delta\omega \cos \omega_m t}{\Delta_o^4} \right] \\ & + \left[\frac{\omega_m^4 \Delta\omega \sin \omega_m t}{\Delta_o^5} \right] - \dots \\ & - \left[\frac{\omega_m \Delta\omega^3 \cos \omega_m t \sin^2 \omega_m t}{2\Delta_o^4} \right] + \dots \end{aligned} \quad (6.8)$$

The first term of the right side of Eq. 6.8 is the frequency modulation on the input signal and the other terms provide some distortion. However, when the locking range is much larger than the modulating signal of input FM signal $-\Delta_o \gg \omega_m$, the other terms become negligible compared to the first term. Thus, the distortion becomes very small under these conditions. Thus, for $\omega_m < \Delta_o$, Eq. 6.8 is almost identical with Eq. 6.5. As a result, a linear operation of the demodulator may be predicted.

The demodulator characteristics can be shown in Fig.6.2. Inside the locking bandwidth A-B, linear characteristics may be obtained. The "breakout" represents the difference beat between the oscillating

demodulator and the RF carrier. This phenomenon will be discussed in the next section.

Similarly, the other mode of operation can be analyzed. Fig.5.1 may be used for explanation of a frequency demodulation scheme, (no use is made of the modulating signal oscillator at the locked oscillator). In this case we connect only the locked oscillator to port 2 of the circulator. An FM signal into the first coupler is divided into two parts. One signal is used for injection locking of the oscillator and the other signal bypasses the oscillator and is combined with the oscillator output by a second coupler. In the coupler the phase-shifted and non-shifted signals from the FM source are added and subtracted as a function of frequency and fed to a crystal detector. From the detector we obtain the base-band output signal. The mechanism is the same as before. It is also understood that the vector-voltage addition and detection may be accomplished by means of a magic tee balanced detector (Appendix-D) or a hybrid detector.

6-3 Experimental Performance of Frequency Demodulation

The experimental setup for this FM signal reception is shown in Fig.6.1. The FM signal was obtained by modulating an X-band BWO with a test signal.

The maximum frequency deviation measurement of the FM signal was made with a spectrum analyzer. By knowing the modulating frequency and the modulating indices at which the carrier and sidebands, respectively, go to zero, we can measure the FM deviation. For a single tone FM signal, any deviation within the limits of the oscillation may

be set up by choosing the correct combinations of modulation index and modulation frequency.

Fig.6.3 shows the oscillating demodulator characteristics of a typical IMPATT diode oscillator (SYA-3200-3) and a typical Gunn diode oscillator (CL-8370-3). The characteristic is very linear over the locking bandwidth of the oscillator. If the carrier deviation extends beyond the locking bandwidth, the circuit will not be able to remain in step with the deviations of the FM carrier. This results in a condition known as "breakout" which can be observed at the extremes of the demodulator characteristics in Fig.6.3(a) and (c). The breakout phenomena represent the difference beats between the deviating carrier and the oscillating demodulator. So long as the carrier frequency deviations remain within the locking range the circuit will be forced or pulled into step with the input signal. In Fig.6.3(b) and (d) all the carrier frequency deviations remain within the locking range and then the circuit is synchronized with the input locking FM signal.

In a multiplex signal situation, or with a single wideband signal, where nearly the entire locking range is occupied by the signal bandwidth, it is important to maintain the free-running frequency equal to the center frequency of the information bandwidth. The voltage tunability of the oscillator would be useful for this purpose.

Eqs. 6.5 and 6.7 show that the maximum variations of $\sin \theta$ or the detected amplitude will be directly proportional to the modulating voltage of the FM input, when the free-running frequency ω_0 is made equal to the center frequency of the FM, ω_c . Experimentally this was found to be the case, as is shown in Fig. 6.4. For a Gunn diode oscillator (CL-8370-4) the measured amplitudes of the detector output

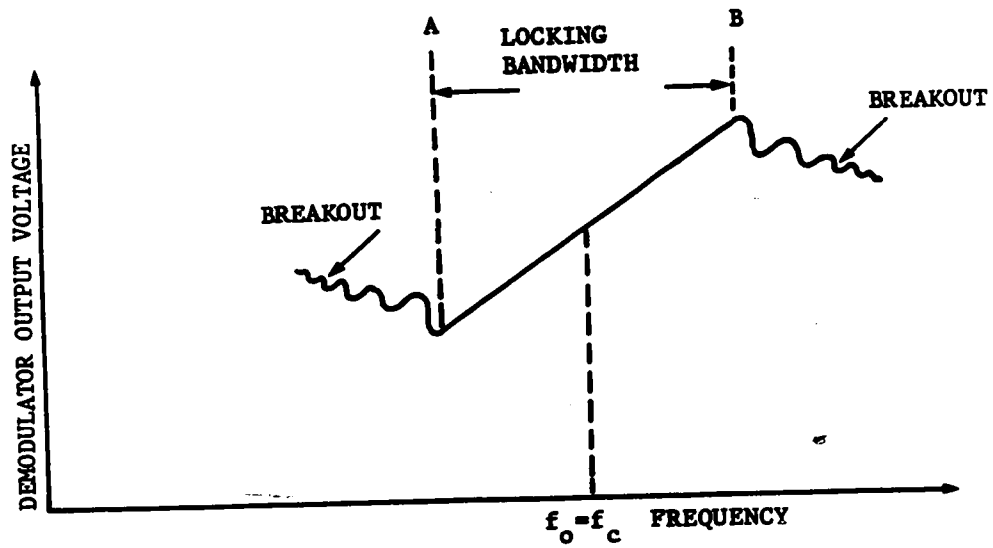


Fig.6-2 DEMODULATOR CHARACTERISTICS SHOWING THE BEATS OCCURING OUTSIDE LOCKING BANDWIDTH.

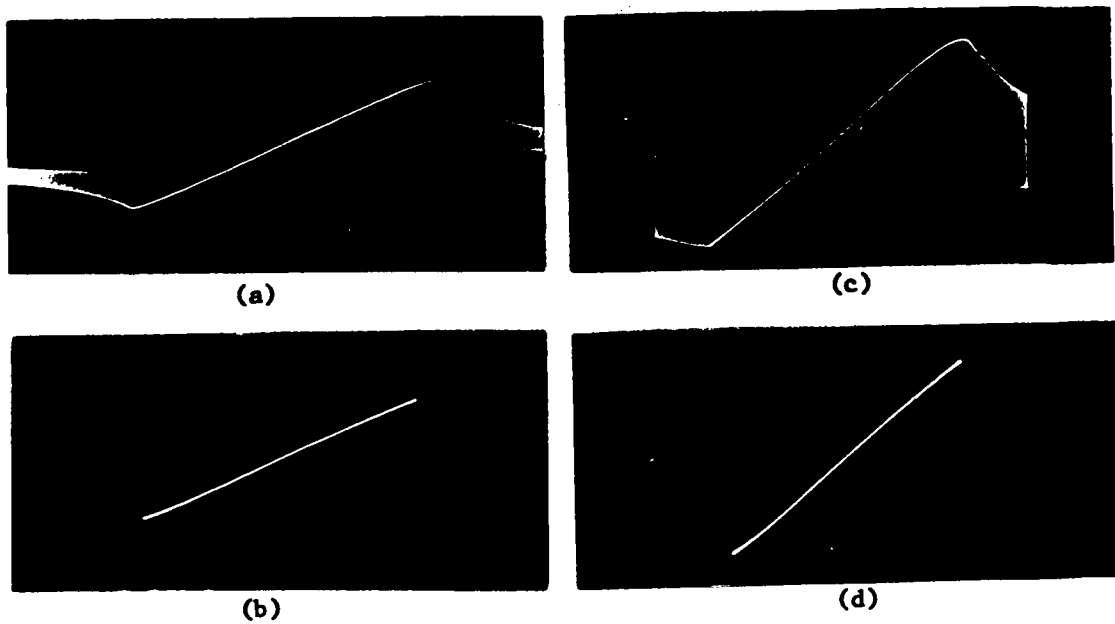
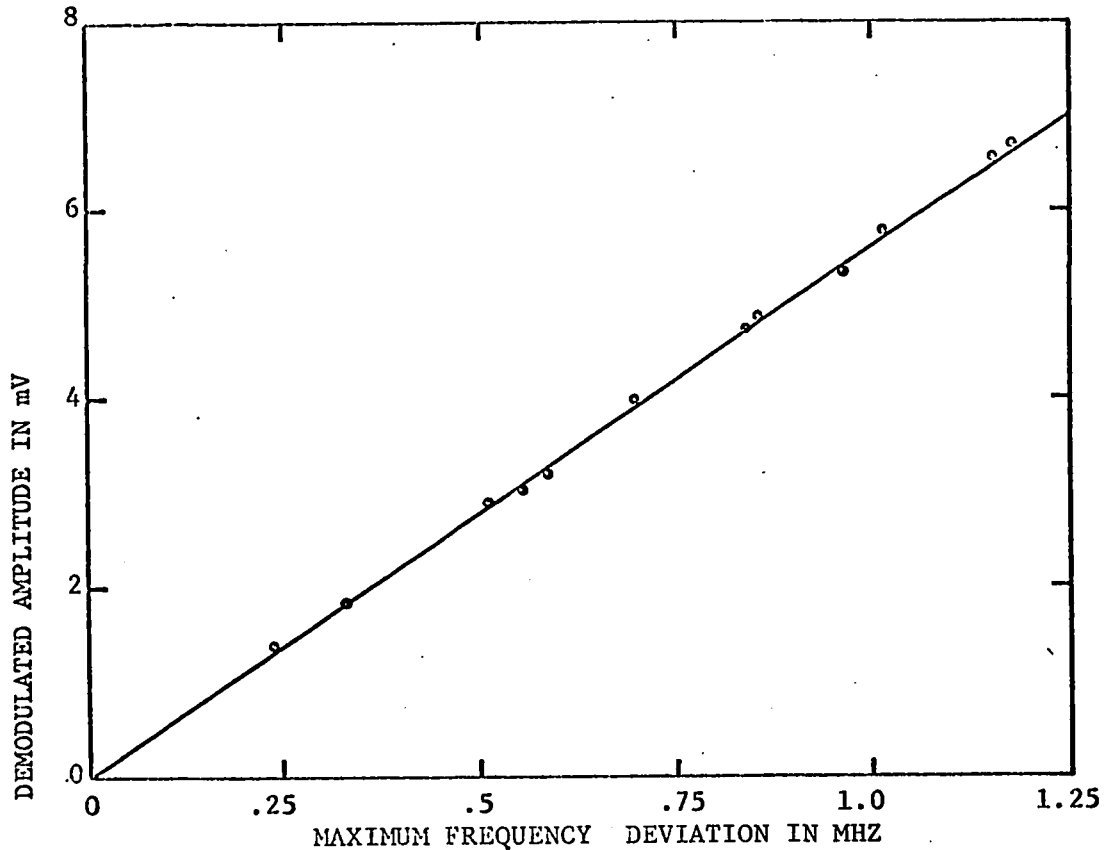


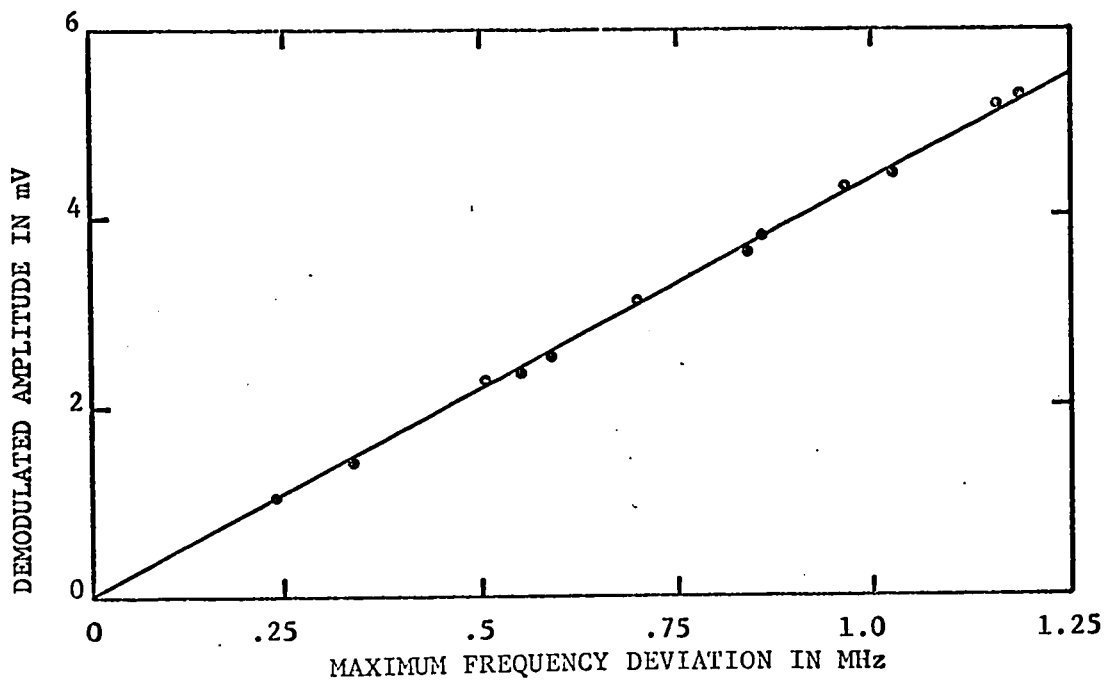
Fig.6-3 (a) and (b) OSCILLOSCOPIC DEMODULATOR CHARACTERISTICS OF AN IMPATT DIODE OSCILLATOR (SYA-3200-3);
 (c) and (d) A GUNN DIODE OSCILLATOR (CL-8370-3);
 Vertical Scale: 22mV/division. Horizontal Scale: 7.7 MHz/division.

voltage versus maximum frequency deviations are plotted in Fig.6.4 for a modulating frequency of 100 KHz and a power gain of 20 dB. For the given operating conditions, the demodulation sensitivity is 5.6 mV per MHz of frequency deviation for the Gunn diode oscillator and it is 4.4 mV per MHz for an IMPATT diode oscillator (SYA-3200-4), as seen in Fig.6.4.

From this analysis, it is shown that linear operation is possible over base-band bandwidths approaching the oscillator locking range.



(a) GUNN DIODE OSCILLATOR (CL-8370-4)



(b) IMPATT DIODE OSCILLATOR (SYA-3200-4)

Fig. 6-4 DEMODULATOR OUTPUT VOLTAGE VS. MAXIMUM FREQUENCY DEVIATION FOR A MODULATING FREQUENCY OF 100 KHz WHEN THE LOCKING GAIN IS 20 dB.

CHAPTER VII

SUMMARY AND CONCLUSIONS

A detailed systematic study of the injection phase-locking properties of microwave IMPATT diode oscillators and of Gunn diode oscillators was carried out by use of the locking equations derived from the loading effect of the locking signal on the oscillator. The results obtained indicate the IMPATT diode and Gunn diode oscillators may be suitable for system applications as microwave FM amplifiers, demodulators, and angle-modulators. Following conclusions can be drawn from the study of injection phase-locking properties:

1. IMPATT and Gunn diode oscillators can be locked in frequency by an external signal which is injected into the oscillator. The mechanism of the locking process depends on (1) the initial frequency difference between the oscillator and the injected signals, (2) the relative amplitude between the oscillator and the injected signals, and (3) the oscillator circuit parameters.
2. The injection phase-locking properties of the microwave oscillator are determined qualitatively by use of the loading effect method in which the injected signal is considered as a reflected wave from a mismatched load. The effective susceptance is a finite positive or negative susceptance added in parallel with the equivalent circuit of the locked one-port oscillator and the locking signals under locked conditions. In addition, the locking signal contributes a negative conductance to the load of the oscillator.

3. The loading effect theory develops locking differential equation which is useful even for comparatively high levels of locking signal power. The resulting differential equation has been solved and the results have been presented graphically with curves which can be used to determine the properties of an injection-locked oscillator required for a desired locking time. When the locking signal amplitude is relatively small compared to the oscillator output, the locking equation reduces to a simple one.
4. The locking figure of merit characterizes the locking efficiency of an oscillator. This parameter is dependent only upon the oscillator circuit and therefore a method of Q measurement by injection phase-locking is simpler and more accurate than a conventional method at microwave frequencies.
5. The injection phase-locked oscillator may be used as an amplifier for frequency-modulated microwave signals, without excessive amplitude modulation. The gains and bandwidths obtained from the CW locking tests indicate that amplification of 20 MHz bandwidth signals at 20 dB gain could be achieved with the IMPATT diode oscillator whose external Q was approximately 98 and that of 36 MHz bandwidth signals at 20 dB gain with the Gunn diode oscillator whose external Q was approximately 52.
52. In order to minimize the distortion in FM signal amplification the center frequency of the input FM signal must be located at the free-running frequency of the oscillator.
6. The modulation suppression of an FM locking signal in the injection-locked oscillator is very small while the FM noise of the oscillator is considerably reduced by the injection phase-locking: this conclusion is

supported by the conservation and suppression rates of modulation, which are derived from the fundamental locking equation of phase angle.

7. Outside the locking range, the phase angle between the oscillator and external signals varies at a relatively slow rate compared to the frequency of oscillation. The pulled oscillations represent, in general, frequency and amplitude modulated waves, but the degree of amplitude modulation is very small. The fundamental frequency of modulation - average beat frequency - decreases as the locking condition is approached. The average frequency of oscillation is shifted from the free-running frequency toward the external frequency by an amount depending on the external signal amplitude and frequency.

8. The locking equation derived from the loading effect has been shown experimentally to be applicable to driven IMPATT and Gunn diode oscillators. The measured basic steady-state locking performance of the oscillators is satisfactory for some system applications. The information necessary to identify an oscillator for system applications is: (1) free-running frequency, (2) output power, and (3) locking figure of merit. The parameters, output power and locking figure of merit, are normally slight functions of frequency.

9. The variation in detected power from the locked oscillator, with locking signal amplitude, appears to support the hypothesis that the detected power is a constructive or destructive interference combination of the oscillator output and reflected locking signal. As the locking signal amplitude increases, nonlinear electronic admittance effects cause the locked oscillator output power to have an asymmetric distribution

about the free-running frequency.

10. It has been verified experimentally that the approximate expressions derived for modulation suppression rates of an injection-locked oscillator can be applied to the IMPATT and the Gunn diode oscillators; in the locking band, the modulation suppression of an FM driving signal in the locked oscillator is very small, while the oscillator noise, which dominates the entire output characteristic, is considerably reduced.

11. Frequency stabilization of a self-excited oscillator has been obtained by using a self-injection phase-locking technique, in which a small fraction of output power is passed through a high Q cavity and injected back into the oscillator itself through a circulator thus heightening the external Q of the oscillator.

12. A type of phase control of bias-modulated IMPATT and Gunn diode oscillators has been achieved by injection of energy from a CW reference signal into the oscillators. An entire frequency locking of bias-modulated oscillators yields a practical phase modulation scheme at microwave frequencies, which might be used directly for communication purposes.

13. Partial pulling properties of the driven oscillator have been used to permit the IMPATT and Gunn diode oscillators to be side-band locked, achieving up-conversion with gain and frequency stability.

14. Another application for the locked oscillator is as a practical frequency demodulator. In one mode of operation, the microwave oscillator diode is simultaneously used for quasi-steady-state phase locking and

detection. Linear operation of the frequency demodulator has been obtained. The measured data verify that the locked IMPATT and the Gunn diode oscillators with an FM locking signal obey the locking equation and agree sufficiently well with the values predicted by the quasi-steady-state solution to the locking equation. In addition, far outside the locking range, the Gunn diode oscillator can be an efficient regenerative mixer for microwave detection, due to the low-frequency negative conductance of Gunn diodes.

REFERENCES

1. B. van der Pol, "*Forced oscillations in a circuit with nonlinear resistance*", Phil. Mag., vol. 3, pp 65-80, January 1927.
2. D.G. Tucker, "*The synchronization of oscillators*", Electronic Engng., vol. 15, pp 415-457, vol. 16, pp 26-114, 1943.
3. C.W. Carnahan and H.P. Kalmus, "*Synchronized oscillators*", Electronics, vol. 17, pp 108-111, August 1944.
4. D.G. Tucker, "*Forced oscillations in oscillator circuits and the synchronization of oscillators*", Journal of the IEE., vol. 92, Part III, p 226, 1945.
5. R. Adler, "*A study of locking phenomena in oscillators*", Proc. IRE, vol. 34, pp 351-357, June 1946.
6. R.D. Huntoon and A. Weiss, "*Synchronization of oscillators*", Proc. of IRE, vol. 35, pp 1415-1423, December 1947.
7. J.C. Slater, "*The phasing of magnetrons*", MIT Research Laboratory of Electronics, Technical Report No. 35, April 1947.
8. E.E. David, Jr., "*Locking phenomena in microwave oscillators*", MIT Research Laboratory of Electronics, Technical Report No. 63, April 1948.
9. R.V. Khokhlov, "*A method of analysis of the theory of sinusoidal self-oscillations*", IRE Trans. on Circuit Theory, pp 398-413, December 1960.
10. R.C. Mackey, "*Injection locking of klystron oscillators*", IRE Trans. on Microwave Theory and Techniques, pp 228-235, July 1962.
11. H.L. Stover and R.C. Shaw, "*Injection locked oscillators as amplifiers for angle modulated signals*", Digest of Technical papers, G-MTT International Symposium 1966.
12. H. Fukui, "*Frequency locking and modulation of microwave silicon avalanche diode oscillators*", Proc. IEEE (Correspondence), vol. 54, No. 10, pp 1475-1477, October 1966.
13. B.W. Hakki, J.P. Beccone and S.E. Plauski, "*Phase-locked GaAs CW microwave oscillators*", IEEE Trans. on Electron Devices (Correspondence), vol. ED - 13, No. 1, pp 194-196, January 1966.
14. K. Kurokawa, "*Noise in synchronized oscillators*", IEEE Trans. on Microwave Theory and Techniques, Vol. MTT-16, pp 234-240, April 1968.
15. M.E. Hines, J.R. Collinet and J.G. Ondria, "*FM noise suppression of an injection phase-locked oscillator*", IEEE Trans. on Microwave Theory and Techniques, vol. MTT-16, pp 738-742, September 1968.

16. W. Shockley, "*Negative resistance arising from transit time in semiconductor diodes*", Bell System Tech. J., vol. 33, p. 799, 1954.
17. W.T. Read, "*A proposed high frequency negative resistance diode*", Bell System Tech. J., vol. 37, pp 401-446, March 1958.
18. R.L. Johnston, B.C. DeLoach, Jr., and B.G. Cohen, "*A silicon diode microwave oscillator*", Bell System Tech. J., vol. 47, p 366, 1964.
19. C.A. Lee, R.L. Badorf, W. Wiegmann, and G. Kaminsky, "*The Read diode - an avalanching, transit-time, negative resistance oscillator*", Appl. Phys. Letters, vol. 6, p. 89, 1965.
20. T. Misawa, "*Negative resistance on p-n junction under avalanche breakdown conditions, Part I and II*", IEEE Trans. on Electron Devices, vol. ED-13, pp 137-151, January 1966.
21. M. Gilden and M.F. Hines, "*Electronic tuning effects in the Read microwave avalanche diode*", IEEE Trans. on Electron Devices, vol. ED-13, pp 169-175, January 1966.
22. B.K. Ridley and T.B. Watkins, "*The possibilities of negative resistance effects in semiconductors*", Proc. Phys. Soc., vol. 78, pp 293-304, August 1961.
23. C. Hilsum, "*Transferred electron amplifiers and oscillators*", Proc. IRE, vol. 50, pp 185-189, February 1962.
24. J.B. Gunn, "*Microwave oscillations of current in III-V semiconductors*", Solid-State Communications, vol. 1, pp 88-91, September 1963.
25. H. Kroemer, "*Theory of the Gunn effect*", Proc. IEEE (Correspondence), vol. 52, p 1736, December 1964.
26. B.K. Ridley, "*Specific negative resistance in solids*", Proc. Phys. Soc. (London), vol. 82, pp 954-966, 1963.
27. D.E. McCumber and A.G. Chynoweth, "*Theory of negative conductance amplification and Gunn instabilities in "two valley" semiconductors*", IEEE Trans. on Electron Devices, vol. ED-13, pp 4-21, January 1966.
28. E.M. Conwell and M.O. Vassel, "*High field distribution function in GaAs*", IEEE Trans. on Electron Devices, vol. ED-13, pp 22-27, January 1966.
29. H. Kroemer, "*Nonlinear space charge domain dynamics in a semiconductor with negative differential mobility*", IEEE Tans. on Electron Devices, vol. ED-13, pp 27-40, January 1966.
30. J.L. Moll, Physics of Semiconductors, New York, McGraw-Hill Book Co., 1964.

31. S.M. Sze, Physics of Semiconductor Devices, New York; Wiley - Interscience, 1969.
32. J.A. Copeland, "*CW Operation of LSA oscillator diodes 44 GHz to 88 GHz*", Bell System Tech. J., vol. 46, pp 284-287, January 1967.
33. J.A. Copeland, "*Bulk negative resistance semiconductor devices*", IEEE Spectrum, vol. 4, pp 71-77, May 1967.
34. H. Kroemer, "*Negative conductance in semiconductors*", IEEE Spectrum, vol. 5, pp 47-56, January 1968.
35. W.A. Edson, "*Noise in oscillators*", Proc. IRE, vol. 48, pp 1454-1466, August 1960.
36. J.A. Mullen, "*Background noise in nonlinear oscillators*", Proc. IRE, vol. 48, pp 1467-1472, August 1960.
37. M.E. Hines, "*Potential applications and noise problem in the Read avalanche diode*", 1966 International Solid-State Circuit Conf., Digest of Tech. Papers, pp 82-83.
38. H.K. Gummel and J.L. Blue, "*A small-signal theory of avalanche noise in IMPATT diodes*", IEEE Trans. on Electron Devices, vol. ED-14, pp 569-580, September 1967.
39. J.G. Josenhaus, "*Noise spectra of Read diode and Gunn oscillators*", Proc. IEEE (Letters), vol. 54, pp 1478-1479, October 1966.
40. R.L. Rulison, G. Gibbons, and J.G. Josenhaus, "*Improved performance of IMPATT diodes fabricated from Ge*", Proc. IEEE, vol. 55, p 223, 1967.
41. D.W. Draysey, W.P.N. Court, and I.B. Bott, "*Noise performance of Gunn microwave generators in X and J band*", Electronics Letters, vol. 2, pp 125-126, March 1966.
42. G.S. Hobson, "*Source of FM noise in cavity controlled Gunn effect oscillators*", Electronics Letters, vol. 3, pp 63-64, February 1967.
43. J.B. Johnson, "*Thermal agitation of electricity in conductors*", Physical Review, vol. 32, pp 97-109, July 1928.
44. J.L. Altman, Microwave Circuits, New York, D. Van Nostrand Company, 1964.
45. T. Isobe and M. Tokida, "*A new microwave amplifier for multichannel FM signal using a synchronized oscillator*", IEEE Journal of Solid-State Circuits, vol. SC 4, December 1969, pp 4000-4008.

46. M.E. Hines, J.R. Colliet, and J.G. Ondira, "*FM noise suppression of an injection phase-locked oscillator*", IEEE Trans on Microwave Theory and Techniques, vol. MTT-16, pp 738-742, September 1968.
47. H.L. Stover, "*The theoretical explanation for the output spectra of unlocked driven oscillators*", IEEE vol. 54, pp 310-311, February 1966.
48. H. Lashinski, "*Periodic pulling and the transition to turbulence in a system with discrete modes*", The symposium on Turbulence of Fluids and Plasmas, Polytechnic Institute of Brooklyn, April 16-18, 1968.
49. M.E. Hines, "*Noise theory for the Read type avalanche diode*", IEEE Trans. on Electron Devices, vol. EC-13, pp 158-163, January 1966.
50. E.A. Faulkner and M.L. Meade, "*Frequency modulation noise in Gunn oscillators*", Electronic Letters, vol. 3, p 419, September 1967.
51. S.L. Johnson, B.H. Smith, and D.A. Calker, "*Noise spectrum characteristics of low noise microwave tubes and solid-state devices*", Proc. of the IEEE, vol. 54, pp 258-265, February 1966.
52. R.H. Dishington, "*Diode phase discriminators*", Proc. IRE, vol. 37, pp 1401-1404, December 1949.
53. W.J. Gruen, "*Theory of AFC synchronization*", Proc. IRE, vol 41, pp 1043 - 1048, August 1953.
54. A.F. Harvey, Microwave Engineering, New York; Academy Press, 1963, pp 767-769.
55. F.M. Gardener, Phaselock Techniques, New York; John Wiley, 1966, pp 58-66.
56. R.V. Pound, Rad. Lab. Series, Vol. 11, New York, McGraw-Hill Book Company, 1947, pp 58-78.
57. V.C. Rideout, "*Automatic frequency control of microwave oscillators*", Proc. IRE, vol. 35, pp 767-771, August 1947.
58. R.V. Pound, "*Frequency stabilization of microwave oscillators*", Proc. IRE, vol. 35, pp 1405-1415, December 1947.
59. W.G. Tuller, W.C. Galloway, and F.P. Zaffarano, "*Recent developments in frequency stabilization of microwave oscillators*", Proc. IRE, vol. 36, pp 794-800, June 1948.

60. M.E. Hines, "*Negative resistance diode power amplification*", Trans. IEEE on Electron Devices, vol. ED-17, pp 1-8, January 1970.
61. N.B. Cramer, "*Characterization and modeling of IMPATT oscillators*", IEEE Trans. on Electron Devices, vol. ED-15, pp 838-846, November 1968.
62. J.L. Blue, "*Approximate-large signal analysis of IMPATT oscillators*", Bell Systems Tech. J., pp 383-396, February 1969.
63. D.L. Scharfetter and H.K. Gummel, "*Large signal analysis of a silicon Read diode oscillator*", IEEE Trans. on Electron Devices, vol. ED-16, pp 64-77, January 1969.
64. W.J. Evens and G.I. Haddad, "*A large-signal analysis of IMPATT diodes*", IEEE Trans. on Electron Devices, vol. ED-15, pp 708-717, October 1968.
65. A.J. Viterbi, "*Acquisition and tracking behaviour of phase-locked loops*", JPL External Publication No. 673, July 14, 1959.
66. G.A. Peterson and B.W. Knight, "*Nonlinear analysis of the Gunn effect*", Bull. Am. Phys. Soc., vol. 11, p 174, March 1966.
67. P. Jochen, "*Equivalent circuit for injection locked negative-resistance oscillators*", Electronics Letters, vol. 6, pp 61-62, February 1970.
68. P.A. Goud, "*Solid-state microwave sources*", The Journal of Microwave Power, vol. 2, pp 99-103, 1968.
69. J. Bartnik, "*Increasing rf power by summing*", Electronics, vol. 39, pp 101-107, May 1966.
70. H. Fukui, "*Frequency locking and modulation of microwave silicon avalanche diode oscillator*", Proc. of the IEEE (Correspondence), vol. 54, pp 1475-1477, October 1966.
71. I. Tatsuguchi, "*A frequency-modulated phase-locked IMPATT power combiner*", 1970 IEEE International Solid-State Circuits Conference Digest of Technical Papers, pp 18-19.
72. S. Mizushina, "*2ⁿ oscillators combined with 3-dB directional couplers for output power summing*", Proc. of the IEEE (Correspondence), vol. 55, pp 2166-2167, December 1967.
73. J.R. Nevarez, and G.J. Herskowitz, "*Output power and load analysis of 2ⁿ injection-locked oscillator combined through an ideal and symmetric hybrid combiner*", IEEE Trans. on Microwave Theory and Techniques, vol. MTT-17, pp 2-10, January 1969.
74. B.W. Hakki and S. Knight, "*Microwave phenomena in bulk GaAs*", IEEE Trans. on Electron Devices, vol. ED-13, pp 94-105, January 1966.

75. I.B. Bott, C. Hilsom, and B.C. Taylor, "*Amplitude and frequency modulation of transferred electron microwave generators*", IEEE Trans. on Electron Devices (Correspondence), vol. ED 13, pp 193-194, January 1966.
76. K. Yokoo, S. Ono and Y. Shibata, "*The electronic tunable Gunn diode oscillator*", IEEE Trans. on Electron Devices, vol. ED 16, pp 494-497, May 1969.
77. B. Martin and G.S. Hobson, "*High speed phase and amplitude modulation of Gunn oscillators*", Electronics Letters, pp 224-226, April 1970.
78. M. Shoji, "*A voltage tunable Gunn effect oscillator*", Proc. of the IEEE (Correspondence), vol. 55, pp 130-131, January 1967.
79. B.S. So and P.A. Goud, "*Injection phase-locking properties of bias-modulated IMPATT diode oscillators*", 8th International Conference Proceedings on Microwave and Optical Generation and Amplification (MOGA) 1970.
80. R.H. Haitz, "*Noise of a self-sustaining avalanche discharge in silicon: low-frequency noise studies*", J. Appl. Phys. vol. 38, p 2935, June 1967.
81. E.F. Scherer, "*Investigation of the noise spectra of avalanche oscillators*", IEEE Trans. on Microwave Theory and Techniques, Vol. MTT 16, pp 781-788, September 1968.
82. J.J. Goedbloed, "*On the upconversion noise of IMPATT-diode oscillator*", 8th International Conference Proc. of MOGA 1970, Amsterdam, Netherlands.
83. A.E. Mostafa, and A.F. Kheireldin, "*Pulled oscillations in a triode oscillator distributed by an external signal*", Special issue on Electronics, Alexandria University Press, pp 17-49, vol. 8, 1969.
84. T.J. Buchanan, "*The frequency spectrum of a pulled oscillator*", Proc. of the IRE, vol. 40, p 958, August 1952.
85. S. Goldman, Frequency Analysis, modulation and noise, New York, McGraw-Hill Book Company, pp 154-156, 1948.
86. Members of the Technical Staff of Bell Telephone Laboratories, Transmission Systems for Communications, Bell Telephone Laboratories, June 1965.
87. T.P. Lee, R.D. Standley, and T. Misawa, "*A 50 GHz Silicon IMPATT diode oscillator and amplifier*", IEEE Trans. on Electron Devices, vol. ED-15, pp 741-747, October 1968.
88. F.M. Gardener, Phaselock Techniques, New York, John Wiley, 1966.

89. J.R. Woodyard, "*Application of the autosynchronized oscillator to frequency demodulation*", Proc. IRE, vol. 25, pp 612-619, May 1937.
90. C.W. Carhahn and H.P. Kalmus, "*Synchronized oscillators as FM receiver limiters*", Electronics, vol 17, pp 108-111, August 1944.
91. G.L. Beers, "*A frequency-dividing locked-in-oscillator frequency-modulation*", Proc. IRE, vol. 32, pp 730-737, December 1944.
92. W.E. Bradley, "*Single stage FM detector*", Electronics, vol 19, pp 88-91, October 1946.
93. M.S. Corrington, "*Locked-in-oscillator TV sound*", Electronics, pp 120-125, March 1951.
94. K. Ishii, "*X-band receiving amplifier*", Electronics, vol 28, pp 202-210, April 1955.
95. K. Ishii, "*Reflex klystrons as receiver amplifiers*", Electronics, vol. 33, pp 56-57, January 1960.
96. K. Ishii, "*The use of reflex klystrons as millimeter wave detectors*", Electronics, vol. 33, pp 82-83, September 1960.
97. A.I. Koc tenki, M.N. Deviatkov, and A.A. Lebed, "*On the application of virtual cathodes for the detection of microwave signals*", Radiotekh. i Elektron, vol. 4, pp 482-488, March 1959.
98. S.A. Kornelov and O.N. Kazbekova, "*Detection in the cathode circuit of an underexcited reflex klystron*", Radiotekh. i Elektron, Vol. 4, pp 475-841, March 1959.
99. J.K. Pulfer, "*Application of a backward wave amplifier to microwave autodyne receiver*", IRE Trans. on Microwave Theory and Techniques, vol. MTT-7, pp 356-359, July 1959.
100. B.G. Whitford, "*The reflex klystron as a microwave detector*", IRE Trans. on Electron Devices, vol ED 8 pp 131-134, March 1961.
101. B.G. Whitford, "*The reflex klystron as a regenerative mixer*", IRE Trans. on Electron Devices, vol. ED 8 , pp 289-293, July 1961.
102. M.E. Mazzone and T.K. Ishii, "*Reflex klystron as subcarrier detector*", Proc. of the IEEE (Correspondence), vol. 53, pp 1755-1756, November 1965.
103. B.W. Hakki, "*GaAs post-threshold microwave amplifier*", Proc. IEEE, vol. 54, p 299, February 1966.
104. S. Nagano, H. Ueno, H. Kondo and H. Murakami, "*Self-excited microwave mixer with a Gunn diode and its applications to Doppler radar*", Electronics and Communication in Japan, vol. 52, pp 112-114, 1969 .

105. G.E. Raue, "*Four unconventional uses for reflex klystrons*", *Microwaves*, vol. 5, pp 34-40, October 1966.
106. J.A. Copeland, "*Stable space charge layers in two-valley semiconductors*", *J. Appl. Phys.* vol. 37, p 3602, August 1966.
107. Ruthroff, "*Injection-locked oscillator FM receiver analysis*", *Bell Systems Tech. J.*, pp 1635-1661, October 1968.
108. D.F. Lawden, Mathematics of Engineering Systems, Ind. ed., pp 328-342, 1959.
109. N. Krylov and N. Bogoliubov, Introduction to Nonlinear Mechanics, Princeton, N.J., Princeton University Press, 1943.

APPENDIX-A

SOME CHARACTERISTICS OF IMPATT DIODES AND GUNN DIODESA-1 Static Characteristics of the IMPATT Diode

If the electric field in the depletion region of a pn junction is sufficiently high that electron-hole pairs are generated by impact ionization, the avalanche breakdown condition is given by the ionization integral³⁰;

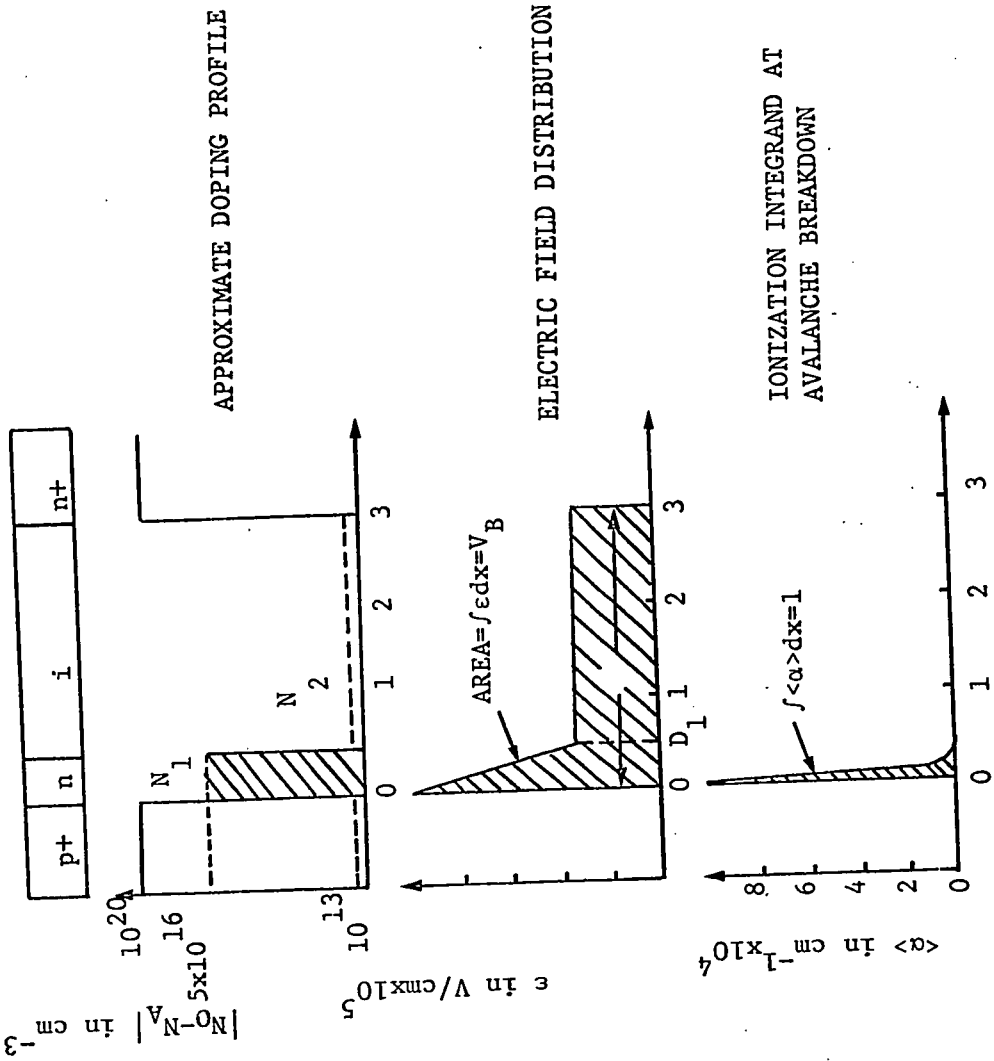
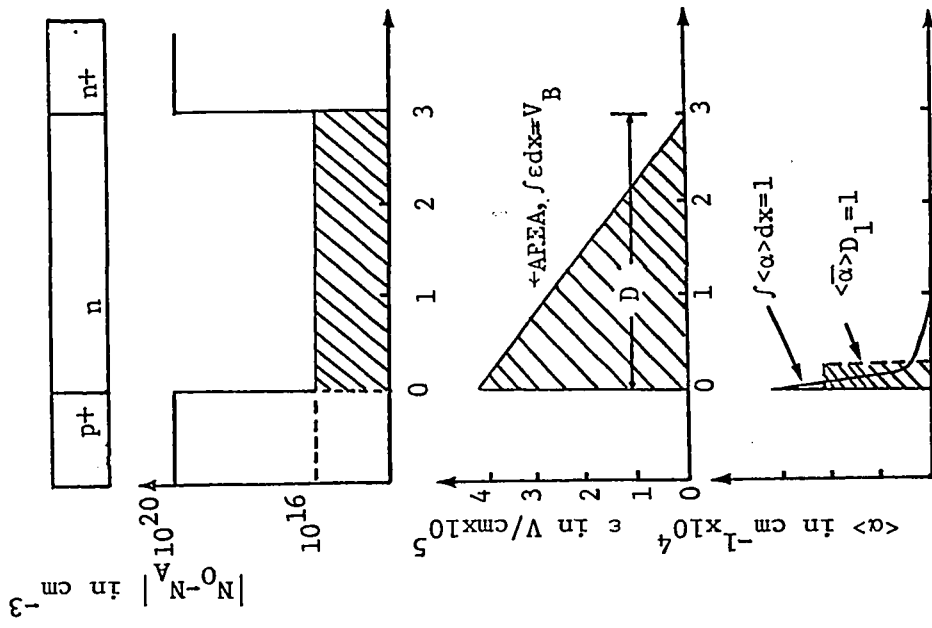
$$\int_0^D \alpha_n \exp\left[-\int_x^D (\alpha_n - \alpha_p) dx\right] dx = 1 \quad (\text{A.1})$$

where α_n and α_p are the ionization rates of the electrons and holes, respectively, and D is the depletion width.

Basic classes of IMPATT diode are the Read diode, the one-sided p-n junction, the linearly graded p-n junction and the p-i-n diode³¹.

Let us consider the static characteristics of the Read diode and of the one-sided abrupt p-n junction. Fig.A.1 shows the doping profile, the electric field, and the ionization integrand at the breakdown condition for a Read diode and for a typical one-sided p-n junction diode. The diode conditions are represented while biased into reverse breakdown. As seen in Fig.A.1, the avalanche region is so highly localized that most of the charge multiplication occurs in a narrow region near the highest field. The drift region is located outside the avalanche region.

For both Read diode and the abrupt p-n junction diode, the region of carrier multiplication is restricted to a narrow region close to the



APPROXIMATE DOPING PROFILE

ELECTRIC FIELD DISTRIBUTION

IONIZATION INTEGRAND AT AVALANCHE BREAKDOWN

(b) ABRUPT p-n JUNCTION (p+ntnt)

(a) READ DIODE (p+ntint)

Fig.A-1

metallurgical junction. Thus, a reasonable definition of the avalanche region width, D_a , is obtained by taking the distance over which 95% of the contribution of the integral in Eq.A.1 occurs:

$$\int_0^D \alpha_n \exp\left[-\int_x^D (\alpha_n - \alpha_p) dx\right] dx = 0.95 \quad (\text{A.2})$$

The drift region is the depletion layer, excluding the avalanche region. The carrier drift velocity is the most important parameter in the drift region. The electric field in this region is high enough so that the generated carriers can travel at their scattering limited velocity, v_s . For silicon, the electric field should be larger than 10^4 V/cm for velocity saturation.

Under operating conditions the IMPATT diode is biased well into avalanche breakdown and the current density is usually very high. The high current density results in a considerable rise in junction temperature and a large space-charge effect, which is the variation of electric field in the depletion region. This effect gives rise to a positive dc incremental resistance for abrupt junctions.

A-2 Dynamic Characteristics of IMPATT Diode

The basic small signal analysis of the Read diode was first considered by Read¹⁷ and developed further by Gilden and Hines²¹. For analysis purposes, the diode may be divided into three regions: 1) the avalanche region, which is assumed to be very thin, so that space charge and signal delay can be neglected; 2) the drift region, where no carriers are generated, and all carriers entering from the avalanche

region travel at their scattering-limited velocity; 3) an inactive end region which adds undesirable parasitic resistance, as shown in Fig.A.2a.

Under the assumption¹⁷ that 1) electrons and holes have equal ionization rates and scattering velocities, 2) the drift current components are much larger than the diffusion component, and 3) the generation rate of electron-hole pairs by avalanche multiplication is large compared to the thermal generation rate, and 4) the breakdown does occur not by direct internal field emission or tunnelling. An equivalent circuit of the avalanche region can be shown²¹ to be as in Fig.A.2b, where the inductance L_a , and capacitance C_a are given as;

$$L_a = \frac{\tau_a}{2\bar{\alpha}' A J_o} \quad (A.3)$$

$$C_a = \frac{\epsilon_s A}{D_a}$$

where τ_a = the transit time across the multiplication region.

$\bar{\alpha}'$ = the derivative of an average value of the ionization rate with respect to the electric field

J_o = the direct current density of diode

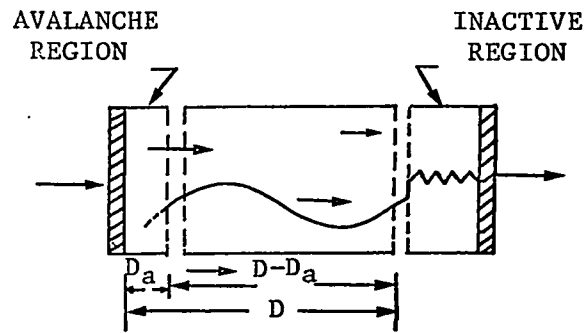
ϵ_s = the dielectric constant of diode, and

A = the active junction area cross-sectional.

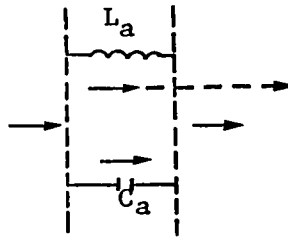
From Eq.A.3, the "avalanche frequency" is given by

$$\omega_a = \sqrt{\frac{2\bar{\alpha}' v_s J_o}{\epsilon_s}} \quad (A.4)$$

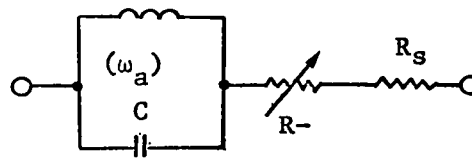
and the impedance for the avalanche region is given by



(a)



(b)



(c)

Fig.A-2

- (a) MODEL OF READ DIODE WITH AVALANCHE REGION, DRIFT REGION AND INACTIVE REGION.
- (b) EQUIVALENT CIRCUIT OF THE AVALANCHE REGION.
- (c) EQUIVALENT CIRCUIT OF READ DIODE FOR SMALL TRANSIT ANGLE. (AFTER GILDEN AND HINES²¹)

$$Z_a = \frac{1}{j\omega C} \left(\frac{1}{1 - \frac{\omega^2 a^2}{\omega^2}} \right) \quad (\text{A.5})$$

An expression for the impedance of the drift region is given²¹ by

$$Z_d \equiv \frac{1}{\omega C_d} \left[\frac{1}{1 - \frac{\omega^2}{\omega_a^2}} \left(\frac{1 - \cos \theta_d}{\theta_d} \right) \right] + \frac{j}{\omega C_d} \left[1 + \frac{1}{1 - \frac{\omega^2}{\omega_a^2}} \left(\frac{\sin \theta_d}{\theta_d} \right) \right] \quad (\text{A.6})$$

$$\text{where } \theta_d = \frac{\omega(D-D_a)}{v_s}$$

$$C_d \equiv \frac{\epsilon_s A}{D-D_a} \quad ; \text{ the capacitance of the drift region.}$$

It is seen from Eq. A.6 that the real part will be negative when $\omega > \omega_a$ and that the real part will be positive for frequencies below ω_a and approached a finite value at low frequencies:

$$R_d(\omega \rightarrow 0) = \frac{(D-D_a)^2}{2A \epsilon_s v_s} \quad (\text{A.7})$$

Actually, the low-frequency small signal resistance results from a space charge resistance in the drift region.

As a result, the total impedance Z , the sum of the impedance of three regions, can be written as;

$$\begin{aligned}
Z = & \frac{(D-D_a)^2}{2 A \epsilon_s v_s} \left(\frac{1}{1 - \frac{\omega^2}{\omega_a^2}} \right) \frac{1 - \cos \theta_d}{\frac{\theta_d^2}{2}} + R_s \\
& + \frac{j}{\omega C_d} \left[\left(\frac{\sin \theta_d}{\theta_d} - 1 \right) - \left(\frac{\frac{\sin \theta_d}{\theta_d} + \frac{D_A}{D-D_a}}{1 - \frac{\omega_a^2}{\omega^2}} \right) \right] \quad (A.8)
\end{aligned}$$

For small transit angles, Eq. A.8 reduces to

$$Z = \frac{(D-D_a)^2}{2A v_s \epsilon_s \left(1 - \frac{\omega^2}{\omega_a^2}\right)} + R_s + \frac{1}{j\omega C} \left(\frac{1}{1 - \frac{\omega_a^2}{\omega^2}} \right) \quad (A.9)$$

where $C \equiv \epsilon_s A/D$; the total depletion layer capacitance. The equivalent circuit correspondence to Eq. A.9 is shown in Fig.A-2c. The first term in Eq. A.9, which corresponds to R_d in the equivalent circuit, becomes negative for $\omega > \omega_a$, and the diode becomes an active device whenever $-R_d > R_s$. The third term in Eq. A.9, which corresponds to the parallel resonant circuit of Fig.A.2c, becomes capacitive for $\omega > \omega_a$ and inductive for $\omega < \omega_a$.

For generalized small signal analysis, the multiple-uniform-layer model was proposed by Misawa²⁰. As discussed before, in the Read diode, the avalanche region is so narrow that the phase shift of the signal within the region is neglected; in the p-i-n diode there is no avalanche-free drift region. By the use of a multiple-uniform-layer model, the intermediate case can be investigated. The diodes in the multiple-layer model behave similar to Read diodes and also exhibit a negative resistance when the transit time of the carriers

becomes a significant fraction of an RF period. The reactance of the diode is inductive at lower frequencies and changes to capacitive beyond the resonant frequency.

A-3 Bulk Differential Negative Conductance of n-type GaAs

In this section, we shall consider the bulk differential negative conductance associated with the Ridley-Watkins-Hilsum transferred electron mechanism.

Let us consider a simple two-valley model of GaAs as shown in Fig.A.3. At zero electric field the carriers are distributed between the two valleys in a manner determined by the energy separation $\Delta\omega$, the lattice temperature T_0 , and the density of states. When a field is applied, a redistribution of the population takes place. We assume that in the lower valley the electrons have an effective mass m_1^* , a mobility μ_1 , and a concentration n_1 , and the density of states is N_1 . In the upper valley the corresponding values are m_2^* , μ_2 , and N_2 . The total carrier concentration is given by $n = n_1 + n_2$. The steady-state conductivity of the two-valley semiconductor can be given by

$$\sigma = q_e (n_1 \mu_1 + n_2 \mu_2) = q_e n \bar{\mu} \quad (\text{A.10})$$

where q_e is the electronic charge and the average mobility

$$\bar{\mu} \equiv \frac{n_1 \mu_1 + n_2 \mu_2}{n_1 + n_2} \quad (\text{A.11})$$

The magnitude of the current density is given by

$$J = \sigma \varepsilon = q_e n \bar{\mu} \varepsilon = q_e n \dot{v} \quad (\text{A.12})$$

where ε is the electric field intensity and

where $\bar{v} = \bar{\mu}\epsilon$ is the magnitude of the average carrier velocity.

For simplicity, let us assume the following conditions for the carrier concentrations over specific ranges of electric field:

$$n_1 \approx n \quad \text{and} \quad n_2 \approx 0 \quad \text{for} \quad 0 < \epsilon < \epsilon_a$$

$$n_1 + n_2 = n \quad \text{for} \quad \epsilon_a < \epsilon < \epsilon_b$$

$$n_1 \approx 0 \quad \text{and} \quad n_2 \approx n \quad \text{for} \quad \epsilon_b < \epsilon$$

Then, the current density is

$$J \approx q_e n \mu_1 \epsilon = q_e n v_1 \quad \text{for} \quad 0 < \epsilon < \epsilon_a$$

$$J = q_e n \bar{\mu}\epsilon = q_e n \bar{v} \quad \text{for} \quad \epsilon_a < \epsilon < \epsilon_b$$

$$J \approx q_e n v_2 \epsilon = q_e n v_2 \quad \text{for} \quad \epsilon < \epsilon_b$$

If $\mu_1 \epsilon_a$ is larger than $\mu_2 \epsilon_b$, there will exist a region of negative differential conductance, as shown in Fig.A.4.

The incremental variation of current density with field is obtained by taking the derivative of Eq. A.12, with respect to the electric field;

$$\frac{\partial J}{\partial \epsilon} = q_e n \frac{\partial \bar{v}}{\partial \epsilon} \quad (\text{A.13})$$

The condition for negative differential conductance can then be written as

$$\frac{\partial \bar{v}}{\partial \epsilon} < 0 \quad (\text{A.14})$$

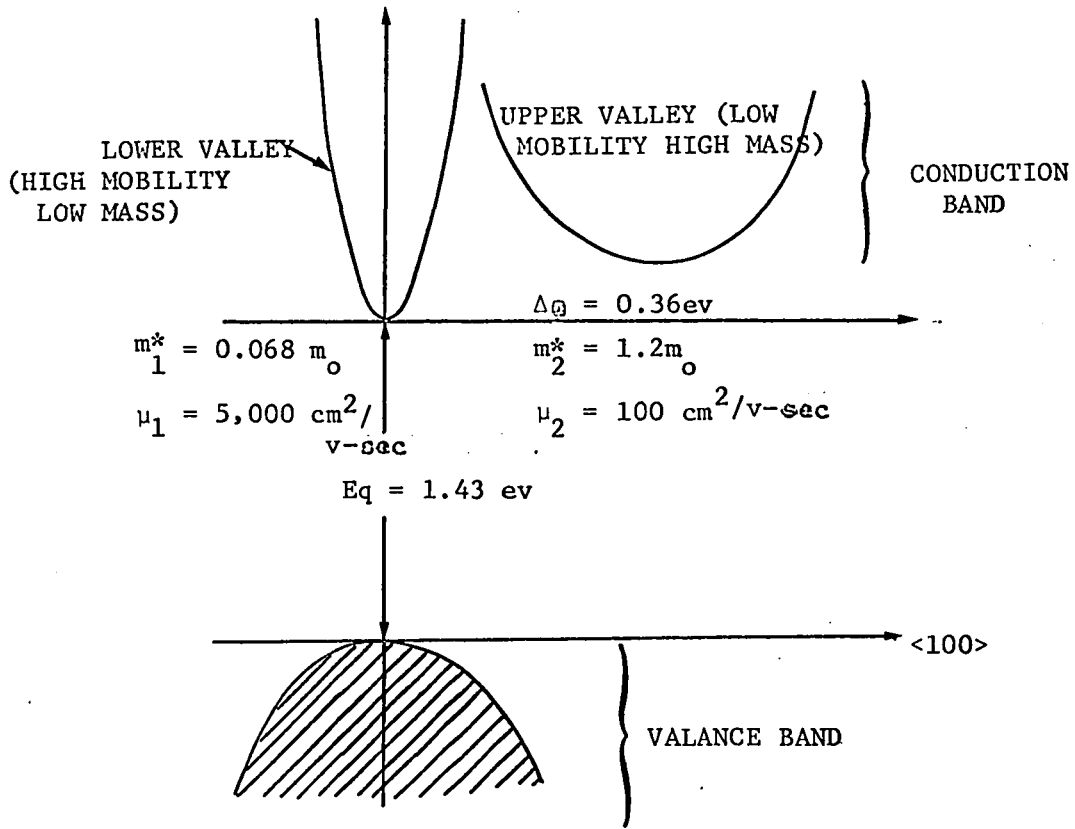


Fig. A-3 SCHEMATIC DIAGRAM SHOWING THE ELECTRON ENERGY VERSUS WAVE NUMBER IN THE REGION OF THE CONDUCTION BAND VALLEYS FOR n-TYPE GaAs

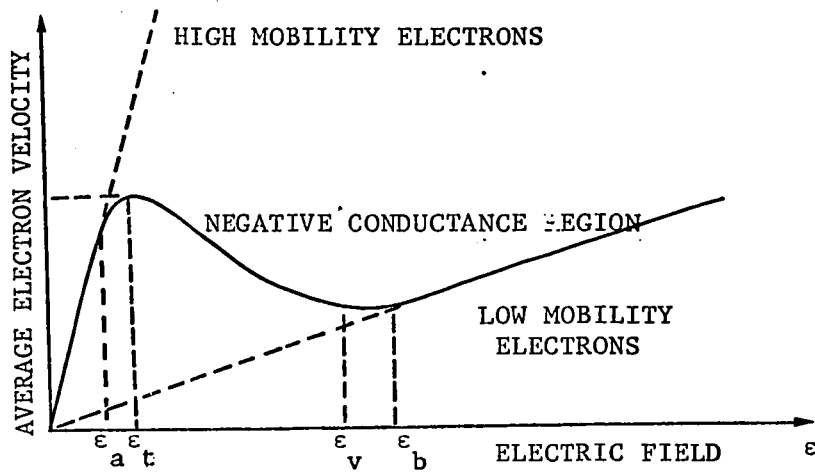


Fig. A-4 AVERAGE VELOCITY VS. ELECTRIC FIELD FOR n-TYPE GaAs.

For the determination of $\overline{dv}/d\epsilon$, a detailed Boltzmann-equation analysis of the high field carriers is required²⁹. For an analytical expression of the velocity-field curve, it is assumed that the carrier populations are instantaneous functions of the electric field³⁰;

$$n_1 = n(1 - F^k)^{-1} \quad (\text{A.15})$$

$$n_2 = nF^k(1 + F^k)^{-1} \quad (\text{A.16})$$

where F is an appropriately normalized electric field, k is a constant and $n = n_1 + n_2 = n_0 + \Delta n$. The average velocity for a given field then becomes

$$\overline{v} = \mu_1 \epsilon \frac{1 + (\mu_2/\mu_1)F^k}{1 + F^k} \quad (\text{A.17})$$

The constants ϵ and k are unknown; however, a choice of $\epsilon = 4.5$ kV/cm and $k = 4.5$ were found to yield reasonably good agreement between theory and experiment³⁰.

APPENDIX-B

GENERAL SOLUTION TO THE LOCKING EQUATION

Let us here solve the differential equation which describes the injection phase-locking properties. By separating variables in Eq. 3.37, the locking equation can be rewritten as

$$\frac{Q_{\text{ext}}(1 + |\Gamma|^2)}{\omega_o |\Gamma|} + \frac{2Q_{\text{ext}}}{\omega_o} \cos\theta \quad d\theta = dt \quad (\text{B.1})$$

$$\frac{\Delta\omega_o Q_{\text{ext}}(1 + |\Gamma|^2)}{\omega_o |\Gamma|} + \frac{2\Delta\omega_o Q_{\text{ext}}}{\omega_o} \cos\theta - \sin\theta$$

with an initial condition

$$\theta(0) = \theta_o \quad (\text{B.2})$$

Let $\xi_1 = \frac{\omega_o |\Gamma|}{Q_{\text{ext}}(1 + |\Gamma|^2)}$ and

$$\xi_2 = \frac{\omega_o}{2 Q_{\text{ext}}} \quad (\text{B.3})$$

Substituting Eq. B.3 into Eq. B.1 yields

$$\left(\frac{\frac{1}{\xi_1} + \frac{1}{\xi_2} \cos\theta}{\frac{\Delta\omega_o}{\xi_1} + \frac{\Delta\omega_o}{\xi_2} \cos\theta - \sin\theta} \right) d\theta = dt \quad (\text{B.4})$$

Thus, from Eq. B.4 a definite integration form is obtained:

$$\int_{\theta_0}^{\theta} \frac{\left(\frac{1}{\xi_1} + \frac{1}{\xi_2} \cos\theta \right)}{\left(\frac{\Delta\omega_0}{\xi_1} + \frac{\Delta\omega_0}{\xi_2} \cos\theta - \sin\theta \right)} d\theta = \int_0^t dt \quad (\text{B.5})$$

Eq. B.5 has two different solutions, depending upon the values of ξ_1 , ξ_2 , and $\Delta\omega_0$.

First, subject to the condition;

$$\left(\frac{\xi_2}{\xi_1} \right)^2 + 1 > \left(\frac{\Delta\omega_0}{\xi_1} \right)^2$$

By substituting Eqs. B.3a and B.3b into the above equation and using Eq. 3.47, we obtain the condition

$$|\Delta\omega_0| < \Delta_1 \quad (\text{B.6})$$

which means that the initial frequency difference is less than the locking range - the locking frequency falls within the locking range.

Under this condition, Eq. B.5 can be rewritten as;

$$\begin{aligned} & \frac{\Delta\omega_0}{\sqrt{1 - \left(\frac{\Delta\omega_0}{\Delta_1} \right)^2}} \ln \frac{\left[\left(\frac{\Delta\omega_0}{\xi_1} - \frac{\Delta\omega_0}{\xi_2} \right) \tan \frac{\theta}{2} - 1 - \sqrt{1 - \left(\frac{\Delta\omega_0}{\Delta_1} \right)^2} \right] \left[\left(\frac{\Delta\omega_0}{\xi_1} - \frac{\Delta\omega_0}{\xi_2} \right) \tan \frac{\theta_0}{2} - 1 + \sqrt{1 - \left(\frac{\Delta\omega_0}{\Delta_1} \right)^2} \right]}{\left[\left(\frac{\Delta\omega_0}{\xi_1} - \frac{\Delta\omega_0}{\xi_2} \right) \tan \frac{\theta}{2} - 1 + \sqrt{1 - \left(\frac{\Delta\omega_0}{\Delta_1} \right)^2} \right] \left[\left(\frac{\Delta\omega_0}{\xi_1} - \frac{\Delta\omega_0}{\xi_2} \right) \tan \frac{\theta_0}{2} - 1 - \sqrt{1 - \left(\frac{\Delta\omega_0}{\Delta_1} \right)^2} \right]} \\ & + \frac{\Delta\omega_0}{\xi_2} (\theta - \theta_0) - \frac{\xi_1}{\xi_2} \ln \left[\frac{\frac{\Delta\omega_0}{\xi_1} + \frac{\Delta\omega_0}{\xi_2} \cos\theta - \sin\theta}{\frac{\Delta\omega_0}{\xi_1} - \frac{\Delta\omega_0}{\xi_2} \cos\theta_0 - \sin\theta_0} \right] \\ & = \xi_1 \left[1 + \left(\frac{\Delta\omega_0}{\xi_2} \right)^2 \right] t \quad (\text{B.7}) \end{aligned}$$

It is worthwhile to note that, when "t" goes to infinity, Eq. B.7 yields the stationary solution. By some mathematical manipulations, we then obtain from Eq. B.7 the stationary condition;

$$\frac{\frac{\Delta\omega}{\xi_1}}{1} - \frac{\frac{\Delta\omega}{\xi_2}}{2} \cos\theta - \sin\theta = 0$$

from which the steady-state phase is obtained as;

$$\theta = \sin^{-1}\left(\frac{\frac{\Delta\omega_o}{\xi_1}}{\sqrt{1 + \left(\frac{\Delta\omega_o}{\xi_2}\right)^2}}\right) + \sin^{-1}\frac{\frac{\Delta\omega_o}{\xi_2}}{\sqrt{1 + \left(\frac{\Delta\omega_o}{\xi_2}\right)^2}} \quad (\text{B.8})$$

Eq. B.8 is identical to Eq. 3.40 which is the steady-state solution to Eq. 3.37, the locking equation for the general case.

Eq. B.7 specifies time as a function of phase and from the equation the phase can be calculated as a function of time. The phase goes from θ_o to θ_{ss} as t goes from 0 to infinity.

Suppose that the magnitude of the reflection coefficient $|\Gamma|$ is very small; in other words, the locking power is very small compared to the locked output power. Then, Eq. B.7 reduces to:

$$\ln \frac{\left[\frac{\Delta\omega_o}{\Delta_o} \tan \frac{\theta}{2} - 1 - \sqrt{1 - \left(\frac{\Delta\omega_o}{\Delta_o} \right)^2} \right] \left[\frac{\Delta\omega_o}{\Delta_o} \tan \frac{\theta_o}{2} - 1 + \sqrt{1 - \left(\frac{\Delta\omega_o}{\Delta_o} \right)^2} \right]}{\left[\frac{\Delta\omega_o}{\Delta_o} \tan \frac{\theta}{2} - 1 + \sqrt{1 - \left(\frac{\Delta\omega_o}{\Delta_o} \right)^2} \right] \left[\frac{\Delta\omega_o}{\Delta_o} \tan \frac{\theta_o}{2} - 1 - \sqrt{1 - \left(\frac{\Delta\omega_o}{\Delta_o} \right)^2} \right]} = \sqrt{1 - \left(\frac{\Delta\omega_o}{\Delta_o} \right)^2} \Delta_o t \quad (\text{B.9})$$

or

$$\theta = 2 \tan^{-1} \left\{ \frac{1}{k} - \frac{\sqrt{1-k^2}}{k} \left[\frac{e^{\sqrt{1-k^2} \Delta_o t} \left(\frac{2}{k} - \frac{1-\sqrt{1-k^2}}{k} - \tan \frac{\theta_o}{2} \right) + \left(\frac{1-\sqrt{1-k^2}}{k} - \tan \frac{\theta_o}{2} \right)}{e^{\sqrt{1-k^2} \Delta_o t} \left(\frac{2}{k} - \frac{1-\sqrt{1-k^2}}{k} - \tan \frac{\theta_o}{2} \right) - \left(\frac{1-\sqrt{1-k^2}}{k} - \tan \frac{\theta_o}{2} \right)} \right] \right\}$$

where $k = \frac{\Delta\omega_o}{\Delta_o}$.

Moreover, when $t \rightarrow \infty$, Eq. B.9 yields a stationary condition for the case of small locking signals:

$$\tan \frac{\theta}{2} = \frac{\omega_o}{\Delta\omega_o} - \frac{\omega_o}{\Delta\omega_o} \sqrt{1 - \left(\frac{\Delta\omega_o}{\Delta_o} \right)^2} \quad \text{or} \quad \theta = \sin^{-1} \left(\frac{\Delta\omega}{\Delta_o} \right) \quad (\text{B.10})$$

Eq. B.10 is identical to Eq. 3.41 which is the steady-state phase angle obtained from the Adler's equation. In addition, it can be shown that the solution to Eq. 3.37 yields the same result as Eq. B.9. Consequently, it indicates that our loading effect method agrees with Adler's approach for relatively small locking signal cases.

Second, impose the condition that

$$|\Delta\omega_o| > \Delta_1 \quad (\text{B.11})$$

Eq. B.11 means that the initial difference frequency is larger than the locking range, that is, the locking frequency falls outside the locking range. Under this condition, Eq. B.5 yields

$$\begin{aligned}
& \frac{2}{\sqrt{\left(\frac{\Delta\omega}{\Delta_1}\right)^2 - 1}} \left[\tan^{-1} \frac{\left(\frac{\Delta\omega_0}{\xi_1} - \frac{\Delta\omega_0}{\xi_2}\right) \tan \frac{\theta}{2} - 1}{\sqrt{\left(\frac{\Delta\omega}{\Delta_1}\right)^2 - 1}} - \tan^{-1} \frac{\left(\frac{\Delta\omega_0}{\xi_1} - \frac{\Delta\omega_0}{\xi_2}\right) \tan \frac{\theta}{2} - 1}{\sqrt{\left(\frac{\Delta\omega}{\Delta_1}\right)^2 - 1}} \right] + \frac{\Delta\omega_0}{\xi_2} (\theta - \theta_0) \\
& - \frac{\xi_1}{\xi_2} \ln \left(\frac{\frac{\Delta\omega}{\xi_1} + \frac{\Delta\omega}{\xi_2} \cos \theta - \sin \theta}{\frac{\Delta\omega}{\xi_1} + \frac{\Delta\omega}{\xi_2} \cos \theta_0 - \sin \theta_0} \right) = \xi_1 \left[1 + \left(\frac{\Delta\omega}{\xi_2}\right)^2 \right] t \quad (\text{B.12})
\end{aligned}$$

For the case of relatively small locking signals ($|\Gamma| \ll 1$) Eq. B.12 can be rewritten as;

$$\left[\tan^{-1} \left(\frac{\frac{\Delta\omega_0}{\Delta_0} \tan \frac{\theta}{2} - 1}{\sqrt{\left(\frac{\Delta\omega_0}{\Delta_0}\right)^2 - 1}} \right) \right]_{\theta_0}^{\theta} = \frac{\sqrt{\left(\frac{\Delta\omega_0}{\Delta_0}\right)^2 - 1}}{2} \Delta_0 t \quad (\text{B.13})$$

It is seen that the phase in Eq. B.13 is a periodic function of time. Eq. B.13 can also be derived directly from Eq. 3.38.

APPENDIX-C

AN APPROXIMATE SOLUTION TO THE DIFFERENTIAL EQUATION OF A LOCKED OSCILLATOR FOR THE FOLLOWING CASES: (1) LOCKING SIGNAL IS FREQUENCY-MODULATED (2) SELF-EXCITED OSCILLATOR IS FREQUENCY-MODULATED.

This appendix presents a method for finding the approximate solution of the locking system in which the locking signal is frequency-modulated or the self-excited oscillator is frequency-modulated.

Let us consider first the case in which the oscillator is driven by an input FM signal;

$$e_1 = A_1 \cos[\omega_c t + \phi(t)] \quad (C.1)$$

where e_1 = applied FM signal

A_1 = constant amplitude of FM

ω_c = carrier frequency

$\phi(t)$ = angle modulation

A typical negative-conductance oscillator, whose free-running frequency and oscillation amplitude are ω_o and A_2 , respectively, will have an output

$$e_2 = A_2 \cos [\omega_c t + \phi(t) - \theta(t)] \quad (C.2)$$

when driven by the input FM signal of Eq. C.1, provided that $\phi(t)$ is a slowly varying function of time and that the input amplitude is very small compared to the oscillator output amplitude. In Eq. C.2 $\theta(t)$

represents the phase tracking error.

From Eq. C.1 the instantaneous frequency of the locking signal can be written as

$$\omega_s(t) = \omega_c + \phi'(t) \quad (C.3)$$

The instantaneous phase difference between the locking and locked signals is, from Eqs. C.1 and C.2, easily seen to be $\theta(t)$.

By substituting Eq. C.3 into Eq. 3.38, the slowly varying function of $\theta(t)$ behaves according to the differential equation

$$\frac{d\theta(t)}{dt} = (\omega_c - \omega_o) + \phi'(t) - \Delta_o \sin \theta(t) \quad (C.4)$$

For simplicity, let ω_c be equal to ω_o and the modulation on the input FM signal be a single frequency sinusoid:

$$\phi'(t) = \Delta\omega \sin \omega_m t \quad (C.5)$$

or

$$\phi(t) = -\frac{\Delta\omega}{\omega_m} \cos \omega_m t$$

where $\Delta\omega$ is the maximum frequency deviation and ω_m is the modulating frequency.

Substitution of Eq. C.5 into Eq. C.4 yields

$$\frac{d\theta}{dt} + \Delta_o \sin \theta = \Delta\omega \sin \omega_m t \quad (C.6)$$

for a symmetric modulation about the free-running frequency.

Provided the input maximum frequency deviation is small compared

to the locking range, the phase angle characteristics can be approximated by a linearized characteristic; $\sin \theta \approx \theta$.

As a result, Eq. C.6 is reduced, substantially, to

$$\frac{d\theta}{dt} + \Delta_o \theta = \Delta\omega \sin \omega_m t \quad (\text{C.7})$$

Since both the dependent variable θ and its derivative $d\theta/dt$ in Eq. C.7 now occur in linear form, a solution can be obtained by means of an integration factor of the form

$$\mu = e^{\Delta_o t}$$

Multiplying both sides of Eq. C.7 by this integration factor, the differential equation reads

$$e^{\Delta_o t} \left[\frac{d\theta}{dt} + \Delta_o \theta \right] = e^{\Delta_o t} \Delta\omega \sin \omega_m t$$

This is equivalent to

$$\frac{d}{dt} [e^{\Delta_o t} \theta] = e^{\Delta_o t} \Delta\omega \sin \omega_m t$$

and the solution of Eq. C.7 is of the form

$$e^{\Delta_o t} \theta = \Delta\omega \int e^{\Delta_o t} \sin \omega_m t + C_o$$

Integrating by parts and dividing both sides by $e^{\Delta_o t}$, we obtain

$$\theta = \frac{\Delta\omega}{\Delta_o \sqrt{1 + \left(\frac{\omega_m}{\Delta_o}\right)^2}} \sin\left[\omega_m t - \tan^{-1} \frac{\omega_m}{\Delta_o}\right] + C_o e^{-\Delta_o t} \quad (\text{C.8})$$

Let us take as an initial condition that at $t = 0$, $\theta = 0$, then

$$C_o = \frac{\omega_m}{\Delta_o^2} \quad (C.9)$$

Substitution of Eq. C.9 into Eq. C.8 yields

$$\theta = \frac{\Delta\omega}{\Delta_o \sqrt{1 + \left(\frac{\omega_m}{\Delta_o}\right)^2}} \sin(\omega_m t - \tan^{-1} \frac{\omega_m}{\Delta_o}) + \frac{\omega_m}{\Delta_o^2} e^{-\Delta_o t} \quad (C.10)$$

The second term of Eq. C.10 is a transient term; it seems to decrease exponentially at a rate determined by the locking bandwidth, decreasing to $\frac{1}{e}$ of its original value after a time $\frac{1}{\Delta_o}$. In the steady state, we have

$$\theta = \frac{\Delta\omega}{\Delta_o \sqrt{1 + \left(\frac{\omega_m}{\Delta_o}\right)^2}} \sin(\omega_m t - \tan^{-1} \frac{\omega_m}{\Delta_o}) \quad (C.11)$$

Eq. C.11 represents the phase-tracking error of the locking system.

In addition, from Eqs. C.2, C.5, and C.11 we can obtain the instantaneous phase deviation $\alpha(t)$ of the locked oscillator from the carrier;

$$\begin{aligned} \alpha(t) &= \theta(t) - \phi(t) \\ &= \frac{\frac{\Delta\omega}{\omega_m}}{\sqrt{1 + \left(\frac{\omega_m}{\Delta_o}\right)^2}} \sin(\omega_m t + \tan^{-1} \frac{\omega_m}{\Delta_o}) \end{aligned} \quad (C.12)$$

It is useful to define a "modulation conservation factor" C_1 being the ratio of the modulation index of the original input FM signal, $\Delta\omega/\omega_m$, to the output modulation index. In other words, the modulation conservation factor represents the ratio of the input peak phase

deviation to the locked output peak phase deviation. The locked output modulation index or the output peak phase deviation can easily be obtained from the instantaneous phase deviation formula of Eq. C.12;

$$\alpha_m = \frac{\frac{\Delta\omega}{\omega_m}}{\sqrt{1 + \left(\frac{\omega_m}{\Delta\omega}\right)^2}} \quad (\text{C.13})$$

Therefore, the modulation conservation factor is

$$C_1 = \sqrt{1 + \left(\frac{\omega_m}{\Delta\omega}\right)^2} \quad (\text{C.14})$$

In this case we can also deduce from Eq. C.14, a "Modulation suppression factor" defined as the reciprocal of the conservation factor:

$$S_1 = \frac{1}{\sqrt{1 + \left(\frac{\omega_m}{\Delta\omega}\right)^2}} \quad (\text{C.15})$$

Let us now consider the second case, in which the self-excited oscillator is frequency-modulated,

$$\omega_o(t) = \omega_c + \Delta\omega \sin \omega_m t, \quad (\text{C.16})$$

and the locking signal is a sinusoid

$$e_1 = A_1 \cos \omega_s t. \quad (\text{C.17})$$

Then the locked oscillator will have an output

$$e_2 = A_2 \cos[\omega_s t - \theta(t)] \quad (\text{C.18})$$

when driven by the input CW signal of Eq. C.17. $\theta(t)$ represents the phase difference between the locking and locked oscillator signals.

As a result, by substituting Eq. C.16 into Eq. 3.38, the slowly varying function of $\theta(t)$ behaves according to

$$\frac{d\theta(t)}{dt} = \omega_s - \omega_c - \Delta\omega \sin \omega_m t - \Delta_o \sin \theta(t) \quad (C.19)$$

As in the first case, let ω_c be equal to ω_s . Then we have

$$\frac{d\theta(t)}{dt} + \Delta_o \sin \theta(t) = -\Delta\omega \sin \omega_m t \quad (C.20)$$

Letting

$$\theta(t) = -\beta(t) \quad (C.21)$$

we obtain a differential equation identical in form to Eq. B.7;

$$\frac{d\beta(t)}{dt} + \Delta_o \sin \beta(t) = \Delta\omega \sin \omega_m t \quad (C.22)$$

In a similar way, the instantaneous phase deviation $\theta(t)$, which is equal to $-\beta(t)$, can be written as

$$\theta(t) = -\frac{\frac{\Delta\omega}{\Delta_o}}{\sqrt{1 + \left(\frac{\omega_m}{\Delta_o}\right)^2}} \sin\left(\omega_m t - \tan^{-1} \frac{\omega_m}{\Delta_o}\right) \quad (C.23)$$

It is very useful to deduce the "modulation suppression factor" for this case. The modulation index of the locked oscillator is represented as the peak phase deviation of the locked oscillator output;

$$\theta_M = \frac{\frac{\Delta\omega}{\Delta_o}}{\sqrt{1 + \left(\frac{\omega_m}{\Delta_o}\right)^2}} \quad (\text{C.24})$$

Consequently, the ratio of θ_M to the original modulation rate $\Delta\omega/\omega_m$ yields the modulation suppression factor;

$$S_2 = \frac{\frac{\omega_m}{\Delta_o}}{\sqrt{1 + \left(\frac{\omega_m}{\Delta_o}\right)^2}}$$

or

$$S_2 = \frac{1}{\sqrt{1 + \left(\frac{\Delta_o}{\omega_m}\right)^2}} \quad (\text{C.25})$$

APPENDIX-D

EFFECT OF ADDITIVE DC POTENTIAL ON AVERAGE FREQUENCY SHIFT

The average dc potential developed at the diode input of the oscillator may be determined from Eq. 3.38 when relatively small locking signals are applied to the oscillator.

Integrating the differential equation over one cycle results in

$$\frac{1}{T_b} \int_0^{T_b} \Delta_o \sin \theta dt = \frac{1}{T_b} \int_0^{T_b} \Delta\omega_o dt - \frac{1}{T_b} \int_{\theta_o}^{\theta_o+2\pi} d\theta \quad (D.1)$$

or
$$\Delta_o \langle \sin \theta \rangle = \Delta\omega_o - \frac{2\pi}{T_b}$$

Substituting Eq. 3.79 into Eq. C.1 yields

$$\Delta_o \langle \sin \theta \rangle = \Delta\omega_o - \Delta\omega_o \sqrt{1 - \left(\frac{\Delta_o}{\Delta\omega_o}\right)^2} \quad (D.2)$$

Eq. D.2 is plotted in Fig.D.1. It is seen that $\Delta_o \sin \theta$, the average frequency shift, is a maximum when $\Delta\omega_o = \Delta_o$ and decreases beyond that point, approaching zero.

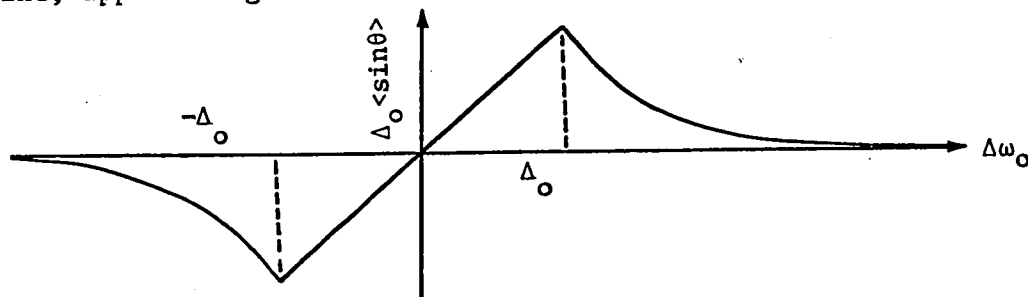


Fig.D-1 PLOT OF $\Delta_o \langle \sin \theta \rangle$ AS A FUNCTION OF $\Delta\omega_o$.

Once the existence of the DC component is recognized, the beat-note of the fundamental frequency, $\Delta\omega_0 \sqrt{1 - \left(\frac{\Delta_0}{\Delta\omega_0}\right)^2}$, is seen to modulate the oscillator.

APPENDIX-E

MICROWAVE PHASE DETECTOR

Consider the arrangement of Fig.D.1, consisting of a magic tee and two microwave square law detectors with detector mounts.

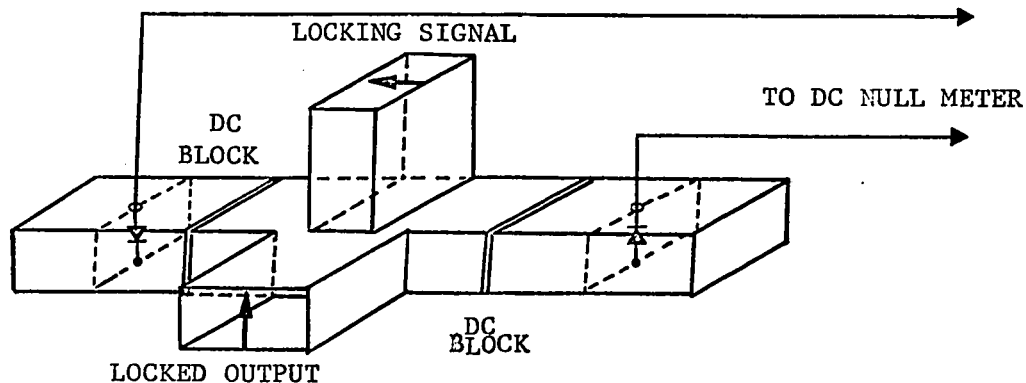


Fig.E-1 MICROWAVE PHASE DETECTOR

The two detector mounts are insulated for dc and video from the E and H arms so that the signals from the two detectors can be subtracted by connecting the detector mount outputs in series opposition. The dc blocks account for the equivalent circuit of Fig.E.2. The two capacitors are actually the cable capacitance; the resistors are about $15\text{ k}\Omega$ each. The two mounts are tuned for maximum dc voltage output. Both detectors should be adjusted as nearly as possible for identical operation.

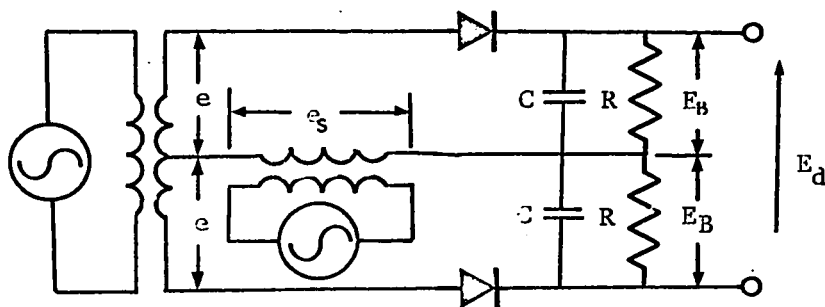


Fig.E-2 EQUIVALENT CIRCUIT OF Fig.E-1.

The two voltages being compared may be represented as

$$e_s = E'_s \sin \omega_s t \quad (\text{E.1})$$

$$e = E' \sin(\omega_s t - \theta) \quad (\text{E.2})$$

Consequently, the outputs of the detectors are expressed as;

$$E_A \propto |e_s + e|^2 = E'_s{}^2 + E'^2 + 2E'_s E' \cos \theta \quad (\text{E.3})$$

$$E_B \propto |e_s - e|^2 = E'_s{}^2 + E'^2 - 2E'_s E' \cos \theta \quad (\text{E.4})$$

Since the output E_d is equal to the difference of the two rectified voltages, then

$$E_d = K_1 \cos \theta \quad (\text{E.5})$$

where K_1 is a proportionality constant which is independent of the phase. In other words, the output is a sinusoidal wave as a function of input phase difference,

Another microwave phase detector may be accomplished by means of a 3-dB coupler as the symmetry of the crystals with respect to the reference plane has no particular significance⁴⁴, except to offset the response curve by a constant angle. Let us consider Fig.E.3. The two voltages being compared have the same form of Eq. E.5. In the coupler, two signals interfere because of the phase difference between them. The detector input may be represented as

$$e_{in} = E'_s \sin \omega_s t + E' \sin(\omega_s t - \theta) \quad (\text{E.6})$$

square-law detected output is expressed as

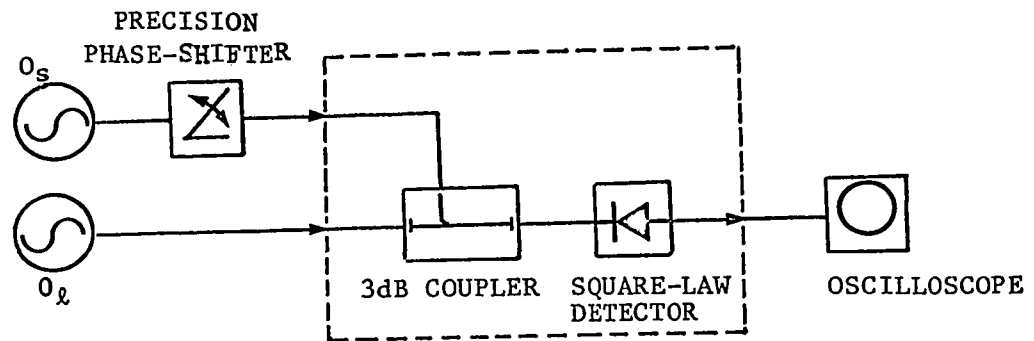


Fig.E-3 A PHASE DETECTOR WITH 3 dB COUPLER.

$$e_{\text{out}} = M_1 (E_s'^2 + E_l'^2 + 2E_s' E_l' \cos \theta) \quad (\text{E.7})$$

where M_1 is the detector conversion constant. Since an electrical length or a phase angle can be adjusted by use of a phase shifter, θ in Eq. E.7 may be replaced by $\theta + 90^\circ$. Then the output is

$$e'_{\text{out}} = M (E_s'^2 + E_l'^2 - 2E_s' E_l' \sin \theta) \quad (\text{E.8})$$

Therefore, the detector output is a sine wave as a function of input phase difference.

If the phase angle is time-modulated by an AC signal, the AC component of the detector output can be represented as

$$v_d = M_2 \sin \theta(t) \quad (\text{E.9})$$

where $M_2 = 2E_s' E_l' M_1 = \text{constant}$.

APPENDIX-F

INJECTION PHASE-LOCKING OF A NONLINEAR CONDUCTANCE DIODE OSCILLATOR

Consider a simple model of a locked oscillator, represented by a resonant circuit G, L, C , a nonlinear element of characteristic

$$i_g = \phi(e) \quad (\text{F.1})$$

and a locking source $i_s(t)$, as shown in Fig.E.1.

For large signal operation, we may express the current flowing through the diode active element in terms of a power series of the RF voltage $e(t)$ across the diode:

$$i_g = a_1 e + a_2 e^2 + a_3 e^3 + \dots \quad (\text{F.2})$$

The diode is assumed to be mounted in a simple, single-tuned circuit, and no significant harmonic voltages appear. Then the fundamental component of current as a function of the RF voltage e can be written as;

$$i_g = a_1 e + a_3 e^3 \quad (\text{F.3})$$

where a_1 is negative and a_3 positive.

Then the differential equation describing the circuit of Fig.E.1 is given by

$$C \frac{de}{dt} + (G + a_1)e + \frac{1}{L} \int e dt + a_3 e^3 = i_s(t) \quad (\text{F.4})$$

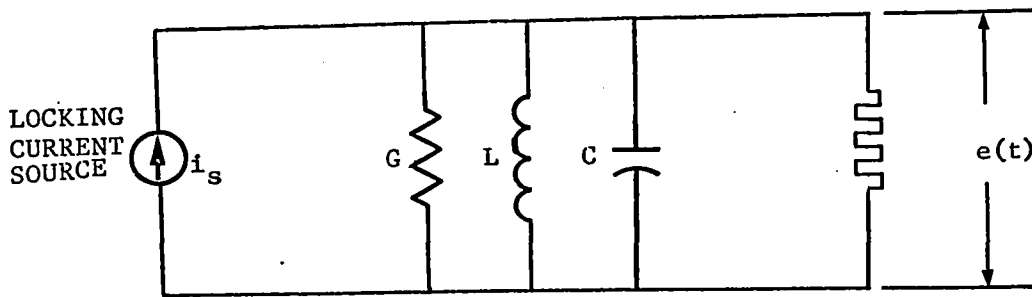


Fig.F-1 AN EQUIVALENT CIRCUIT OF THE INJECTION PHASE-LOCKED OSCILLATOR OF NONLINEAR CONDUCTANCE DIODE.

Under the above assumptions, the RF voltage across the resonant circuit can be given by

$$e(t) = E(t) \cos[\omega t - \theta(t)] \quad (\text{F.5})$$

where $E(t)$ and $\theta(t)$ do not change appreciably over one cycle of the oscillation.

Under these conditions, de/dt and $\int edt$ can be approximately obtained as

$$\frac{de}{dt} = -E\left(\omega - \frac{d\theta}{dt}\right) \sin(\omega t - \theta) + \frac{dE}{dt} \cos(\omega t - \theta) \quad (\text{F.6})$$

and

$$\int edt = \left(\frac{E}{\omega} + \frac{E}{\omega^2} \frac{d\theta}{dt}\right) \sin(\omega t - \theta) + \frac{1}{\omega^2} \frac{dE}{dt} \cos(\omega t - \theta) \quad (\text{F.7})$$

Substituting Eqs. F.5 and F.6, and F.7 into Eq. F.4, multiplying by $\sin(\omega t - \theta)$ or $\cos(\omega t - \theta)$ and integrating with respect to time over one cycle of the oscillation, because of the orthogonal relations between sine and cosine functions, we obtain an approximate differential equation¹⁰⁸⁻¹⁰⁹:

$$\left(-\omega C - \frac{1}{\omega L}\right) + \left(C + \frac{1}{\omega^2 L}\right) \frac{d\theta}{dt} = \frac{2}{ET_0} \int_0^t i_s(t) \sin(\omega t - \theta) dt \quad (\text{F.8})$$

$$\left(C + \frac{1}{\omega^2 L}\right) \frac{dE}{dt} + \left(G + a_1 + \frac{3}{4} a_3 E^2\right) E = \frac{2}{T_0} \int_{t-T_0}^t i_s(t) \cos(\omega t - \theta) dt \quad (\text{F.9})$$

For a steady-state free-running oscillation, since $d\theta/dt = 0$, $dE/dt = 0$, and $i_s = 0$, we obtain the frequency ω_0 and the amplitude E_0 of the oscillation;

$$\omega_0 = \frac{1}{\sqrt{LC}} \quad (\text{F.10})$$

and

$$E_0 = \frac{4}{3} \left(\frac{a_1' - G}{a_3} \right) \quad (\text{F.11})$$

where $a_1' = -a_1 = |a_1|$.

The free-running power p_0 of the oscillator is given by

$$\begin{aligned} P_0 &= \frac{1}{2} G E_0^2 \\ &= \frac{2G}{3a_3} (a_1' - G) \end{aligned} \quad (\text{F.12})$$

Power output is parabolic as a function of G , peaking when

$$G = \frac{a_1'}{2} \quad (\text{F.13})$$

and having a maximum value

$$\max P_0 = \frac{a_1'^2}{6 a_3} \quad (\text{F.14})$$

For analysis purposes let the locking current source $i_s(t)$ be written as:

$$i_s(t) = I_s \cos \omega_s t \quad (\text{F.15})$$

Substitution of Eq. F.15 into Eqs. F.8 and F.9 yields:

$$\left(-\frac{1}{\omega L} - \omega C\right) + \left(C + \frac{1}{\omega^2 L}\right) \frac{d\theta}{dt} = -\frac{I_s}{E} \sin \theta \quad (\text{F.16})$$

$$\left(C + \frac{1}{\omega^2 L}\right) \frac{dE}{dt} + \left(G + a_1 + \frac{3}{4} a_3 E^2\right) E = I_s \cos \theta \quad (\text{F.17})$$

For the steady-state of the locked oscillator, $d\theta/dt$ or $\theta = \text{constant}$ and $dE/dt = 0$. Let

$$\omega_s = \omega_o + \Delta\omega_o \quad (\text{F.18})$$

where $\Delta\omega_o = \text{initial frequency difference}$. In this case, substitution of Eq. F.18 into Eq. F.16 yields;

$$\frac{\Delta\omega_o}{\omega_o} = \frac{1}{Q_{\text{ext}}} \frac{E_s}{E} \quad (\text{F.19})$$

where E_s is taken as the effective locking voltage at the optimum load condition, and Q_{ext} is the external Q of the oscillator.

Substitution of Eq. F.11 into Eq. F.17 yields

$$E^2 = E_o^2 \left(1 + \frac{E_s}{E} \cos \theta\right) \quad (\text{F.20})$$

It is very interesting to note that the nonlinear conductance diode oscillator does not introduce any modification in the locking range, but only modifies the output voltage, resulting in the modified power output.